

**NMR Studies on Transition Metal Catalyzed  
Hydroformylation and Carbonylation Using  
Parahydrogen Induced Polarization**

---

by

**Dexin Guan**

**A Thesis Submitted to the Department of Chemistry**

**for the Degree of Doctor of Philosophy**

The University of York

Department of Chemistry

September, 2013



## Abstract

This thesis presents a number of mechanistic studies using parahydrogen that enable the detection of an array of reaction intermediates; species are detected through PHIP and One-Proton-PHIP. The reactions studied involve iridium, rhodium and palladium catalysts and are hydrogenation, hydroformylation and hydrocarbonylation.

For iridium, the following complexes were synthesized:  $\text{Ir}(\eta^3\text{-C}_3\text{H}_5)(\text{CO})(\text{PR}_2\text{R}')_2$  (**15a-15e**), where **15a**,  $\text{PR}_2\text{R}' = \text{PMe}_3$ ; **15b**,  $\text{PPhMe}_2$ ; **15c**,  $\text{PPh}_2\text{Me}$ ; **15d**,  $\text{P}(p\text{-tol})_3$ ; **15e**,  $\text{PPh}_3$ . The following intermediates were detected by PHIP:  $\text{Ir}(\eta^3\text{-C}_3\text{H}_5)(\text{H}_2)(\text{CO})(\text{PR}_2\text{R}')$  (**18A** and **18B**),  $\text{Ir}(\text{H})_2(\eta^1\text{-C}_3\text{H}_5)(\text{CO})_2(\text{PMe}_3)_2$  (**33A** and **33B**). Reaction pathways for hydrogenation and hydroformylation were proposed on the basis of these studies.

For rhodium, the following species were synthesized:  $\text{Rh}(\eta^3\text{-C}_3\text{H}_5)(\text{PPh}_3)_2$  (**16**). The Rh system proved much more reactive under hydroformylation conditions which prevented further study.

For palladium, the complexes,  $[(\text{BCOPE})\text{Pd}(\text{CH}_3\text{OH})_2](\text{OTf})_2$  (**12a**) and  $[(^t\text{BuCOPE})\text{Pd}(\text{H}_2\text{O})_2](\text{OTf})_2$  (**12b**) were prepared. Now the carbonylation intermediates,  $[\text{PdH}(\text{BCOPE})(\text{CO})](\text{OTf})$  (**13a-3**),  $[(\text{BCOPE})\text{Pd}(\text{CPh}=\text{CHPh})(\text{CD}_3\text{OD})](\text{OTf})$  (**40a-1**),  $(\text{BCOPE})\text{Pd}(\text{CPh}=\text{CHPh})(\text{OTf})$  (**40a-4**),  $[(\text{BCOPE})\text{Pd}(\mu\text{-H})(\mu\text{-CO})\text{Pd}(\text{BCOPE})][\text{OTf}]$  (**43a**),  $[(\kappa^2\text{-BCOPE})(\kappa^1\text{-BCOPE})\text{Pd}(\text{H})_2](\text{OTf})_2$  (**70a**),  $[(\text{BCOPE})\text{Pd}(\text{CD}_3\text{COCPh}=\text{CHPh})(\text{CO})](\text{OTf})_2$  (**72a**),  $[\text{Pd}(\text{BCOPE})\text{Pd}(\text{CO-CPh}=\text{CHPh})(\text{CO})](\text{OTf})$  (**73a**) were detected. These observations were used to propose a reaction cycle for the methoxycarbonylation of diphenyl acetylene.

## *Table of contents*

# **Table of contents**

<b>ABSTRACT</b>	<b>1</b>
<b>TABLE OF CONTENTS</b>	<b>2</b>
<b>LIST OF FIGURES</b>	<b>10</b>
<b>LIST OF TABLES</b>	<b>17</b>
<b>ACKNOWLEDGEMENTS</b>	<b>20</b>
<b>DECLARATION</b>	<b>21</b>
<b>CHAPTER 1 INTRODUCTION</b>	<b>22</b>
<b>1.1 Catalysis in industry</b>	<b>23</b>
1.1.1 Catalysis and its importance	23
1.1.2 Homogenous and heterogeneous catalysis	23
1.1.3 Homogenous catalysis and its applications	24
1.1.4. Carbonylation	25
1.1.4.1 What is carbonylation	25
1.1.4.2: Hydroformylation versus Reppe carbonylation	26
<b>1.2 Mechanistic study on homogeneous catalysis</b>	<b>27</b>
1.2.1 Why mechanistic study is important?	27
1.2.2 Elemental reactions in homogeneous catalysis	27
1.2.2.1 Ligand exchange: association and dissociation	28
1.2.2.2 Insertion and migratory insertion	29
1.2.2.3 De-insertion and $\beta$ -elimination	30
1.2.2.4 Oxidative addition	30
1.2.2.5 Reductive elimination	31
1.2.2.6 Hydrogen activation by heterolytic cleavage	31
1.2.3 Methods of mechanistic study	31
1.2.3.1 Chemical methods	31
1.2.3.2 Analytical methods	32
1.2.3.3 Theoretical methods	33

<b>1.3 Hydroformylation</b>	<b>33</b>
1.3.1 Hydroformylation: discovery, definition and application	33
1.3.2 Catalyst evolution	35
1.3.2.1 Unmodified first generation catalyst	35
1.3.2.2 Modified first generation catalyst	36
1.3.2.3 The second generation catalyst	37
1.3.2.4 Expanding ligands	38
1.3.2.5 The third generation catalyst	41
1.3.2.6 New generation (or 4th) catalyst	42
1.3.3 General mechanism of hydroformylation	42
1.3.4 Reactivity and selectivity	45
1.3.4.1 Parameters that determines the selectivity	45
1.3.4.2 Selectivity on unmodified catalyst system:	47
1.3.4.3 Selectivity on Rh/PPh <sub>3</sub> system:	48
<b>1.4 Reppe carbonylation</b>	<b>49</b>
1.4.1 History	49
1.4.2 Catalysts for Reppe carbonylation	50
1.4.3 Carbonylation mechanisms	50
1.4.3.1 Alkene carbonylation	50
1.4.3.2 Alkyne carbonylation	51
1.4.4 Intermediates	52
1.4.4.1 Palladium monohydride complexes	52
1.4.4.2 Palladium vinyl complexes	54
1.4.4.3 Palladium alkyl complexes:	55
<b>1.5 Parahydrogen and its NMR application</b>	<b>57</b>
1.5.1 History, concept and preparation of parahydrogen	57
1.5.2 NMR properties of <i>ortho</i> and <i>parahydrogen</i>	58
1.5.3 NMR programs and terms related with this study	59
1.5.3.1 Homonuclear Correlation spectroscopy (COSY)	59
1.5.4.2 Heteronuclear correlation spectroscopy (HMQC)	60
1.5.4.3 NOESY	61
1.5.4.4 $\pi/4$ pulse NMR experiments	61
1.5.4.5 OPSY	61
1.5.4.6 Virtual coupling	62
1.5.4: An example of PHIP	63
1.5.5 Applications of PHIP	65

## Table of contents

1.5.5.1 On detecting organometallic species:	65
1.5.5.2 On the mechanistic studies	65
1.5.5.3 Other applications of PHIP	66
<b>1.6 Aim on Ir/Rh catalysed hydroformylation</b>	<b>67</b>
1.6.1 Why Ir/Rh allyl complexes	67
1.6.1.1 Ligand hapticity	67
1.6.1.2 Spectroscopic properties	67
1.6.1.3. The $\pi$ - $\sigma$ interconversions of allyl ligands	68
1.6.1.4 The fluxional behaviour of the allyl group	68
1.6.2 Aim on $M(\eta^3\text{-C}_3\text{H}_5)(\text{CO})(\text{PPh}_3)_2$ (where M = Rh, Ir) catalyzed hydroformylation	69
1.6.2.1 Background	69
1.6.2.2 Precursors	69
1.6.2.3 Fluxionality and Characterization	70
1.6.2.4 Expected reaction of $\text{Ir}(\eta^3\text{-C}_3\text{H}_5)(\text{CO})(\text{PR}_2\text{R}')_2$ (15) with $\text{H}_2$	70
1.6.2.5 NMR study on the reaction of $\text{Ir}(\eta^3\text{-C}_3\text{H}_5)(\text{CO})(\text{PR}_2\text{R}')_2$ with $\text{CO}/\text{H}_2$	72
<b>1.7 Aim on Pd catalysed carbonylation</b>	<b>75</b>
1.7.1 Background	75
1.7.2 Precursors	76
1.7.3 Study on palladium catalysed carbonylation	76
1.7.4 Further study on palladium catalysed diphenyl acetylene hydrogenation	79
<b>CHAPTER 2 NMR STUDY ON IRIDIUM CATALYSED HYDROFORMYLATION</b>	<b>80</b>
<b>2.1 Introduction</b>	<b>81</b>
<b>2.2 Synthesis of the precursors</b>	<b>81</b>
<b>2.3 Results from reactions involving <math>\text{Ir}(\eta^3\text{-C}_3\text{H}_5)(\text{CO})(\text{PMe}_3)_2</math> (15a)</b>	<b>82</b>
2.3.1 NMR characterization of $\text{Ir}(\eta^3\text{-C}_3\text{H}_5)(\text{CO})(\text{PMe}_3)_2$ (15a)	82
2.3.2 Reactions of $\text{Ir}(\eta^3\text{-C}_3\text{H}_5)(\text{CO})(\text{PMe}_3)_2$ (15a) with <i>parahydrogen</i>	86
2.3.2.1 Reaction of 15a with <i>parahydrogen</i> at 233 K	86
2.3.2.2 Reactions of $\text{Ir}(\eta^3\text{-C}_3\text{H}_5)(\text{CO})(\text{PMe}_3)_2$ (15a) with <i>parahydrogen</i> at 253 K	89
2.3.2.3 Reactions of $\text{Ir}(\eta^3\text{-C}_3\text{H}_5)(\text{CO})(\text{PMe}_3)_2$ (15a) with <i>parahydrogen</i> at 298 K	90
2.3.2.4 Short conclusion	92
2.3.3 Reaction of $\text{Ir}(\eta^3\text{-C}_3\text{H}_5)(\text{CO})(\text{PMe}_3)_2$ (15a) with $\text{CO}$ ( $^{12}\text{CO}$ and $^{13}\text{CO}$ )	95
2.3.3.1 Reaction of $\text{Ir}(\eta^3\text{-C}_3\text{H}_5)(\text{CO})(\text{PMe}_3)_2$ (15a) with $\text{CO}$ at 203 K	95
2.3.3.2 Reaction of $\text{Ir}(\eta^3\text{-C}_3\text{H}_5)(\text{CO})(\text{PMe}_3)_2$ (15a) with $\text{CO}$ at 298 K	97

2.3.3.3 Short conclusion	100
2.3.4 Reaction of $\text{Ir}(\eta^3\text{-C}_3\text{H}_5)(\text{CO})(\text{PMe}_3)_2$ (15a) with CO and H <sub>2</sub>	101
2.3.4.1 Control reaction of 15a with CO and H <sub>2</sub> at 203 K	101
2.3.4.2 Reaction of $\text{Ir}(\eta^3\text{-C}_3\text{H}_5)(\text{CO})(\text{PMe}_3)_2$ (15a) with CO and H <sub>2</sub> at 283 K	101
2.3.4.3 Reaction of $\text{Ir}(\eta^3\text{-C}_3\text{H}_5)(\text{CO})(\text{PMe}_3)_2$ (15a) with CO and H <sub>2</sub> at 298 K	103
2.3.4.4 Reaction of $\text{Ir}(\eta^3\text{-C}_3\text{H}_5)(\text{CO})(\text{PMe}_3)_2$ (15a) with CO and H <sub>2</sub> at 313 K	105
2.3.5 Conclusion for 15a	106
<b>2.4 Results from reactions involving <math>\text{Ir}(\eta^3\text{-C}_3\text{H}_5)(\text{CO})(\text{PMe}_2\text{Ph})_2</math> (15b)</b>	<b>108</b>
2.4.1 Synthesis and characterization of 15b	108
2.4.1.1 Synthesis of 15b	108
2.4.1.2 Characterization of $\text{Ir}(\eta^3\text{-C}_3\text{H}_5)(\text{CO})(\text{PMe}_2\text{Ph})_2$ (15b)	109
2.4.2 Reaction of $\text{Ir}(\eta^3\text{-C}_3\text{H}_5)(\text{CO})(\text{PMe}_2\text{Ph})_2$ with <i>parahydrogen</i>	111
2.4.2.1 Reaction of $\text{Ir}(\eta^3\text{-C}_3\text{H}_5)(\text{CO})(\text{PMe}_2\text{Ph})_2$ (15b) with <i>parahydrogen</i> at 233 K	111
2.4.2.1 Reaction of $\text{Ir}(\eta^3\text{-C}_3\text{H}_5)(\text{CO})(\text{PMe}_2\text{Ph})_2$ (15b) with <i>parahydrogen</i> at 298 K	111
2.4.3 Reaction of $\text{Ir}(\eta^3\text{-C}_3\text{H}_5)(\text{CO})(\text{PMe}_2\text{Ph})_2$ (15b) with CO ( <sup>12</sup> CO and <sup>13</sup> CO)	113
2.4.3.1 Reaction of $\text{Ir}(\eta^3\text{-C}_3\text{H}_5)(\text{CO})(\text{PMe}_2\text{Ph})_2$ (15b) with CO at 203 K ( <sup>12</sup> CO and <sup>13</sup> CO)	113
2.4.4 Reaction of $\text{Ir}(\eta^3\text{-C}_3\text{H}_5)(\text{CO})(\text{PMe}_2\text{Ph})_2$ (15b) with CO and <i>parahydrogen</i>	114
2.4.5 Conclusion for 15b	119
<b>2.5 NMR studies of fluxional behaviour of 15a-15e</b>	<b>120</b>
2.5.1 Line shape simulation	120
2.5.2 Calculation of the activation parameters	120
<b>2.6 Conclusion</b>	<b>121</b>
<b>CHAPTER 3 STUDIES OF RHODIUM CATALYSED HYDROFORMYLATION</b>	<b>123</b>
<b>3.1 Introduction</b>	<b>124</b>
<b>3.2 Synthesis &amp; characterization of <math>\text{Rh}(\eta^3\text{-C}_3\text{H}_5)(\text{PPh}_3)_2</math> (16)</b>	<b>124</b>
3.2.1 Synthesis	124
3.2.2 NMR characterization of $\text{Rh}(\eta^3\text{-C}_3\text{H}_5)(\text{PPh}_3)_2$ (16)	125
3.2.3 XRD studies	128
<b>3.3 Control Reaction of <math>\text{Rh}(\eta^3\text{-C}_3\text{H}_5)(\text{PPh}_3)_2</math> with <i>parahydrogen</i></b>	<b>131</b>
3.3.1 Reaction of $\text{Rh}(\eta^3\text{-C}_3\text{H}_5)(\text{PPh}_3)_2$ with <i>parahydrogen</i> in toluene-d <sub>8</sub>	131
3.3.2 Reaction of the detected product $\text{Rh}(\text{H})_2(\text{PPh}_3)_2(\mu\text{-H})_2\text{Rh}(\text{PPh}_3)_2$ (46) with CO	135
3.3.3 Reaction of $\text{Rh}(\eta^3\text{-C}_3\text{H}_5)(\text{PPh}_3)_2$ with acetonitrile-d <sub>3</sub>	136

## ***Table of contents***

3.3.4 Reaction of $\text{Rh}(\eta^3\text{-C}_3\text{H}_5)(\text{PPh}_3)_2$ with <i>parahydrogen</i> in acetonitrile- $\text{d}_3$ at 298K	137
3.3.5 Reaction of $\text{Rh}(\eta^3\text{-C}_3\text{H}_5)(\text{PPh}_3)_2$ with <i>parahydrogen</i> in acetonitrile- $\text{d}_3$ at 273 K	141
3.3.6 Discussion & Conclusion	143
<b>3.4 Control reaction of <math>\text{Rh}(\eta^3\text{-C}_3\text{H}_5)(\text{PPh}_3)_3</math> with CO (<math>^{12}\text{CO}</math> or <math>^{13}\text{CO}</math>)</b>	<b>144</b>
3.4.1 Background	144
3.4.2 Reaction of $\text{Rh}(\eta^3\text{-C}_3\text{H}_5)(\text{PPh}_3)_2$ (16) with CO at 203 K	145
3.4.3 Reaction of $\text{Rh}(\eta^3\text{-C}_3\text{H}_5)(\text{PPh}_3)_2$ with CO at 233 K	150
<b>3.5 Reaction of <math>\text{Rh}(\eta^3\text{-C}_3\text{H}_5)(\text{PPh}_3)_2</math> with CO and <math>\text{H}_2</math> in toluene-<math>\text{d}_8</math></b>	<b>152</b>
<b>3.6 Conclusion</b>	<b>152</b>
<b>CHAPTER 4 NMR STUDY ON PALLADIUM CATALYSED CARBONYLATION MECHANISM</b>	<b>154</b>
<b>4.1: Results &amp; Introduction</b>	<b>155</b>
4.1.1 Results	155
4.1.2 Synthesis and characterization of the catalysts and expected product	156
4.1.2.1 Synthesis of catalysts	156
4.1.2.2 Structures of catalysts	157
4.1.2.3 Synthesis of the carbonylation product 44 and its NMR characterization	157
<b>4.2 Control reactions for 12a</b>	<b>160</b>
4.2.1 Reaction of 12a and <i>parahydrogen</i>	160
4.2.1.1 Background	161
4.2.1.2 Re-examination of the reaction of 12a and hydrogen	162
4.2.2 Reaction of 12a with CO	163
4.2.2.1 Background	163
4.2.2.2 Re-examination of the reaction of 12a and CO	164
4.2.3 Reaction of 12a, CO and $\text{H}_2$ in methanol- $\text{d}_4$	164
4.2.3.1 Background	164
4.2.3.2 Re-examination of the reaction of 12a, CO and $\text{H}_2$	166
4.2.4 Reaction of 12a with diphenyl acetylene	166
4.2.5 Reaction of 12a with diphenyl acetylene and CO in methanol- $\text{d}_4$	166
4.2.6 Short conclusion	166
<b>4.3 Diphenyl acetylene carbonylation catalysed by 12a</b>	<b>166</b>
4.3.1 Introduction	166



## List of contents

4.3.1.1 Reaction and study methods	166
4.3.1.2 NMR parameters	167
4.3.2 NMR study in methanol	167
4.3.2.1 Overview	167
4.3.2.2 Detection of species that does not contain CO	168
4.3.2.3 Detection of the product: <i>cis</i> -PhCH=CPhCOOCD <sub>3</sub> (44)	176
4.3.2.4 Detection of CO containing intermediates	178
4.3.2.5 Detection of species of low-intensity	178
4.3.2.6 Study with NaOTf: Detection of Pd[(BCOPE)(CPh=CHPh)(OTf) (40a-4)	183
4.3.2.7 Reaction of 12a, diphenyl acetylene with CO and <i>parahydrogen</i> in ethanol-d <sub>6</sub>	184
4.3.2.8 Short conclusion	185
4.3.3 NMR studies of 12a catalyzed carbonylation in dichloromethane-d <sub>2</sub>	185
4.3.3.1 Control reaction	185
4.3.3.2 Overview of reaction	186
4.3.3.3 Detection of intermediates	187
4.3.3.4 Reaction of (12a), diphenyl acetylene, with CO and H <sub>2</sub> in tetrachloroethane-d <sub>2</sub> at 343K	189
4.3.3.5 Kinetic study	190
4.3.4 Impact of other reagents	190
4.3.4.1 Methanol	191
4.3.4.2 Water	191
4.3.4.3 NaCl	191
4.3.5 Short conclusion	192
<b>4.4 Diphenylacetylene carbonylation catalysed by 12b</b>	<b>192</b>
4.4.1 Diphenylacetylene carbonylation catalysed by [Pd( <sup>t</sup> BuCOPE)(OH <sub>2</sub> ) <sub>2</sub> ](OTf) <sub>2</sub> (12b) in methanol-d <sub>4</sub>	192
4.4.2 The reaction of 12b diphenylacetylene, with CO and <i>parahydrogen</i> in dichloromethane-d <sub>2</sub>	196
<b>4.5 Studies using other substrates</b>	<b>198</b>
4.5.1 Carbonylation of <i>cis</i> -stilbene catalysed by 12a	199
4.5.2 Carbonylation of styrene catalysed by 12a and 12b	199
4.5.2.1 The reaction of 12a and styrene in methanol-d <sub>4</sub>	199
4.5.2.2 The reaction of 12a, styrene and CO in methanol-d <sub>4</sub>	199
4.5.2.3 The reaction of 12a, styrene, with CO and <i>parahydrogen</i> in methanol-d <sub>4</sub>	199
4.5.2.4 Reaction of 12b, styrene and CO in methanol-d <sub>4</sub>	202
4.5.3 Carbonylation of phenyl acetylene	203
4.5.3.1 Reaction of Phenyl acetylene and 12a in methanol-d <sub>4</sub>	204
4.5.3.2 Reaction of 1a, phenyl acetylene and CO/ <i>p</i> -H <sub>2</sub> in dichloromethane-d <sub>2</sub>	204

## *Table of contents*

<b>4.6 Discussion &amp; Conclusion</b>	<b>204</b>
4.6.1 Discussion	204
4.6.2 Overall mechanism of diphenyl acetylene carbonylation	210
<b>CHAPTER 5 NMR STUDY ON DIPHENYL ACETYLENE HYDROGENATION USING MONOPHOSPHINE SUPPORTED PALLADIUM CATALYST</b>	<b>211</b>
<b>5.1 Results</b>	<b>212</b>
<b>5.2 Synthesis and NMR characterization of Pd(PMePh<sub>2</sub>)<sub>2</sub>(OTf)<sub>2</sub> (45)</b>	<b>213</b>
<b>5.3 Control reactions</b>	<b>214</b>
5.3.1 Reaction of Pd(PMePh <sub>2</sub> ) <sub>2</sub> (OTf) <sub>2</sub> (45) with H <sub>2</sub>	214
5.3.2 Reaction of 45 and diphenyl acetylene	223
<b>5.4 Study on Pd(PMePh<sub>2</sub>)<sub>2</sub>(OTf)<sub>2</sub> (45) catalyzed diphenyl acetylene hydrogenation</b>	<b>224</b>
5.4.1 NMR studies	224
5.4.1.1 Detection of [Pd(PMePh <sub>2</sub> ) <sub>2</sub> (CHPh-CH <sub>2</sub> Ph)](OTf) (82)	224
5.4.1.2 Detection of compound 83	226
5.4.1.3 Detection of compound 84	228
5.4.2 ESI-MS investigation	230
<b>5.5 Discussion and Conclusion</b>	<b>231</b>
<b>CHAPTER 6 EXPERIMENTAL</b>	<b>232</b>
<b>6.1 General Conditions</b>	<b>233</b>
6.1.1 General Conditions	233
<b>6.2 Synthesis for chapter 2</b>	<b>233</b>
6.2.1 Synthesis of IrCl(CO)(PMe <sub>3</sub> ) <sub>2</sub> (12a)	233
<b>6.3 Synthesis for Chapter 3</b>	<b>234</b>
<b>6.4 Synthesis for Chapter 4 and 5</b>	<b>234</b>
6.4.1 Synthesis of complexes	234
6.4.1.1 Reagents	234
6.4.1.2 Synthesis for Chapter 4 and 5	235
6.4.2 NMR sample preparation	235

<b>APPENDICES</b>	<b>236</b>
Appendix 1: Calculation of the activation parameters of 15a-15e	236
Appendix 2: The crystallographic data for 16	239
<b>LIST OF ABBREVIATIONS</b>	<b>252</b>
<b>REFERENCES</b>	<b>254</b>
<b>STRUCTURE OF COMPLEXES</b>	<b>263</b>

## List of Figures

Figure 1: Distribution of the hydroformylation products .....	34
Figure 2: Structure of UC-44; the combination of UC-44 and rhodium proved to be the most active and selective hydroformylation catalyst. ....	40
Figure 3: High performance bisphosphine ligands for hydroformylation .....	41
Figure 4: Active species in $\text{HRh}(\text{CO})(\text{PPh}_3)_3$ catalyzed low-pressure hydroformylation.....	44
Figure 5: Illustration of Tolman angle, where the P-M bond length is averagely 2.24 Å.....	46
Figure 6: Types of substrates for hydroformylation .....	47
Figure 7: Structure of $\text{Rh}(\text{alkyl})(\text{CO})_3$ isomers, the key intermediates in unmodified rhodium precursor catalyzed hydroformylation .....	48
Figure 8: Structure of palladium catalysts for carbonylation.....	50
Figure 9: Structure of monohydride species when $[(\text{BCOPE})\text{Pd}(\text{CH}_3\text{OH})_2](\text{OTf})_2$ (12a) or $[(\text{tBuCOPE})\text{Pd}(\text{H}_2\text{O})_2](\text{OTf})_2$ (12b) catalyze the hydrogenation of diphenyl acetylene .....	53
Figure 10: Structure of palladium vinyl hydride species that are detected in $(\text{PEt}_3)\text{Pd}(\text{OTf})_2$ catalyzed diphenyl acetylene hydrogenation .....	54
Figure 11: The molar rotation energy of hydrogen on temperature.....	57
Figure 12: Left: A simple model for generating parahydrogen. Right: Schematic of the parahydrogen rig used at York .....	58
Figure 13: (a): A normal NMR experiment on a $\text{MH}_2$ moiety without hyperpolarisation. (b): An NMR experiment on a $\text{MH}_2$ moiety formed after reacting with the parahydrogen.....	59
Figure 14: The 2D $^1\text{H}$ - $^1\text{H}$ COSY pulse sequence .....	60
Figure 15: The 2D HMQC sequence.....	60
Figure 16: The NOESY sequence.....	61
Figure 17: The OPSY program a): $^1\text{H}$ ; b): 2D $^1\text{H}$ - $^1\text{H}$ COSY .....	62
Figure 18: The $^1\text{H}$ NMR spectrum recorded in acetone- $\text{d}_6$ shows virtual coupling, in contrast of that in $\text{CDCl}_3\text{-d}_1$ .....	62
Figure 19: The $^1\text{H}$ NMR spectra showing the formation of $\text{cis-trans-Ir}(\text{H})_2\text{Cl}(\text{CO})(\text{PPh}_3)_2$ by reacting $\text{IrCl}(\text{CO})(\text{PPh}_3)_2$ with parahydrogen.....	64
Figure 20: Comparison of the thermal hydride signals shows an enhancement of 2000 for $\text{cis-trans-Ir}(\text{H})_2\text{Cl}(\text{CO})(\text{PPh}_3)_2$ .....	64
Figure 21: A $^{31}\text{P}$ NMR spectrum of $\text{cis-trans-Ir}(\text{H})_2\text{Cl}(\text{CO})(\text{PPh}_3)_2$ , an enhancement factor of 8 was estimated for this signal .....	64
Figure 22: Intermediates that were detected for the hydrogenation of alkenes using $\text{Rh}(\text{Cl})(\text{PPh}_3)_3$ catalyst.....	66
Figure 23: The hapticity of the allyl ligand, the $\eta^3$ form and the $\eta^1$ form.....	67
Figure 24: Structures of 15a-15e .....	69
Figure 25: Structure of 16 .....	70

Figure 26: Possible reaction intermediates that could be detected during the hydrogenation of the allyl ligand in compounds 15a-15e, according to the routes described in the text .....	72
Figure 27: Intermediates that are detected during the [(BCOPE)Pd(OH <sub>2</sub> ) <sub>2</sub> ](OTf) <sub>2</sub> catalysed hydrogenation of diphenyl acetylene .....	75
Figure 28: Structure of carbonylation catalysts in my research .....	76
Figure 29: Structure of monohydride species in [(BCOPE)Pd(OH <sub>2</sub> ) <sub>2</sub> ](OTf) <sub>2</sub> catalyzed diphenyl acetylene carbonylation .....	76
Figure 30: Structure of vinyl species in 12a catalyzed diphenyl acetylene carbonylation .....	77
Figure 31: Intermediates that were detected by PHIP in (PEt <sub>3</sub> ) <sub>2</sub> Pd(OTf) <sub>2</sub> catalysed diphenyl acetylene hydrogenation .....	79
Figure 32: Structure of compound 45 .....	79
Figure 33: (a): A <sup>31</sup> P NMR spectrum of IrCl(CO)(PMe <sub>3</sub> ) <sub>2</sub> , the starting material; (b): an in-situ <sup>31</sup> P NMR spectrum of the solution produced after adding allyl magnesium bromide to IrCl(CO)(PMe <sub>3</sub> ) <sub>2</sub> for 2 hours; this suggests that the conversion of IrCl(CO)(PMe <sub>3</sub> ) <sub>2</sub> to 15a has occurred .....	82
Figure 34: Structure of 15a .....	83
Figure 35: Region of the 2D <sup>1</sup> H- <sup>1</sup> H COSY dataset used to reveal the inequivalence of five protons for the allyl group in 15a at 203 K.....	84
Figure 36 (a): 2D <sup>1</sup> H- <sup>13</sup> C HMQC spectrum that correlates proton and carbon signals as indicated; (b): cross peak expansion showing the correlation of the <sup>1</sup> H resonance at δ 4.83 and the <sup>13</sup> C centre at δ 55.8 thereby revealing <sup>31</sup> P splittings.....	84
Figure 37: The <sup>31</sup> P NMR spectra of 15a at 203 K and 298 K .....	85
Figure 38: Hydride region of (a) <sup>1</sup> H{ <sup>31</sup> P} and (b) <sup>1</sup> H NMR spectra used to confirm the formation of Ir(η <sup>3</sup> -C <sub>3</sub> H <sub>5</sub> )(H <sub>2</sub> )(CO)(PMe <sub>3</sub> ) (18aA and 18aB) when 15a reacts with parahydrogen at 233 K.....	87
Figure 39: 2D <sup>1</sup> H- <sup>31</sup> P HMQC dataset that links the hydride signals due to 18aA and 18aB to the corresponding <sup>31</sup> P centres; where the blue cross peak suggests cis coupling while the red peak results when the same experiment is re-run for a trans coupling. ....	88
Figure 40: The (a) <sup>1</sup> H and (b) <sup>1</sup> H{ <sup>31</sup> P} NMR spectra that suggests the formation of 18aA, 18aB and 19aB at 253 K.....	89
Figure 41: The orientation of the hydride and phosphine ligands on the iridium centre, suggested by their coupling pattern (other ligands omitted).....	89
Figure 42: NOe NMR spectra showing magnetization transfer to a <sup>1</sup> H NMR signal at δ 1.26 due to the cis PMe <sub>3</sub> ligands when the hydride signal at δ -10.12 was selectively irradiated .....	90
Figure 43: Structure of 19aB.....	90
Figure 44: Structure of 23aA.....	91
Figure 45: Structures of 24aA and 24aB.....	92
Figure 46: Expansion of the 2D <sup>1</sup> H- <sup>31</sup> P HMQC dataset that correlates of hydride signals of 24aA and 24aB with corresponding <sup>31</sup> P centres .....	92

## List of Figures

Figure 47: a): The $^{31}\text{P}$ NMR spectrum that monitored the control reaction of 15a and CO; b): the $^{31}\text{P}$ NMR spectrum of 28a when $^{13}\text{C}$ was used, the $^{13}\text{C}$ - $^{31}\text{P}$ coupling in 28a suggests the inequivalence of the phosphine ligands and the equivalence of two CO ligands. ....	96
Figure 48: A 2D $^1\text{H}$ - $^1\text{H}$ COSY spectrum at 203 K revealed formation of several new species after the reaction of 15a with CO at 298 K: Red: iridium allyl species; blue: iridium acyl species; Purple: decomposition products; Green, isomerization products .....	98
Figure 49: Expansion of 2D $^1\text{H}$ - $^{31}\text{P}$ HMQC dataset that shows the correlation between the $^1\text{H}$ NMR signals at $\delta$ -9.61 and $\delta$ 2.87 to the $^{31}\text{P}$ centre at $\delta$ -58.9 .....	101
Figure 50: Expansion of the 2D $^1\text{H}$ - $^{13}\text{C}$ HMQC dataset that confirms the trans orientation of CO ligand and the hydride ligands for the new product .....	102
Figure 51: (a) $^1\text{H}$ and (b) $^1\text{H}\{^{31}\text{P}\}$ NMR spectra showing the hydride region. These spectra indicate the formation of several new species when 15a reacts with a 1:2 mixture of CO and $\text{H}_2$ at 303K. ...	103
Figure 52: Expansion of the 2D $^1\text{H}$ - $^{31}\text{P}$ HMQC spectrum that differentiate the overlapped signals at $\delta$ -9.60 and $\delta$ -9.61 in the second dimension. ....	104
Figure 53: Structure of 39aA .....	106
Figure 54: Multinuclear NMR data of 39aA collected at 298 K .....	108
Figure 55: Structure of 15b .....	109
Figure 56: Intermediates and organometallic products that are detected in reaction of $\text{Ir}(\eta^3\text{-C}_3\text{H}_5)(\text{CO})(\text{PMe}_2\text{Ph})_2$ (15b) with parahydrogen at 298 K .....	112
Figure 57: The structure of 33bA and 33bB .....	115
Figure 58: The line shape simulation of the $^{31}\text{P}$ NMR spectra for 15a. a) 203 K; b) 223K; 1): experimental spectrum; 2): calculated spectrum .....	120
Figure 59: The Eyring plot for fluxional process of 15a .....	121
Figure 60: The in-situ $^{31}\text{P}$ NMR spectrum of 16 that was recorded in diethyl ether at 298 K. A drop of benzene- $d_6$ was added to this sample for shim and lock calibration .....	124
Figure 61: The structure of an $\eta^3$ -allyl ligand .....	125
Figure 62: Part of a 2D $^1\text{H}$ - $^1\text{H}$ COSY NMR spectrum that correlates the proton signals at $\delta$ 5.23, $\delta$ 3.05, and $\delta$ 2.53 due to the $\eta^3$ -allyl group in 16 .....	125
Figure 63: Expansion taken from a $^1\text{H}$ - $^{31}\text{P}$ HMQC NMR spectrum that shows the correlations between the $^{31}\text{P}$ signal at $\delta$ 41.9 and the proton signals at $\delta$ 3.05 (a), and $\delta$ 2.53 (b) due to 16 .....	127
Figure 64: Plot of a $^1\text{H}$ - $^{13}\text{C}$ HMQC NMR experiment which correlates the proton signals at $\delta$ 3.05 and $\delta$ 2.53 with a $^{13}\text{C}$ NMR signal at $\delta$ 58.55, with $J_{\text{PC}} = J_{\text{RhC}} = 10$ Hz .....	127
Figure 65: Molecular structure of 16: ORTEP view showing 51.3% and 48.7% probability ellipsoids for 16A and 16B. ....	129
Figure 66: (a) and (b): Region of the 1D NMR spectra showing the hydride region that was recorded when 16 reacted with parahydrogen in toluene- $d_8$ ; (a): $^1\text{H}$ ; (b): $^1\text{H}\{^{31}\text{P}\}$ ; (c): Spots taken from the 2D $^1\text{H}$ - $^1\text{H}$ COSY spectrum that links the two hydride resonances $\delta$ -8.30 and $\delta$ -15.18 .....	132

Figure 67: Expansions taken from a $^1\text{H}$ - $^{31}\text{P}$ HMQC NMR spectrum showing the correlation of the hydride signals at $\delta$ -8.30 and $\delta$ -15.18 with two $^{31}\text{P}$ centres at $\delta$ 54.41 and $\delta$ 49.22. ....	133
Figure 68: Structure of $\text{Rh}(\text{H})_2(\text{PPh}_3)_2(\mu\text{-H})_2\text{Rh}(\text{PPh}_3)_2$ (46) and a similar complex, $\text{Rh}(\text{H})_2[\text{P}(\text{NMe}_2)_3]_2(\mu\text{-H})_2\text{Rh}[\text{P}(\text{NMe}_2)_3]_2$ .....	133
Figure 69: The conformation of isomers of 46 .....	134
Figure 70: Structure of $\text{Rh}(\text{H})_2(\text{PPh}_3)_2(\mu\text{-H})_2\text{Rh}(\text{PPh}_3)_2$ (46) and related complexes.....	134
Figure 71: Structure of $\text{RhH}(\text{CO})(\text{PPh}_3)_3$ (1) and $\text{RhH}(\text{CO})_2(\text{PPh}_3)_2$ (2ee) .....	136
Figure 72: Structure of propene .....	138
Figure 73: $^1\text{H}\{^{31}\text{P}\}$ NMR spectrum taken from the reaction of $\text{Rh}(\eta^3\text{-C}_3\text{H}_5)(\text{PPh}_3)_2$ and parahydrogen at 298 K, where polarized signals due to propene, propane and a rhodium alkyl species are observed.....	138
Figure 74: Structures of 49A and 49B .....	139
Figure 75: The $^1\text{H}$ - $^{31}\text{P}$ NMR spectrum that links the hydrides signals at $\delta$ -16.96 and $\delta$ -17.14 with their $^{31}\text{P}$ neighbours. ....	139
Figure 76: Structure of $\text{Rh}(\text{H})_2(\text{PPh}_3)_2(\mu\text{-Br})_2\text{Rh}(\text{PPh}_3)_3$ (52) .....	140
Figure 77: Structure of 50, 51 .....	140
Figure 78: (a) $^1\text{H}$ spectrum taken from the hydride region when 11 reacts with parahydrogen at 263K. (b) The $^1\text{H}\{^{31}\text{P}\}$ spectrum. (c) Expansion of the COSY spectrum that correlates the $^1\text{H}$ signals at $\delta$ -10.47 and $\delta$ -16.94. ....	142
Figure 79: COSY experiments that correlates three proton signals at $\delta$ 4.84, $\delta$ 2.91, and $\delta$ 1.723 due to the $\eta^3$ -allyl group in $\text{Rh}(\eta^3\text{-C}_3\text{H}_5)(\text{CO})(\text{PPh}_3)_2$ (14).....	145
Figure 80: 1D $^{31}\text{P}$ NMR spectra of $\text{Rh}(\eta^3\text{-C}_3\text{H}_5)(\text{CO})(\text{PPh}_3)_2$ at 188 K, 203 K, and 233 K revealing its high fluxionality. (a): at 233 K using $^{12}\text{CO}$ ; (b): at 188 K using $^{12}\text{CO}$ ; (c): at 203 K using $^{13}\text{CO}$ , D and E show expansion of the signal with/without $^{13}\text{CO}$ .....	146
Figure 81: Two conformations of 14 in the toluene solution .....	146
Figure 82: The $^1\text{H}$ - $^{13}\text{C}$ HMQC NMR spectrum that correlated three protons signals at $\delta$ 4.84, $\delta$ 2.82 and $\delta$ 1.77 with corresponding carbon resonances.....	147
Figure 83: The structure of $\text{Rh}(\eta^3\text{-C}_3\text{H}_5)(\text{CO})_2(\text{PPh}_3)$ (62) .....	149
Figure 84: The $^1\text{H}$ - $^1\text{H}$ COSY spectrum indicates the formation of two $\eta^1$ -allyl contained products.....	150
Figure 85: Part of the $^1\text{H}$ and $^1\text{H}\{^{31}\text{P}\}$ NMR spectra of 62A and 62B.....	151
Figure 86: Structure of 62A and 62B.....	151
Figure 87: Structures of 12a and 12b.....	155
Figure 88: A $^{31}\text{P}$ NMR spectrum of 12a .....	157
Figure 89: NOESY experiments reveal several spatially close protons in 45.....	158
Figure 90: Reaction of $[(\text{BCOPE})\text{Pd}(\text{H}_2\text{O})_2](\text{OTf})_2$ with hydrogen in acidic solution gives 67a .....	161
Figure 91: Structures of the monohydride species (13a) that are reported in this thesis.....	162

## List of Figures

Figure 92: The hydride region of $^1\text{H}$ (a, vertical scale: 32, 128 scans) and $^1\text{H}\{^{31}\text{P}\}$ (b: vertical scale: 2; 4,000 scans) NMR spectra recorded to monitor the reaction of 12a with parahydrogen in tetrachloroethane- $d_2$ at 323 K .....	162
Figure 93: Structure of $[\text{Pd}_2(\text{BCOPE})_2(\text{CO})_2](\text{OTf})_2$ (69a).....	163
Figure 94: Structure of 42a .....	164
Figure 95: The $^1\text{H}\{^{31}\text{P}\}$ NMR spectrum recorded during the reaction of 12a, diphenyl acetylene- $d_{10}$ , CO and parahydrogen, suggesting the formation of a range of reaction intermediates and products at 323 K. ....	168
Figure 96: The correlation of the PHIP enhanced signals at $\delta$ 5.02, $\delta$ 3.10 and $\delta$ 2.93 due to 41a is revealed by 2D $^1\text{H}$ - $^1\text{H}$ COSY NMR. ....	169
Figure 97: The integration of a $^1\text{H}$ OPSY NMR spectrum shows the level of polarization that sits in the 'CHPh-CH <sub>2</sub> Ph' sites in 41a .....	169
Figure 98: Correlation of $^1\text{H}$ and $^{31}\text{P}$ signals at $\delta$ 32.2 and $\delta$ 42.1 using $\pi/4$ 2D $^1\text{H}$ - $^{31}\text{P}$ HMQC experiments. ....	170
Figure 99: Structures of type 40a complexes .....	172
Figure 100: (a): A $\pi/4$ experiment taken from the reaction of 1a, diphenyl acetylene and CO/ $p$ -H <sub>2</sub> shows the signals at $\delta$ -8.56 and $\delta$ -8.59 have both in-phase and antiphase component. ....	173
Figure 101: Possible structures that fit the hydride signal at $\delta$ -8.60.....	173
Figure 102: Correlation of hydride signals at $\delta$ -8.56 and $\delta$ -8.59 due to 12a with $^{31}\text{P}$ resonances.....	174
Figure 103: Structure of 44. ....	176
Figure 104: $^1\text{H}$ NMR spectra showing the region that contains the diagnostic signal for 44 when $^{12}\text{CO}$ (a) and $^{13}\text{CO}$ (b) were used. (c): the correlation of this proton signal to the carbon centre at $\delta$ 168.1 is recorded via a 2D measurement.....	176
Figure 105: Expansion of the $^1\text{H}$ - $^{13}\text{C}$ HMQC dataset showing the correlation of the proton signal at $\delta$ 7.84 to the corresponding carbon centres at (a) $\delta$ 132.6 and (b) $\delta$ 140.5. ....	177
Figure 106: $\alpha$ -phenyl-cinnamic ester derivatives detected in this study.....	177
Figure 107: Structure of 42a .....	178
Figure 108: $^1\text{H}$ NMR spectra shows the dependence of [Pd]/CO ratio for the $^1\text{H}$ NMR signal at $\delta$ 6.90 .....	179
Figure 109: Structure of 40a-4 .....	180
Figure 110: Region of the (a) $^1\text{H}\{^{31}\text{P}\}$ (b) $^1\text{H}$ and NMR spectra taken from the reaction of 12a, diphenyl acetylene and CO/ $p$ -H <sub>2</sub> . ....	181
Figure 111: Possible structure for 71a.....	181
Figure 112: Expansion of the $^1\text{H}$ NMR signal at $\delta$ 5.08 under different conditions. (a): using normal CO at 313 K, (b): $^1\text{H}\{^{31}\text{P}\}$ $^{13}\text{CO}$ at 308 K. $\text{C}^1\text{H}$ , $^{13}\text{CO}$ at 308 K.....	182
Figure 113: Structure of 72a .....	182
Figure 114: $^1\text{H}$ and $^1\text{H}\{^{31}\text{P}\}$ spectrum of additional alkyl complexes 42a-3 and 41a-3.....	183



Figure 115: Structure of 42a and 41a-3.....	183
Figure 116: Structure of [Pd(BCOPE)(CPh=CHPh)(CH <sub>3</sub> CH <sub>2</sub> OD)](OTf) (40-5).....	184
Figure 117: <sup>1</sup> H NMR spectrum shows selective hydrogen addition to the 'CH <sub>2</sub> Ph' site in 41a when the reaction was undertaken in dichloromethane-d <sub>2</sub> at 308 K .....	186
Figure 118: The <sup>1</sup> H and <sup>1</sup> H { <sup>31</sup> P } spectra taken from the reaction of 1a, diphenyl acetylene and CO/p-H <sub>2</sub> in dichloromethane-d <sub>2</sub> at 313 K revealed the formation of an acyl species 73a .....	187
Figure 119: Structure of 73a .....	188
Figure 120: The <sup>1</sup> H and <sup>1</sup> H { <sup>31</sup> P } NMR spectra showing the formation of a monohydride species 13a-3 .....	189
Figure 121: Structure of 13a-3 .....	189
Figure 122: (a): <sup>1</sup> H NMR spectrum upon adding 5 μl H <sub>2</sub> O to the same sample. (b): <sup>1</sup> H NMR spectrum taken from the reaction of 12a, diphenyl acetylene with CO/H <sub>2</sub> .....	191
Figure 123: Region of the organic region of a <sup>1</sup> H NMR spectrum that was recorded during the reaction of 12b, diphenyl acetylene and CO/p-H <sub>2</sub> at 333 K .....	194
Figure 124: Structure of 71bA and 71bB.....	194
Figure 125: Structures of 43bA and 43bB .....	195
Figure 126: Structure of 73bA and 73bB.....	196
Figure 127: (a): <sup>1</sup> H NMR spectra recorded at 323 K when 12b reacts with diphenylacetylene, CO and parahydrogen in dichloromethane-d <sub>2</sub> which reveal the formation of the monohydride complexes 13b-3; (b): expansion of a <sup>1</sup> H- <sup>31</sup> P HMQC dataset showing correlations between these hydride signal of 13bA-3 and the resonances of its two <sup>31</sup> P coupling partners. ....	198
Figure 128: Structure of 75a .....	199
Figure 129: (a): A <sup>1</sup> H- <sup>1</sup> H COSY dataset revealed the correlation of <sup>1</sup> H NMR signals for 75a. (b): Expansions of the <sup>1</sup> H and <sup>1</sup> H { <sup>31</sup> P } NMR spectra as shown to illustrate the δ 1.44 and δ 4.84 signals due to 75a .....	200
Figure 130: A <sup>1</sup> H- <sup>31</sup> P HMQC dataset showing correlation between the signal at δ 1.43 and two <sup>31</sup> P centres which resonate at δ 31.6 and δ 42.7 in 75a; the signal at δ 4.84 connects with just one <sup>31</sup> P centre at δ 31.6 .....	200
Figure 131: Structure of 75bA .....	202
Figure 132: (a): The COSY dataset revealed the evidence of CH <sub>3</sub> -CH-Pd group in 75bA. (b): Expansion of the <sup>1</sup> H- <sup>31</sup> P HMQC dataset that correlates the CH <sub>3</sub> -CH group to two <sup>31</sup> P centres.....	203
Figure 133: Region of the <sup>1</sup> H NMR spectrum when 12a catalyses the reaction of phenyl acetylene and parahydrogen, indicating the formation of 75a .....	204
Figure 134: The proposed cationic and neutral mechanism for 12a catalysed hydrogenation of diphenyl acetylene 46.....	205
Figure 135: The formation of palladium hydride clusters from complexes 13 .....	206

## List of Figures

Figure 136: The structures of 40a and 75a, the colour labelling stands for the level of polarization. Blue: weak or moderate;.....	209
Figure 137: Structures of the intermediates and products that are detected when 45 reacts hydrogen .....	212
Figure 138: Additional organometallic products detected in 45 catalyzed diphenyl acetylene hydrogenation.....	213
Figure 139: The $^{31}\text{P}$ NMR spectrum of $\text{Pd}(\text{PMePh}_2)_2(\text{OTf})_2$ (45) (298 K, in $\text{CD}_2\text{Cl}_2$ ) .....	214
Figure 140: Structures of $[\text{PdH}(\text{PMe}_2\text{Ph})_3](\text{OTf})$ (77) and $\text{PdH}(\text{PPh}_2\text{Me})_2(\text{OTf})$ (78) .....	215
Figure 141: Selective regions of (a): $^1\text{H}\{^{31}\text{P}\}$ and (b): $^1\text{H}$ NMR spectra that illustrate the formation of 77 and 78 when 45 reacts with hydrogen.....	215
Figure 142: Selected regions of the NMR spectra used to indicate the formation of 79. (a): $^1\text{H}$ and (b) $^1\text{H}\{^{31}\text{P}\}$ .....	217
Figure 143: 2D $^1\text{H}$ - $^1\text{H}$ COSY dataset that connects the $^1\text{H}$ NMR signals for 79A and 79B .....	218
Figure 144: Region of the $^1\text{H}$ NMR spectrum showing the formation of several hydride contained species when 45 reacts with parahydrogen.....	221
Figure 145: Possible structure for 80.....	222
Figure 146: The $^1\text{H}$ NMR spectra at 248 K and 298 K suggested the dynamic behaviour for 81 .....	222
Figure 147: The structure of 81 .....	222
Figure 148: Expansion of the 2D $^1\text{H}$ - $^1\text{H}$ OPSY-COSY NMR spectrum that links the polarized signals at $\delta$ 2.95, $\delta$ 2.57 and $\delta$ 3.90, with internal $^1\text{D}$ OPSY spectra and external $^1\text{D}$ $\pi/4$ $^1\text{H}$ NMR spectrum as horizontal and vertical projections respectively. ....	225
Figure 149: Structure of $[\text{Pd}(\text{PMePh}_2)_2(\text{CHPh-CH}_2\text{Ph})](\text{OTf})$ (82).....	225
Figure 150: The 2D $^1\text{H}$ - $^{31}\text{P}$ HMQC dataset that correlates the $^1\text{H}$ NMR signals at $\delta$ 2.95, $\delta$ 2.57 and $\delta$ 3.90 to two $^{31}\text{P}$ centres at $\delta$ 2.4 and $\delta$ 14.3 .....	225
Figure 151: Structure of new product 83 that is detected in the $\text{Pd}(\text{PMePh}_2)_2(\text{OTf})_2$ catalysed hydrogenation of diphenyl acetylene and its known $\text{PEt}_3$ analogue. ....	227
Figure 152: Region of the $^1\text{H}$ NMR spectrum and the coupling assignment for hydride resonance at $\delta$ - 7.34 due to 83 .....	227
Figure 153: Expansion of the 2D $^1\text{H}$ - $^1\text{H}$ COSY dataset showing the correlation between the $^1\text{H}$ NMR signals at $\delta$ 2.23, $\delta$ 2.84 and $\delta$ 3.62.....	228
Figure 154: Region of the $^1\text{H}$ NMR spectrum and coupling assignment for hydride resonance at $\delta$ - 10.10 due to 84 .....	229
Figure 155: Structure of 84 .....	229
Figure 156: Summary of structures of 82-84 .....	231

## List of Tables

Table 1: Features of homo- and heterogeneous catalysis.....	24
Table 2: Examples of homogeneous reactions catalyzed by transition metal complexes.....	25
Table 3: Industrial carbonylation reactions .....	26
Table 4: Features of hydroformylation and Reppe carbonylation.....	27
Table 5: The uses of n-butyraldehyde and 2-butyraldehyde.....	34
Table 6: The hydroformylation results of 1-hexene using Co <sub>2</sub> (CO) <sub>8</sub> /2PR <sub>3</sub> as the catalyst precursor. (160 °C, 70 atm. 1.2:1 H <sub>2</sub> /CO) <sup>71</sup> .....	37
Table 7: The composition of two-phase solvent systems for hydroformylation .....	41
Table 8: Electronic and steric parameters of PR <sub>3</sub> type ligands .....	46
Table 9: The hydroformylation selectivity to different substrates using unmodified rhodium catalyst	48
Table 10: Selected values of reaction rate constants and regioisomeric ratios in Rh <sub>4</sub> (CO) <sub>12</sub> catalysed styrene hydroformylation, Kb/Kn: the elimination rate of the branched(b)/linear(l) acyl complex .....	48
Table 11: The NMR pulse sequences used in parahydrogen related study .....	65
Table 12: Multinuclear NMR data for 15a (in toluene-d <sub>8</sub> ).....	86
Table 13: Multinuclear NMR data for 18aA and 18aB (233 K in toluene-d <sub>8</sub> ) .....	93
Table 14: Multinuclear NMR Data for 19aB (253 K in in toluene-d <sub>8</sub> ).....	94
Table 15: NMR Data for 23aA (283 K in toluene-d <sub>8</sub> ).....	94
Table 16: Multinuclear NMR data for 24aA and 24aB (298 K in toluene-d <sub>8</sub> ) .....	95
Table 17: Multinuclear NMR data for 28a (203 K in toluene-d <sub>8</sub> ) .....	97
Table 18: NMR data of η <sup>1</sup> -C <sub>3</sub> H <sub>5</sub> contained complexes that formed when 1a reacts with CO at 298 K....	99
Table 19: NMR data of CO insertion products that formed when 15a reacts with CO at 298 K.....	99
Table 20: NMR data of P-CH <sub>2</sub> -CH=CH <sub>2</sub> contained complexes that formed when 15a reacts with CO at 298 K.....	100
Table 21: Multinuclear NMR data for 33aA (283 K in toluene-d <sub>8</sub> ) .....	107
Table 22: Selected NMR data of 33eB (303K in toluene-d <sub>8</sub> ) .....	107
Table 23: Selected multinuclear NMR data of 19aA collected at 303K.....	108
Table 24: Multinuclear NMR data for 15b (203 K in toluene-d <sub>8</sub> ) .....	110
Table 25: Multinuclear NMR data for 18bA and 18bB (233K in toluene-d <sub>8</sub> ).....	111
Table 26: Multinuclear NMR Data for 19aB (253 K in toluene-d <sub>8</sub> ).....	112
Table 27: NMR Data for 23bA (298 K in toluene-d <sub>8</sub> ) .....	112
Table 28: Multinuclear NMR data of 24bA and 24bB.....	113
Table 29: Multinuclear NMR data for 28b (233 K in toluene-d <sub>8</sub> ) .....	114
Table 30: Multinuclear NMR data for 33bA (283 K in toluene-d <sub>8</sub> ).....	116
Table 31: Multinuclear NMR data for 33bB (303K in toluene-d <sub>8</sub> ).....	116
Table 32: Selected multinuclear NMR data for 39bA (298 K in toluene-d <sub>8</sub> ).....	118

## List of Tables

Table 33: Multinuclear NMR data for 39bB (298 K in toluene-d <sub>8</sub> ) .....	119
Table 34: The activation parameters for 15a-15e.....	121
Table 35: Multinuclear NMR data for 16 (298 K in toluene-d <sub>8</sub> ).....	128
Table 36: Selected bond lengths (Å) and angles (°) of 16A and 16B.....	130
Table 37: A comparison of the structural parameters for 16 and other known rhodium allyl species	131
Table 38: Multinuclear NMR data for 46 (273 K in toluene-d <sub>8</sub> ).....	135
Table 39: NMR data for 47 (273 K in toluene-d <sub>8</sub> ).....	137
Table 40: NMR data for the hydride species when 54 reacts with hydrogen.....	141
Table 41: Multinuclear NMR data for 14 (in toluene-d <sub>8</sub> ) .....	148
Table 42: Selected multinuclear NMR data for 61 (in toluene-d <sub>8</sub> ) .....	150
Table 43: Complexes formed when the reaction of Rh(η <sup>3</sup> -C <sub>3</sub> H <sub>5</sub> )(CO)(PPh <sub>3</sub> ) <sub>2</sub> with <sup>13</sup> CO was warmed to 233 K .....	152
Table 44: Multinuclear NMR data for α-phenyl-cinnamic acid (298 K in methanol-d <sub>4</sub> ).....	159
Table 45: Multinuclear NMR data for 45 (298 K methanol-d <sub>4</sub> ) .....	160
Table 46: Selected NMR data for 41a (308 K in methanol-d <sub>4</sub> ).....	171
Table 47: Multinuclear NMR data for 40a-1 (308 K in methanol-d <sub>4</sub> ).....	172
Table 48: Multinuclear NMR data for 70a (308 K in CD <sub>3</sub> OD).....	175
Table 49: Experimental conditions used when studying the CO dependence for 40a-4 .....	179
Table 50: The impact of the [Pd]/CO ratio on the intensity of the related species .....	180
Table 51: NMR data for 66 (308 K in ethanol-d <sub>1</sub> ).....	184
Table 52: NMR data for 73a (315 K in CD <sub>2</sub> Cl <sub>2</sub> ).....	188
Table 53: Experiments used to study the impact of methanol .....	190
Table 54: Selected multinuclear NMR data for 41b (308 K CD <sub>2</sub> Cl <sub>2</sub> ) .....	193
Table 55: Intermediates detected in 12b catalysed diphenyl acetylene carbonylation and their NMR properties .....	195
Table 56: Multinuclear NMR data for 73b isomers (315 K in toluene-d <sub>8</sub> ) .....	197
Table 57: Multinuclear NMR data for 13b-3 isomers (315 K in CD <sub>2</sub> Cl <sub>2</sub> ) .....	198
Table 58: Multinuclear NMR data for 75a (298 K in CD <sub>3</sub> OD).....	202
Table 59: Selective multinuclear NMR data for 75bA.....	203
Table 60: Multinuclear NMR data for 45 (298 K in CD <sub>2</sub> Cl <sub>2</sub> ) .....	214
Table 61: Selective NMR data for 77 (298 K in CD <sub>2</sub> Cl <sub>2</sub> ).....	216
Table 62: Selective NMR data for 78 (248 K in CD <sub>2</sub> Cl <sub>2</sub> ).....	217
Table 63: Multinuclear NMR data of 79A and 79B .....	219
Table 64: NMR data for 78 (298 K in CD <sub>2</sub> Cl <sub>2</sub> ) .....	223
Table 65: NMR data for 79 (in CD <sub>2</sub> Cl <sub>2</sub> ) .....	223
Table 66: Multinuclear NMR data for 82 (308 K in CD <sub>3</sub> OD).....	226
Table 67: Multinuclear NMR data for 83 (315 K in CD <sub>2</sub> Cl <sub>2</sub> ) .....	230

## *List of Tables*

<b>Table 68: Selected multinuclear NMR data for 84 (313 K in CD<sub>2</sub>Cl<sub>2</sub>) .....</b>	<b>230</b>
<b>Table 69: Ligand exchange rate constants for 15a from 203 K to 293 K .....</b>	<b>236</b>
<b>Table 70: Eyring plot data for 15a .....</b>	<b>236</b>
<b>Table 71: The reaction rate and rate constants for 15b from 203 K to 293 K .....</b>	<b>237</b>
<b>Table 72: The reaction rate and rate constants for 15c from 203 K to 293 K.....</b>	<b>237</b>
<b>Table 73: The reaction rate and rate constants for 15d from 203 K to 293 K .....</b>	<b>238</b>

## *Acknowledgements*

### **Acknowledgements**

I am in great debt to my supervisor, Prof. Simon Duckett, for his inspiration and every support during this study. I am also grateful to my thesis adviser Prof. Richard Douthwaite for his discussions and suggestions. I would like to thank the departmental staff, Alice (graduate school), Adrian (XRD), Brian, Abbigail (glass workshop), Heather (NMR centre), Karl (mass spectrometry centre), Stephen, and Mike (stores) for their kind help.

Many thanks to the group members, Alex, Barbara, Beatriz, Chris, Fran, Iman, Jose, Kate, Kevin, Louise, Lyrelle, Majid, Marianna, Michael, Naser, Ralf, Richard (Green), Richard (John), Ryan, and Sarah, for their help on my research, thesis writing and everyday life. Special thanks to John, who is in collaboration with me in the study on palladium.

Thanks to Wild Fund (University of York) and China Scholarship Council for financial support.

Lastly, a big thanks to all my family members for everything they have done for me.

## **Declaration**

Herein I declare that all the result within this thesis is the original work of the author, unless it's specifically stated and referenced. It has not been submitted for any other degree.

Dexin Guan \_\_\_\_\_

## **Chapter 1 Introduction**

*1.1 Catalysis in industry*

*1.2 Mechanistic study on homogeneous catalysis*

*1.3 Hydroformylation*

*1.4 Reppe carbonylation*

*1.5 Parahydrogen and its NMR applications*

*1.6 Aim on Ir/Rh catalysed hydroformylation*

*1.7 Aim on Pd catalysed carbonylation*



## 1.1 Catalysis in industry

### 1.1.1 Catalysis and its importance

Catalysis is of paramount importance in chemistry, where it features in the chemical industry and the total synthesis of organic molecules. According to a recent report, catalysis is involved in the production of 90 % of the chemicals. Not surprisingly, the catalyst industry contributes more than 10 trillion US dollars to world GDP, and occupies 2 % of total chemistry related investments.<sup>1</sup> The use of catalysis not only makes many reactions more practicable but also improves their efficiency by reducing the activation barrier to reactions.

Catalysis contributes to the production of fundamental chemicals: iron catalysts for ammonia, vanadium oxide for sulphuric acid and transition metal catalysts for a wide range of chemicals and materials by functionalizing hydrocarbons, which are readily available from petroleum. Chemical feed stocks switched from coal to petroleum after the establishment of the OXO process, one of the largest and most important homogeneous catalytic processes.

Catalysis also offers potential for developing sustainable resources by reducing energy input and thereby moving us away from fossil fuel reliance. Photolysis of water produces molecular hydrogen and oxygen, which help to make better use of solar energy.<sup>2-4</sup> Reduction of CO<sub>2</sub> provides an alternative pathway to obtain CO, formaldehyde and methanol from biomass. The turnover frequency of this reaction has reached 100 per hour using N-heterocyclic carbene supported copper (I) catalysts.<sup>5-8</sup> The use of catalysts also leads to simple processing, better selectivity and environmental affinity. In one word, catalysis is the key discipline for sustainable development and will be very important for future world development.

Much has been done in this realm; however, more challenges remain for chemistry researchers: low turnover limits CH<sub>4</sub> activation applications and selectivity must be improved further in hydroformylation of internal alkenes. Photolysis of water suffers from low turnover value and hence less efficient use of solar energy.<sup>9</sup> There is a long way to go if we compare artificial chemistry processes with biocatalysts.

### 1.1.2 Homogenous and heterogeneous catalysis

There are two types of catalysis, homogeneous and heterogeneous, according to the media where the catalysis occurs. Homogeneous catalysis, by definition, refers to those reactions in which the reactants and catalyst exist in one phase; while heterogeneous catalysis refers to

## Chapter one

those reactions in which the reactants exist in two or more phases.<sup>10</sup> Table 1 summarizes the differences of homo- and heterogeneous catalysis

**Table 1: Features of homo- and heterogeneous catalysis**

	<b>Homogeneous</b>	<b>Heterogeneous</b>
Active site	Active sites on catalyst molecules	Hot spots on catalyst surface
Product separation	Hard (distillation)	Easy (filtration)
Selectivity	Choice of metal, ligands	Particle and pore size, character of catalytic site, element composition, type of support material, other external parameters.
Catalyst improvement	Geometric and electronic tuning	Very complicated

Homo- and heterogeneous catalysis are therefore distinct. In homogeneous catalysis, catalysts are dispersed at molecular level and all of the catalyst molecules are active; whereas only surface sites are accessible and active for the heterogeneous catalysts. The reactivity of homogeneous catalysts is determined mainly by metal and ligands. It can be improved by changing the electronic and steric properties of the ligands. The reactivity of heterogeneous catalysts is more determined by pore size, elemental composition, character of active sites, and the nature of the support. On this basis, homogeneous catalysis is preferred for mechanistic study. The history and chemistry of some important homogenous catalysis such as hydrogenation, hydroformylation and carbonylation reactions are detailed in the following section.

### 1.1.3 Homogenous catalysis and its applications

Homogeneous catalysis is a large family that includes traditional reactions such as ester hydrolysis, Diels-alder reactions, and transition metal catalyzed reactions. The earliest example of homogeneous catalysis dates back to a gaseous catalysis called the 'lead chamber process', where sulfur dioxide was oxidized to sulfur trioxide by  $\text{NO}_2$ .  $\text{NO}_2$  was recovered by oxidizing  $\text{NO}$  with air. Nowadays, transition metal catalyzed reactions are the core of chemistry due to the expanding of organometallic chemistry. Therefore the definition of homogeneous catalysis now narrows to transition metal compounds catalyzed reactions.

The first example of transition metal catalyzed homogeneous reactions is titanium catalyzed olefin polymerization (Ziegler-Natta catalyst, Nobel Prize in 1963). Examples of other important homogeneous catalysis are summarized in Table 2. As seen in Table 2, the choice of ligand is important: as combination of the same metal and different ligands give very different products from the same starting material.

**Table 2: Examples of homogeneous reactions catalyzed by transition metal complexes**

Technology	Catalysts	Products	Applications
Hydrogenation and asymmetric hydrogenation	Ru, Rh etc.	Variable	
Hydroformylation of olefins	Rh/PPh <sub>3</sub>	Alcohols	Paints, plasticizers
Hydrocyanation of butadiene	Ni, Pd	Nitriles	Nylons
Carbonylation of methanol	[RhI <sub>2</sub> (CO) <sub>2</sub> ] <sup>-</sup>	Acetic acid	Plastics, paints, coatings
Olefin metathesis	Ru etc.	A wide range of molecules	Renewable, plastics, total synthesis, etc.
Oligomerization of olefins	Ti, etc.	Long chain olefins	Co-monomers for PE
Polymerization of olefins	Ti	PE, PP	Plastics
C-C coupling reactions	Pd	A wide range of molecules	Organic synthesis

#### 1.1.4. Carbonylation

##### 1.1.4.1 What is carbonylation

Carbonylation refers to reactions that introduce a carbonyl into an organic or inorganic substrate. These reactions entail the transformation of abundant substrates, such as alkenes or methanol, into carbonyl containing products. Carbonylation is also termed as hydrocarboxylation or hydroesterification, if the reactions produce acid or ester. The chemistry and industrial use of carbonylation is well reviewed.<sup>11,12</sup> Table 3 summarizes several typical carbonylation processes.

Table 3: Industrial carbonylation reactions

	Starting material	Catalysts	reagents	products
Hydroformylation	Olefins	Co /PR <sub>3</sub> Rh/ PR <sub>3</sub>	CO/H <sub>2</sub>	Aldehydes alcohol
Reppe carbonylation	Olefin or acetylene	Co or Pd	CO/H <sub>2</sub> CO/water CO/alcohol	Aldehydes acid ester
Methanol carbonylation	Methanol	[RhI <sub>2</sub> (CO) <sub>2</sub> ]	CO	Acetic acid

### 1.1.4.2: Hydroformylation versus Reppe carbonylation

Carbonylation includes hydroformylation and Reppe carbonylation. Hydroformylation is a mature technology that converts terminal alkenes, especially C<sub>2</sub>-C<sub>4</sub> alkenes, into aldehydes or alcohols consequently. This process will be further discussed in **Section 1.3**. However, hydroformylation is less useful for the following:

1. long-chain alkenes (> C<sub>8</sub>)
2. less active internal alkenes
3. carboxylic acid or ester products are required.

The Reppe carbonylation converts unsaturated hydrocarbons into aldehydes, acids and esters. They are important complementary to hydroformylation. Reppe carbonylation is more useful under two conditions: when carboxyl acids or esters (> C<sub>6</sub>) are required, in which case the hydroformylation routine takes three to four steps; and when less inert internal alkenes are used as the substrates. Table 4 summarizes the differences of hydroformylation and carbonylation.

Table 4: Features of hydroformylation and Reppe carbonylation

	Hydroformylation	Reppe carbonylation
CO source	Synthesis gas (cheaper)	CO
Other reagents	No	Nucleophile
Catalyst	Co or Rh	Ni or Pd
Product	Aldehyde/alcohol	Aldehyde/acid/ester
Substrates	Alkenes	Alkenes, alkynes, dienes
To other functional groups	Sensitive	Tolerant

## 1.2 Mechanistic study on homogeneous catalysis

### 1.2.1 Why mechanistic study is important?

Due to the large capacity of homogeneous catalysis, any substantial improvement on these reactions can bring in massive benefits. The core improvement is to explore new catalysts of better performance. However, catalyst design is a very complicated matter, involving those aspects such as catalytic performance, cost, reaction conditions etc. Successful catalysts always require a compromise. For example, Rh/PPh<sub>3</sub> catalysts are widely used in industrial hydroformylation reactions due to the versatility of phosphine ligands; although many other phosphine ligands show much better reactivity and selectivity.<sup>13,14</sup> Nowadays, catalyst design is becoming more and more systematic with the development of theoretical chemistry. A very recent example is the synthesis of new bisphosphine ligands after the proposal of natural bite angle theory.<sup>15-18</sup> To achieve this, a clear understanding on the catalysis mechanism is necessary.

In the following section, some related terms and elemental reactions are presented, **Section 1.2.3** deals with the methodology for mechanistic studies.

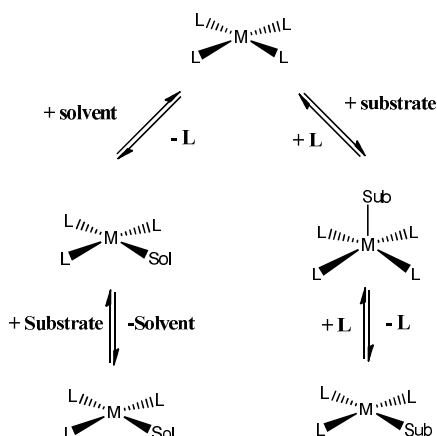
### 1.2.2 Elemental reactions in homogeneous catalysis

The mechanism of a schematically simple reaction might be very complicated. The following section deals several closely related elemental steps that are involved in homogeneous catalysis. They are ligand exchange, insertion and de-insertion, oxidative addition, reductive elimination and hydrogen activation.<sup>14,19</sup>

## Chapter one

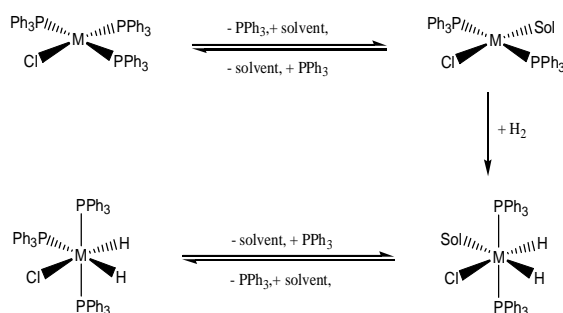
### 1.2.2.1 Ligand exchange: association and dissociation

The core principle of catalysis is to bring together the reactants. To achieve this, a vacant site on the catalyst is necessary. In most cases, catalysis starts with creating a vacant site by ligand association or dissociation, as illustrated in Scheme 1.



*Scheme 1: Two pathways for ligand exchange: the association and the dissociation mechanism*

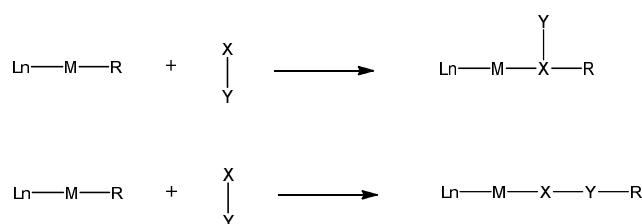
Ligand dissociation is very common in complexes that contain a group VIII metal centre. For example, the hydrogenation catalyzed by Wilkinson's catalyst starts with catalyst solvation, followed by hydrogen addition, as shown in Scheme 2.<sup>20-22</sup> The ligand exchange is important in the hydroformylation process, where  $PPh_3$  and CO concentration are at least two orders of magnitude higher than the metal content. The ligand exchange reaction at least partly determines the reaction rates, as well as its selectivity.



*Scheme 2:  $RhCl(PPh_3)_3$  catalyzed hydrogenation starts with  $PPh_3$ /solvent exchange to create a site that allows dihydrogen addition*

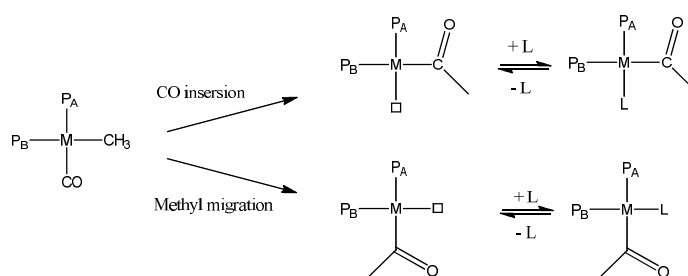
### 1.2.2.2 Insertion and migratory insertion

The insertion reaction refers to those where a coordinated molecule, such as CO, alkene, or alkyne, interposes itself to an existing cationic bond, normally metal carbon bond or metal hydrogen bond. Two types of insertion processes are illustrated in Scheme 3. The essential condition for the insertion step is that the groups involved must be *cis* orientated.<sup>19</sup> Two important insertion reactions are the CO insertion into a metal-carbon bond and the alkene insertion to a metal-hydrogen bond.



**Scheme 3: 1, 1 insertion and 1, 2 insertion**

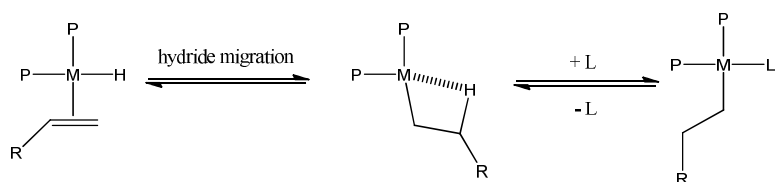
As shown in Scheme 4, there are two pathways to describe CO insertion: insertion and migration, which can be differed spectrally by using asymmetric phosphorus ligands<sup>23</sup> or by theoretical calculations. The migration mechanism is more suitable to describe most of these reactions. However, most of manganese and iron carbonyl complexes follow the migratory mechanism (For more information, See Section 1.2.2.3).



**Scheme 4: Insertion mechanism and migratory insertion mechanism**

The second important reaction is called hydride migratory insertion as shown in Scheme 5. In this reaction, the created vacant site could be stabilized by the interaction a  $\beta$ -hydrogen or another incoming ligand.

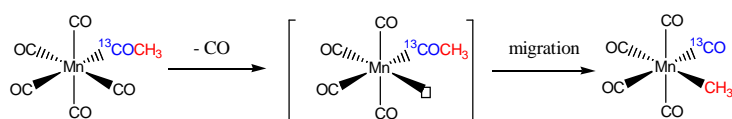
## Chapter one



**Scheme 5:** Hydride migration to the bound alkene leads to the formation of an alkyl ligand, which can be stabilized by  $\beta$ -hydrogen agostic interaction

### 1.2.2.3 De-insertion and $\beta$ -elimination

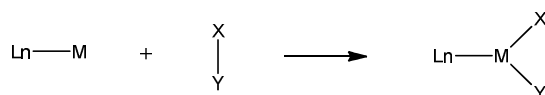
De-insertion is the reverse reaction of migratory insertion. A vacant site in *cis* is required for de-insertion. For example, when  $\text{Mn}(^{13}\text{COMe})(\text{CO})_5$  is heated, the new methyl group always appeared in *cis* relative to  $^{13}\text{CO}$  in the product.<sup>24</sup>  $\beta$ -elimination is the reverse reaction of the hydride migratory insertion.  $\beta$ -Elimination is usually not desired and it can be suppressed by modifying the reaction conditions.<sup>14</sup>



**Scheme 6:** The orientation of the two new groups for de-insertion was indicated by heating  $\text{Mn}(^{13}\text{COMe})(\text{CO})_5$

### 1.2.2.4 Oxidative addition

Oxidative addition represents a reaction where an XY formulated molecule adds to a metal centre, accompanied by breaking the X-Y bond and formation of M-X and M-Y bonds. In this reaction, the oxidation state of both the X and Y group are reduced by one, whereas the oxidation state, d-electron account and the coordination number of the metal centre increases by two. This oxidative addition process is illustrated in Equation 1.

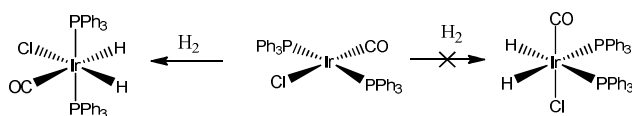


**Equation 1:** Oxidative addition of XY

There are generally four types of oxidative addition reaction mechanisms: concerted,  $\text{S}_{\text{N}}2$ , ionic, or radical reaction. Most oxidative additions follow the concerted mechanism. The



concerted pathway applies to those diatomic molecules lacking in  $\pi$ -bonding, especially dihydrogen.<sup>23</sup>



*Scheme 7: The dihydrogen addition to Vaska's complex, an example for oxidative addition*

### 1.2.2.5 Reductive elimination

Reductive elimination is the reverse reaction of oxidative addition. It always goes pair wise with oxidative addition. In a typical catalytic cycle, an oxidative addition is followed by insertion, and then by reductive elimination to give a product and regenerate the catalyst. It should be noted that C-C coupling reactions are always irreversible due to the high energy difference between the C-C bond and two M-C bonds.<sup>14</sup>

### 1.2.2.6 Hydrogen activation by heterolytic cleavage

Dihydrogen can be activated by transition metal complexes by several methods, like oxidative addition, heterolytic cleavage and  $\sigma$ -bond metathesis. Oxidative addition of hydrogen to  $d^8$ -iridium and rhodium complexes is very common, as described in the last section.<sup>20,25-27</sup> In the heterolytic cleavage process, a dihydrogen molecule splits into a proton and a metal hydride. For example, the reaction of  $\text{RuCl}_2(\text{PPh}_3)_3$  and hydrogen might involve a heterolytic cleavage process.<sup>28,29</sup> Such a process can be promoted by the presence of base. In the case of  $\sigma$ -bond metathesis, the heterolytic cleavage of hydrogen does not involve a 2+2 intermediate, therefore metal dihydrogen complexes can be observed during this process.<sup>29</sup>

## 1.2.3 Methods of mechanistic study

At least three methods contribute to establish a mechanism. They are chemical, analytical and theoretical methods.

### 1.2.3.1 Chemical methods

The chemical methods are the primary methods to understand a reaction by varying reaction temperature, pressure, catalysts and the substrates and comparing different catalytic behaviors under different conditions. Kinetic measurement is useful to give the rate equation.

## Chapter one

Sometimes, if necessary, compounds involved in the reaction can be isolated for analytical measurements. Based on the information which those experiments provide, a hypothetical of a mechanism could be proposed.

### 1.2.3.2 Analytical methods

Analytical measurement plays an important role in mechanistic studies. They include X-ray diffraction (XRD), *in-situ* IR, NMR, <sup>30-34</sup> UV, elemental analysis, mass spectroscopy and chromatography. The practical methods and results for the study of carbonylation were recently reviewed by Diebolt. <sup>35</sup>

When it is possible to use XRD techniques, it provides useful information on molecular structure and other bonding parameters of the bonding in the complex. Recently, X-ray Absorption Fine Structure Spectroscopy (XAFS) and Extended X-ray Absorption Fine Structure Spectroscopy (EXAFS), proved to be powerful for *in-situ* structural studies, where the number and nature of ligands, bond distances and disorders in the coordination sphere around the absorbing atom could be provided. Combination of UV visible spectroscopy and Time Resolved EXAFS provides more detailed information on homogeneous catalysis. <sup>36-38</sup>

The *in-situ* IR measurements are advantageous over the NMR methods, in which the concentration and the natural abundance problem could be largely overcome. Although in some cases the consumption of gaseous reactants could happen, IR methods are especially useful for reactions involving metal carbonyls. Qualitative study could be achieved by measuring the binding mode of CO ligands. In the case of hydroformylation, the ligand exchange reaction, and CO insertion reaction can be studied using this method. <sup>39,40</sup>

*In-situ* NMR methods are also informative and useful in mechanistic study. However, there are many drawbacks. Firstly, certain concentration is required to obtain good signal-to-noise. Low concentration compounds and intermediates, detection of elements with low NMR sensitivity are hard. <sup>41</sup> In addition, some useful signals might be masked by intensive resonances of free ligands. Secondly, the fast consumption of gaseous reactants and the diffusion problems make it hardly possible to obtain 'real' *in-situ* conditions. Thirdly, the NMR experiments can only be run at limited pressure and temperature, although some high pressure NMR (HP-NMR) experiments help to expanded the range of measurements. <sup>42</sup> Fourthly and especially for hydroformylation, the ligand concentrations in the practicable

reactions are often two orders of magnitude higher than normal NMR study experiments, which will affect the equilibrium and selectivity significantly.<sup>43,44</sup>

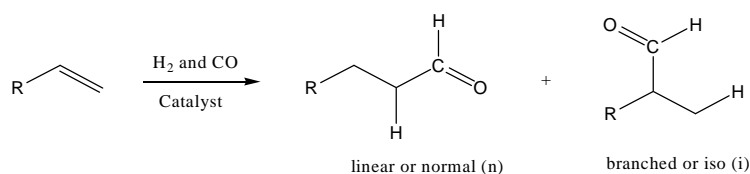
The drawbacks of *in-situ* NMR experiments can be largely overcome by using *parahydrogen* assisted NMR methods. Recent research by Duckett group gives clear insight to  $\text{RhCl}(\text{PPh}_3)_3$  and  $(\text{BCOPE})\text{Pd}(\text{OTf})_2$ , [where BCOPE is  $(\text{C}_8\text{H}_{14})\text{PCH}_2\text{-CH}_2\text{P}(\text{C}_8\text{H}_{14})$ ] catalyzed hydrogenation<sup>20,45-47</sup> and Co/Ir catalyzed hydroformylation mechanism.<sup>30-32</sup>

### 1.2.3.3 Theoretical methods

Quantum chemistry gives further insights into molecular processes by simulating 3D structures and thermodynamic profiles. Reaction energies, activation barriers, the transition and final states can be calculated. These help to explore rate-determining steps and selectivity of alternative reaction pathways. Theoretical methods can be used to pre-screen catalysts and make new catalyst design simpler and faster. The quantum studies become a standard method for catalysis after 30-year developments and became the topic of the Nobel Prize in 1998.<sup>48-51</sup>

## 1.3 Hydroformylation

### 1.3.1 Hydroformylation: discovery, definition and application



#### *Equation 2: Hydroformylation*

Hydroformylation was discovered and formulated by Otto Roelen when investigating cobalt catalyzed Fischer-Tropsch reactions.<sup>52</sup> It is one of the oldest and most important chemical processes. Equation 2 illustrates this reaction, in which terminal olefins, sometimes internal olefins, are converted to aldehydes and their derivatives. Regioselectivity is important, and the linear products are preferred due to their higher commercial value. The side reactions include alkene isomerization and alkene hydrogenation, but does not include the aldehyde hydrogenation, as most of the products are subsequently hydrogenated to alcohols. Today, hydroformylation remains the largest homogeneous catalytic process in chemical industry. Its annual capacity exceeded 9 million tons in 2009.

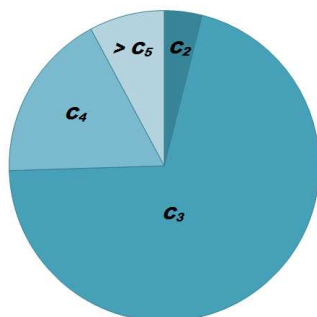


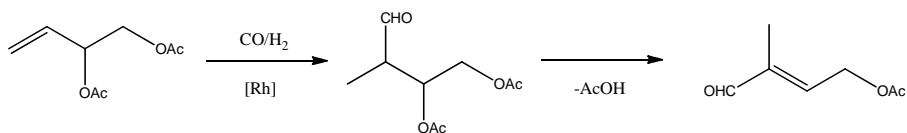
**Figure 1: Distribution of the hydroformylation products**

The hydroformylation products, especially terminal alcohols, can be used as solvents (C<sub>3</sub> - C<sub>7</sub>), plasticizers (C<sub>8</sub> - C<sub>12</sub>) or detergents (C<sub>12</sub> - C<sub>19</sub>), and are thus of great importance. According to statistical data, shown in Figure 1, the production of n-butyraldehyde from propene, using Rh/TPPTS catalyst combination, occupies 72 % of hydroformylation capacity. Most of the butyraldehyde produced by this reaction is hydrogenated to alcohols. The derivations of butyraldehyde and their use are demonstrated in Table 5.

**Table 5: The uses of n-butyraldehyde and 2-butyraldehyde**

	<i>n</i> -Butyraldehyde		<i>i</i> -Butyraldehyde	
Reagent	Product	use	product	use
	2-Ethylhexanol	Plasticiser as phthalic and phosphoric acid ester		
H <sub>2</sub>	n-Butanol	Plasticiser, solvent	i-Butanol	Plasticiser, solvent
HCHO Ca(OH) <sub>2</sub>	Trimethyl-propane	Plasticiser, lubricant, polyester resin	Neo-pentylglycol	Polyester resins
O <sub>2</sub>	Butyric acid		i-butyric acid	
Alcohol	Polyvinyl	Safety glasses		

In addition, hydroformylation, especially asymmetric hydroformylation, is also involved in the total synthesis of fine chemicals. These results were reviewed by Siegel<sup>53</sup> and recently by Breit.<sup>54</sup> As an example, the total synthesis of Vitamin A involves hydroformylation.<sup>53</sup> The BASF process for Vitamin A involves an ylide reaction of C<sub>15</sub> moiety and a C<sub>5</sub> moiety. The C<sub>5</sub> moiety, *trans*-3-formyl-2-butenyl acetate was prepared by hydroformylation of 1-vinylethylene diacetate using rhodium catalyst, as shown in Scheme 8.



**Scheme 8: The hydroformylation step that is involved in the synthesis of vitamin A**

Closely related to my thesis, the catalyst evolution (**Section 1.3.2**), the mechanistic study (**Section 1.3.3**), and the regioselectivity (**Section 1.3.4**) of hydroformylation will be discussed in detail in the following section.

### 1.3.2 Catalyst evolution

Although many complexes are active in the hydroformylation process, almost all of the hydroformylation catalysts are cobalt and rhodium based.<sup>55</sup> Cobalt catalyst, modified or unmodified, dominated before the 1970s.<sup>56</sup> The rhodium catalysts became the main stream after the discovery of the Rh/PPh<sub>3</sub> catalyst; even though Rh is much more expensive than cobalt. Nowadays, 75 % of the hydroformylation process is rhodium based. The modified cobalt catalyst is only used by Shell for internal olefin substrates, in conjunction with Shell Higher Olefin Process (SHOP).<sup>55,57-59</sup>

#### 1.3.2.1 Unmodified first generation catalyst

The original catalyst was cobalt based, although its exact composition was not known at that time. The first commercialized catalyst was dicobalt octacarbonyl, which is active to most of internal or terminal alkenes.<sup>60-62</sup> Some important facts were noted at the very early stage. Firstly, higher CO partial pressure decreases the reaction rate, the isomerization rate, but promotes the selectivity. Secondly, increasing H<sub>2</sub>/CO ratio showed limited impact on the reaction rate. Thirdly, increasing temperature accelerates hydroformylation, isomerization as well as other side reactions. A conclusion was made that the real catalytic species was HCo(CO)<sub>3</sub> rather than HCo(CO)<sub>4</sub>. These two species are in equilibrium under hydroformylation conditions. At lower CO pressure, RCo(CO)<sub>3</sub> has a life time that is long enough to undergo  $\beta$ -H elimination and slightly increases the chance to form the linear CO product over the branched.<sup>56,63-66</sup>

Following research revealed that the thermal stability of HCo(CO)<sub>4</sub> is a key factor under hydroformylation conditions: HCo(CO)<sub>4</sub> is only stable under certain CO pressure at given temperature. This explains why higher CO pressure is needed. Typical hydroformylation

## Chapter one

happens at 110 - 180 °C, under 200 - 300 bar.<sup>67</sup> Considering the aldehyde was partly hydrogenated to alcohol (5 - 12 %), even higher H<sub>2</sub>/CO ratio must be used. The overall 1 : b ratio of dicobalt octacarbonyl catalyzed hydroformylation varies from 3 to 4, depending on reaction conditions and the nature of the substrates.

Another advantage of this process is the easy recovery of the catalyst. BASF oxidizes the catalyst waste to Co<sup>2+</sup>, which is consequently reduced to HCo(CO)<sub>4</sub> again under CO/H<sub>2</sub>, while Exxon treat the catalyst waste with NaOH to produce Na[Co(CO)<sub>4</sub>], which is extracted, and transformed into HCo(CO)<sub>4</sub> by treating it with H<sub>2</sub>SO<sub>4</sub> and CO/H<sub>2</sub>.<sup>56,68,69</sup>

Rhodium carbonyl species such as Rh<sub>4</sub>(CO)<sub>12</sub> have limited application to hydroformylation. This is because the hydrolysis of rhodium carbonyl usually requires very high temperature, which slows the reaction rate to unacceptable value.<sup>68</sup> Recently, it was reported that the catalytic performance of Rh<sub>4</sub>(CO)<sub>12</sub> can be dramatically improved by adding HMn(CO)<sub>5</sub> as the co-catalyst. The increasing reaction rate was ascribed to binuclear elimination to produce aldehydes.<sup>69</sup>

### 1.3.2.2 Modified first generation catalyst

In 1961, Slauch and Mullineaux at Shell reported that adding trialkyl phosphine to cobalt carbonyl catalyst leads to much higher regioselectivity, albeit the reaction rate is slower.<sup>70</sup> Addition of phosphine also prevents the unwanted cobalt plating, even at higher temperatures. As a result, the CO pressure for such a catalytic system can be reduced to 50 - 100 atm. These facts are explained by the formation of the less active but more selective species HCo(CO)<sub>3</sub>(PR<sub>3</sub>) (where R = alkyl). Its inactive nature can be compensated for raising the reaction temperature. In addition, the modified catalyst HCo(CO)<sub>3</sub>(PR<sub>3</sub>) is more active for hydrogenation. This leads to smooth conversion of aldehydes to alcohols in a one-pot reaction.

The choice of phosphine ligands is important as the electronic property of HCo(CO)<sub>3</sub>(PR<sub>3</sub>) must be considered: the electron donating phosphine ligand leads to a more electron rich metal centre and stronger cobalt-carbonyl bonding. The higher regioselectivity arises from steric reasons. The catalytic behavior of HCo(CO)<sub>3</sub>(PR<sub>3</sub>) type complexes with different phosphine are summarized in Table 6.<sup>71</sup> The nature of these phosphine ligands could be presented by electronic and steric parameters. These parameters will be further discussed in **Section 1.3.4.1.**

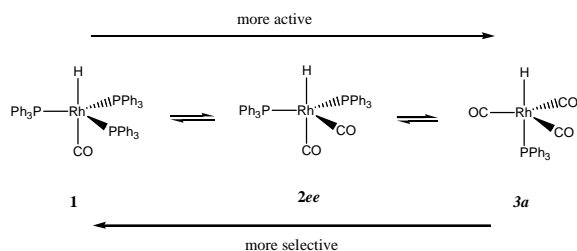
**Table 6: The hydroformylation results of 1-hexene using  $\text{Co}_2(\text{CO})_8/2\text{PR}_3$  as the catalyst precursor. (160 °C, 70 atm. 1.2:1  $\text{H}_2/\text{CO}$ )<sup>71</sup>**

	pKa	Tolman $\gamma$ ( $\text{cm}^{-1}$ )	Cone Angle	k ( $10^3 \text{ min}^{-1}$ )	linear product (%)	Aldehyde to alcohol
$\text{P}^i\text{Pr}_3$	9.4	2059.2	160	2.8	85.0	-
$\text{PEt}_3$	8.7	2061.7	132	2.7	89.6	0.9
$\text{PPr}_3$	8.6	2060.9	132	3.1	89.5	1.0
$\text{PBu}_3$	8.4	2060.3	136	3.3	89.6	1.1
$\text{PEtPh}_2$	6.3	2063.7	136	5.5	84.6	2.2
$\text{PEtPh}_2$	4.9	2066.7	140	8.8	71.7	4.3
$\text{PPh}_3$	2.7	2068.9	145	14.1	62.4	11.7

The modified cobalt catalysts are still being used today, as there is no other satisfactory alternative found for internal olefins. This process is used predominantly by Shell to produce detergent grade alcohols. However, the exact phosphine is not published.

### 1.3.2.3 The second generation catalyst

Although Slaugh and Mullineaux patented the Rh/phosphine combinations in 1961,<sup>70</sup> it is widely believed that Wilkinson's work led the way to rhodium catalyzed hydroformylation.<sup>22,39,40,44,72-75</sup> In this research, a range of triarylphosphine containing Rh(I)-Cl complexes were found to be active for hydroformylation. However, the real catalytic species is considered to be the known complex  $\text{HRh}(\text{CO})(\text{PPh}_3)_3$  (**1**)<sup>76,77</sup> rather than the Rh(I)-Cl species. According to their research,  $\text{HRh}(\text{CO})(\text{PPh}_3)_3$  converts a range of 1-alkenes to corresponding aldehydes under very mild condition (25° C, 1 atm. 1 : 1  $\text{CO}/\text{H}_2$ ) with the l : b ratio as high as 20 : 1. Hydrogenation is almost negligible. The only drawback is the low reaction rate at room temperature. Attempts to increase the reaction temperature or pressure decrease the regioselectivity. Wilkinson's discovery inspired intensive research on  $\text{HRh}(\text{CO})(\text{PPh}_3)_3$  catalyzed hydroformylation.<sup>33,72,73,75,78</sup>



**Scheme 9: active species in  $\text{HRh}(\text{CO})(\text{PPh}_3)_3$  catalyzed hydroformylation**

The next critical discovery is that adding free triphenylphosphine to the reaction leads to increasing l : b ratio, even at higher temperatures. This announced the birth of the Rh/  $\text{PPh}_3$  catalyst. The first plant using Rh/ $\text{PPh}_3$  catalyst was built in 1976 by Union Carbide, in conjunction with Davy Power gas and Johnson Matthey. Afterwards, the rhodium catalyst gradually began to replace cobalt in hydroformylation.

In Rh/ $\text{PPh}_3$  catalyzed hydroformylation, the selectivity was determined by the  $[\text{Rh}] : \text{CO} : \text{PPh}_3$  ratio. In general, increasing CO pressure favors more active catalyst  $\text{HRh}(\text{CO})_3(\text{PPh}_3)$ , as shown in Scheme 9, while adding extra phosphine will inhibit this. The selectivity reaches a high at 17 : 1 when 820 equivalents of  $\text{PPh}_3$  is added to a solution that contains 0.5 mM  $[\text{Rh}]$ . Selectivity cannot be improved further on adding more phosphine, even using melted triphenylphosphine. The commercial catalyst contains 0.1 mM  $[\text{Rh}]$  and 0.4 M triphenylphosphine for propene hydroformylation, producing a l : b ratio of 8 - 10 : 1 in the product. Rh/ $\text{PPh}_3$  catalyzed propene hydroformylation is used by BASF, Union Carbide and Mitsubishi, with different technological features. Nowadays, Rh/ $\text{PPh}_3$  remains the most popular hydroformylation catalyst and accounts for 80 % of total hydroformylation capacity.

#### 1.3.2.4 Expanding ligands

After the discovery of the Rh/ $\text{PPh}_3$  system, studies were made to improve the catalyst performance. Two interesting families must be mentioned: the electron poor phosphite ligands and the bisphosphine/biphosphite ligands.

The phosphite ligands have many advantages over the phosphine ligands, such as easier preparation and simpler catalyst separation. However, the most attractive aspect lies in the fact that phosphites are better  $\pi$ -acceptors than phosphines. Phosphite ligands therefore decrease the electron density on the metal centre and the strength of the metal-carbonyl bond.



In addition, the electron withdrawing group on the phosphite ligands also promotes the reactivity. Some electron poor phosphite based catalysts even show considerable activity to inert alkenes.<sup>43,79</sup>

Hydroformylation using phosphite ligands was studied by Pruett and Smith at Union Carbide Corporation. They reported that electron poor ligands lead to better selectivity than electron rich ligands. This was achieved by comparing the reactivity of 4-methoxyl and 4-chloro substituted triphenyl phosphite ligands.<sup>43,79</sup> Van Leeuwen and his co-workers discovered another highly reactive and selective catalytic system for hydroformylation using extremely bulky phosphite ligands. The high reactivity could be explained by the exclusive formation of the monoligated catalyst for steric reasons in Rh/tris(2-tert-butylphenyl)phosphite catalyzed hydroformylation. The combination of [Rh] and tris(2,2,2-trifluoroethyl)phosphite catalyzed hydroformylation of 1-octene has a rate of 161,000 mol/ Rh<sup>-1</sup> h<sup>-1</sup> with moderate selectivity. These catalysts are so active that they are active to 1,2- and 2,2-dialkylalkenes, and therefore prospective ligands for the 4<sup>th</sup> generation catalyst. (**Section 1.3.2.6**) Commercial application of bulky phosphite ligands in the hydroformylation process includes the production of 3-methylpentane-1, 5-diol from 3-methylbut-3-en-1-ol.<sup>79,80</sup>

The importance of catalytic systems that contains bisphosphine or bisphosphite ligands was realized as early as the discovery of rhodium catalyzed hydroformylation. Although they do not guarantee high linearity, the bisphosphine or bisdiphosphite ligands modified system seems to prove a convenient way to create a precursor with phosphine ligands in equatorial position.

The original research on bisphosphite containing catalysts was patented by Bryant at UCC. To my knowledge, both the bridge length and the bite angle impact the selectivity greatly. The best result is achieved using bridging biphenyl and bulky groups on the phosphorus centre. As an example, the UC-44/Rh catalyst gave a selectivity of over 30 : 1 for terminal alkenes and over 25 : 1 for 2-butene.<sup>81</sup> The structure of UC-44 is illustrated in Figure 2.

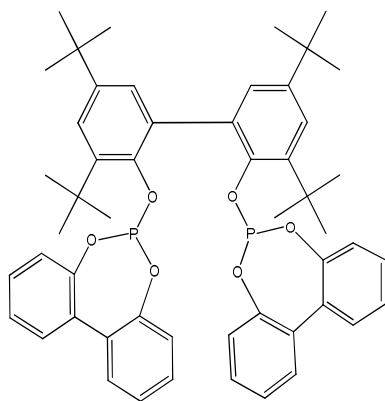


**Figure 2: Structure of UC-44; the combination of UC-44 and rhodium proved to be the most active and selective hydroformylation catalyst.**

The initial work on common bisphosphine ligands showed neither acceptable reactivity nor selectivity. Sanger reported moderate selective results on addition of bisphosphine to  $\text{HRh}(\text{CO})(\text{PPh}_3)_3$  at mild conditions.<sup>82,83</sup> Pittman studied the same reaction at higher temperature and pressure, with the 1 : b ratio dropped to 1.<sup>84</sup> Dppb based catalysts was discovered by Matsumoto and Tamura at Kuraray Co. and licensed by ARCO Chemicals to produce 1,4-butanediol from allyl alcohol. They found a stable catalyst system can be produced on addition of equal molar of dppb to  $\text{HRh}(\text{CO})(\text{PPh}_3)_3$ . Adding more dppb to the reaction or simply using only dppb lead to poor reaction rates and selectivity. The arm on-arm off mechanism proposed by Matsumoto explains the selectivity. However, no direct evidence was provided. Therefore, the mechanism of the bisphosphine system is far from well understood.<sup>85</sup>

Novel bisphosphine ligands have been developed by several groups. A highly selective BISBI/Rh catalyst was reported by Devon and co-workers at Texas Eastman.<sup>54,86</sup> Propene can be hydroformylated with a 1 : b ratio of 30 at standard conditions (95 - 125 °C, 16 atm. of  $\text{CO}/\text{H}_2$ ,  $[\text{Rh}] = 1.5 \text{ mM}$ , phosphine/Rh = 2.4), which is much higher compared with the commercial Rh/ $\text{PPh}_3$  catalyst despite its halved reaction rate. If the reaction rate was not considered, the selectivity can be optimized to 288 : 1 under certain conditions. The Xantphos family was developed by the Leeuwen group at University of Amsterdam. They give high selectivity and similar rates to BISBI.<sup>87,88</sup> Structure of the BISBI and Xantphos family ligand are illustrated in Figure 3. In addition, accompanied with the ligand discovery, theoretical work was used to explain these high-performance catalysts. The high selectivity of BISBI and Xantphos family is explained by the bite angle effects that lead to the formation of specific intermediates.<sup>87,89-91</sup>

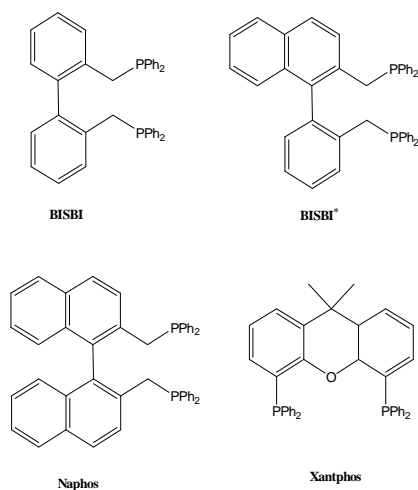


**Figure 3: High performance bisphosphine ligands for hydroformylation**

### 1.3.2.5 The third generation catalyst

Some drawbacks in Rh/PPh<sub>3</sub> catalyst cannot be ignored. The most notable problem is the ecological and economical catalyst separation. This problem was overcome by using biphasic catalysis. The concept of biphasic catalysis aims at simple, economical product separation under mild conditions. Different compositions for biphasic system are summarized in Table 7. Their application to hydroformylation has been achieved on the laboratory scale (ionic liquid/organic liquid,<sup>92</sup> supercritical CO<sub>2</sub>/ ionic liquid,<sup>93</sup> perfluoro organic liquid/organic liquid) and the industrial scale (water/organic liquid).<sup>94</sup> A water-organic biphasic hydroformylation process was developed by Rhone Poulenc and Ruhr Chemie AG in 1982, which led to an industrial scale hydroformylation process in aqueous solution.<sup>94</sup>

**Table 7: The composition of two-phase solvent systems for hydroformylation**

<b>Polar phase</b>	<b>Less polar phase</b>
Water miscible solvent	Organic solvent
Fluorous organic solvent	Organic solvent
Polarized organic solvent	Non polar organic solvent
Ionic liquid	Organic solvent

The core of such progress was the discovery of the sulfonated catalyst: HRh(CO)[P(Ph-*m*-SO<sub>3</sub>Na)<sub>3</sub>]<sub>3</sub> (TPPTS), which is highly charged and therefore water soluble. In this process, extra phosphine, normally 60 - 80 equivalents relative to [Rh], is necessary to prevent the

## Chapter one

catalyst deactivating. Such a catalytic system gives improved yield, higher selectivity (94 : 6 at phosphine/Rh ratio of 80/1) and sufficient product purity. The combination of Rh/BFNAS, shows even higher selectivity (1 : b ratios: 98 : 2 at P/Rh 7 : 1), however, the industrial use of the BINAS modified catalyst was limited due to the high cost of the ligands. The Rh/TPPTS based catalytic process only applies to propene, butylenes and pentene due to the poor solubility of longer alkenes in water. Neither is this process suitable for ethylene hydroformylation, for the product propanol, is too miscible with water.

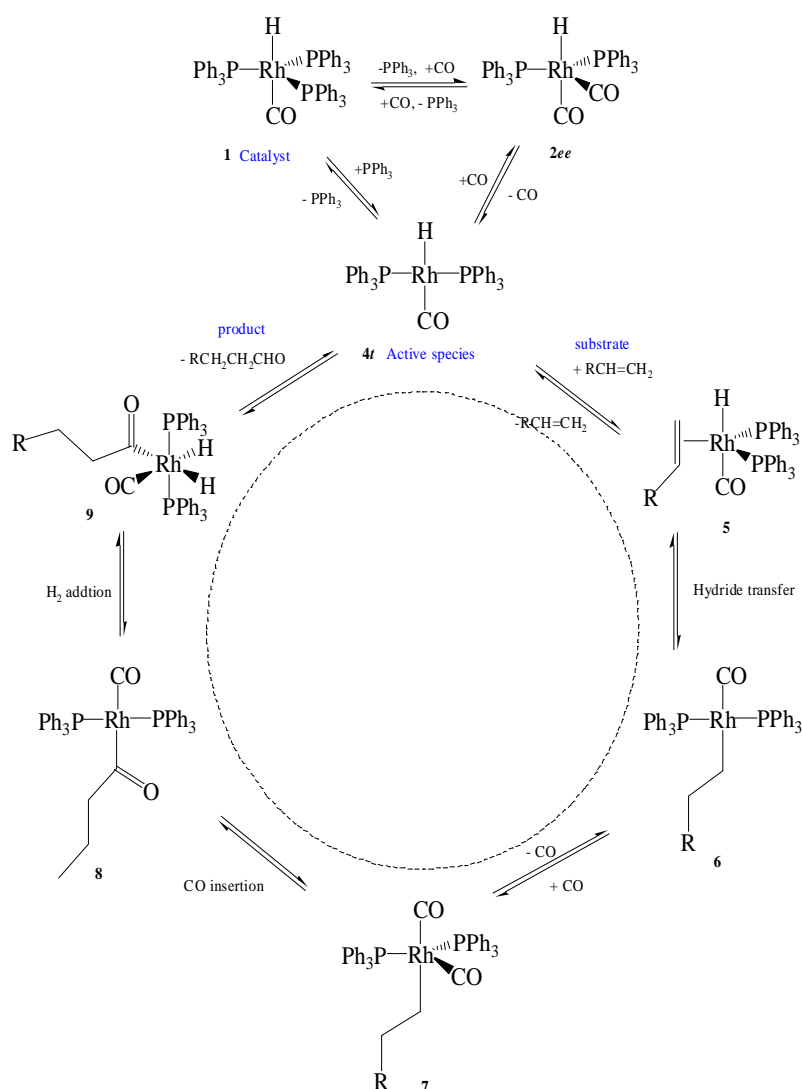
### 1.3.2.6 New generation (or 4th) catalyst

The fourth generation hydroformylation catalyst focuses on the less active internal alkenes. To achieve this, the catalyst must be a highly active as an isomerization catalyst. The isomerization product and hydroformylation acyl intermediate (which should prefer  $\beta$ -elimination rather than CO insertion) must firstly form the terminal alkene. The terminal alkene can then be hydroformylated to linear products. The hydroformylation reaction of internal alkenes can be ignored due to their inactive nature.

So far, the use of fourth generation catalyst remains a great challenge. Very few examples show acceptable results. Van Leeuwen and Roobeek reported an early example using a monophosphite ligand with an electron-withdrawing group leading to moderate selectivity. The phosphite ligands help to accelerate the isomerization rate which leads to high selectivity for the linear product.<sup>95</sup> Bryant at UCC reported hydroformylation of 2-butene using rhodium/bulky diphosphite based catalyst, with 1 : b = 3.<sup>81</sup> Improved results were obtained by Du Pont and DSM by using electron poor ligands, where the selectivity reached 97 % for a linear product when 2-hexene was hydroformylated.<sup>96</sup>

### 1.3.3 General mechanism of hydroformylation

The general hydroformylation mechanism is illustrated in Scheme 10. using the Rh/PPh<sub>3</sub> catalyst and a terminal alkene substrate, based on the analogy to the modified cobalt catalyst.<sup>65,66,73,97</sup> This mechanism is in good accordance with the experimental and theoretical results and accepted by most researchers. Scheme 10 illustrates the major species present under mild hydroformylation conditions (298 K, 1 atm. of CO/H<sub>2</sub>, catalyst concentration 10<sup>-2</sup> M - 10<sup>-1</sup> M). It is different to 'real' hydroformylation conditions (343 K - 393 K, 10 - 30 atm. of CO/H<sub>2</sub>, catalyst concentration 10<sup>-3</sup> M), but is a very good approximation to my study.

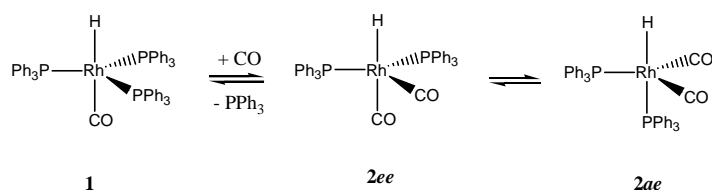


**Scheme 10: General hydroformylation mechanism using the  $\text{HRh}(\text{CO})(\text{PPh}_3)_3$  and alkene substrate**

The starting complex  $\text{HRh}(\text{CO})(\text{PPh}_3)_3$  (**1**) was prepared and structurally characterized independently by Vaska and Wilkinson.<sup>76</sup> Compound **1** has a trigonal pyramidal structure with the hydride and carbonyl ligand in the axis, according to corresponding NMR and crystallography studies.<sup>91</sup> When exposed to an atmospheric pressure of carbon monoxide in solution, one phosphine ligand in **1** is replaced by a CO ligand, yielding  $\text{HRh}(\text{CO})_2(\text{PPh}_3)_2$  (**2**).<sup>33,44</sup> Compound **2** has two isomers: the *ee* isomer contains two equivalent phosphine ligands in an equatorial position, while the *ae* isomer contains two inequivalent phosphine ligands, one in equatorial and the other in apical position. Brown and co-workers suggested the *2ee* isomer was thermodynamically preferred.<sup>33</sup> Further CO/ $\text{PPh}_3$  exchange leads to formation of  $\text{HRh}(\text{PPh}_3)(\text{CO})_3$  (**3**) under even higher CO pressure. Magnetization transfer NMR experiment suggests both **1** and **2** undergo phosphine exchange with free phosphine at a

## Chapter one

rate much higher than the catalytic reaction. This indicates the inter-conversion of **1** and **2** is reversible.



**Scheme 11:** Catalytic precursors that are formed by  $PPh_3/CO$  exchange in  $HRh(CO)(PPh_3)_3$  catalyzed low pressure hydroformylation.

All the species discussed above are electronically saturated. Therefore, ligand dissociation must happen if catalysis is to occur. Ligand dissociation of phosphine or CO, from an equatorial position of **1** and **2** respectively lead to a square planar monohydride complex **4**, which is considered to be the real catalytic species under low pressure hydroformylation conditions. Complex **4** should have both *trans* and *cis* forms. However, the detection of type **4** species is rare. The only example is the  $HRh(CO)(PCy_3)_2$ ,<sup>98</sup> while the type **4<sub>c</sub>** complex has never been observed.

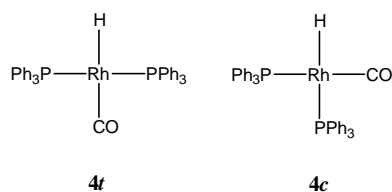


**Figure 4:** Active species in  $HRh(CO)(PPh_3)_3$  catalyzed low-pressure hydroformylation.

Complexation of free alkene to complex **4** leads to another trigonal bipyramidal compound **5**. However, no observation of **5** type compounds has been reported. Duckett et al. reported a similar rhodium dihydride species that contains an alkene ligand.<sup>20</sup> The conversion of **4** and **5** is believed to be reversible. This is supported by the fact that isomerization of styrene could be achieved in the presence of **1** without an external hydrogen source.<sup>33</sup> This step involves  $\beta$ -hydride elimination of the alkyl group, as described in **Section 1.2.2.3**.

Complex **5** transforms to another square planar complex **6** after the alkene migratory insertion. This step is believed to be irreversible at low temperature ( $< 70^\circ C$ ) and high partial pressure of CO ( $> 10$  atm.). Thus the conversion of **5** to **6** could be the selectivity determining step. The reaction of **6** with hydrogen gives hydrogenation products. **6** can also combine another CO molecule to reform the trigonal bipyramidal complex **7**. Complex **7** undergoes a

second migratory insertion to give the acyl complex **8**. Complex **8** reacts with hydrogen to yield the aldehyde and regenerate the catalyst **4** via a dihydride complex **9**. Several type **8** complexes are known, while little information is known for type **7** and **9** complexes. Brown has observed that the *ae* isomer of **9** isomer dominates due to steric factor, in contrast with complex **2**, where the *ee* isomer is favoured.<sup>33</sup>

In conclusion, Rh/PPh<sub>3</sub> catalyzed hydroformylation involves six elemental steps, as presented in Scheme 10. Side reaction might happen in each step. The reaction under industrial conditions is more complicated due to ligands exchange.

The hydroformylation of dienes shows great similarity to that of alkenes. The key intermediates are transition metal allyl complexes.<sup>75</sup>

### 1.3.4 Reactivity and selectivity

#### 1.3.4.1 Parameters that determines the selectivity

The catalyst selectivity has been determined by both electronic and steric factors, as reviewed by Tolman in 1977.<sup>99,100</sup> The overall electronic properties of a ligand are represented by the parameter  $\chi$ . High  $\chi$  values stand for strong  $\pi$ -acceptors and poor  $\sigma$ -donors (i.e. electron withdrawing), while low  $\chi$  value for strong  $\sigma$ -donors and poor  $\pi$ -acceptors (i.e. electron giving). The electronic parameter of phosphine ligands are measured by the vibrational frequency of corresponding (PR<sub>3</sub>)Ni(CO)<sub>3</sub> type complexes.<sup>100</sup> If other ligands increase the density of  $\pi$  electrons on the metal, the C-O bond is weakened and  $\nu(\text{CO})$  decreases. Conversely, if other ligands compete with CO for  $\pi$ -back bonding,  $\nu(\text{CO})$  increases. The  $\chi$  values of common phosphine ligands are shown in Table 8, which was refined by Bartik, where substitution effects on the triarylphosphines were considered.<sup>101</sup>

The steric factor is represented by cone angle value  $\theta$ , which is defined as the solid angle formed with the metal at the vertex and the hydrogen atoms at the perimeter of the cone. Table 8 illustrates the  $\chi$  and  $\theta$  value of several phosphine ligands. The overall impact varies with different catalytic systems.

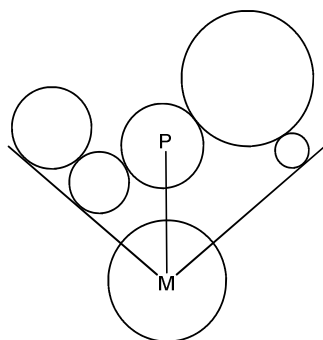


Figure 5: Illustration of Tolman angle, where the P-M bond length is averagely 2.24 Å

Table 8: Electronic and steric parameters of PR<sub>3</sub> type ligands

PR <sub>3</sub>	pK <sub>a</sub>	Tolman $\chi$ (cm <sup>-1</sup> )	Cone Angle °
P( <i>i</i> -Pr) <sub>3</sub>	9.4	2059.2	160
PEt <sub>3</sub>	8.7	2061.7	132
PPr <sub>3</sub>	8.6	2060.9	132
PBu <sub>3</sub>	8.4	2060.3	136
PEt <sub>2</sub> Ph	6.3	2063.7	136
PEtPh <sub>2</sub>	4.9	2066.7	140

When a bisphosphine is considered, the steric factor becomes more complicated. Tolman originally expanded the steric factor to bisphosphine ligands by defining the average cone angle as the angle between the M-P bond and the bisector of the P-M-P angle. Such a definition still remains a good approximation for bisphosphine ligands.<sup>101</sup> However, the coordination of bisphosphine ligands is dynamic and flexible, according to recent studies by Casey and Diekes. There are different coordinated intermediates in catalysis, for example, 90° is preferred in octahedral and square planar complexes, while 109° is preferred in tetrahedral complexes.<sup>91,102</sup>

The steric factors of the substrates should also be considered, Figure 6 illustrates common substrates that are used in the hydroformylation process regarding the substitution on the double bond.



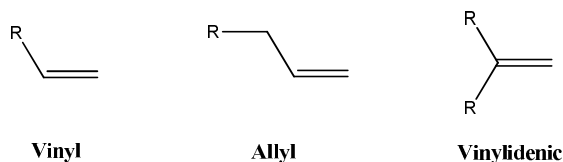


**Figure 6: Types of substrates for hydroformylation**

### 1.3.4.2 Selectivity on unmodified catalyst system:

Several unmodified rhodium complexes serve as catalyst precursors, such as  $\text{Rh}_4(\text{CO})_{12}$ ,  $[\text{Rh}(\text{CO})_2(\text{acac})]$ ,  $[\text{RhCl}(\text{CO})_2]_2$ ,  $[\text{Rh}(\text{COD})(\text{OAc})]_2$  and  $[\text{Rh}(\text{COD})_2](\text{BPh}_4)$ . The real catalytic species is believed to be  $\text{HRh}(\text{CO})_n$ , where  $n = 3, 4$  under hydroformylation conditions. These two species are highly unstable and recombine to rhodium clusters if no hydrogen or substrate is present.<sup>18</sup> Research on unmodified rhodium catalyzed hydroformylation provide for a simple model to understand how selectivity occurs, where key intermediates are less and the ligand impact is weaker compared with modified catalysts.

During the  $\text{HRh}(\text{CO})_n$  catalyzed hydroformylation, the formation of the alkyl intermediate is irreversible at low temperature, where the side reactions such as isomerization and  $\beta$ -elimination are almost negligible at this stage. The selectivity is decided by the ratio of the two alkyl intermediates. Electronic factor dominate at this point if no bulky substrates are involved. Branched alkyl complexes are preferred due to delocalization of negative charge owing to the inductive effect, therefore branched products predominate. This trend is more evident when the substrate contains one or more electron withdrawing group.<sup>103,104</sup> However, the substituent group on the alkenes prevents the CO insertion if it's too large. Vinylidene substrates only give linear products due to this.<sup>105</sup> Increasing the reaction temperature favours the formation of the linear product. This was observed for different substrates. For styrene, the l : b ratio is 36 : 64 at 403 K, in contrast to 2 : 98 at 293 K. The two relevant reactions,  $\beta$ -elimination and CO de-insertion cannot be ignored at higher temperature. There is an equilibrium between the metal alkyl and acyl species at higher temperature. The hydrogenolysis of metal-acyl complexes is now the rate determining step. However, the hydrogenolysis of linear acyl complexes is faster than branched ones due to the difference on steric properties.<sup>18,106,107</sup>  $\beta$ -Hydride elimination only happens with allylic substrates to give more active terminal alkenes, which leads to a quick consumption of the branched alkyl isomers. Such progress can be studied by H-D exchange experiments. No deuterated substrates are detected under mild conditions on mixing protio substrate and Rh-D species.

## Chapter one

[108, 109] Table 9 illustrates experimental results when representative substrates are hydroformylated by  $\text{Rh}_4(\text{CO})_{12}$ .<sup>103,108</sup>

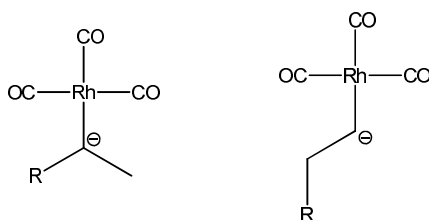


**Figure 7: Structure of  $\text{Rh}(\text{alkyl})(\text{CO})_3$  isomers, the key intermediates in unmodified rhodium precursor catalyzed hydroformylation**

**Table 9: The hydroformylation selectivity to different substrates using unmodified rhodium catalyst**

Substrates	T (°C)	P (bar)	Reaction times (h)	l:b ratio
Substituted styrene	20	60	16	95/5-98/2
Fluoroethene	80	110	6	100/0
3,3 -Dimethylbutene	20	60	16	0/100
2-Methylpropene	100	100	1	0/100

**Table 10: Selected values of reaction rate constants and regioisomeric ratios in  $\text{Rh}_4(\text{CO})_{12}$  catalysed styrene hydroformylation,  $K_b/K_n$ : the elimination rate of the branched(b)/linear(l) acyl complex**

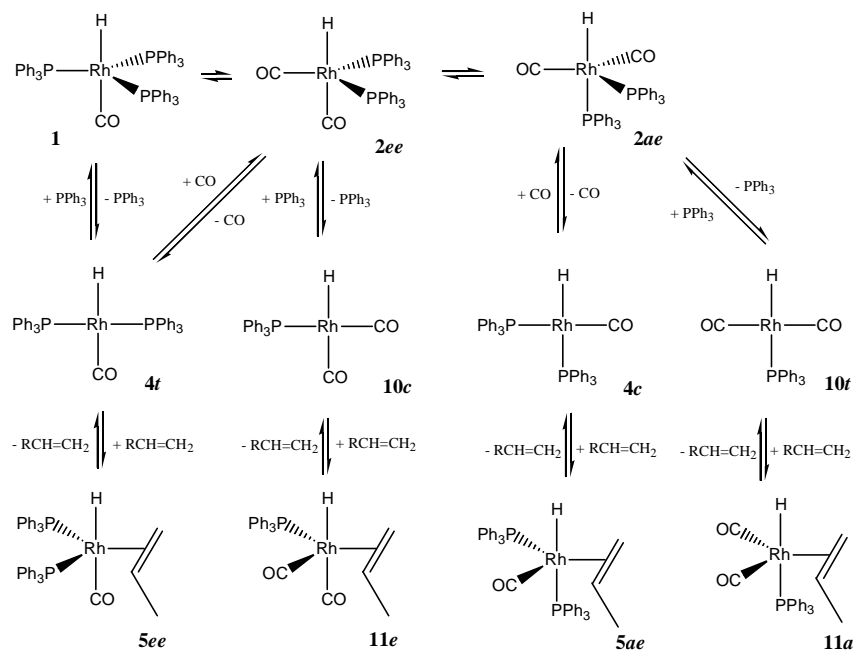
	At 298 K	At 403 K		At 298 K	At 403 K
$K_b$	0.93	4.18	3b : 3l	97.5/2.5	87.5/12.5
$K_n$	1.27	10.3	b : l	96.7/3.3	66/34

### 1.3.4.3 Selectivity on $\text{Rh}/\text{PPh}_3$ system:

The selectivity of the  $\text{Rh}/\text{PPh}_3$  system is dependent on  $\text{Rh}/\text{PPh}_3$  ratio, CO pressure and temperature. The structure of substrates is also considered.

At high concentration of  $\text{PPh}_3$ , the resting state of the catalyst is **1**. **1** only gives a square planar hydride complex **4t** after losing a phosphine ligand. The catalyst resting state is **2** at low concentrations of  $\text{PPh}_3$ , **2ee** gives **4t** and **4c** isomers after losing a CO ligand, while **2ea** gives **10c** and **10t** isomers. Wilkinson suggested that the selectivity was determined by the

distribution of **4t**, **4c**, **10c** and **10t**. Higher concentrations of **4t** gives more linear product. In their research, *trans*-HRh(CO)(PPh<sub>3</sub>)<sub>2</sub>, gave a l : b ratio of 20, whereas HRh(CO)<sub>2</sub>(PPh<sub>3</sub>) gave a l : b ratio of 4. Their conclusion is in good accordance with propene hydroformylation using the HRh(CO)(PPh<sub>3</sub>)<sub>3</sub> catalyst. However, high concentration of **4t** does not guarantee high linearity. When a large excess of dppe or dppp are used, where **4t** type species dominates among these species, selectivity was only moderate.



**Scheme 12: The distribution and inter-conversion of active species in HRh(CO)(PPh<sub>3</sub>)<sub>2</sub> catalysed hydroformylation.**

There are two conditions for the application of Wilkinson's conclusion. Firstly, the alkene association must be irreversible; the inter conversion of **5** and **11** isomers must be slow if it is to be ignored. Secondly, there must not be a very bulky group on the substrate.

As discussed, the selectivity is a comprehensive result of the steric and electronic factors.

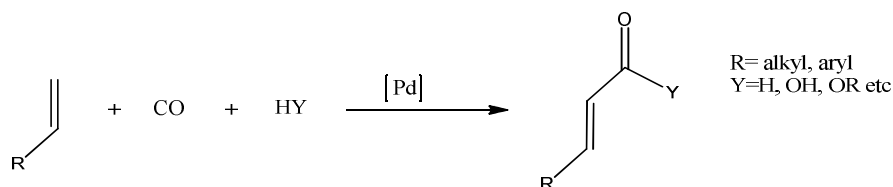
## 1.4 Reppe carbonylation

### 1.4.1 History

Reppe carbonylation converts alkene substrates into their acid derivatives, as shown in Equation 3. It can be catalyzed by many transition metal based catalysts. The first application of Reppe carbonylation converted acetylene, CO, and water into acrylic acid, using Ni(CO)<sub>4</sub> as catalyst.<sup>11</sup> Similar process is still used by BASF. However, Ni(CO)<sub>4</sub> is not preferred due to

## Chapter one

its high toxicity. Rhodium catalysed Monsanto's acetic acid synthesis occupies 25 % of acetic acid production all over the world.<sup>11</sup> The first palladium catalysed Reppe-carbonylation was developed by BASF. Although patented by Shell in the late 1980s, the importance of palladium catalysts was not realized until the last decade. Palladium catalysed carbonylation also enables the synthesis of a wide range of compounds that contains heterocycles.<sup>109</sup>



**Equation 3: Reppe carbonylation**

### 1.4.2 Catalysts for Reppe carbonylation

Pd(II) complexes that contains two phosphine ligands are the best catalysts for carbonylation. The two phosphine ligands must be *cis* to promote the selectivity. Based on that, it was not surprising that bisphosphines have great advantage over monophosphine ligands. In addition, the other two coordination sites in the catalyst molecule must be occupied by weakly bound anions like OAc<sup>-</sup> and OTf<sup>-</sup> ion, which could be easily replaced by solvent, CO or the substrates.

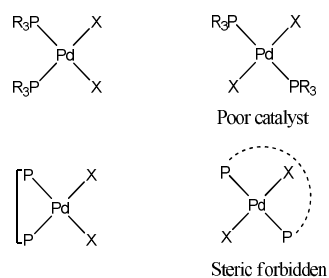


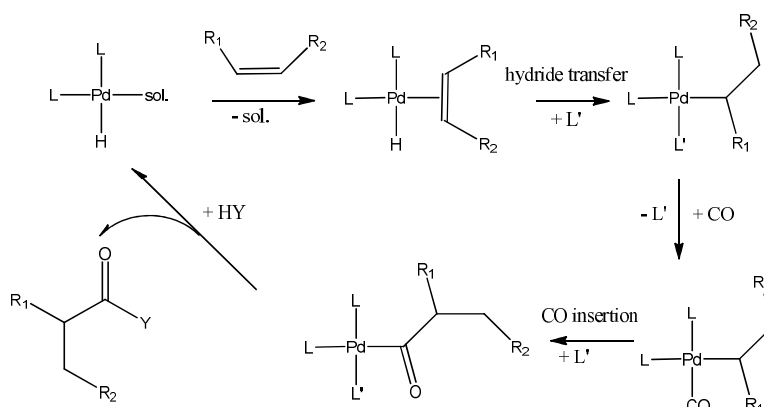
**Figure 8: Structure of palladium catalysts for carbonylation**

### 1.4.3 Carbonylation mechanisms

#### 1.4.3.1 Alkene carbonylation

Although palladium catalysed carbonylation is so widely used in organic catalysis, the mechanistic study of those reactions was not so straightforward. Deactivation of catalysts, and formation of palladium clusters and colloids, brought heterogeneous character to those

reactions. Now two distinct mechanisms for palladium catalysed carbonylation are proposed by researchers: the monohydride mechanism and the alkyloxy carbonyl mechanism.

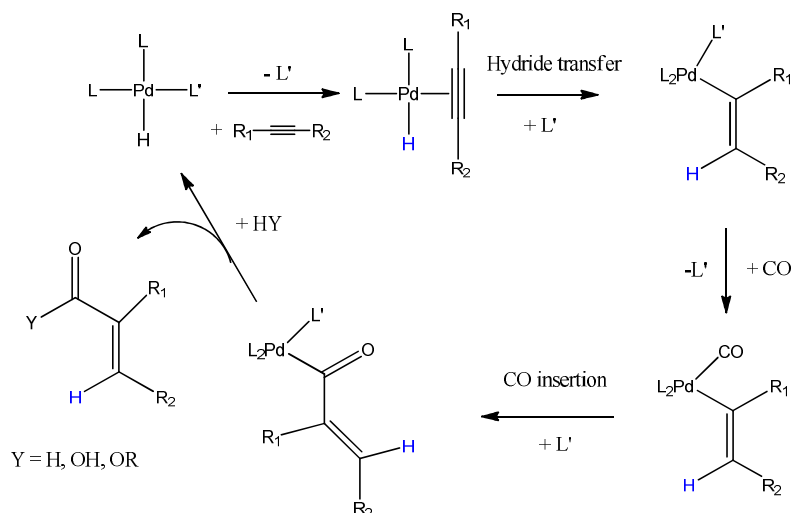


**Scheme 13: The hydride mechanism for palladium catalysed alkene carbonylation**

The first mechanism, termed the ‘monohydride mechanism’, is illustrated in Scheme 13, where palladium monohydride species are proposed to be the active species. It gives an alkyl intermediate after alkene association and consequent hydride migration. CO imposes itself into the Pd-C bond after replacing a ligand, to form an acyl species. Nucleophilic attack by  $\text{OH}^-$  or  $\text{CH}_3\text{O}^-$  produces the acid or ester product, where the monohydride species can be regenerated by their counter cation  $\text{H}^+$ . According to this mechanism, the nature of the key intermediate, the palladium acyl complex, determines the selectivity. However, direct detection of such species is very rare. The properties of palladium alkyl species are discussed in **Section 1.4.4.3**.

### 1.4.3.2 Alkyne carbonylation

Mechanistic research on alkyne carbonylation with palladium complexes was relatively rare. The proposed alkyne carbonylation mechanism is similar with alkenes, as illustrated in Scheme 14.<sup>110</sup>



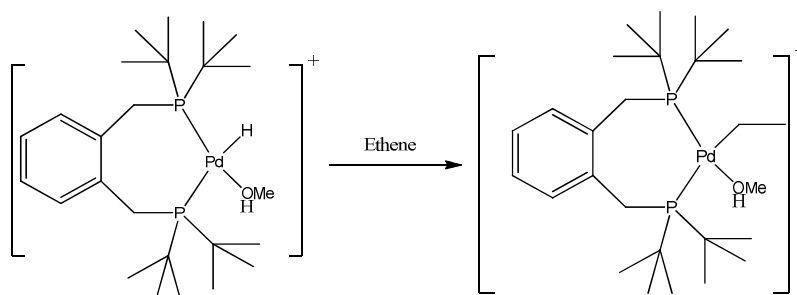
**Scheme 14: Monohydride mechanism for palladium catalyzed alkyne carbonylation**

## 1.4.4 Intermediates

### 1.4.4.1 Palladium monohydride complexes

In these reactions, palladium monohydride species  $[(PR_3)_2PdH]^+$  are often considered to be catalyst precursors. The chemistry property of monohydride species is determined by the backbone phosphine ligands. The chemistry of cationic palladium monohydride species  $(P)_2PdHX$ , where  $X = Cl, Br$ , is rich. [106] However, they are too stable to catalyse. The *in-situ* detection of more active species  $(P)_2PdH(L)$  (where  $L =$  solvent or other weakly bind ligand) is very rare.

There are two possible pathways to produce monohydride species in catalysis, depending on the source of the hydride. The first one route is protonation. The hydride has a solvent origin in this reaction. In 2002, a monohydride complex  $[Pd(d^t bpx)H(MeOH)](OTf)$ , where  $d^t bpx = 1, 2-(CH_2P^t Bu_2)_2C_6H_4$ , was prepared and studied by Clegg and co-workers. Their study also included the subsequent reaction of  $[Pd(d^t bpx)H(MeOH)](OTf)$  with ethylene to give a palladium ethyl product. However, their study was not catalytic. <sup>111,112</sup>.



**Equation 4: Structure of  $[Pd(dtbpx)H(MeOH)](OTf)$  and its consequent reaction with ethene**

The second way to produce a monohydride species involves hydrogen activation. The exact activation mechanism could be heterocleavage or oxidative addition. Heterocleavage mechanism is in good agreement with most of the experimental results. This reaction can be promoted by adding suitable base to the reaction. Konya et al reported dramatic improvement on reactivity as well as selectivity on  $[(BCOPE)Pd(CH_3OH)_2](OTf)_2$  (**12a**) catalysed alkene hydroformylation by adding small amount of a halide ion to the reaction. Adding a large excess of  $X^-$  terminates the catalysis. This supports the heterolytic splitting manner of hydrogen in catalysis, where  $X^-$  serves as Lewis base.<sup>113</sup> Joaquín and co-workers also reported the detection of  $[(BCOPE)PdH(pyridine)](OTf)$  (**13a-2**) in hydrogenation of diphenyl acetylene using NMR methods, which confirms the necessity of hydrogen if carbonylation reactions to occur.<sup>46</sup>

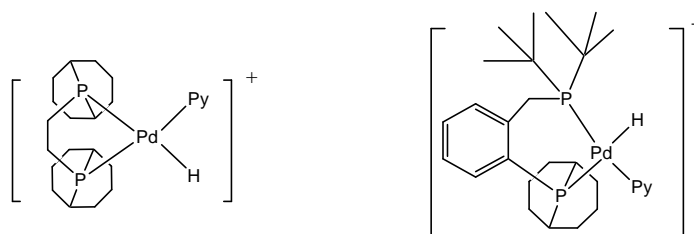


**Figure 9: Structure of monohydride species when  $[(BCOPE)Pd(CH_3OH)_2](OTf)_2$  (**12a**) or  $[(tBuCOPE)Pd(H_2O)_2](OTf)_2$  (**12b**) catalyze the hydrogenation of diphenyl acetylene**

In addition, the oxidative addition manner of hydrogen to palladium is less important but cannot be excluded, even the example of hydrogen addition to molecular palladium species are extremely rare. Only two examples of hydrogen addition to molecular palladium species are reported in brief before our study, using  $PdCl_2(PCy_3)_2$  and  $[Pd(tBuCOPE)(OH)_2](OTf)_2$  (**12b**) precursor. In our previous research on  $(PEt_3)_2Pd(OTf)_2$  catalysed diphenyl acetylene hydrogenation, a palladium vinyl hydride species  $[trans-(PEt_3)_2PdH(CPh=CHPh)](OTf)$  was

## Chapter one

detected and characterized by NMR spectroscopy using PHIP. The correlation of the hydride signal and the vinyl signal suggested that they are from the same *parahydrogen* molecule.<sup>45</sup>

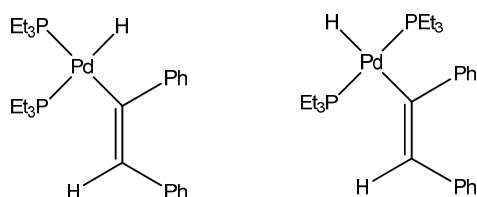
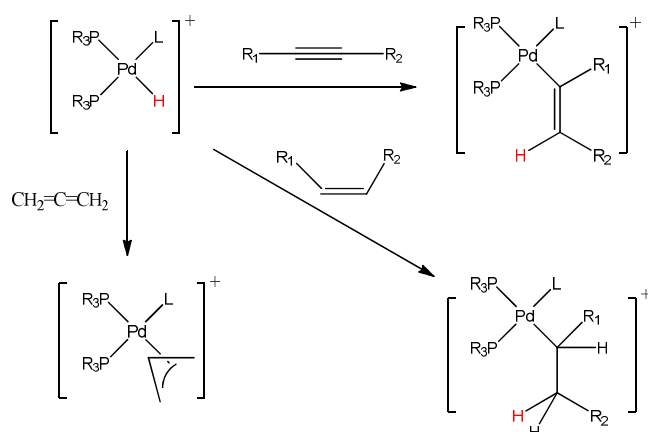


**Figure 10: Structure of palladium vinyl hydride species that are detected in  $(PEt_3)Pd(OTf)_2$  catalyzed diphenyl acetylene hydrogenation**

The interactions of palladium monohydride complex and unsaturated hydrocarbons, such as alkenes, alkynes and dienes, are well established, as shown in Scheme 15. We must note that the monohydride is more reactive to alkynes rather than alkenes. If this catalyst is added to a mixture of them, the alkene was inert until the alkyne is all consumed.

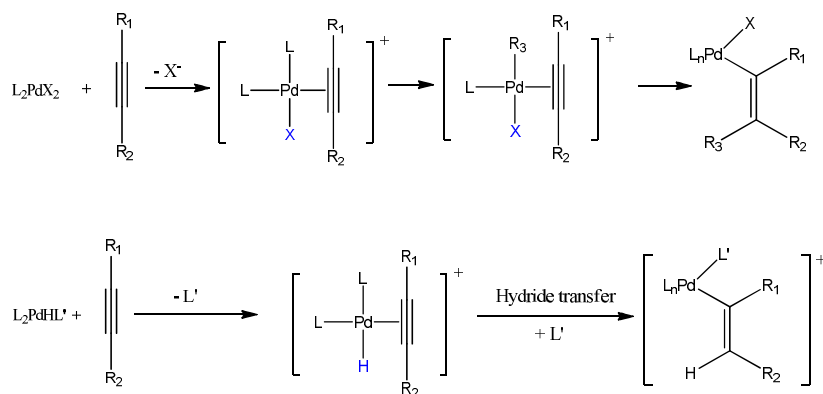


**Scheme 15: Chemistry of palladium monohydride complexes**

### 1.4.4.2 Palladium vinyl complexes

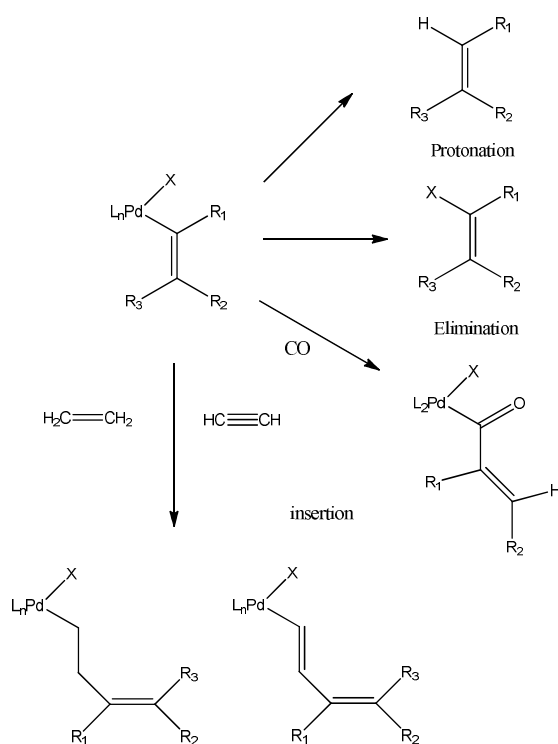
Palladium vinyl complexes are generated from the interaction of palladium hydride species and alkynes, where the transferable group must be *cis*. It could form from a hydride or an alkyl group.<sup>114</sup> As shown in Scheme 16, the vinyl species are generated after migration. Similar results were also found for the nickel analogue.<sup>115</sup>





**Scheme 16: Generation of palladium vinyl complexes by interaction of palladium monohydride species and free alkyne.**

The palladium vinyl complex can eliminate an alkene, or produce a chain growing product after insertion of a small molecule. The chemistry of palladium vinyl complexes are illustrated in Scheme 17.



**Scheme 17: Chemistry of palladium vinyl complexes**

#### 1.4.4.3 Palladium alkyl complexes:

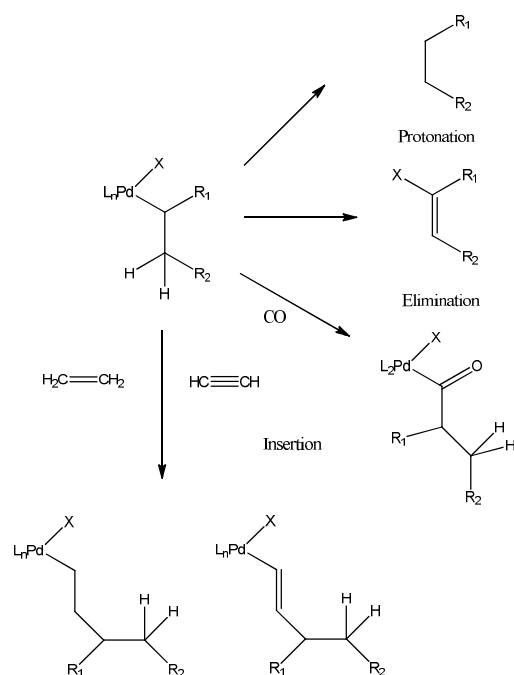
The first method to prepare palladium alkyl complexes involves the interaction of a palladium monohydride complex, and a free alkene, especially for ethene/ $CO$  co-polymerization and

## Chapter one

carbonylation. The second method involves oxidative addition of an alkyl halide to Pd(0) centre. Addition of benzyl chloride to Pd(PPh<sub>3</sub>)<sub>4</sub> gives PdCl(CH<sub>2</sub>Ph)(PPh<sub>3</sub>)<sub>2</sub>. This product dimerizes and yields a binuclear complex Pd<sub>2</sub>(Cl)<sub>2</sub>(CH<sub>2</sub>Ph)<sub>2</sub>(PPh<sub>3</sub>)<sub>2</sub>. This method applies to a wide range of alkyl and aryl halides.<sup>116</sup> A very similar complex, PdCl(Ph)(PPh<sub>3</sub>)<sub>2</sub> was prepared and characterized by <sup>31</sup>P NMR spectroscopy and XRD methods.<sup>117</sup> All of these examples involves the oxidative addition to Pd(0) species. No example for Pd(II) species have been reported. However, similar addition electron rich nickel (II) centres can be found to yield Ni(IV) alkyl products.<sup>118</sup>

The β-agostic interaction must be considered when dealing with palladium alkyl species. It also makes the β-elimination and hydrogen exchange possible. NMR experiments show evidence that this η<sup>3</sup>-η<sup>1</sup> conversion happens in solution, even the η<sup>1</sup> form is not thermally favoured. Kinetic study and experiments with labelled material ascribes *ortho*-hydrogen activation and hydrogen exchange to this η<sup>3</sup>-η<sup>1</sup> conversion.

The chemistry of palladium alkyl complexes are summarised in Scheme 18.



**Scheme 18: Chemistry of palladium alkyl complexes**

## 1.5 Parahydrogen and its NMR application

### 1.5.1 History, concept and preparation of parahydrogen

The concept of *parahydrogen* was proposed by Heisenberg in 1927. Pure *parahydrogen* was isolated one year later. However, its importance was not realized until the discovery of its applications in NMR.<sup>30,41,47,119,120</sup>

Dihydrogen contains four spin states:  $\alpha\alpha$ ,  $\beta\beta$ ,  $\alpha\beta+\beta\alpha$  and  $\alpha\beta-\beta\alpha$ . The first three isomers are triply degenerate and symmetric, and comprise *ortho*hydrogen. The  $\alpha\beta-\beta\alpha$  isomer is anti-symmetric and referred as *parahydrogen*. They are extremely close in energy therefore almost equally populated at room temperature. *Parahydrogen* is intrinsically the more stable, as its rotational quantum number can be as low as 0, because of the exclusion principle. This fact is exploited the production of *parahydrogen* at low temperature.

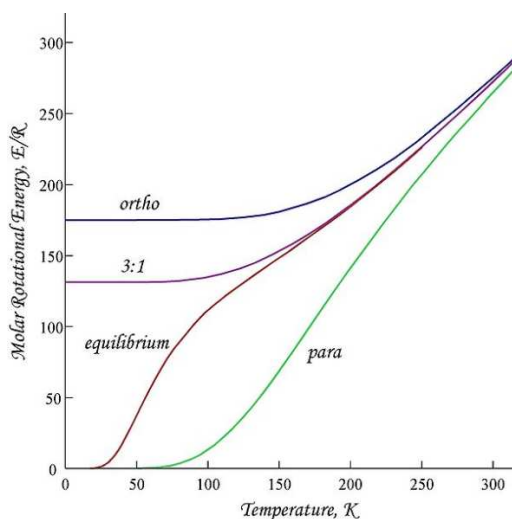


**Figure 11: The molar rotation energy of hydrogen on temperature<sup>1</sup>**

The proportion of *parahydrogen* increases when temperature is lowered. Figure 11 presents the temperature dependence of *ortho* and *parahydrogen* isomers. According to it, *parahydrogen* presents almost 100 % concentration at 20 K. Paramagnetic catalysts must be used to convert of *ortho*hydrogen to *parahydrogen*. *Parahydrogen* is stable for days in the absence of the catalyst. Figure 12 demonstrates the models of the equipments that are used to produce *parahydrogen* in York.

<sup>1</sup> picture taken from wikipedia, no further information given

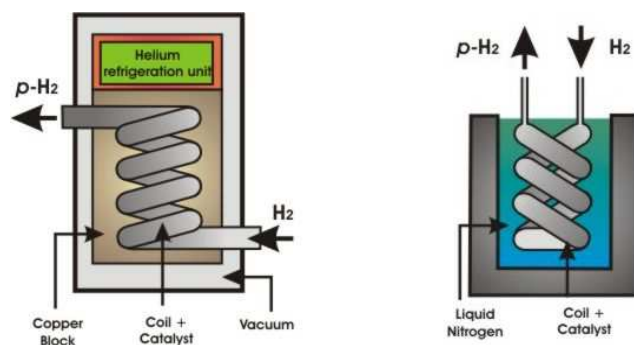
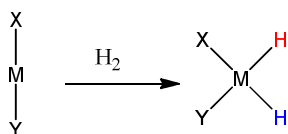


Figure 12: Left: A simple model for generating parahydrogen. Right: Schematic of the parahydrogen rig used at York<sup>2</sup>

### 1.5.2 NMR properties of *ortho* and *parahydrogen*

The two spins in *orthohydrogen* isomers are aligned; therefore the overall molecule has a net magnetic moment and can be observed in an NMR experiment. In *parahydrogen*, however, the spins are opposed, making it NMR silent. However, when *parahydrogen* reacts and its symmetry is broken, the *parahydrogen* effects can be seen provided the reaction proceeds in a spin correlated manner. This can be readily achieved when an  $MH_2$  containing product is formed and the two protons are magnetically inequivalent. (See Equation 5)



Equation 5: Oxidative addition of hydrogen to transition metal centre

When normal hydrogen is used in the reaction, the four spin combinations in dihydrogen are conserved in the new  $MH_2$  group. The NMR signals that are normally seen in a 1D NMR spectrum for such a species would be two doublets. The four possible configurations in the product are also populated approximately equally. Since the intensity of an NMR signal is proportional to the population difference between the energy levels, the number of nuclei capable of undergoing transitions is small, leading to a signal that is normally of very low intensity. This situation is illustrated in Figure 13-a, where approximately 1 in 30,000 nuclei are capable of undergoing a detectable transition at a field of 9.4 T. If only one of the spin configurations of hydrogen, the  $\alpha\beta$ - $\beta\alpha$  state, is used, it would selectively populate only two of

<sup>2</sup> Pictures taken from the SBD group website

the spin states in the product. Because of the resultant hyperpolarisation, a term used to indicate the populations of each energy level are different to the usual Boltzmann distribution, the NMR signals of the product are greatly increased. This phenomenon has been termed as *Parahydrogen Induced Polarization (PHIP)*.<sup>41</sup> It is easy to see if the enhancement has worked, since the resultant signals are now antiphase; one set in absorption and the other in emission. This situation is illustrated in Figure 13-b. **Section 1.5.5** shows how this work when  $\text{IrCl}(\text{CO})(\text{PMePh}_2)_2$  was used.

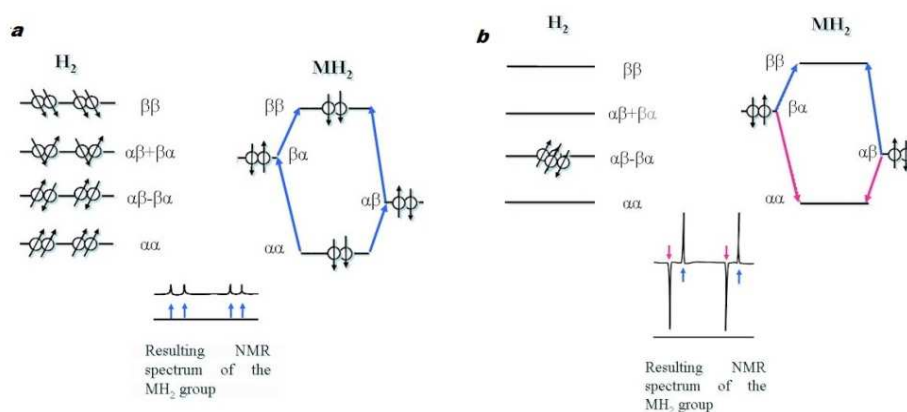


**Figure 13:** (a): A normal NMR experiment on a  $\text{MH}_2$  moiety without hyperpolarisation. (b): An NMR experiment on a  $\text{MH}_2$  moiety formed after reacting with the parahydrogen.

The term ‘One-Proton PHIP’ is used to describe the reactions in which only one proton ends up into the new organic product. This phenomenon is based on a strong coupling in the dihydride species before reductive elimination. The enhancement factor for One-Proton PHIP is normally much smaller than PHIP. One-Proton PHIP was observed for the  $-\text{CHO}$  signal, when  $\text{cis-PtCl}_2(\text{CO})(\text{PPh}_3)\text{-SnCl}_2$  catalyses the hydroformylation of 1-hexane.<sup>121</sup>

### 1.5.3 NMR programs and terms related with this study

#### 1.5.3.1 Homonuclear Correlation spectroscopy (COSY)

Homonuclear correlation spectroscopy (COSY) is the most popular 2D NMR experiment. It correlates spins from single isotopes that couple with each other. A standard  $90^\circ$  COSY sequence consists of a preparation time (single pulse, p1), evolution time (t1), a mixing period (single pulse p2) and measurement period (t2). The COSY sequence is illustrated in Figure 14.

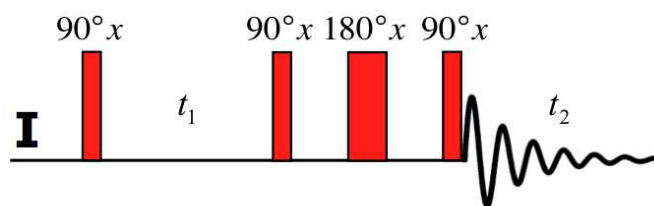


Figure 14: The 2D  $^1\text{H}$ - $^1\text{H}$  COSY pulse sequence

A typical COSY dataset contains two types of peaks; the diagonal peaks that correspond to peaks in the 1D NMR experiment, and cross peaks which indicate the couplings between pairs of nuclei. Cross peaks result from a phenomenon called magnetization transfer, and their presence indicates that two nuclei are coupled which have the two different chemical shifts that make up the cross peak's coordinates. The COSY sequence is not only useful for  $^1\text{H}$ , but also applies to  $^{31}\text{P}$  and  $^{13}\text{C}$  that contains stable  $\frac{1}{2}$  spin states.

#### 1.5.4.2 Heteronuclear correlation spectroscopy (HMQC)

Heteronuclear correlation spectroscopy gives signals based upon coupling between nuclei of two different types. Often one of the two nuclei are protons and another "heteronucleus". This is because the low natural abundance of most heteronuclei would result in the proton spectrum being overwhelmed with signals from molecules with no active heteronuclei, making it useless for observing the desired, coupled signals. With the advent of techniques for suppressing these undesired signals, inverse correlation experiments such as HSQC, HMQC, and HMBC are actually much more common today. The HMQC experiment provides correlation between protons and their attached heteronuclei through the heteronuclear scalar coupling; while the HQSC experiment detects long range coupling between proton and carbon (two or three bonds away) with great sensitivity.

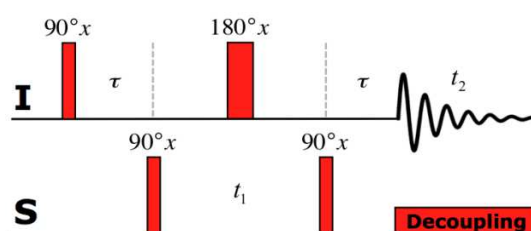
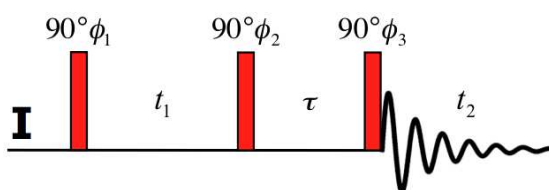


Figure 15: The 2D HMQC sequence

### 1.5.4.3 NOESY

In NOESY, the nuclear overhauser cross relaxation between nuclear spins during the mixing period is used to establish the correlations. The spectrum obtained is similar to COSY, with diagonal peaks and cross peaks, however the cross peaks connect resonances from nuclei that are spatially close rather than those that are through-bond coupled to each other. NOESY spectra also contain extra axial peaks which do not provide extra information and can be eliminated through a difference experiment by reversing the phase of the first pulse.



**Figure 16: The NOESY sequence**

The pulse sequence consists of three  $90^\circ$  pulses. The first and second pulses are separated by the variable time  $t_1$ , followed by a constant mixing time  $\tau_m$ , the third pulse and the acquisition of the FID.

### 1.5.4.4 $\pi/4$ pulse NMR experiments

In order to observe the polarisation of protons resulting from *parahydrogen*, all pulse programs need to be modified to have a  $45^\circ$  pulse angle. A  $90^\circ$  pulse will tilt the spins in such a way that they cancel, and the signals will completely disappear. This simple change can be made to any pulse program and as a result, PHIP can be performed on a multitude of experiments, including 2D experiments. Using an HMQC sequence, it is possible to sensitise heteronuclei in a molecule, an essential technique for identified the species detected with PHIP.

### 1.5.4.5 OPSY

As discussed in **Section 1.5.1**, the inherent low sensitivity of NMR method can be overcome by signal amplification due to adding *parahydrogen*. However, the background of other thermal resonance must be seriously considered. In a catalytic reaction with 100 fold substrate to catalyst, given the signals of a reaction intermediate, which represent 1 % of the catalyst concentration, are enhanced by 1000 fold, the ratio of hyperpolarized signal to the

## Chapter one

background is still 1 : 10.<sup>122</sup> That means that there is still a large possibility that the polarized signals are masked by other thermal signals due to the substrate and the solvent. A solution to suppress the background was using fully deuterated substrate.<sup>46</sup> However, this method is expensive for routine research.

Only *parahydrogen* spectroscopy (OPSY) was developed to suppress the thermal signals by using a PFG based quantum coherence filter. This method was not only applicable to 1D experiment but also to 2D COSY and HMQC experiments. Figure 17 illustrated the pulse sequence of 1D and 2D HMBC experiments. By suppressing the thermal proton signals, OPSY also allows the replacement of deuterated solvents by protio solvents.

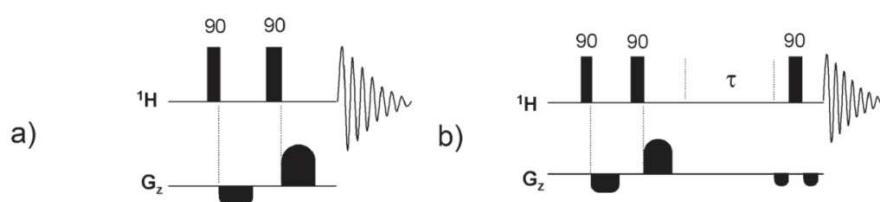


Figure 17: The OPSY program a):  $^1\text{H}$ ; b): 2D  $^1\text{H}$ - $^1\text{H}$  COSY

### 1.5.4.6 Virtual coupling

The term ‘virtual coupling’ was defined by Reich as follows:<sup>123</sup>

*‘Virtual coupling refers to an NMR phenomenon in which apparently first-order multiplets contain false coupling information. In extreme cases, protons that are not actually coupled will show splitting. More commonly, the magnitude of coupling constants obtained by first-order analysis is incorrect.’*

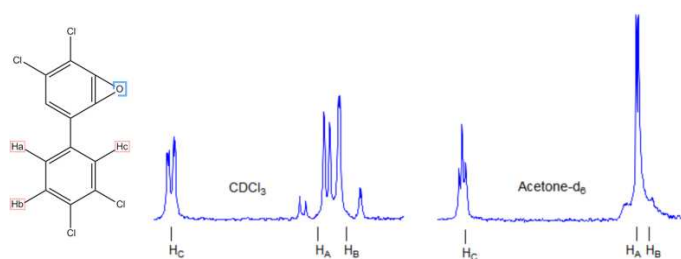


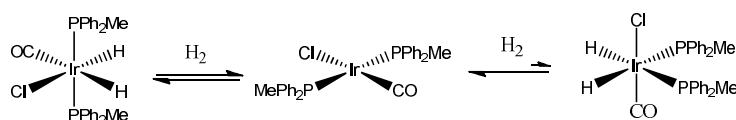
Figure 18: The  $^1\text{H}$  NMR spectrum recorded in acetone- $d_6$  shows virtual coupling, in contrast of that in  $\text{CDCl}_3\text{-}d_1$



This phenomenon can be demonstrated using the compound as shown in Figure 18. In its  $^1\text{H}$  NMR spectrum,  $\text{H}_\text{A}$  and  $\text{H}_\text{B}$  are quasi-first order in  $\text{CDCl}_3$ , However, when acetone- $\text{d}_6$  was used, now  $\text{H}_\text{A}$  and  $\text{H}_\text{B}$  are superimposed, the  $\text{H}_\text{C}$  appears as a triplet, as if  $\text{H}_\text{A}$  and  $\text{H}_\text{B}$  were equally coupled to  $\text{H}_\text{C}$ .

#### 1.5.4: An example of PHIP

Vaska's complex,  $\text{IrCl}(\text{CO})(\text{PPh}_3)_2$  is known to reversibly add dihydrogen to form the six coordinate Ir(III) dihydride species *cis-trans*- $\text{Ir}(\text{H})_2\text{Cl}(\text{CO})(\text{PPh}_3)_2$ .<sup>27,124</sup> The *cis-cis*-isomer of  $\text{Ir}(\text{H})_2\text{Cl}(\text{CO})(\text{PPh}_3)_2$  is not thermally favoured and cannot be detected by normal NMR experiments.<sup>26</sup> As part of my research, the  $\text{PPh}_2\text{Me}$  analogue  $\text{IrCl}(\text{CO})(\text{PPhMe}_2)_2$  was prepared and its reaction with *parahydrogen* was examined.



**Scheme 19: Oxidative addition of hydrogen to Vaska's complex *trans*- $\text{IrCl}(\text{CO})(\text{PMePh}_2)_2$  gives *cis-trans*- $\text{Ir}(\text{H})_2\text{Cl}(\text{CO})(\text{PPh}_3)_2$**

Figure 19 illustrates the hydride region of the  $^1\text{H}$  NMR spectrum when  $\text{IrCl}(\text{CO})(\text{PPhMe}_2)_2$  reacts with *parahydrogen*. The enhanced signals for the  $\text{Cl}$ - $\text{Ir}$ - $\text{CO}$  axis addition product *cis-trans*- $\text{Ir}(\text{H})_2\text{Cl}(\text{CO})(\text{PPh}_2\text{Me})_2$  are observed at  $\delta$  -8.36 and  $\delta$  -17.76. Figure 20 illustrated the  $^1\text{H}$  NMR spectra when dq-OPSY pulse was used, suggesting the two hydride ligands are from the same *parahydrogen* molecule. The enhancement of these two signals is estimated to be 2000 by comparing their intensities with a thermal spectrum, as shown in Figure 20. Figure 19 shows how the  $\text{P}$ - $\text{Ir}$ - $\text{P}$  axis addition product, *trans-trans*- $\text{Ir}(\text{H})_2\text{Cl}(\text{CO})(\text{PPh}_3)_2$  was detected, which is not seen if normal hydrogen was used. In addition, Figure 21 shows the single-scan  $^{31}\text{P}$  NMR spectra of *cis-trans*- $\text{Ir}(\text{H})_2\text{Cl}(\text{CO})(\text{PPh}_3)_2$ , whereas the  $^{31}\text{P}$  NMR signals for other species are almost invisible. The enhancement for this signal was estimated to be 8.

Chapter one

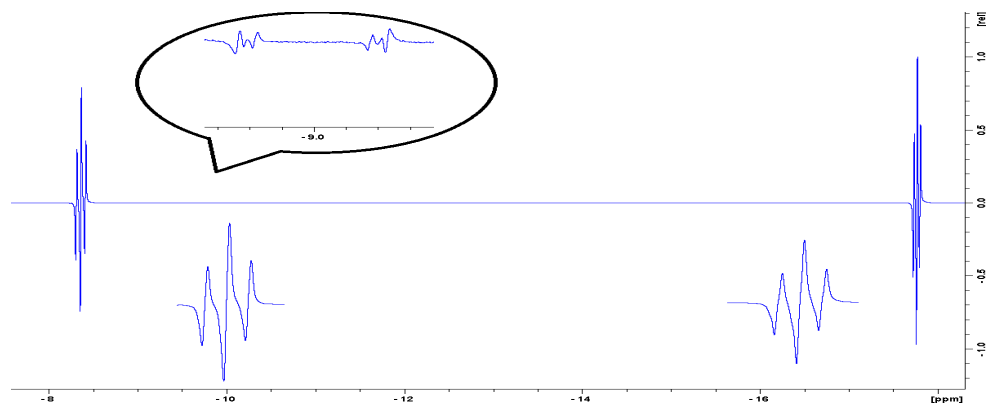


Figure 19: The  $^1\text{H}$  NMR spectra showing the formation of *cis-trans-Ir(H)<sub>2</sub>Cl(CO)(PPh<sub>3</sub>)<sub>2</sub>* by reacting *IrCl(CO)(PPh<sub>3</sub>)<sub>2</sub>* with parahydrogen

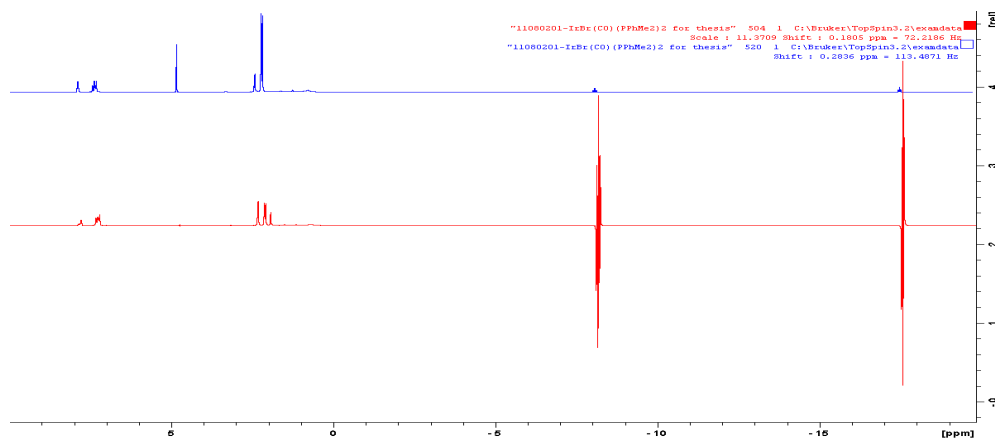


Figure 20: Comparison of the thermal hydride signals shows an enhancement of 2000 for *cis-trans-Ir(H)<sub>2</sub>Cl(CO)(PPh<sub>3</sub>)<sub>2</sub>*

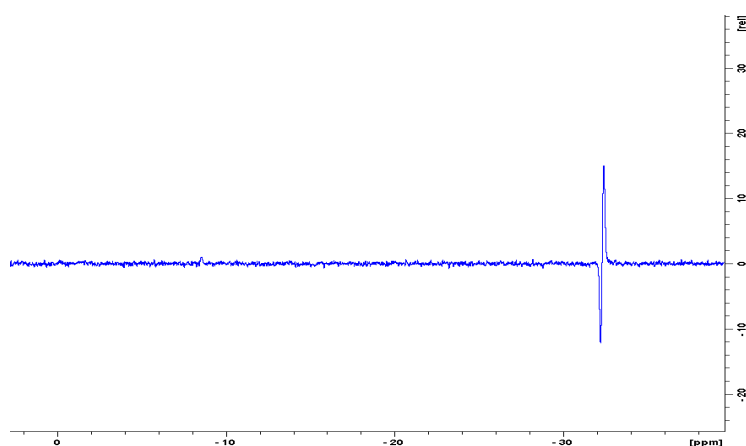


Figure 21: A  $^{31}\text{P}$  NMR spectrum of *cis-trans-Ir(H)<sub>2</sub>Cl(CO)(PPh<sub>3</sub>)<sub>2</sub>*, an enhancement factor of 8 was estimated for this signal

## 1.5.5 Applications of PHIP

### 1.5.5.1 On detecting organometallic species:

As we have discussed above, *parahydrogen* induced polarization (PHIP), in conjunction with corresponding NMR experiments, is a very useful method for mechanistic study, Table 11 summarizes NMR sequences variants. The most direct use of PHIP is the detection of hydrogen addition products. A example is, when *parahydrogen* was added to  $\text{RhCl}(\text{PPh}_3)_3$ , the enhanced signal due to  $\text{RhCl}(\text{H})_2(\text{PPh}_3)_3$  was detected.<sup>20</sup> however, this method also applies to the detection of other spin  $\frac{1}{2}$  heteronucleus.

**Table 11: The NMR pulse sequences used in *parahydrogen* related study**

Pulse programs	Aims
	Sites containing p-H <sub>2</sub> enhanced signals
COSY	Homonuclei signals via scalar couplings
nOe	Spatial arrangement of nuclei
HMQC	Heteronuclei signals via scalar couplings
EXSY	Site exchange and reaction kinetics
MRI	Images

The detection of other spin  $\frac{1}{2}$  heteronucleus is even harder than proton using normal NMR sequences. The sensitivities of  $^{19}\text{F}$ ,  $^{31}\text{P}$ ,  $^{13}\text{C}$ ,  $^{15}\text{N}$  decrease by factors of 1.2, 15, 64 and  $10^4$  respectively, compared with  $^1\text{H}$ . The characterization is further exacerbated if the natural abundances are taken into account ( $^{13}\text{C}$ , 1.108%,  $^{15}\text{N}$ , 0.37%), which reduces the sensitivities of  $^{13}\text{C}$  and  $^{15}\text{N}$  to 1 :  $1.2 \times 10^8$  and 1 :  $8.7 \times 10^9$  respectively. However, the NMR signals for these nuclei can be enhanced by scalar coupling with hydride ligand, which has a *parahydrogen* origin. When  $[\text{Ir}(\text{H})_2(\text{PCy}_3)(\text{Py})_3][\text{BF}_4]$  and free pyridine were used as the catalyst and substrate and a single scan  $^{13}\text{C}$  experiment was recorded, 823 fold polarization on pyridine was observed. If standard pulse with 20 seconds recovery delay was used for this experiment, 67000 scans (three months) are necessary to obtain the spectrum of the same quality.

### 1.5.5.2 On the mechanistic studies

Studies have been investigated into the hydrogenation and hydroformylation mechanism using PHIP by characterizing low-concentration intermediates and studying the kinetic

## Chapter one

behaviour of those species. The hydrogenation mechanism of Wilkinson's catalyst was studied by PHIP.<sup>20</sup> Specifically, when the reaction between  $\text{RhCl}(\text{PPh}_3)_3$  and styrene was examined, an  $\text{Rh}(\text{alkene})\text{Cl}(\text{PPh}_3)_2(\text{H})_2$  type species was detected. The NMR signal from this compound was not seen unless *parahydrogen* was used. The detection of dihydride species confirmed the original proposal on this reaction.

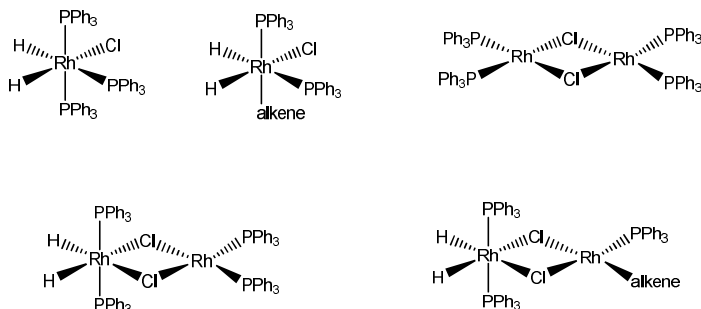


**Figure 22: Intermediates that were detected for the hydrogenation of alkenes using  $\text{Rh}(\text{Cl})(\text{PPh}_3)_3$  catalyst**

Dimeric species were also observed in the reaction.  $\text{Rh}(\text{Cl})(\text{PPh}_3)_3$  is known to dimerise to  $[\text{RhCl}(\text{PPh}_3)_2]_2$  in solution.<sup>20</sup> Reaction of  $[\text{RhCl}(\text{PPh}_3)_2]_2$  with parahydrogen leads to the formation of  $\text{Rh}(\text{H})_2(\text{PPh}_3)_2(\mu\text{-Cl})_2\text{Rh}(\text{PPh}_3)_2$  and  $[\text{Rh}(\text{H})_2(\text{PPh}_3)_2(\mu\text{-Cl})_2]_2$ . In the presence of an alkene substrate, signals for  $\text{Rh}(\text{H})_2(\text{PPh}_3)_2(\mu\text{-Cl})_2\text{Rh}(\text{PPh}_3)(\text{alkene})$  were also detected. The direct hydrogen transfer of  $\text{Rh}(\text{H})_2(\text{PPh}_3)_2(\mu\text{-Cl})_2\text{Rh}(\text{PPh}_3)(\text{alkene})$  into ethylbenzene proceeded at a rate of  $1 \text{ s}^{-1}$  at 295 K. These results confirmed that the opportunity to produce binuclear resting states when bridging ligands are present.

### 1.5.5.3 Other applications of PHIP

It has also been shown that polarisation transfer, from parahydrogen, cannot only occur through hydride transfer, which makes it possible for the associated NMR signal from catalytic species and hydrogenated product to be enhanced. But also via by scalar coupling with other nucleus allowing corresponding ligands to polarized. The latter routine, termed Signal Amplification by Reversible Exchange (SABRE), has potential clinic applications on NMR imaging.<sup>41,119,125</sup>

## 1.6 Aim on Ir/Rh catalysed hydroformylation

Part of this thesis focuses on the mechanistic studies on hydroformylation and hydrogenation, using Ir/Rh allyl compounds as the catalysts. The chemistry, NMR properties and fluxionality of transition allyl compounds are presented in **Section 1.6.1**.

### 1.6.1 Why Ir/Rh allyl complexes

#### 1.6.1.1 Ligand hapticity

The allylic metal compounds are a large family. They can contain allyl ligand only, such as  $M(\text{allyl})_2$ , ( $M = \text{Ni, Pd, Pt}$ ),  $M(\text{allyl})_3$  ( $M = \text{Co, Rh, Ir}$ ), or compounds with ‘mixed’ ligands such as phosphines, halides, pyridine,  $\text{Cp}^-$ , COD, etc.<sup>126-131</sup> Some of the metal allyl complexes, especially the palladium and nickel species, are good precursors or intermediates for the coupling reaction of carbon and other nucleus.<sup>132-134</sup> There are generally two types allyl ligand hapticity: the  $\eta^3$  form and the  $\eta^1$  form, as shown in Figure 23. The hapticity of allyl ligands can be studied by IR and NMR methods.

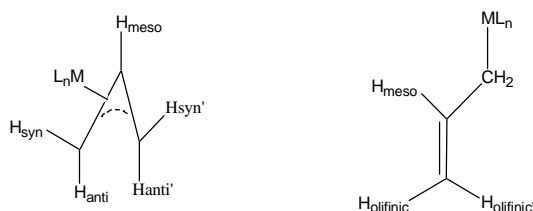


**Figure 23:** The hapticity of the allyl ligand, the  $\eta^3$  form and the  $\eta^1$  form

#### 1.6.1.2 Spectroscopic properties

In the  $\eta^3$  allyl group, all of the three carbons are interacting with the metal centre through a delocalized  $\pi$  system. The *anti*-protons are closer to the metal centre in geometry, so they will project on the metal coordination sphere and cause destabilizing effect. Therefore the *anti*-protons will resonate at higher field than the *syn* hydrogens due to the different shielding effect. In the proton spectrum of the  $\eta^3$ -allyl group, The  $H_{\text{meso}}$  normally appear from  $\delta$  4.5 to  $\delta$  5.5; while the  $H_{\text{syn}}$  is mostly seen between  $\delta$  2.5 to  $\delta$  3.0. The  $H_{\text{anti}}$  generally appears from  $\delta$  2 to  $\delta$  2.5. Two *syn* protons or *anti* protons are sometimes equivalent due to fluxionality.

In the  $\eta^1$ -allyl group, two vinyl protons resonate near  $\delta$  5.0 as two doubles, while the  $H_{\text{meso}}$  is normally found at lower field from  $\delta$  5.9 to  $\delta$  6.8. The chemical shift of  $\text{CH}_2$  protons is more

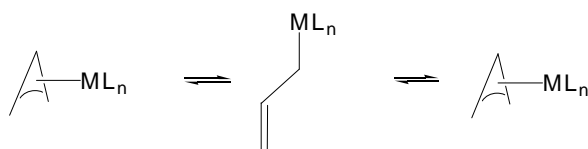
## Chapter one

dependent on the metal centre it was attached to, typically  $\delta$  2.5 - 2.8 if they are binding to a metal centre,  $\delta$  3.5 - 4.1 if bonded to CO-metal unit.

The  $\eta^3$  allyl has a characteristic infrared absorption at  $1455\text{ cm}^{-1}$ , which is typical delocalized C-C stretching frequency.

### 1.6.1.3. The $\pi$ - $\sigma$ interconversions of allyl ligands

The metal allyl complexes are generally more stable than corresponding alkene adducts, however, most of the rhodium and cobalt allyl compounds are very sensitive to air. The other disadvantage of rhodium allyl complexes is the tendency for C-C coupling and C-H activation. Although there are also other routes for the decompositions include disproportion and C-H activation. We believe the  $\pi$ - $\sigma$ - $\pi$  inter conversion plays important role in the decomposition and many other reactions like ligand exchange, oxidation-addition, and ligand isomerization.



**Scheme 20: the  $\pi$ - $\sigma$ - $\pi$  mechanism that explains allyl isomerization.**

Some of the metal-allyl compounds are fluxional molecules. There are two reasons cause the fluxion behaviour: the  $\pi$ - $\sigma$ - $\pi$  inter-conversion and the allyl rotation. The  $\pi$ - $\sigma$ - $\pi$  inter-conversion involves unsaturated intermediate, which can be trapped by pyridine ligands, while the allyl rotating does not results in new unsaturated species. NMR methods were again a useful tool to provide information to reveal how this dynamic progress happens by analysis the line shape of the  $^1\text{H}$  and  $^{31}\text{P}$  NMR spectra at variable temperatures.

### 1.6.1.4 The fluxional behaviour of the allyl group

The fluxional molecules are defined as molecules that can interconvert rapidly with respect to a reference time scale. The most common timescale for nuclear magnetic spectroscopy is millisecond ( $10^{-3}$  s). The rate constant for this inter-conversion is given by the Eyring equation.<sup>135</sup>

## 1.6.2 Aim on $M(\eta^3\text{-C}_3\text{H}_5)(\text{CO})(\text{PPh}_3)_2$ (where $M = \text{Rh}, \text{Ir}$ ) catalyzed hydroformylation

### 1.6.2.1 Background

Studies on alkene hydroformylation are extensive.<sup>15,17,22,34,44,53,55,59,60,82,83,90,136-143</sup> However, very little attention has been focussed on the hydroformylation of dienes. The mechanism of the hydroformylation of dienes is not as clear as that for alkenes. The Ir/Rh allyl complexes are key intermediates in this process.<sup>51,75,140</sup>

The first example of transition metal allyl complexes is  $\text{Ir}(\eta^3\text{-C}_3\text{H}_5)_3$ , however, the structure and chemistry of  $M(\eta^3\text{-C}_3\text{H}_5)_3$  (where  $M = \text{Ir}, \text{Rh}$ ), were not fully realized until recently.<sup>126,128,144,145</sup> Shaw reported a group of air stable rhodium allyl complexes and their conversion with each other.<sup>52</sup> However, the importance of transition metal allyl complexes in catalysis were not realized until Wilkinson's study on  $M(\eta^3\text{-C}_3\text{H}_5)(\text{CO})(\text{PPh}_3)_2$  ( $M = \text{Rh}, \mathbf{14}, \text{Ir}, \mathbf{15e}$ ).<sup>75</sup> The study of  $\text{Rh}(\eta^3\text{-C}_3\text{H}_5)(\text{CO})(\text{PPh}_3)_2$  in hydroformylation was not possible due to its high fluxionality and poor stability. NMR characterization of  $\text{Rh}(\eta^3\text{-C}_3\text{H}_5)(\text{CO})(\text{PPh}_3)_2$  gives little information due to their fluxional behaviour.

### 1.6.2.2 Precursors

In my research, I have prepared the five iridium compounds,  $\text{Ir}(\eta^3\text{-C}_3\text{H}_5)(\text{CO})(\text{PR}_2\text{R}')_2$  (**15a-15e**, where **15a**,  $\text{PR}_2\text{R}' = \text{PMe}_3$ ; **15b**,  $\text{PPhMe}_2$ ; **15c**,  $\text{PPh}_2\text{Me}$ ; **15d**,  $\text{P}(p\text{-tol})_3$ ; **15e**,  $\text{PPh}_3$ , as hydroformylation precursors. Their structures are shown in Figure 24.

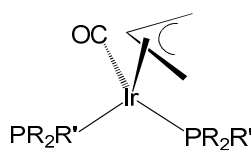


**Figure 24: Structures of 15a-15e**

The rhodium analogue  $\text{Rh}(\eta^3\text{-C}_3\text{H}_5)(\text{CO})(\text{PPh}_3)_2$  (**14**) is highly unstable even in solid state. Therefore, a similar stable complex,  $\text{Rh}(\eta^3\text{-C}_3\text{H}_5)(\text{PPh}_3)_2$  (**16**), was prepared. It is expected to yield  $\text{Rh}(\eta^3\text{-C}_3\text{H}_5)(\text{CO})(\text{PPh}_3)_2$  *in-situ* on exposing to CO. The structure of **16** is shown in Figure 25.

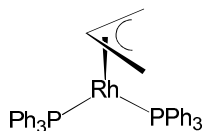


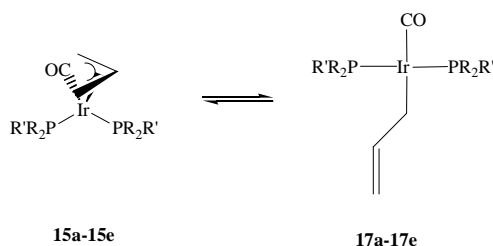
Figure 25: Structure of 16

### 1.6.2.3 Fluxionality and Characterization

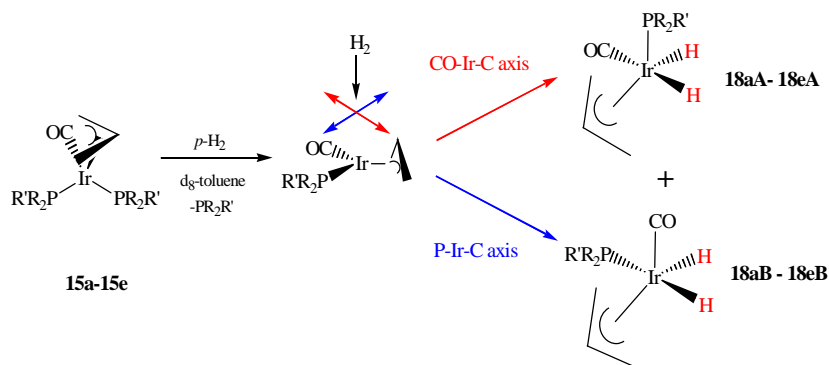
Whilst these compounds are known, their fluxional behaviour received little attention. As we discussed in **Section 1.6.1.4**, two reasons bring fluxionality to the complexes that contains allyl ligand, the  $\pi$ - $\sigma$ - $\pi$  inter-conversion and allyl rotation. They can be studied by both chemical and analytical methods. In my studies, pyridine was used to trap the  $\eta^1$  form of these species, whereas the analytical methods aids in calculating the exchange rates and other thermal parameters by analysing the corresponding  $^{31}\text{P}$  NMR spectrum, which was obtained over a temperature range from 188 K to 298 K

### 1.6.2.4 Expected reaction of $\text{Ir}(\eta^3\text{-C}_3\text{H}_5)(\text{CO})(\text{PR}_2\text{R}')_2$ (**15**) with $\text{H}_2$

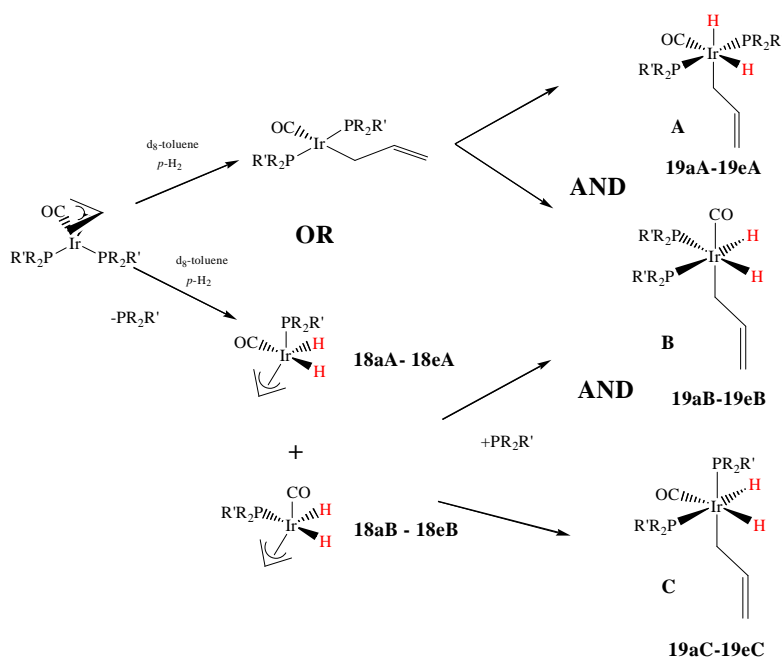
We are expecting the following changes to occur in solution when  $\text{H}_2$  reacts with  $18e^-$  compound  $\text{Ir}(\eta^3\text{-C}_3\text{H}_5)(\text{CO})(\text{PR}_2\text{R}')_2$  (**15**). Firstly, if  $\text{Ir}(\eta^3\text{-C}_3\text{H}_5)(\text{CO})(\text{PR}_2\text{R}')_2$  (**15**) were to add  $\text{H}_2$  directly it must do so as the  $16e^-$   $\eta^1$  form **17**, as shown in Equation 6; Secondly, If  $\text{H}_2$  addition were to occur to the  $\eta^3$  form, a ligand must be lost from  $\text{Ir}(\eta^3\text{-C}_3\text{H}_5)(\text{CO})(\text{PR}_2\text{R}')_2$  in order to generate the necessary vacant coordination site and the required 16 electron count, as shown in Scheme 21. This ligand could be either CO or phosphine. Products **18** and **19** with the structures shown in Scheme 22 are therefore the expected products resulting from phosphine loss. It should be noted that **18** can be converted into **19** by the addition of phosphine after an initial allyl hapticity change from  $\eta^3$ - $\eta^1$ .

Equation 6: The  $\eta^3$ - $\eta^1$  conversion of  $\text{Ir}(\eta^3\text{-C}_3\text{H}_5)(\text{CO})(\text{PR}_2\text{R}')_2$



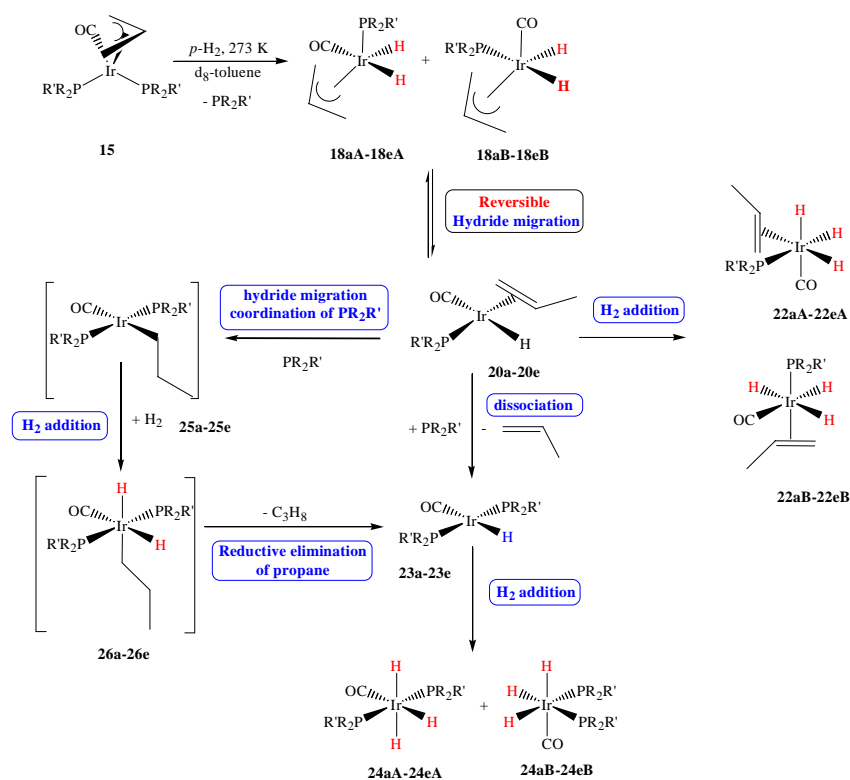


**Scheme 21:** Expected  $H_2$  addition products after ligand loss



**Scheme 22:** Further products that are expected to see by hydrogen addition to **15**

However, compound **18** should also be able to undergo hydride transfer to one of the carbon centres of the allyl ligand. This process results in the formation of the  $16e^-$  alkene complex  $IrH(CO)(PR_3)(propene)$  (**20**). Should parahydrogen be used, and the hydride exchange process be reversible, then PHIP would be expected to be seen in **20**, or  $IrH(CO)(PR_3)_2(propene)$  (**21**) after phosphine association. Subsequent trapping by  $H_2$  rather than phosphine would be predicted to lead to  $IrH_3(CO)(PR_3)(propene)$  (**22**) with either further hydrogenation or propene dissociation being possible. These chemical changes are illustrated in Scheme 23. Figure 26 provides a list of the potential reaction intermediates that might therefore be detected by PHIP.



**Scheme 23:** Possible reactions pathways for the  $H_2$  addition products, 15a-15e, to form the related trihydride complexes and either propene or propane.

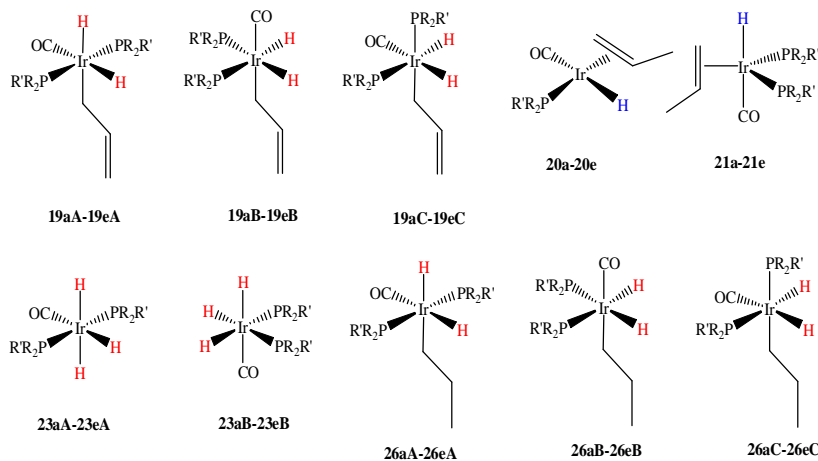
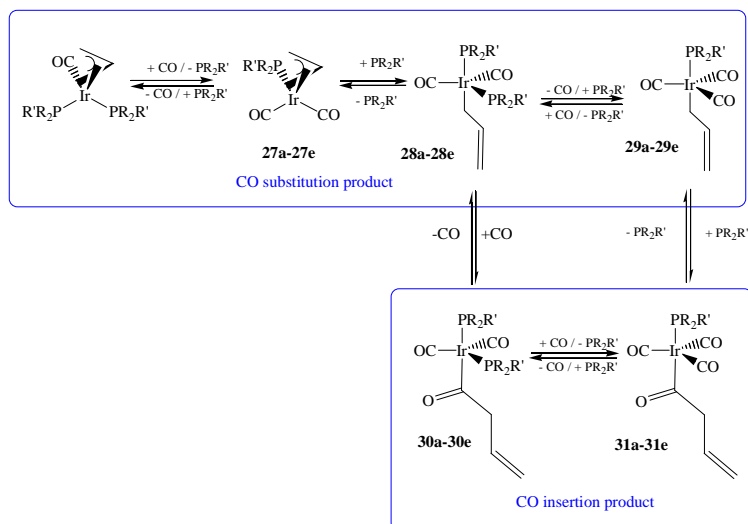


**Figure 26:** Possible reaction intermediates that could be detected during the hydrogenation of the allyl ligand in compounds 15a-15e, according to the routes described in the text

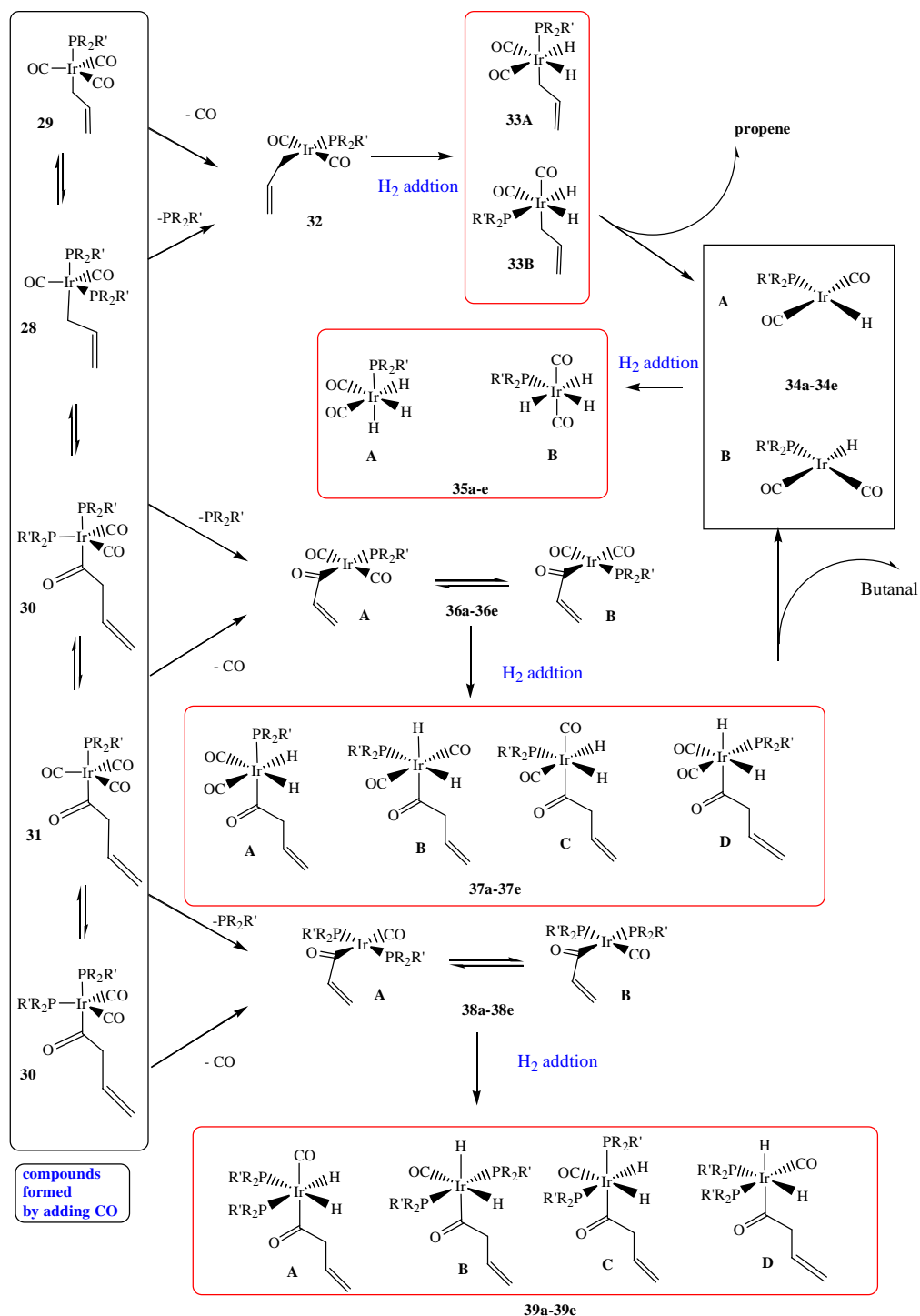
### 1.6.2.5 NMR study on the reaction of $Ir(\eta^3-C_3H_5)(CO)(PR_2R')_2$ with $CO/H_2$

The possible reaction pathways associated with the reaction of **15** with CO are shown in Scheme 24. When **15** is treated with carbon monoxide, the carbonyl ligand might exchange

with the free carbon monoxide to give **27**, which could possibly be detected at this point. Further CO substitution will occur to form **28** or **29**. These reactions are reversible in the P-*(p-tol)*<sub>3</sub> and PPh<sub>3</sub> case, to form equilibrium of **27d-27e**, **28d-28e**, and **29e-29e** according to previous study in our group.<sup>32</sup> The acyl species **30** and **31** are formed by CO insertion. Scheme 24 illustrates possible reactions when compound **15** is treated with CO.



**Scheme 24:** Possible ligand substitution and CO insertion products formed in the reaction of complexes **12a-12e** and carbon monoxide.



**Scheme 25: Proposed hydroformylation mechanism involving Ir(η<sup>3</sup>-C<sub>3</sub>H<sub>5</sub>)(CO)(PR<sub>2</sub>R')<sub>2</sub> and the key reaction intermediates that are expected to be involved. Complexes in red square show PHIP**

According to our previous study, If H<sub>2</sub> is present at this stage; compounds **28** and **29** are expected to add hydrogen after losing a phosphine or carbonyl ligand rather than insert a CO ligand to form a 16e<sup>-</sup> compound **17** or **32**. This progress was considered to be the side

reaction (hydrogenation) and can be suppressed by adding a large excess CO. The CO insertion product, **30** and **31** are expected to add hydrogen likewise, to form dihydride species **37** and **39**. They are expected to eliminate butanal and form  $\text{IrH}(\text{CO})_2(\text{PR}_2\text{R}')_2$ . (**34**) or  $\text{IrH}(\text{CO})_2(\text{PR}_2\text{R}')_2$ . (**23**) The formation of **23** and **34** suggests the accomplishment of a catalytic cycle. These processes are illustrated in Scheme 25. We should note the rhodium and cobalt analogues of compound **23**, which is the real catalytic precursor, can be generated by ligand loss and exchange from the widely used catalyst  $\text{HM}(\text{CO})(\text{PR}_2\text{R}')_3$ , where  $\text{M} = \text{Co}, \text{Rh}$ .

In general, we are expecting to see *parahydrogen* enhancement on compounds **19**, **20**, **21**, **23** and **26** in the hydrogenation progress, as shown in Figure 26, and **33**, **35**, **37**, and **39** in the hydroformylation progress, as shown in Scheme 25. Signals for organic products, propene, propane or butanal could also be polarized. A full map of hydroformylation will be illustrated by detecting these *in-situ* species.

## 1.7 Aim on Pd catalysed carbonylation

### 1.7.1 Background

The palladium complex  $[(\text{BCOPE})\text{Pd}(\text{CH}_3\text{OH})_2](\text{OTf})_2$  (**12a**) and is an efficient catalyst for the hydroformylation of internal alkenes.<sup>143,146,147</sup> Previous studies in York suggested that **12a** also catalyze the selective hydrogenation of diphenyl acetylene.<sup>46</sup> In these studies,  $(\text{BCOPE})\text{PdH}^+$  (**13a**) is proposed to be the catalytic species. NMR study revealed the presence of the pyridine adduct of **13a** and three additional intermediates: **40a-1**, **40a-2**, and **41**, as shown in Figure 29 and Figure 27 respectively.

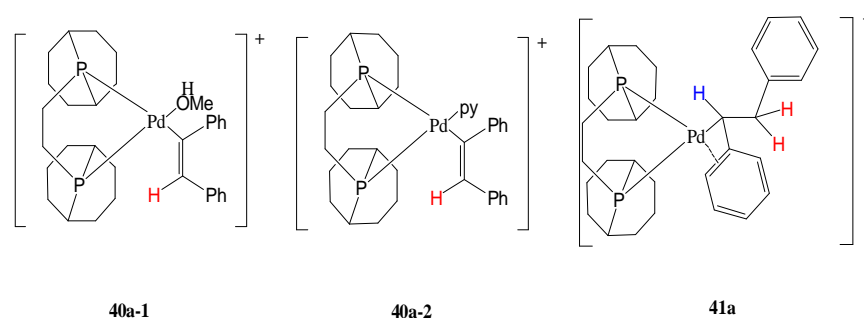


**Figure 27: Intermediates that are detected during the  $[(\text{BCOPE})\text{Pd}(\text{OH}_2)_2](\text{OTf})_2$  catalysed hydrogenation of diphenyl acetylene**

## Chapter one

### 1.7.2 Precursors

In my research, two catalyst precursors were prepared to study the carbonylation of diphenyl acetylene. Their structures are illustrated in Figure 28. They are expected to catalyse the carbonylation of a range of alkyne substrates.

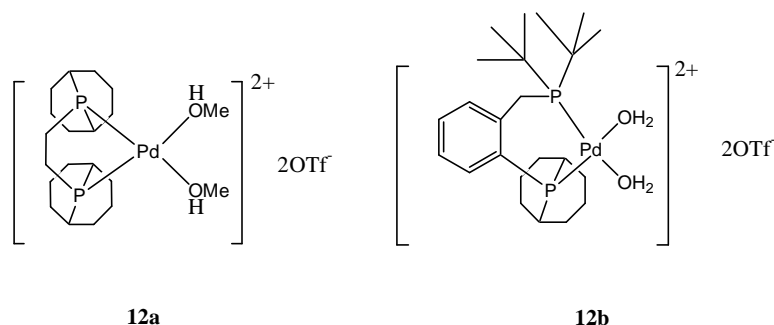


Figure 28: Structure of carbonylation catalysts in my research

### 1.7.3 Study on palladium catalysed carbonylation

The proposal of this research will be presented using  $[(\text{BCOPE})\text{Pd}(\text{CH}_3\text{OH})_2](\text{OTf})_2$  (**12a**) in the following section.

**12a** is expected to be reduced by methanol, to yield the hydride species **13a**.<sup>146</sup> Complex **13** can also be trapped by OTf, methanol, CO, or pyridine. If CO is present, a stable dimeric complex  $[(\text{BCOPE})\text{Pd}(\mu\text{-H})(\mu\text{-CO})\text{Pd}(\text{BCOPE})]$  (**43**) could also be formed. All of these species could be in equilibrium with **13**. Figure 29 illustrates the structure of the monohydride species that might be detected in my study.

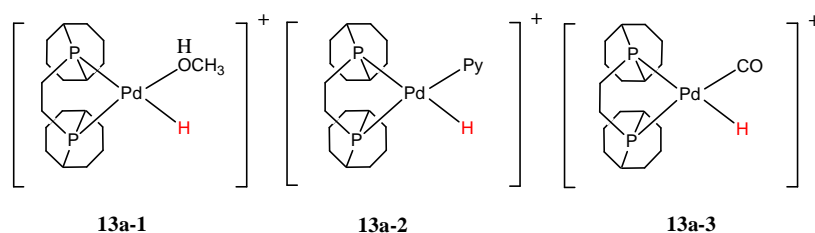
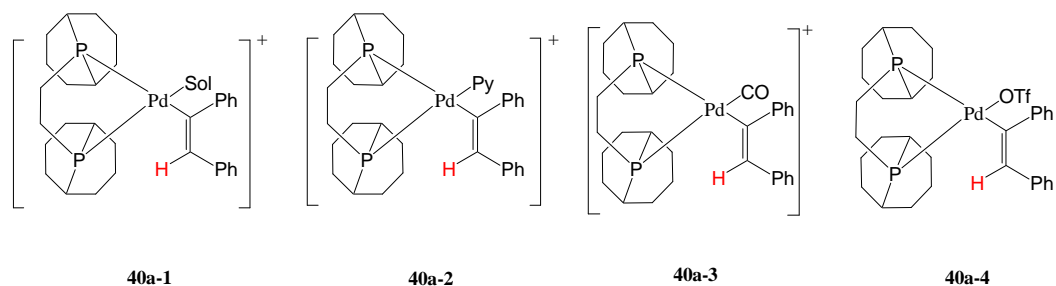


Figure 29: Structure of monohydride species in  $[(\text{BCOPE})\text{Pd}(\text{OH}_2)_2](\text{OTf})_2$  catalyzed diphenyl acetylene carbonylation

Association of diphenyl acetylene to  $(\text{BCOPE})\text{PdH}^+$  should give a palladium alkyne complex. However, this complex is not stable if the hydride transfer is fast enough. Hydride migration could give the vinyl species **40a**. The vinyl complex can be stabilized by, methanol (**40a-1**),

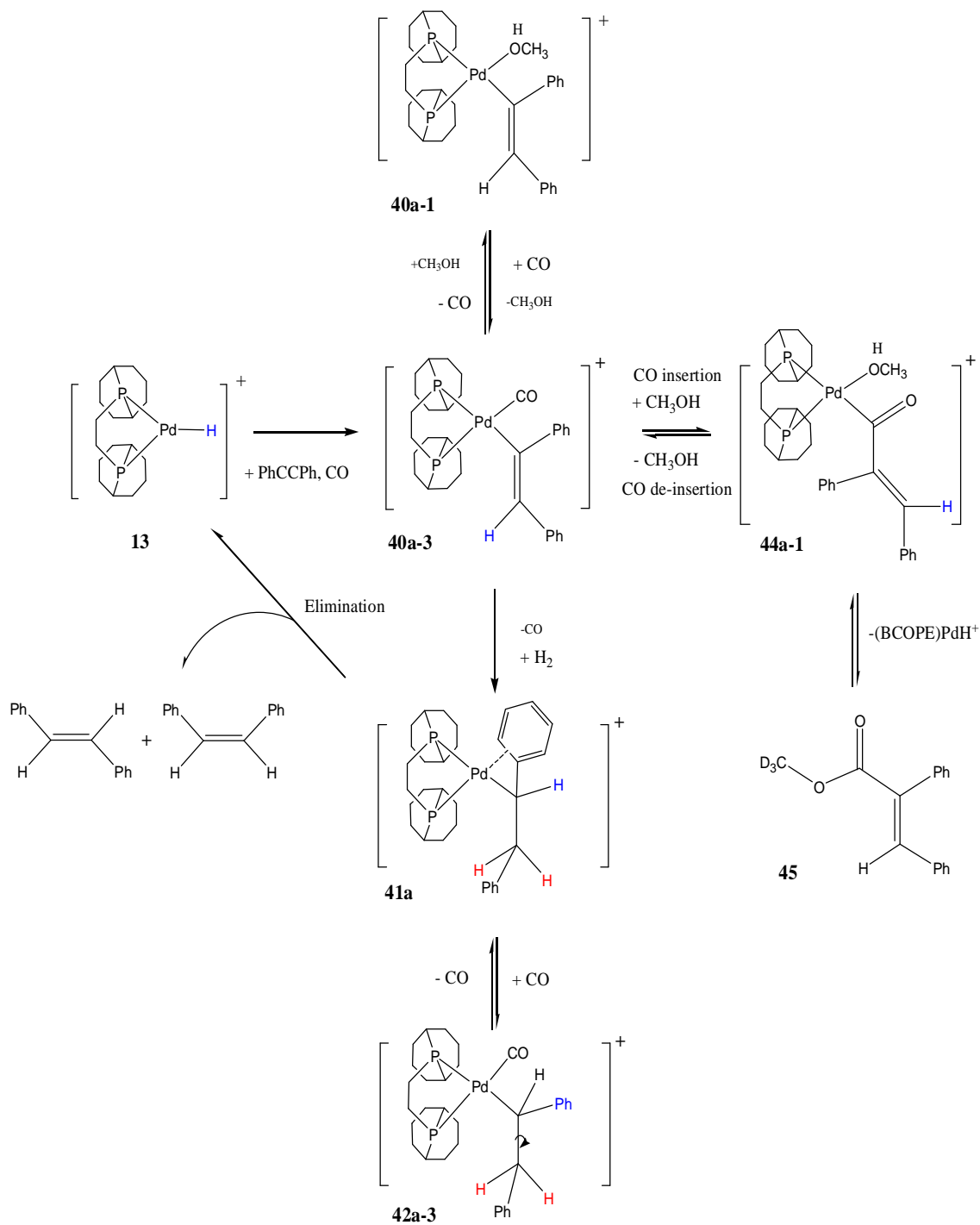
pyridine (**40a-2**), CO (**40a-3**) or OTf (**40a-4**). The structures of potential type **40a** complexes are demonstrated in Figure 30.



**Figure 30: Structure of vinyl species in 12a catalyzed diphenyl acetylene carbonylation**

The vinyl species **40a** then reacts with a range of reagents during catalysis. Hydrolysis of **40a** yields *cis*-stilbene, the semihydrogenation product. It can also be hydrogenated further to palladium alkyl species [(BCOPE)Pd(alkyl)][OTf] (**41a**). **41a** is thermally stable by the  $\eta^3$  interaction. However, its  $\eta^1$  form can also be stabilized by, methanol (**42a-1**), pyridine (**42a-2**), CO (**42a-3**) or OTf (**42a-4**). In the presence of CO, Compound **42a-3** allows a migratory insertion to give a palladium acyl species **43a**. In addition, if the substrate is abundant, the chain prolonged reaction (alkyne polymerization) could happen. However, the nature of the BCOPE ligand favours carbonylation rather than alkyne polymerization or alkyne/CO copolymerization.

The nucleophilic attack on the palladium acyl species by  $\text{CH}_3\text{OH}$  or  $\text{H}_2\text{O}$  yields esters or acids (carbonylation), while hydrolysis yields the corresponding aldehyde (hydroformylation). These reactions are determined by the nature of phosphine ligand, the reagents that are used, and the temperature.



**Scheme 26: The proposed mechanism for diphenyl acetylene hydrogenation, hydroformylation and hydroesterification**

The proposed mechanism of **12a** catalysed diphenyl acetylene hydrogenation and carbonylation is illustrated in Scheme 26. We are aiming at detecting the palladium monohydride species **13a**, vinyl species **40**, alkyl species **41**, acyl species **43**, the organic products, including **44** and stilbene isomers by PHIP. The organometallic products can be



stabilized by methanol, CO or OTf. We also should note that most of these species mentioned in this section show One-Proton-PHIP, the corresponding NMR signals will therefore be in emission.

#### 1.7.4 Further study on palladium catalysed diphenyl acetylene hydrogenation

Catalysts that contains monophosphine ligands shows different catalytic behaviour to those complexes that contains bisphosphine ligands. Two possible path ways are proposed for this reaction, termed cationic or neutral mechanism.<sup>45,46</sup> The active species is  $[(PR_3)PdH]^+$  in the cationic route, as we described in **Section 1.7.3**. However, for the neutral mechanism, an alternative active palladium (0) species  $(PR_3)Pd$  is proposed. Its presence was partly supported by detection of  $(PR_3)_2Pd(H)(vinyl)$  during  $(PEt_3)_2Pd(OTf)_2$  catalysed hydrogenation.<sup>45</sup> Similar to **13a** catalyzed reactions, the two hydrogen atoms in the hydrogenation product now are from the same dihydrogen molecule. Figure 31 illustrates the structure of intermediates that are detected in  $(PEt_3)_2Pd(OTf)_2$  catalysed hydrogenation.<sup>45</sup> They are very different from those when  $(BCOPE)Pd(OTf)_2$  or  $(^tBuCOPE)Pd(OTf)_2$  are used and suggested that a neutral mechanism pathway could be possible. Therefore the reaction must be further explored with expanded ligands.

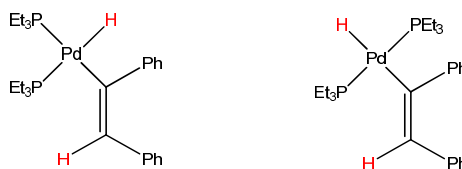


**Figure 31: Intermediates that were detected by PHIP in  $(PEt_3)_2Pd(OTf)_2$  catalysed diphenyl acetylene hydrogenation**

In my research, a palladium catalyst that contains  $PPh_2Me$  ligands (**45**) was synthesised, as illustrated in Figure 32. Their reactivity to hydrogen and the catalytic behaviour during diphenyl acetylene hydrogenation therefore will be of great interest. This work will be presented in **Chapter 5**.

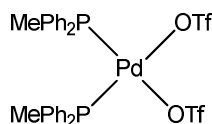


**Figure 32: Structure of compound 45**

## *Chapter two*

### **Chapter 2 NMR study on iridium catalysed hydroformylation**

#### *2.1 Introduction*

#### *2.2 Synthesis of precursors*

#### *2.3 Results from reactions involving $\text{Ir}(\eta^3\text{-C}_3\text{H}_5)(\text{CO})(\text{PMe}_3)_2$ (**15a**)*

#### *2.4 Results from reactions involving $\text{Ir}(\eta^3\text{-C}_3\text{H}_5)(\text{CO})(\text{PMe}_2\text{Ph})_2$ (**15b**)*

#### *2.5 NMR studies of fluxional behaviour of **15a-15e***

#### *2.6 Conclusion*

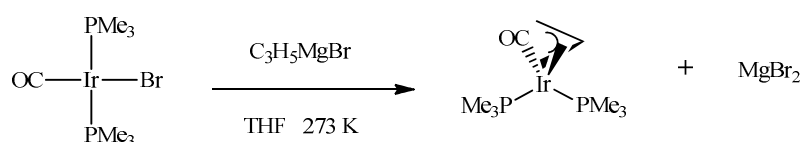
## 2.1 Introduction

A series of NMR studies on iridium catalysed hydroformylation will be presented in this chapter. Previous studies using the precursor  $\text{Ir}(\eta^3\text{-C}_3\text{H}_5)(\text{CO})(\text{PPh}_3)_2$  (**15e**), revealed that two hydrogen addition products,  $\text{Ir}(\text{H})_2(\eta^1\text{-C}_3\text{H}_5)(\text{CO})_2(\text{PPh}_3)$  (**33eA**) and  $\text{Ir}(\text{H})_2(\text{COCH}_2\text{CH}=\text{CH}_2)(\text{CO})_2(\text{PPh}_3)$ , (**37eA**) are formed when **15e** reacts with CO and parahydrogen.<sup>32</sup> My research focused on studying the reactivity of precursors that contain small cone angle phosphine ligands under hydroformylation conditions. These precursors are  $\text{Ir}(\eta^3\text{-C}_3\text{H}_5)(\text{CO})(\text{PR}_2\text{R}')_2$  (**15a-b**, where **15a**,  $\text{PR}_2\text{R}' = \text{PMe}_3$ ; **15b**,  $\text{PPhMe}_2$ )

In this chapter, the synthesis of these complexes is presented in **Section 2.2**. NMR studies concerning **15a** and **15b** are discussed in **Section 2.3** and **2.4** respectively. All the intermediates and organometallic complexes detected in this study are air sensitive and short-lived and therefore not suitable for isolation. In addition, complexes **15a-15e** show interesting fluxional behaviour. It was studied by line shape analysis of the corresponding  $^{31}\text{P}$  NMR spectra at variable temperatures. This work will be provided in **Section 2.5**

## 2.2 Synthesis of the precursors

Compounds **15a-15e** were synthesized by treating  $\text{IrX}(\text{CO})(\text{PR}_2\text{R}')_2$ , where  $\text{X} = \text{Cl}$ , or  $\text{Br}$ , with 10 equivalents of allyl magnesium bromide in THF, according to Equation 7. They were isolated as yellow solid.



**Equation 7: Synthesis of  $\text{Ir}(\eta^3\text{-C}_3\text{H}_5)(\text{CO})(\text{PMe}_3)_2$  (**15a**) from  $\text{IrBr}(\text{CO})(\text{PMe}_3)_2$**

Precursors **15a-15c** that are prepared in this manner are of sufficient purity for NMR study. As shown in Figure 33, *in-situ* NMR experiments reveal that **15a** is the only organometallic product in solution, while **15d** and **15e** contain approximately 15 %  $\text{HIr}(\text{CO})(\text{PR}_2\text{R}')_3$ . However, these impurities are readily removed by recrystallizing them in toluene/hexane. Detailed synthetic procedure for **15a** will be described in **Section 6.2**. **15a-15e** are very soluble in THF and toluene but almost insoluble in saturated hydrocarbons. However, **15a** and **15b** decompose when dissolved in dichloromethane that is purified by standard methods. All these compounds are moderately air sensitive in the solid state.

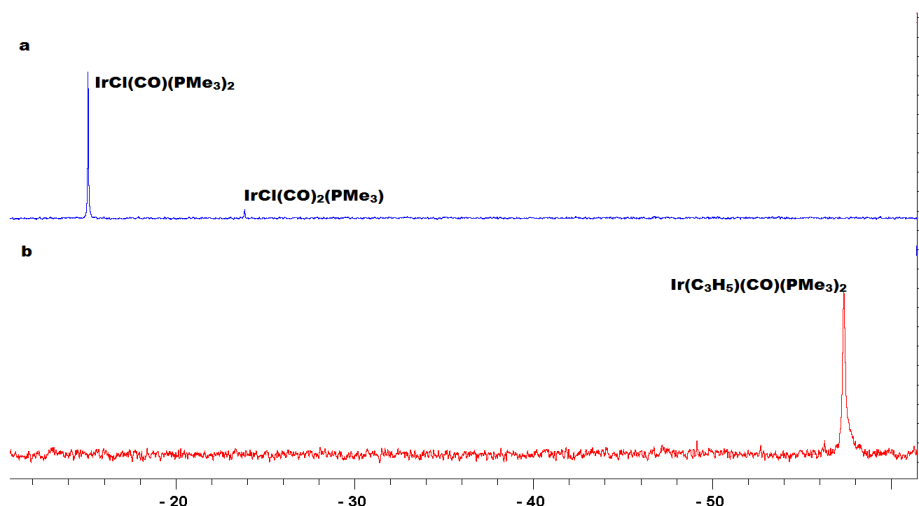


**Figure 33:** (a): A  $^{31}\text{P}$  NMR spectrum of  $\text{IrCl}(\text{CO})(\text{PMe}_3)_2$ , the starting material; (b): an in-situ  $^{31}\text{P}$  NMR spectrum of the solution produced after adding allyl magnesium bromide to  $\text{IrCl}(\text{CO})(\text{PMe}_3)_2$  for 2 hours; this suggests that the conversion of  $\text{IrCl}(\text{CO})(\text{PMe}_3)_2$  to **15a** has occurred

## 2.3 Results from reactions involving $\text{Ir}(\eta^3\text{-C}_3\text{H}_5)(\text{CO})(\text{PMe}_3)_2$ (**15a**)

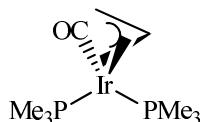
### 2.3.1 NMR characterization of $\text{Ir}(\eta^3\text{-C}_3\text{H}_5)(\text{CO})(\text{PMe}_3)_2$ (**15a**)

**15a** was characterized by NMR methods. A sample of **15a** was prepared by dissolving 20 mg of this compound in 0.6 ml toluene- $d_8$ . When a  $^1\text{H}\{^{31}\text{P}\}$  NMR spectrum of such a sample was recorded at 298 K, a single resonance is observed at  $\delta$  1.22 for the  $\text{PMe}_3$  groups. This resonance is split into a triplet of 3.4 Hz due to coupling to  $^{31}\text{P}$ . This splitting is an example of virtual coupling, where the simple triplet results because the normally invisible  $J_{\text{PP}}$  coupling is larger than  $J_{\text{HP}}$ . At this stage, the corresponding  $^{31}\text{P}^{148}$  NMR spectrum shows a broad singlet at  $\delta$  -57.48, but upon cooling below 273 K, this resonance broadens, suggesting elements of fluxional behaviour. **Section 1.6.1.3** detailed how transition metal allyl complexes can show fluxional behaviour. The results of this study of **15a-15e** will be discussed further in **Section 2.5**.

In addition, a highly coupled quintet of 5.3 Hz was also visible in the  $^1\text{H}\{^{31}\text{P}\}$  NMR spectrum at  $\delta$  4.60. This signal is due to the  $\text{CH}_{\text{meso}}$  group of the allyl ligand. Integration of the CH proton and the  $\text{PMe}_3$  group signals suggests that they are contained in **15a** in the ratio 1 : 18. Surprisingly, no other resonance for the allyl group was visible at this point. However, upon cooling to 230 K, this CH proton signal moved to  $\delta$  4.74 and a second allyl resonance appeared as a broad peak at  $\delta$  2.76. 2D  $^1\text{H}$ - $^1\text{H}$  COSY spectroscopy correlated the

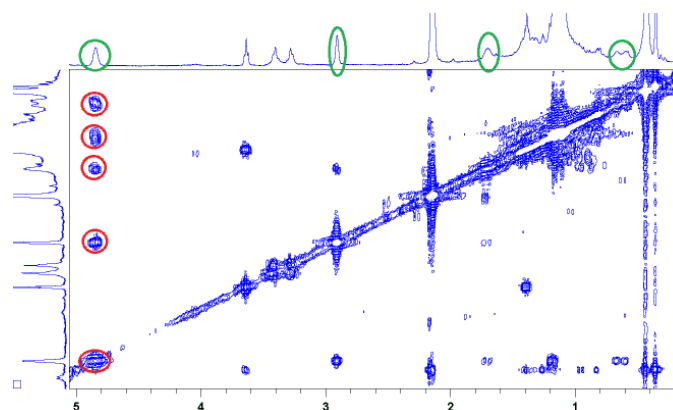
third signal for the allyl ligand, at  $\delta$  1.08, to the resonance at  $\delta$  4.74. The visible effects seen on these signals are therefore further evidence of fluxionality. These data do however confirm that **15a** contains a  $\text{Ir}(\eta^3\text{-C}_3\text{H}_5)(\text{PMe}_3)_2$  grouping.

We further note that a  $^{13}\text{C}$  signal for the CO group in **15a** has been detected at  $\delta$  186.0 thereby confirming these NMR data arise from  $\text{Ir}(\eta^3\text{-C}_3\text{H}_5)(\text{CO})(\text{PMe}_3)_2$  (**15a**). The structure of **15a** is shown in Figure 34.

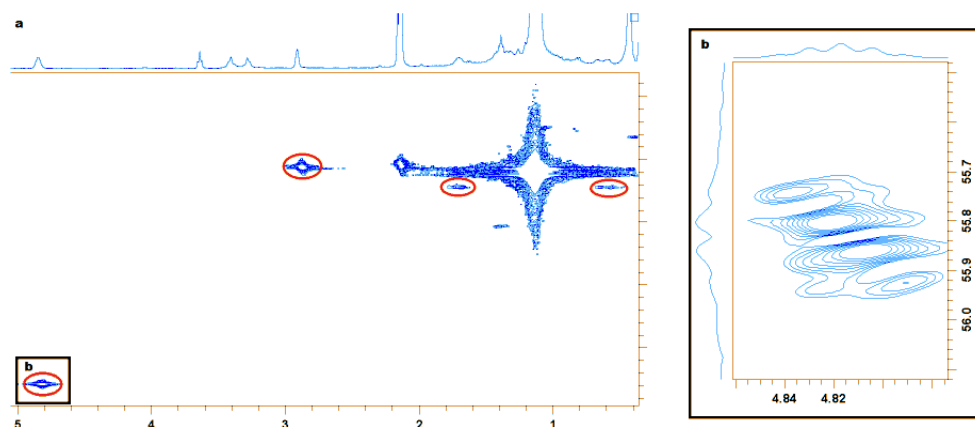


**Figure 34: Structure of 15a**

In order to suppress this potential exchange process, the remaining NMR spectra were recorded at 203 K, which is the lowest practical temperature for this solvent system. The  $\eta^3$ -allyl ligand now produced five distinct resonances at  $\delta$  4.83 (m),  $\delta$  2.90 (s, br), 1.70 (s, br),  $\delta$  1.17 (overlap) and  $\delta$  0.62 (d). The signal at  $\delta$  4.83 couples with all the other four resonances and therefore is due to  $\text{H}_{\text{meso}}$  in the allyl group. Figure 35 illustrates the key region of the 2D  $^1\text{H}$ - $^1\text{H}$  COSY spectrum at this stage. In addition, an  $^1\text{H}$ - $^{13}\text{C}$  HMQC experiment revealed that the  $\delta$  2.90 and  $\delta$  1.7 signals of **15a** couple to a carbon centre through a one-bond coupling to a signal at  $\delta$  21.2, whereas the other two protons, which resonate at  $\delta$  1.17 and 0.62, are attached to a second carbon centre at  $\delta$  24.4. The correlation spectrum showing these proton resonances and the corresponding  $^{13}\text{C}$  signals are illustrated in Figure 36. These data therefore confirm that **15a** contains an  $\eta^3\text{-C}_3\text{H}_5$  group wherein all five protons are inequivalent at 203 K. These data match that expected for an  $\eta^3$ -allyl ligand as described in **Section 1.6.1.2**.

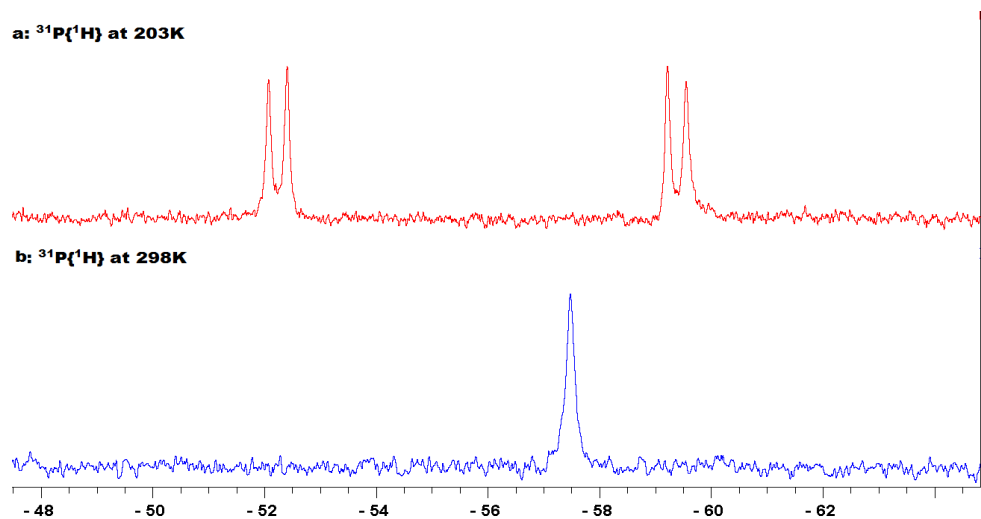


**Figure 35:** Region of the 2D  $^1\text{H}$ - $^1\text{H}$  COSY dataset used to reveal the inequivalence of five protons for the allyl group in **15a** at 203 K.



**Figure 36 (a):** 2D  $^1\text{H}$ - $^{13}\text{C}$  HMQC spectrum that correlates proton and carbon signals as indicated; **(b):** cross peak expansion showing the correlation of the  $^1\text{H}$  resonance at  $\delta$  4.83 and the  $^{13}\text{C}$  centre at  $\delta$  55.8 thereby revealing  $^{31}\text{P}$  splittings

In the corresponding  $^{31}\text{P}^{148}$  spectrum, two doublets appear at  $\delta$  -52.1 and  $\delta$  -59.3, which share a common coupling of 54.2 Hz at 203 K. Figure 37 shows a comparison of the  $^{31}\text{P}^{148}$  NMR spectra at 203 K and 298 K. The  $\delta$  1.22  $\text{PMe}_3$   $^1\text{H}$  signal also shows substantial broadening at 203 K. This information suggests that rotation of the allyl ligand is suppressed by cooling and a structure wherein all five all of the allyl protons and the two phosphines are inequivalent is adopted. The full NMR data of **15a** at 203 K are summarized in Table 12.

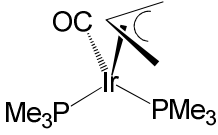


*Figure 37: The  $^{31}\text{P}$  NMR spectra of 15a at 203 K and 298 K*

An examination of the effect of temperature on the  $^{31}\text{P}^{148}$  NMR spectrum in order to determine that rate of allyl rotation will be presented in **Section 2.5**.

## Chapter two

Table 12: Multinuclear NMR data for 15a (in toluene-d<sub>8</sub>)

			
Group / nucleus	Chemical shift (δ)	Multiplicity	Coupling constants (Hz)
<b><sup>1</sup>H</b>			
PMe <sub>3</sub>	1.13 <sup>a</sup>	t, overlapped	J <sub>HP</sub> = 3.4 (virtual coupling)
η <sup>3</sup> -Allyl-CH	4.83 <sup>a</sup> 4.60 <sup>b</sup>	quint	J <sub>HH</sub> = 5.4
Allyl-CH <sub>2</sub>	2.90 <sup>a</sup>	br	
	1.70 <sup>a</sup>	br	
	1.17 <sup>a</sup>	br	
	0.62 <sup>a</sup>	d, br	J <sub>PH</sub> ~ 23.8
Allyl-CH <sub>2</sub>	2.76 <sup>c</sup>		
	1.08 <sup>c</sup>		
<b><sup>31</sup>P</b>			
	-52.1 <sup>a</sup>	d, br	J <sub>PP</sub> = 54.2
	-59.3 <sup>a</sup>	d, br	J <sub>PP</sub> = 54.2
	-57.48 <sup>b</sup>	br,	
<b><sup>13</sup>C</b>			
η <sup>3</sup> -Allyl-CH <sub>2</sub> =	20.8. <sup>a</sup>	d, d	J <sub>PC</sub> = 25, 13
η <sup>3</sup> -Allyl-CH <sub>2</sub> =	24.5 <sup>a</sup>	m	
η <sup>3</sup> -Allyl-CH	55.6 <sup>a</sup>	m	J <sub>PC</sub> = 12.8, 6.5
CO	186.0 <sup>a</sup>	d, br	J <sub>PC</sub> = 4.7
<b>Temperature</b>	a: 203 K; b at 298 K; c: at 233 K		

### 2.3.2 Reactions of Ir(η<sup>3</sup>-C<sub>3</sub>H<sub>5</sub>)(CO)(PMe<sub>3</sub>)<sub>2</sub> (15a) with parahydrogen

#### 2.3.2.1 Reaction of 15a with parahydrogen at 233 K

When a sample of **15a** that was dissolved in toluene-d<sub>8</sub> was added to *parahydrogen* and monitored by NMR spectroscopy at 203 K, four *p*-H<sub>2</sub> enhanced hydride signals were



detected at  $\delta$  -11.37,  $\delta$  -11.51,  $\delta$  -11.74 and  $\delta$  -11.95 according to the corresponding  $^1\text{H}\{^{31}\text{P}\}$  NMR spectrum. It should be noted that 233 K proved to yield stronger enhancements for these resonances and over a longer period, thereby aiding in the characterisation of these products. Figure 38 shows the corresponding  $^1\text{H}$  and  $^1\text{H}\{^{31}\text{P}\}$  NMR spectra at 233 K.

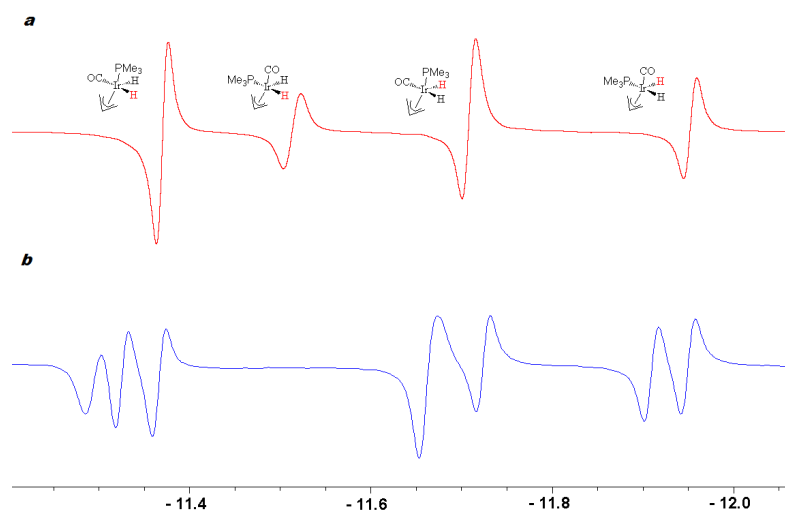


**Figure 38: Hydride region of (a)  $^1\text{H}\{^{31}\text{P}\}$  and (b)  $^1\text{H}$  NMR spectra used to confirm the formation of  $\text{Ir}(\eta^3\text{-C}_3\text{H}_5)(\text{H}_2)(\text{CO})(\text{PMe}_3)$  (18aA and 18aB) when 15a reacts with parahydrogen at 233 K**

In the corresponding  $^1\text{H}$  NMR spectrum, the hydride resonance at  $\delta$  -11.37 possessed a  $^{31}\text{P}$  coupling of 16.4 Hz, which signifies a *cis* ligand arrangement. Its partner at  $\delta$  -11.74 also exhibited a *cis*  $J_{\text{HP}}$  coupling of 25.6 Hz. In contrast, the resonances at  $\delta$  -11.51 and -11.95 exhibit  $J_{\text{HP}}$  couplings of 164.2 and 15.8 Hz respectively. A series of 2D NMR experiments, the *para*- $^1\text{H}$ - $^1\text{H}$  COSY and the *para*- $^1\text{H}$ - $^{31}\text{P}$  HMQC variants, confirmed that the hydrides signals at  $\delta$  -11.37 and  $\delta$  -11.74 arise from one complex which is formed by  $\text{H}_2$  addition over the CO-Ir-C axis with correlations to a phosphine ligand which providing for a single resonance at  $\delta$  -47.44. The two further hydride signals, at  $\delta$  -11.51 and  $\delta$  -11.95 arise from a second complex that is formed by  $\text{H}_2$  addition over the P-Ir-CO axis and these signals correlate with a  $^{31}\text{P}$  NMR signal at  $\delta$  -55.97; a  $^1\text{H}$  methyl resonance is located at  $\delta$  1.48 in addition to this. A section taken from the corresponding 2D  $^1\text{H}$ - $^{31}\text{P}$  HMQC dataset is illustrated in Figure 39.

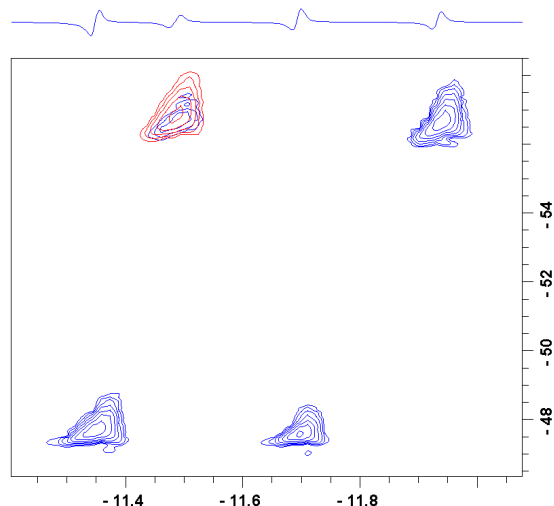
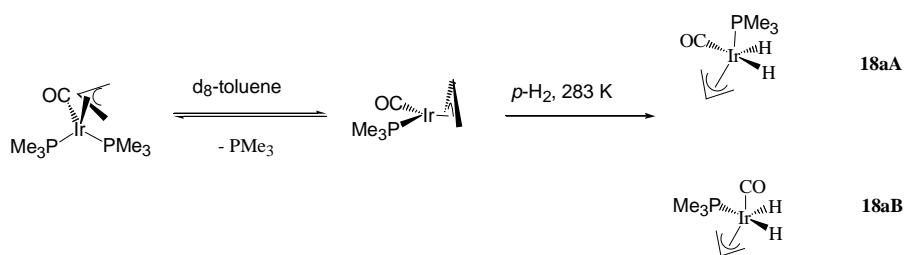


**Figure 39:** 2D  $^1\text{H}$ - $^{31}\text{P}$  HMQC dataset that links the hydride signals due to **18aA** and **18aB** to the corresponding  $^{31}\text{P}$  centres; where the blue cross peak suggests *cis* coupling while the red peak results when the same experiment is re-run for a *trans* coupling.

Based on the information collected, these species are confirmed to be the pair of phosphine loss products, **18aA** and **18aB**, shown in Scheme 27. **18aA** and **18aB** are formed in the ratio 5 : 3 at 233 K. Adding  $^{13}\text{C}$ CO to this sample aids in the detection of the necessary  $^{13}\text{C}$  data for this complex. The carbonyl group for **18aA** was located in this way, although the detection of the carbonyl group in **18aB** was not achieved due to its short life time and need to employ a *cis*-coupling for transfer. The signals for the allyl group were also not detected. Nevertheless, the NMR data for **18aA** and **18aB** are presented in Table 13.



**Scheme 27:** Reaction of  $\text{Ir}(\eta^3\text{-C}_3\text{H}_5)(\text{CO})(\text{PMe}_3)_2$  (**15a**) with parahydrogen at 203 K

A further product was formed when the sample was kept at 233 K for one hour, the hydride signal of which was of a 2<sup>nd</sup> order [AX]<sub>2</sub> type and centred at  $\delta$  -9.94. The  $^{31}\text{P}$  NMR signal for this new species was detected at  $\delta$  -57.44. The new product was assigned to **19aB** according to the following experiments (see **Section 2.3.2.2**). The hydride chemical shift of

**19aB** is slightly temperature dependent, appearing at  $\delta$  -9.94 and 233 K, at  $\delta$  -10.02 and 253 K, and at  $\delta$  -10.12 at 283 K )

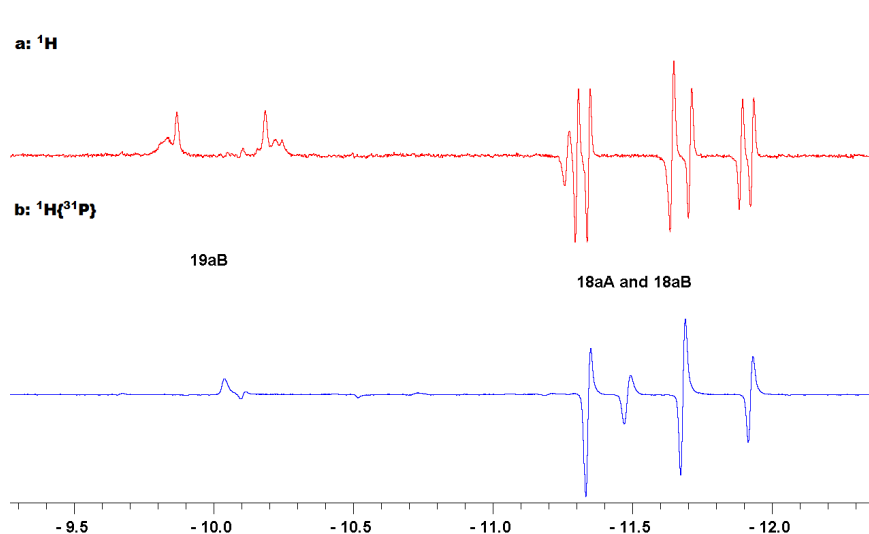


**Figure 40:** The (a)  $^1\text{H}$  and (b)  $^1\text{H}\{^{31}\text{P}\}$  NMR spectra that suggests the formation of 18aA, 18aB and 19aB at 253 K

### 2.3.2.2 Reactions of $\text{Ir}(\eta^3\text{-C}_3\text{H}_5)(\text{CO})(\text{PMe}_3)_2$ (15a) with parahydrogen at 253 K

When this sample was warmed to 253 K, this 2<sup>nd</sup> order hydride resonance showed weak PHIP. Figure 40 shows the corresponding  $^1\text{H}$  and  $^1\text{H}\{^{31}\text{P}\}$  NMR spectra for this signal, suggesting that the hydride signal processes a large splitting of 145.5 Hz due to  $|J_{\text{P}(\text{trans})\text{H}} + J_{\text{P}(\text{cis})\text{H}}|$ . The  $^{31}\text{P}$  signal for this product is detected at  $\delta$  -59.03 according to the 2D  $^1\text{H}$ - $^{31}\text{P}$  HMQC measurements. When a 2D  $^1\text{H}$ - $^1\text{H}$  COSY experiment was recorded, no other hydride resonance was detected to couple with this signal. Therefore it must rise from a chemically equivalent hydrogen addition product, which contains a *cis-cis*- $\text{Ir}(\text{H})_2(\text{PMe}_3)_2$  grouping with a square planar ligand arrangement, as shown in Figure 41. This new product becomes the dominant hydride species and is stable at 253 K for tens of minutes, which allows its further characterization.

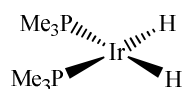


**Figure 41:** The orientation of the hydride and phosphine ligands on the iridium centre, suggested by their coupling pattern (other ligands omitted)

## Chapter two

When a selective nOe experiment was recorded and the hydride signal at  $\delta$  -10.12 was selectively excited, magnetization transfer to a proton that resonates at  $\delta$  1.26 was observed, as illustrated in Figure 42. The signal at  $\delta$  1.26 also couples with the  $^{31}\text{P}$  signal at  $\delta$  -59.03 according to a 2D  $^1\text{H}$ - $^{31}\text{P}$  HMQC experiment. Therefore it is ascribed to be the  $\text{PMe}_3$  group in the new product. The 2D  $^1\text{H}$ - $^{31}\text{P}$  HMQC experiment also linked the  $^{31}\text{P}$  NMR signal to another  $^1\text{H}$  NMR signal at  $\delta$  1.95, which has a  $J_{\text{PH}}$  of 6.6 Hz and a further  $J_{\text{HH}}$  splitting of 7 Hz. When the 2D  $^1\text{H}$ - $^1\text{H}$  COSY experiment was recorded, correlation between the  $^1\text{H}$  NMR signals at  $\delta$  1.95 and  $\delta$  6.94 was observed. They appeared in a 2 : 1 ratio in intensity. The  $^1\text{H}$  NMR signals at  $\delta$  6.94 also coupled with two further  $^1\text{H}$  NMR signals at  $\delta$  4.60 and  $\delta$  4.76. Therefore the signals at  $\delta$  1.95,  $\delta$  4.60,  $\delta$  4.76 and  $\delta$  6.94 were assigned to an  $\eta^1$  group. **19aA** also contains a carbonyl ligand even though it was not directly detected in these measurements. The proposed structure of **19aB** is shown in Figure 43.

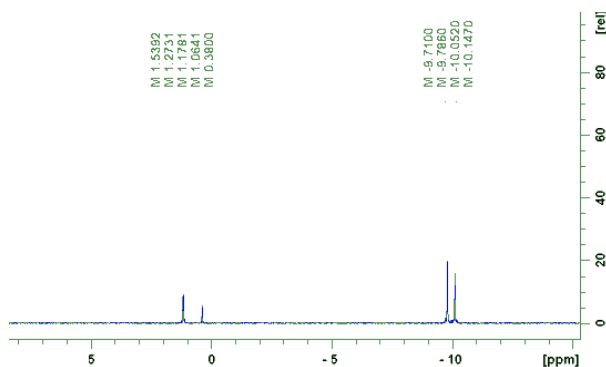


**Figure 42:** NOe NMR spectra showing magnetization transfer to a  $^1\text{H}$  NMR signal at  $\delta$  1.26 due to the *cis*  $\text{PMe}_3$  ligands when the hydride signal at  $\delta$  -10.12 was selectively irradiated

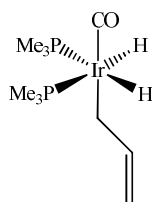


**Figure 43:** Structure of **19aB**

### 2.3.2.3 Reactions of $\text{Ir}(\eta^3\text{-C}_3\text{H}_5)(\text{CO})(\text{PMe}_3)_2$ (**15a**) with *parahydrogen* at 298 K

When a further sample was warmed to 298 K, the hydride region of the resulting NMR spectrum became even more complicated. Now the hydride signals due to **18aA** and **18aB** appear at  $\delta$  -11.41,  $\delta$  -11.73,  $\delta$  -11.56 and  $\delta$  -11.98 and very strong polarization on propene

and propane was detected. This supports that the suggestion that dihydrogen addition is the first step for hydrogenation of **15a**. We note the similarity with rhodium catalyzed hydrogenation.<sup>20</sup> Non-polarized signals for hydrogenation products, propene and propane are detected when such a measurement is repeated, first at 233 K, and then warming the sample to 298 K.

In addition to these known species, a hydride signal was visible at  $\delta$  -9.74 in these experiments. This signal couples with two equivalent  $^{31}\text{P}$  signals through a *cis* coupling of 20.8 Hz. However, the corresponding  $^{31}\text{P}$  signal was not detected due to its short lifetime. The 2D  $^1\text{H}$ - $^1\text{H}$  COSY experiment suggests that this hydride couples with no other hydride resonances and the transient complex was therefore assigned to be a monohydride species. When  $^{13}\text{C}$ CO was used, this signal shows a  $^{13}\text{C}$  splitting of 40.2 Hz thereby confirming a *trans* ligand arrangement. According to this information, and the analogy with the known species  $\text{HIr}(\text{CO})(\text{PPh}_3)_2$ , this new product is assigned to *trans*- $\text{HIr}(\text{CO})(\text{PMe}_3)_2$  (**23aA**) as shown in Figure 44. The NMR data for **23aA** is summarized in Table 15.

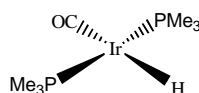


**Figure 44: Structure of 23aA**

Four further thermal hydride signals were detected at  $\delta$  -10.61,  $\delta$  -10.82,  $\delta$  -11.06 and  $\delta$  -10.71 when the reaction time was prolonged. The hydride signal at  $\delta$  -10.61 coupled with the one at  $\delta$  -11.06 through a coupling of -4.7 Hz, they were formed with ratio of 2 : 1 and therefore were assigned to a trihydride species. Both of them possess two *cis* phosphine splittings of 18.1 Hz and 22.4 Hz respectively. The corresponding  $^{31}\text{P}$  centre was located at  $\delta$  -49.53 according to the 2D  $^1\text{H}$ - $^{31}\text{P}$  HMQC experiment. This product was therefore assigned as *fac*- $\text{Ir}(\text{H})_3(\text{CO})(\text{PMe}_3)_2$  (**24aA**). Similarly, the signal at  $\delta$  -10.82 and  $\delta$  -10.71 was assigned to be *mer*- $\text{Ir}(\text{H})_3(\text{CO})(\text{PMe}_3)_2$  (**24aB**). The structures of **24aA** and **24aB** are illustrated in Figure 45. Figure 46 illustrates the correlation of these hydride signals with the expected  $^{31}\text{P}$  centres. The detection of  $^{13}\text{C}$  data for **24a** was achieved by adding  $^{13}\text{C}$ CO to the sample. **24aA** and **24aB** are formed at a ratio of 10 : 9 at this stage. Their NMR data is summarized in Table 16.

## Chapter two

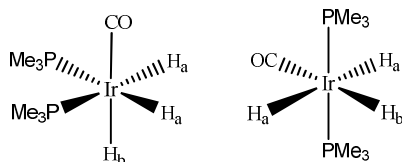


Figure 45: Structures of 24aA and 24aB

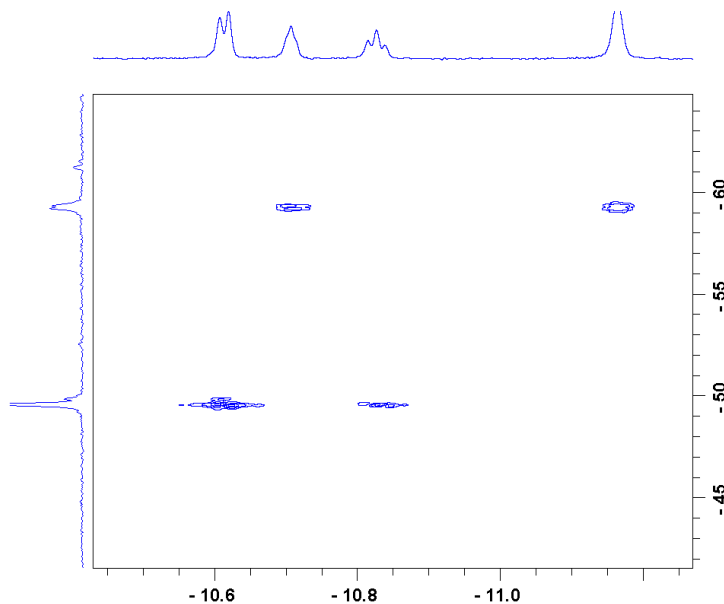


Figure 46: Expansion of the 2D <sup>1</sup>H-<sup>31</sup>P HMQC dataset that correlates of hydride signals of 24aA and 24aB with corresponding <sup>31</sup>P centres

### 2.3.2.4 Short conclusion

Ir( $\eta^3$ -C<sub>3</sub>H<sub>5</sub>)(CO)(PMe<sub>3</sub>)<sub>2</sub> (**15a**) was prepared and characterized by NMR methods. **15a** is fluxional and gives three <sup>1</sup>H NMR signals at 233 K but five distinct signals at 203 K for the allyl group.

The hydrogenation of **15a** yields propene and propane as the final products. This reaction was studied by control reactions, which allowed the detection of a range of reaction intermediates.

At 233 K, the phosphine loss occurs to form the 16e<sup>-</sup> intermediate Ir( $\eta^3$ -allyl)(CO)(PMe<sub>3</sub>). It can be trapped as the dihydride adduct **18aA** and **18aB**, as shown in Scheme 27. **18aA** and **18aB** were detected and characterized by PHIP. **18aA** and **18aB** transform into **19aB** after re-association of the PMe<sub>3</sub> ligand. **19aB** is the dominant product at 253 K. **19aB** was characterized by NMR methods and its structure is well defined.

**15a** might isomerise to the  $\eta^1$  form  $\text{Ir}(\eta^3\text{-C}_3\text{H}_5)(\text{CO})(\text{PMe}_3)_2$  (**17**). Hydrogen addition can happen over the C-Ir-CO or the P-Ir-P axis on **17**. The former routine leads to strong polarization in *cis-trans*- $\text{Ir}(\text{H})_2(\eta^1\text{-allyl})(\text{CO})(\text{PMe}_3)_2$  (**19aA**). However, **19aA** is not observed during my studies. The direct hydrogen addition to the **17** is therefore not seen.

Hydride transfer in **19aB** would be expected to produce  $\text{Ir}(\text{H})(\text{propene})(\text{CO})(\text{PMe}_3)$  (**20a**). Elimination of propene from **20a** would then produce the detected complex  $\text{HIr}(\text{CO})(\text{PMe}_3)_2$  (**23aA**). **23aA** was partly characterized in this study, as it has a short life time. Nevertheless, the structure of **23aA** is confirmed by the subsequent formation of **24aA** and **24aB**. **24aA** and **24aB** are stable at 298 K.

The second hydride transfer in **19aB** yields an iridium alkyl species **25a**. **25a** allows another hydrogen addition to give propane and **23aA**. However, **25a** is highly unstable and cannot be detected. Propene is always present in the final products. This suggests that the multistep hydrogenation of triple bonds/dienes is a consequence of reactions that proceeded without dissociation of the hydrogenation product until the final step.

**Table 13: Multinuclear NMR data for 18aA and 18aB (233 K in toluene- $d_8$ )**

Group / nucleus	Chemical shift ( $\delta$ ) and multiplicity	Coupling constants (Hz)	Chemical shift ( $\delta$ ) and multiplicity	Coupling constants (Hz)
<b><math>^1\text{H}</math></b>				
hydride	-11.44 (d, d)	$J_{\text{HH}} = -5.1$ $J_{\text{PH}} = 16.4$	-12.03	$J_{\text{HH}} = -6.1$ $J_{\text{PH}} = 15.8$
	-11.77 (d, d)	$J_{\text{HH}} = -5.1$ $J_{\text{PH}} = 25.6$ $J_{\text{HC}} \sim 40$	-11.60	$J_{\text{HH}} = -6.1$ $J_{\text{PH}} \sim 164.2$
<b><math>^{31}\text{P}</math></b>				
	-47.47	-	-56.97	-
<b><math>^{13}\text{C}</math></b>				
CO	175.69	$J_{\text{PC}} = 6 \text{ Hz}$	-	

Chapter two

Table 14: Multinuclear NMR Data for 19aB (253 K in in toluene- $d_8$ )

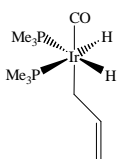
			
Group / nucleus	Chemical shift ( $\delta$ )	Multiplicity	Coupling constant (Hz)
<b><math>^1\text{H}</math></b>			
hydride	-10.02, -10.12 (283 K)	2 <sup>nd</sup> order	$ \text{J}_{\text{P}(\text{trans})\text{H}} + \text{J}_{\text{P}(\text{cis})\text{H}} $ =145.5 Hz
PMe <sub>3</sub>	1.16	overlap	-
Ir-CH <sub>2</sub>	1.95	d, d	$\text{J}_{\text{PH}} = 6.6, \text{J}_{\text{HH}} = 7$
CH=	6.94	m	$\text{J}_{\text{HH}} = 10, 17, 7$
=CH <sub>2</sub>	4.60	d	$\text{J}_{\text{HH}} = 17$
=CH <sub>2</sub>	4.76	d	$\text{J}_{\text{HH}} = 10$
<b><math>^{31}\text{P}</math></b>			
	-57.70, -59.03 (283 K)	s	
<b><math>^{13}\text{C}</math></b>			
CO	173.98	t	$\text{J}_{\text{PC}} = 5.0$ Hz
Reference:11022503 and 12030901			

Table 15: NMR Data for 23aA (283 K in toluene- $d_8$ )

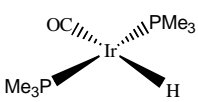
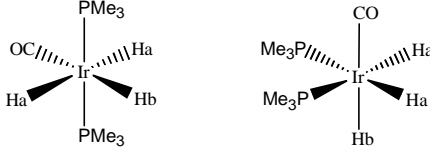
			
Group / nucleus	Chemical shift ( $\delta$ )	Multiplicity	Coupling constant (Hz)
<b><math>^1\text{H}</math></b>			
Hydride	-9.74	t	$\text{J}_{\text{PH}} = 20.8$
<b><math>^{13}\text{C}</math></b>			
CO	173.2	t	$\text{J}_{\text{PC}} = 4.6$

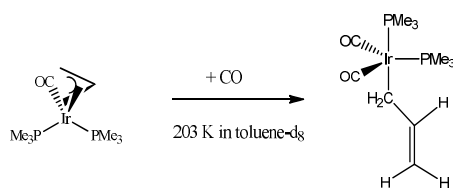


Table 16: Multinuclear NMR data for 24aA and 24aB (298 K in toluene-*d*<sub>8</sub>)

				
	Isomer A		Isomer B	
Group / nucleus	Chemical shift (δ) and multiplicity	Coupling constants (Hz)	Chemical shift (δ) and multiplicity	Coupling constants (Hz)
<b><sup>1</sup>H</b>				
H <sub>a</sub>	-10.61 (t, d)	J <sub>HP(cis)</sub> = 18.1 J <sub>HH</sub> = -4.7	-11.16 (2 <sup>nd</sup> order)	J <sub>PH(trans)</sub> + J <sub>PH(cis)</sub>   = 128 J <sub>HH</sub> = -2.4
H <sub>b</sub>	-10.82 (t, t)	J <sub>PH(cis)</sub> = 22.4 J <sub>HH</sub> = -4.7	-10.71	J <sub>HH</sub> = -2.4 J <sub>PH(cis)</sub> = 22
PMe <sub>3</sub>	1.51	-	1.32	-
<b><sup>31</sup>P</b>				
	-49.53	J <sub>PP</sub> = 32	-59.31	J <sub>PP</sub> = 32
<b><sup>13</sup>C</b>				
	180.13	-	178.4	-
Reference:11022503				

### 2.3.3 Reaction of Ir(η<sup>3</sup>-C<sub>3</sub>H<sub>5</sub>)(CO)(PMe<sub>3</sub>)<sub>2</sub> (**15a**) with CO (<sup>12</sup>CO and <sup>13</sup>CO)

#### 2.3.3.1 Reaction of Ir(η<sup>3</sup>-C<sub>3</sub>H<sub>5</sub>)(CO)(PMe<sub>3</sub>)<sub>2</sub> (**15a**) with CO at 203 K



#### Scheme 28: Reaction of **15a** with CO at 203 K

When a sample of **15a** in toluene-*d*<sub>8</sub> was exposed to CO and a <sup>31</sup>P<sup>148</sup> NMR spectrum recorded at 203 K, the <sup>31</sup>P NMR signals at δ -52.1 and δ -59.3 due to **15a** were replaced by two further doublet signals at δ -53.91 and δ -63.30, which share a common coupling of 21 Hz. This value is significantly smaller than that found in **15a** (54 Hz), which suggests that

## Chapter two

the two phosphine ligands are now *cis* in the product **28a**. **28a** is stable at 203 K for several hours, which aids its full characterization.

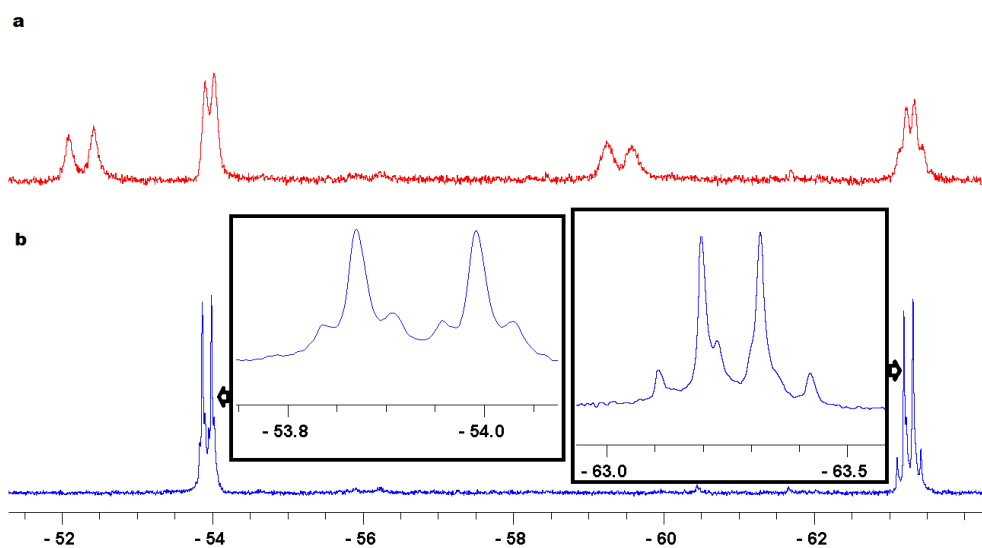


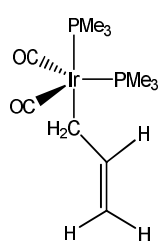
**Figure 47:** a): The  $^{31}\text{P}$  NMR spectrum that monitored the control reaction of **15a** and CO; b): the  $^{31}\text{P}$  NMR spectrum of **28a** when  $^{13}\text{C}$  CO was used, the  $^{13}\text{C}$ - $^{31}\text{P}$  coupling in **28a** suggests the inequivalence of the phosphine ligands and the equivalence of two CO ligands.

When  $^{13}\text{C}$  CO is used, the  $^{31}\text{P}$  NMR signal at  $\delta$  -52.1 showed two further  $J_{\text{PC}}$  splittings of 11 Hz, while the splittings on the signal at  $\delta$  -59.31 are 32 Hz. This would suggest the equivalence of two  $^{13}\text{C}$  CO ligands. Figure 47 illustrated the  $^{31}\text{P}^{148}$  NMR spectrum of the new product. When a  $^{13}\text{C}^{148}$  NMR spectrum was recorded, only a doublet of doublets is seen at  $\delta$  190.5 for this species, where  $J_{\text{PC}} = 11$  Hz and 32 Hz respectively. This is indicative of a terminal CO group in the new product.

In corresponding  $^1\text{H}$  NMR spectrum, two new doublet signals appeared at  $\delta$  5.43 ( $J_{\text{HH}} = 16.6$  Hz) and  $\delta$  4.99 ( $J_{\text{HH}} = 9.2$  Hz). Both of them show strong coupling to a proton NMR signal  $\delta$  7.10. The signal at  $\delta$  7.10 couples with a further signal at  $\delta$  2.72 according to the 2D  $^1\text{H}$ - $^1\text{H}$  COSY experiment. This information suggests that the allyl ligand in **28a** is in its  $\eta^1$  form. The 2D  $^1\text{H}$ - $^{13}\text{C}$  HMQC experiment revealed that the signals at  $\delta$  5.43 and 4.99 were attached to a single carbon centre which resonates at  $\delta$  104.5, while the  $\delta$  2.72 proton signal connected to a  $^{13}\text{C}$  resonance at  $\delta$  119.6, due to an Ir-CH<sub>2</sub> group. The  $\delta$  7.10 resonance and the carbon signal it attaches to overlap with the solvent and was not located.

A  $^1\text{H}$ - $^{31}\text{P}$  HMQC NMR spectrum of **28a** also shows that it yields a  $^1\text{H}$  resonance at  $\delta$  0.86 which couples to a  $^{31}\text{P}$  resonance at  $\delta$  -63.30, while a second methyl resonance at  $\delta$  1.06 couples with the  $^{31}\text{P}$  resonance at  $\delta$  -53.91. These signals are assigned to a methyl group in **28a**. These data suggest that **28a** is the 18 electron complex  $\text{Ir}(\eta^1\text{-C}_3\text{H}_5)(\text{CO})_2(\text{PMe}_3)_2$ , as shown in Scheme 28. NMR data for **28a** is presented in Table 17.

**Table 17: Multinuclear NMR data for 28a (203 K in toluene- $d_8$ )**

			
Group / nucleus	Chemical shift ( $\delta$ )	Multiplicity	Coupling constants (Hz)
<b><math>^1\text{H}</math></b>			
$\text{PMe}_3$ (a)	0.86 (a)	-	
$\text{PMe}_3$ (e)	1.06 (b)	-	
$=\text{CH}_2$	5.43	d	$J_{\text{HH}} = 16.6$
$=\text{CH}_2$	4.99	d	$J_{\text{HH}} = 9.2$
$=\text{CH}$	7.10	overlap	
$\text{Ir-CH}_2$	2.72	-	
<b><math>^{31}\text{P}</math></b>			
$\text{PMe}_3$ (a)	-63.3(a)	d, d	$J_{\text{PP}} = 21, J_{\text{PC}} = 32$
$\text{PMe}_3$ (e)	-53.91(b)	d, d	$J_{\text{PP}} = 21, J_{\text{PC}} = 11$
<b><math>^{13}\text{C}</math></b>			
$\eta^1\text{-Allyl-CH}_2=$	104.5	-	
$\eta^1\text{-Allyl-CH}_2$	119.6	-	
CO	190.47	d, d	$J_{\text{PC}} = 11, 32$

### 2.3.3.2 Reaction of $\text{Ir}(\eta^3\text{-C}_3\text{H}_5)(\text{CO})(\text{PMe}_3)_2$ (**15a**) with CO at 298 K

**28a** is stable at 203 K for a couple of hours. However, when the sample is warmed to 298 K, the  $^1\text{H}$  NMR spectrum now becomes very complicated and a number of further products were formed. The sample was kept at 298 K for one hour before being re-cooled to 203 K. Figure 48 illustrates part of the 2D  $^1\text{H}$ - $^1\text{H}$  COSY dataset that was subsequently recorded at

## Chapter two

203 K. There are four types of complex evident at this stage, as shown in Figure 48. They are Ir- $\eta^1$ -allyl species, Ir-vinyl species (branched product by allyl isomerization), Ir-acyl species (CO insertion), and P- $\eta^1$ -allyl species (decomposing product). They are grouped according to their key CH<sub>2</sub> chemical shift.

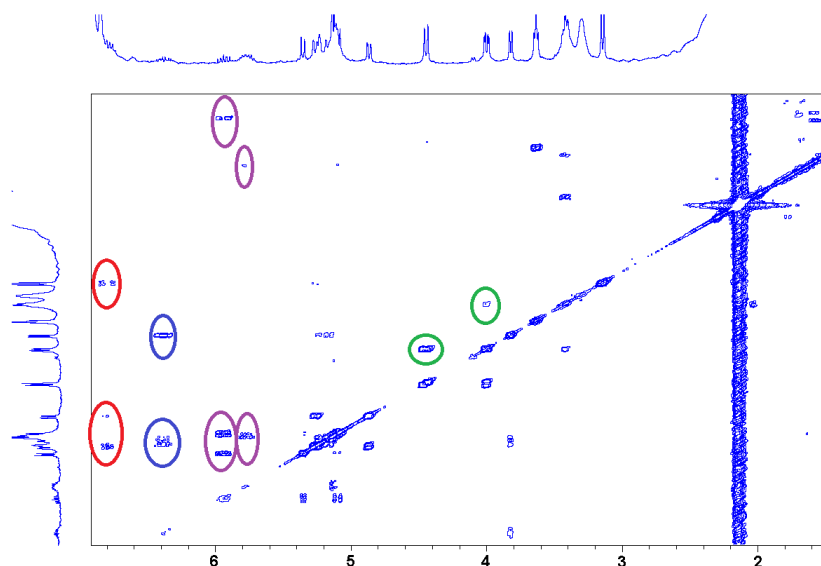


**Figure 48:** A 2D  $^1\text{H}$ - $^1\text{H}$  COSY spectrum at 203 K revealed formation of several new species after the reaction of 15a with CO at 298 K: Red: iridium allyl species; blue: iridium acyl species; Purple: decomposition products; Green, isomerization products

Two sets of  $^1\text{H}$  NMR resonances due to an  $\eta^1$ -allyl group are present at this stage, as summarized in Table 18. The most distinguishable resonances are detected at  $\delta$  6.80,  $\delta$  5.28,  $\delta$  4.79 and  $\delta$  3.16. The corresponding 2D  $^1\text{H}$ - $^{31}\text{P}$  HMQC experiment correlated a  $^{31}\text{P}$  NMR signal at  $\delta$  -60.6 to the proton signal at  $\delta$  3.16, the methyl of which resonates at  $\delta$  0.74. This compound only contains one  $^{31}\text{P}$  signal and is therefore assigned to *e*-Ir( $\eta^1$ -C<sub>3</sub>H<sub>5</sub>)(CO)<sub>3</sub>(PMe<sub>3</sub>) (**29aA**). A non-complete, and much weaker set of  $\eta^1$ -allyl resonances, are detected at  $\delta$  2.39 (2H),  $\delta$  4.84 (1H) and  $\delta$  6.01 (1H). None of these signals show substantial  $^{31}\text{P}$  coupling and they are therefore proposed to be *a*-Ir( $\eta^1$ -C<sub>3</sub>H<sub>5</sub>)(CO)<sub>3</sub>(PMe<sub>3</sub>) (**29aB**).

**Table 18: NMR data of  $\eta^1$ -C<sub>3</sub>H<sub>5</sub> contained complexes that formed when 1a reacts with CO at 298 K**

	Ir( $\eta^1$ -C <sub>3</sub> H <sub>5</sub> )(CO) <sub>2</sub> (PMe <sub>3</sub> ) <sub>2</sub> ( <b>28a</b> )	Ir( $\eta^1$ -C <sub>3</sub> H <sub>5</sub> )(CO) <sub>3</sub> (PMe <sub>3</sub> ) ( <b>29aA</b> )	<i>a</i> -Ir( $\eta^1$ -C <sub>3</sub> H <sub>5</sub> )(CO) <sub>3</sub> (PMe <sub>3</sub> ) ( <b>29aB</b> )
<b><sup>1</sup>H</b>			
CH	7.10	6.80 (m)	-
=CH <sub>2</sub>	4.99	5.28 (d, overlap)	6.01
=CH <sub>2</sub>	5.43	4.89 (d, d J <sub>HH</sub> = 9.6 Hz, 3 Hz)	4.84 (overlap)
Ir-CH <sub>2</sub>	2.72	3.16	2.39
PMe <sub>3</sub>	0.86, 1.06	0.74	-
<b><sup>31</sup>P</b>			
	-54.0, -63.3	-60.6	-

In addition, a range of proton signals due to two CO insertion products were also detected, as summarized in Table 19. The resonance at  $\delta$  3.84 couples with a <sup>31</sup>P signal at  $\delta$  -62.4 and is constant with the formation of Ir(CO- $\eta^1$ -C<sub>3</sub>H<sub>5</sub>)(CO)<sub>2</sub>(PMe<sub>3</sub>)<sub>2</sub> (**30a**). The NMR properties and assignment of these signals are listed in Table 19.

**Table 19: NMR data of CO insertion products that formed when 15a reacts with CO at 298 K**

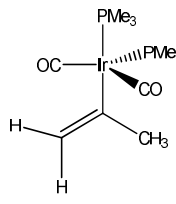
	Ir(COCH <sub>2</sub> CH=CH <sub>2</sub> )(CO) <sub>2</sub> (PMe <sub>3</sub> ) <sub>2</sub> ( <b>30a</b> )	Ir(COCH <sub>2</sub> CH=CH <sub>2</sub> )(CO) <sub>3</sub> (PMe <sub>3</sub> ) ( <b>31a</b> )
<b><sup>1</sup>H</b>		
CH	6.38 (m)	6.61 (m)
=CH <sub>2</sub>	5.15 (overlap)	5.18 (overlap <sup>13</sup> C at $\delta$ 115.5)
=CH <sub>2</sub>	5.24 (overlap)	5.26 (overlap <sup>13</sup> C at $\delta$ 115.5)
Ir-CH <sub>2</sub>	3.84	4.09 (d, J <sub>HH</sub> = 6.5 Hz)
PMe <sub>3</sub>	0.86 (J <sub>PH</sub> = 8 Hz)	-
<b><sup>31</sup>P</b>		
	-62.4	-

A branched product is also present at this stage according to the detection of three mutually coupled signals at  $\delta$  3.41,  $\delta$  4.01 and  $\delta$  4.44. They are ascribed to its methyl proton and two vinyl protons in **28a\_2**. These proton signals also correlate with a <sup>31</sup>P signal at  $\delta$  -53.4. However, when the 2D <sup>1</sup>H-<sup>31</sup>P HMQC pulse sequence was used, two proton signals due to

## Chapter two

PMe<sub>3</sub> were detected, which confirms that two PMe<sub>3</sub> ligands exist in this molecule. Selected NMR data of **28a\_2** is listed in Table 20.

**Table 20: NMR data of P-CH<sub>2</sub>-CH=CH<sub>2</sub> contained complexes that formed when 15a reacts with CO at 298 K**

	
<b><sup>1</sup>H</b>	
CH <sub>3</sub>	3.41 (s)
CH <sub>2</sub>	4.01 (d, J <sub>HH</sub> = 11 Hz)
CH <sub>2</sub>	4.44 (d, d J <sub>HH</sub> = 11 Hz, 14 Hz)
PMe <sub>3</sub>	1.12, 1.31
<b><sup>31</sup>P</b>	-5.34

### 2.3.3.3 Short conclusion

A control reaction between **15a** and CO was followed by NMR spectroscopy at 203 K and 298 K. The reaction of Ir(η<sup>3</sup>-C<sub>3</sub>H<sub>5</sub>)(CO)(PMe<sub>3</sub>)<sub>2</sub> (**15a**) with CO at 203 K proved to be highly selective, with the CO association product Ir(η<sup>3</sup>-C<sub>3</sub>H<sub>5</sub>)(CO)<sub>2</sub>(PMe<sub>3</sub>)<sub>2</sub> (**28a**) being formed. **28a** was characterized by multinuclear NMR methods. In contrast, when a sample of Ir(η<sup>3</sup>-C<sub>3</sub>H<sub>5</sub>)(CO)<sub>2</sub>(PMe<sub>3</sub>)<sub>2</sub> (**28a**) that was dissolved in toluene-d<sub>8</sub> was warmed to room temperature, a large range of CO/PMe<sub>3</sub> exchange products, and CO insertion products, were formed. These products have not been fully characterised but serve to indicate the complexity of this simple system.

In addition, catalyst deactivation might happen via the cleavage of a P-Me bond, to give a new organic products which contains a P-CH<sub>2</sub>CH=CH<sub>2</sub> grouping. We note similar reactions with HRh(CO)(PPh<sub>3</sub>)<sub>3</sub> have been found to lead to the rhodium plating under real hydroformylation conditions.

### 2.3.4 Reaction of $\text{Ir}(\eta^3\text{-C}_3\text{H}_5)(\text{CO})(\text{PMe}_3)_2$ (**15a**) with CO and $\text{H}_2$

#### 2.3.4.1 Control reaction of **15a** with CO and $\text{H}_2$ at 203 K

The reaction of  $\text{Ir}(\eta^3\text{-C}_3\text{H}_5)(\text{CO})(\text{PMe}_3)_2$  with  $^{13}\text{CO}$  and  $\text{H}_2$  was then followed. In order to do this, a sample of **15a** was prepared and exposed to 3 atm. of CO/*p*- $\text{H}_2$  mixture (1 : 2) in dry ice/acetone. During these manipulations, the sample was kept at below 195 K

When such a sample was examined by NMR spectroscopy at 203 K, the formation of **28a** was indicated, as described in **Section 2.3.3.1**. We note that **28a** was the only species in solution until the sample was warmed to 283 K.

#### 2.3.4.2 Reaction of $\text{Ir}(\eta^3\text{-C}_3\text{H}_5)(\text{CO})(\text{PMe}_3)_2$ (**15a**) with CO and $\text{H}_2$ at 283 K

When the sample was examined at 283 K, a polarized hydride signal was visible at  $\delta$  -9.61 in the corresponding  $^1\text{H}\{^{31}\text{P}\}$  NMR spectrum. This signal possessed a *cis*  $^{31}\text{P}$  splitting of 22.8 Hz. When 2D  $^1\text{H}$ - $^{31}\text{P}$  HMQC experiment was recorded, a  $^{31}\text{P}$  centre that resonated at  $\delta$  -58.9 was detected.

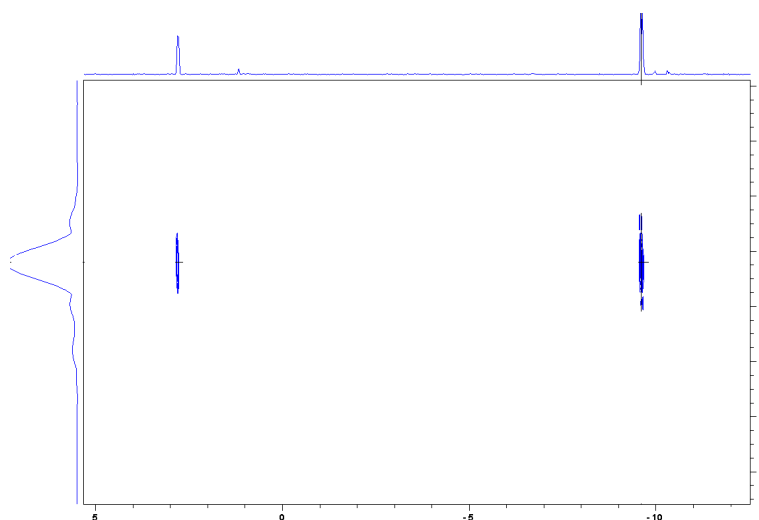


**Figure 49:** Expansion of 2D  $^1\text{H}$ - $^{31}\text{P}$  HMQC dataset that shows the correlation between the  $^1\text{H}$  NMR signals at  $\delta$  -9.61 and  $\delta$  2.87 to the  $^{31}\text{P}$  centre at  $\delta$  -58.9

When 2D  $^1\text{H}$ - $^1\text{H}$  COSY pulse sequence was used, the correlation between the hydride signal which appeared at  $\delta$  -9.61 and another polarized signal at  $\delta$  2.83 due to an Ir- $\text{CH}_2$  group, was observed. The highly coupled signal at  $\delta$  2.83 proved to possess a  $^{31}\text{P}$  splitting of 8 Hz, and two further  $^1\text{H}$  splittings of 8.7 Hz and 2.2 Hz due what are vinyl hydrogen and hydride

## Chapter two

couplings respectively. This suggests that hydride signal is *cis* to an allyl group. A 2D  $^1\text{H}$ - $^{31}\text{P}$  HMQC experiment was used to linked the hydride signal at  $\delta$  -9.61, and the  $^1\text{H}$  NMR signal at  $\delta$  2.83, to the same  $^{31}\text{P}$  signal at  $\delta$  -58.9. Figure 49 illustrated part of the HMQC dataset. The remaining signals for the allyl group in this product were detected at  $\delta$  6.62,  $\delta$  6.71 and  $\delta$  5.0 according to the COSY dataset.

When  $^{13}\text{C}$  was used, the hydride signal at  $\delta$  -9.61 became 2<sup>nd</sup> ordered and showed a large splitting of 48 Hz due to  $|J_{\text{CH}(\text{trans})}+J_{\text{CH}(\text{cis})}|$ . In the corresponding 2D  $^1\text{H}$ - $^{13}\text{C}$  HMQC experiment, this signal correlated with a  $^{13}\text{C}$  signal at  $\delta$  173.2 due a terminal CO ligand, as shown in Figure 50.

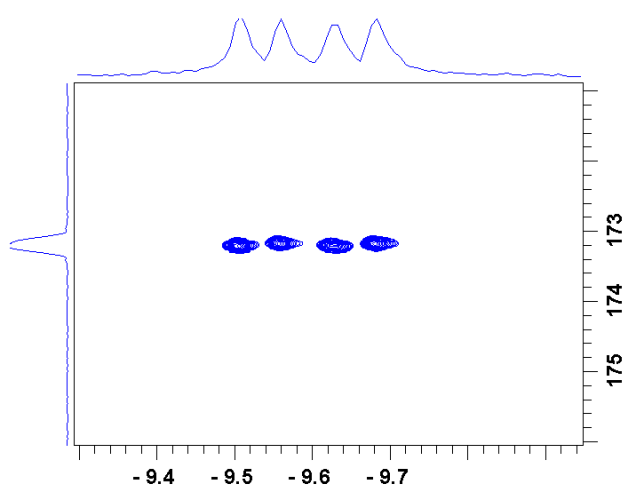
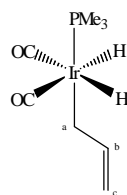


**Figure 50:** Expansion of the 2D  $^1\text{H}$ - $^{13}\text{C}$  HMQC dataset that confirms the *trans* orientation of CO ligand and the hydride ligands for the new product

On this basis, the new product contains two chemically equivalent hydride ligands that are mutually *cis*. A  $\text{PMe}_3$  ligand, and an  $\eta^1$ -allyl ligand, are *cis* to both of them. The new compound also contains two CO ligands in the same plane where the two hydride ligands are. The magnetic inequivalence in hydrides is caused by coupling to the two magnetically inequivalent  $^{13}\text{C}$  nuclei of the CO ligand. These data are attributed to **33aA**. The structure of **33aA** is illustrated in Scheme 29, and the NMR data for **33aA** is summarized in Table 21.





Scheme 29: Structure of 33aA

### 2.3.4.3 Reaction of $\text{Ir}(\eta^3\text{-C}_3\text{H}_5)(\text{CO})(\text{PMe}_3)_2$ (15a) with CO and $\text{H}_2$ at 298 K

When the sample was warmed to 298 K, the intensity of **33aA** grew in. In the meantime, several additional polarized signals were detected. All of these signals contain both *in-phase* and *antiphase* components and therefore must arise from *parahydrogen* addition products. The corresponding  $^1\text{H}$  and  $^1\text{H}\{^{31}\text{P}\}$  spectra are illustrated in Figure 51.

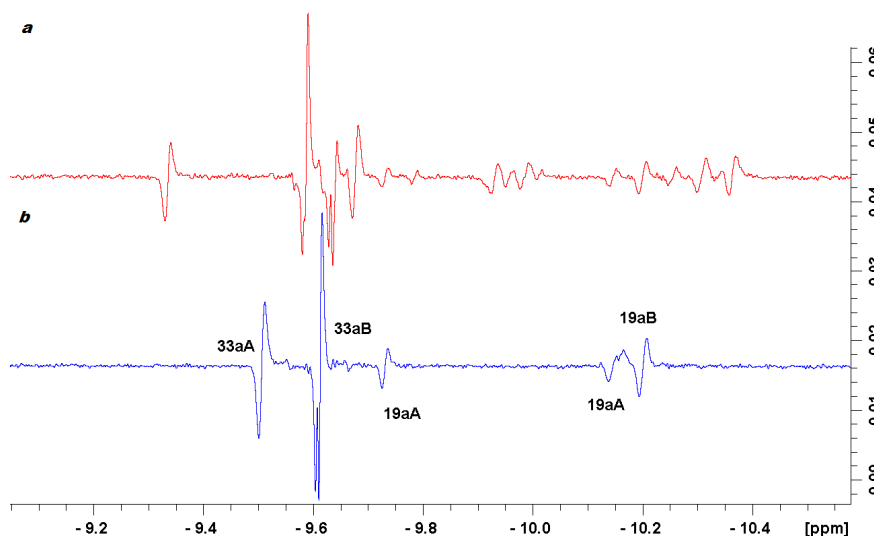


**Figure 51:** (a)  $^1\text{H}$  and (b)  $^1\text{H}\{^{31}\text{P}\}$  NMR spectra showing the hydride region. These spectra indicate the formation of several new species when 15a reacts with a 1:2 mixture of CO and  $\text{H}_2$  at 303K.

The hydride signal at  $\delta$  -9.48 has a large  $^{31}\text{P}$  splitting of 135.5 Hz due to a  $\text{PMe}_3$  ligand that is *trans*, and a further  $^1\text{H}$ - $^1\text{H}$  coupling of -5 Hz. The corresponding  $^{31}\text{P}$  centre was detected at  $\delta$  -60.41 according to the 2D  $^1\text{H}$ - $^{31}\text{P}$  HMQC experiments. When a 2D  $^1\text{H}$ - $^1\text{H}$  COSY pulse sequence was used, its hydride partner was located at  $\delta$  -9.60, which overlapped with the signal at  $\delta$  -9.61 due to **33aA**. However, these signals could be differentiated in the second dimension when a 2D  $^1\text{H}$ - $^{31}\text{P}$  HMQC spectrum was recorded. Figure 52 illustrates the part of an HMQC dataset which contains the correlation data for these two signals with two

## Chapter two

distinct  $^{31}\text{P}$  NMR centres. In addition, this  $^1\text{H}$ - $^{31}\text{P}$ -HMQC measurement also confirms that the signal at  $\delta$  -9.60 carries a  $^{31}\text{P}$  coupling of 25.3 Hz.

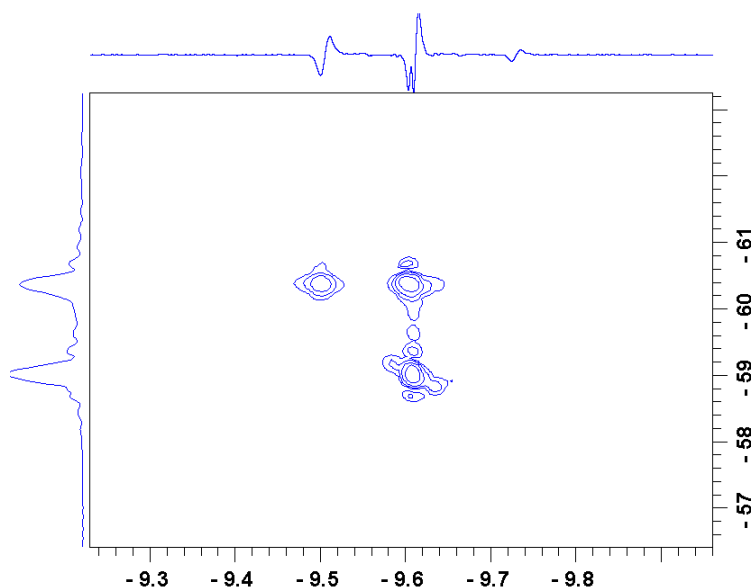
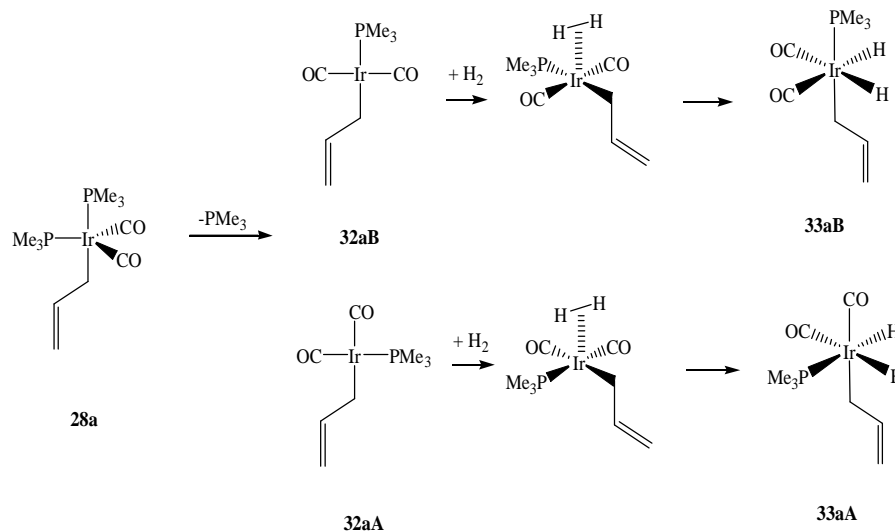


**Figure 52:** Expansion of the 2D  $^1\text{H}$ - $^{31}\text{P}$  HMQC spectrum that differentiate the overlapped signals at  $\delta$  -9.60 and  $\delta$  -9.61 in the second dimension.

When  $^{13}\text{C}$  was used, the signal at  $\delta$  -9.48 showed an extra  $^{13}\text{C}$  splitting of 4 Hz. Furthermore, the hydride signal at  $\delta$  -9.61 showed a large  $^{13}\text{C}$  splitting (ca.  $\sim$  40 Hz due to overlap) thereby suggesting a *trans* CO ligand. A carbonyl resonance was located at  $\delta$  172.6 by a 2D  $^1\text{H}$ - $^{13}\text{C}$  HMQC experiment.

The new compound contains two hydride ligands that resonated at  $\delta$  -9.48 and  $\delta$  -9.61. The signal at  $\delta$  -9.61 is *trans* to a CO ligand that resonates at  $\delta$  172.6, while the hydride at  $\delta$  -9.48 is *trans* to a  $\text{PMe}_3$  ligand. It must also contain a second CO ligand and an  $\eta^1$ -allyl ligand, although they are not directly observed in these measurements. This product was assigned to **33aB**. The NMR data for **33aB** is listed in Table 22.

The resonance polarization of **33aA** and **33aB** lasts for more than one hour before the sample was warmed to 313 K, which suggests they are undergoing hydride-hydrogen exchange. As shown in Scheme 30, the detection of **33a** revealed the presence of **32a**, a  $\text{PMe}_3$  lose product of **28a**.



**Scheme 30:** the formation of detected products **33aA** and **33aB** involves the hydrogen addition to **32a** isomers, the phosphine loss products of **28a**.

#### Detection of **19aA** and **19aB**

At this stage, the hydride resonance due to **19aB** was also detected. The NMR properties of **19aB** have been presented in Section 2.3.4.2. In the meantime, two mutually coupled hydride signals at  $\delta$  -10.20 and  $\delta$  -9.72 were also visible. Both of them showed *cis*  $^{31}\text{P}$  couplings of 21.7 Hz and 22.7 Hz respectively. They are proposed to arise from **19aA**, as hydrogenation of the allyl group does not occur at this stage. They are formed by hydrogen addition to the CO loss product of **28a**.

#### 2.3.4.4 Reaction of $\text{Ir}(\eta^3\text{-C}_3\text{H}_5)(\text{CO})(\text{PMe}_3)_2$ (**15a**) with CO and $\text{H}_2$ at 313 K

When the sample was kept at 313 K for one hour, a further 2<sup>nd</sup> order resonance was observed at  $\delta$  -9.68. It simplified to singlet on  $^{31}\text{P}$  decoupling, with  $|J_{\text{P}(\text{trans})\text{H}} + J_{\text{P}(\text{cis})\text{H}}| = 104$  Hz. When a 2D  $^1\text{H}$ - $^{31}\text{P}$  HMQC experiment was recorded, a  $^{31}\text{P}$  centre that resonates at  $\delta$  -53.48 was correlated to this hydride signal. The 2D  $^1\text{H}$ - $^{31}\text{P}$  HMQC experiments also linked the  $^{31}\text{P}$  NMR signal at  $\delta$  -53.48 with two further proton resonances at  $\delta$  1.25 due to the  $\text{PMe}_3$  ligand and  $\delta$  3.88, which falls into the region for the acyl species rather than allyl species and therefore suggest the formation of the CO insertion product. 2D  $^1\text{H}$ - $^1\text{H}$  COSY experiment located other signals in the acyl group at  $\delta$  5.11 (d, overlapped),  $\delta$  5.14 (d, overlapped) and  $\delta$  6.36 (m). The splitting pattern for this new product was very similar to that of the known species **19aB**. These data confirm **39aA** has the structure as illustrated in Figure 53.

## Chapter two

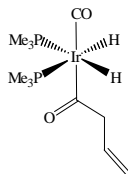


**Figure 53: Structure of 39aA**

The hydride signal due to **39aA** increased in intensity and became the dominate species after 24 hours. It was stable at room temperature for several days. The products **24aA** and **24aB** are also formed after hydrogenation.

### 2.3.5 Conclusion for 15a

The hydroformylation mechanism of **12a** was studied by NMR methods.

Control reactions revealed the priority of CO association to yield **28a** rather than hydrogen addition to **15a**, especially at lower temperature. (203 K to 283 K) Therefore the reaction with CO starts with  $\text{Ir}(\eta^1\text{-C}_3\text{H}_5)(\text{CO})_2(\text{PMe}_3)_2$  (**28a**) rather than  $\text{Ir}(\eta^3\text{-C}_3\text{H}_5)(\text{CO})(\text{PMe}_3)_2$  (**15a**). This agrees with the fact that higher CO pressures suppress hydrogenation, which was realized as early as the first application of hydroformylation.

Compound **28a** undergo  $\text{PMe}_3$  and CO loss to give  $\text{Ir}(\eta^1\text{-C}_3\text{H}_5)(\text{CO})_2(\text{PMe}_3)$  (**32a**) and  $\text{Ir}(\eta^1\text{-C}_3\text{H}_5)(\text{CO})(\text{PMe}_3)_2$  (**17a**). They are not directly detected due to their low concentration. However, their  $\text{H}_2$  addition product, **33a** and **19a** are detected by PHIP. The reaction at 303 K finally yields a stable CO insertion product **39aA** selectively; no other isomer of **39a** was detected.

Table 21: Multinuclear NMR data for 33aA (283 K in toluene- $d_8$ )

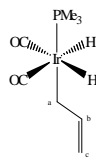
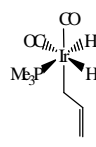
			
Group / nucleus	Chemical shift ( $\delta$ )	Multiplicity	Coupling constant (Hz)
<b><math>^1\text{H}</math></b>			
hydride	-9.61	d, d 2 <sup>nd</sup> order (using $^{13}\text{C}$ O)	$J_{\text{PH}} = 22.8$ , $J_{\text{HHa}} = 2.2$ $ J_{\text{HC(cis)}} + J_{\text{HC(trans)}}  = 48$
Ir- $\text{CH}_2$	2.82	d, d, d	$J_{\text{PH}} = 8$ , $J_{\text{HH}} = -8.7$ , -2.2
Ir- $\text{CH}_2\text{CH}=\text{CH}_2$	6.62 6.71	br, m	
Ir- $\text{CH}_2\text{CH}$	5.0		
$\text{PMe}_3$	1.09		
<b><math>^{31}\text{P}</math></b>			
	-58.9	d	$J_{\text{PC}} = 4.8$
<b><math>^{13}\text{C}</math></b>			
CO	173.17	d	$J_{\text{PC}} = 4.8$

Table 22: Selected NMR data of 33eB (303K in toluene- $d_8$ )

			
Group / nucleus	Chemical shift ( $\delta$ )	Multiplicity	Coupling constants (Hz)
<b><math>^1\text{H}</math></b>			
hydride a	-9.50	d, d,d	$J_{\text{P(trans)H}} = 135.5$ , $ J_{\text{HCcis}} + J_{\text{HCcis}}  = 4$ , $J_{\text{HH}} = -5$
hydride b	-9.60	d,d	$J_{\text{P(cis)H}} = 25.3$ $J_{\text{HH}} = -5$
<b><math>^{31}\text{P}</math></b>			
	-60.41		$J_{\text{P(trans)H}} = 135.5$ , $J_{\text{P(cis)H}} = 25.3$
<b><math>^{13}\text{C}</math></b>			
<i>trans</i> -CO	172.6	-	

## Chapter two

Table 23: Selected multinuclear NMR data of 19aA collected at 303K

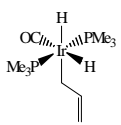
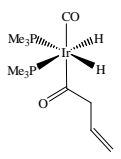
			
	Chemical shift (δ)	Multiplicity	Coupling constant/ Hz
<b><sup>1</sup>H</b>			
hydride	-10.20	t	$J_{P(cis)H} = 21.7$
	-9.72	t	$J_{P(cis)H} = 22.7$

Figure 54: Multinuclear NMR data of 39aA collected at 298 K

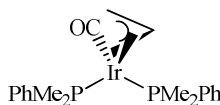
			
	Chemical shift (δ)	Multiplicity	Coupling constant/ Hz
<b><sup>1</sup>H</b>			
hydride	-9.68	2 <sup>nd</sup> order	$ J_{P(trans)H} + J_{P(cis)H}  = 104$
CO-CH <sub>2</sub>	3.84	t, t	$J_{HH} = 5.0, J_{HH} = 1.4$
CH	6.49	m	
CH-CH <sub>2</sub>	5.19	br, overlapped	
PMe	1.25		
<b><sup>31</sup>P</b>			
	-53.48		
<b><sup>13</sup>C</b>			
CO	178.7	t	$J_{PC} = 5.0$
Ir-CO-CH <sub>2</sub>	233.0	d, t	$J_{CC} = 25.0; J_{PC} = 9.0$
CH=CH <sub>2</sub>	114.1		

## 2.4 Results from reactions involving Ir(η<sup>3</sup>-C<sub>3</sub>H<sub>5</sub>)(CO)(PMe<sub>2</sub>Ph)<sub>2</sub> (15b)

### 2.4.1 Synthesis and characterization of 15b

#### 2.4.1.1 Synthesis of 15b

**15b** is synthesized in the same manner as **15a**. The detailed synthetic procedure is described in Section 6.2.

2.4.1.2 Characterization of  $\text{Ir}(\eta^3\text{-C}_3\text{H}_5)(\text{CO})(\text{PMe}_2\text{Ph})_2$  (**15b**)

**Figure 55: Structure of 15b**

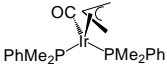
When a sample of **15b**, that was dissolved in toluene- $d_8$ , was examined at 298 K, a highly coupled signal is visible at  $\delta$  4.45 due to the  $CH$  group of the  $\eta^3$  allyl ligand, whereas the signals for other protons of the allyl group were not visible at this stage. In the corresponding  $^{31}\text{P}^{148}$  NMR spectrum, a broad peak is visible at  $\delta$  -39.91. It is further broadened when the sample was cooled to 273 K, suggesting similar fluxionality as seen for **15a**. When the sample was cooled to 233 K, three mutually coupled  $^1\text{H}$  NMR signals were visible at  $\delta$  4.60,  $\delta$  2.97 and  $\delta$  1.06. They are assigned to the *meso*-, *syn*- and *anti*-hydrogen of the  $\eta^3$  allyl group respectively.

The sample was then cooled to 203 K, where the full characterization of **15b** was completed. At 203 K, two sharp doublet NMR signals were visible at  $\delta$  32.5 and  $\delta$  43.2 in the corresponding  $^{31}\text{P}^{148}$  NMR spectrum, suggesting the suppression of allyl rotation. The temperature dependence of  $^{31}\text{P}$  NMR signals is consistent with the  $^1\text{H}$  NMR measurements, now five signals are observed at  $\delta$  4.68 (m),  $\delta$  3.02 (br),  $\delta$  1.63 (br, overlapped),  $\delta$  1.12 (d, t  $J_{\text{PH}} = 10$  Hz,  $J_{\text{HH}} = 6$  Hz) and  $\delta$  0.56 (d, d,  $J_{\text{PH}} = 27$  Hz,  $J_{\text{HH}} = 5$  Hz). A 2D  $^1\text{H}$ - $^{31}\text{P}$  HMQC experiment correlated the  $^{31}\text{P}$  centre at  $\delta$  43.2 to  $^1\text{H}$  NMR signals at  $\delta$  4.68,  $\delta$  1.12 and  $\delta$  0.56, whereas the  $^{31}\text{P}$  centre at  $\delta$  32.5 couples to  $^1\text{H}$  NMR signals at  $\delta$  3.02 and  $\delta$  1.63. In the 1D  $^{13}\text{C}^{148}$  NMR spectrum, a  $^{13}\text{C}$  NMR signal was detected at 185.9 due to the terminal CO in **15b**.

We also note that the two methyl groups in each  $\text{PMe}_2\text{Ph}$  ligand become inequivalent at 203 K. 2D  $^1\text{H}$ - $^{31}\text{P}$  HMQC experiments correlated two  $^1\text{H}$  signals at  $\delta$  1.44 and  $\delta$  1.27 to the  $^{31}\text{P}$  signal at  $\delta$  43.2, whereas two further  $^1\text{H}$  NMR signals at  $\delta$  1.42 and  $\delta$  1.26 connect to the  $^{31}\text{P}$  NMR signal at  $\delta$  32.5. These data confirm **15b** to be  $\text{Ir}(\eta^3\text{-C}_3\text{H}_5)(\text{CO})(\text{PMe}_2\text{Ph})_2$ . Full NMR data for **15b** is summarized in Table 24.

Chapter two

Table 24: Multinuclear NMR data for 15b (203 K in toluene-d8)

			
Group / nucleus	Chemical shift ( $\delta$ )	Multiplicity	Coupling constants (Hz)
<b><math>^1\text{H}</math></b>			
PMe	1.22 (233 K)		
<i>syn-CH<sub>2</sub></i>	4.60 (233 K)	m	$J_{\text{HH}} = 5.4$
<i>anti-CH<sub>2</sub></i>	2.93(233 K)	br	-
CH <sub>2</sub>	1.04 (233 K)	br	-
CH	4.68		
<i>syn-CH<sub>2</sub></i>	3.02	br	
<i>syn-CH<sub>2</sub></i>	1.63	overlapped	
<i>anti-CH<sub>2</sub></i>	1.12	d, t	$J_{\text{PH}} = 10, J_{\text{HH}} = 6$
<i>anti-CH<sub>2</sub></i>	0.56	d, d	$J_{\text{PH}} = 27, J_{\text{HH}} = 5$
<i>PMe</i>	1.44 1.27	d, t d, d	$J_{\text{HH}} = 5,$ $J_{\text{PH}} = 6$
<i>PMe</i>	1.42 1.26	d, t d, d	$J_{\text{HH}} = 5$ $J_{\text{PH}} = 6$
<i>ortho-H</i>	7.27	d	$J_{\text{HH}} = 12$
<i>melta-H</i>	7.07	overlapped	
<i>ortho-H</i>	7.37	d	$J_{\text{HH}} = 12$
<i>melta-H</i>	7.08	overlapped	
<i>para-H</i>	7.66	overlapped	
<b><math>^{31}\text{P}</math></b>			
	-33.96	d	$J_{\text{PP}} = 54$
	-43.49	d	$J_{\text{PP}} = 54$
<b><math>^{13}\text{C}</math></b>			
CH <sub>2</sub>	24.0	d	$J_{\text{PC}} = 40$
CH <sub>2</sub>	27.7	-	
CH	60.3	-	
CO	185.9	s	




## 2.4.2 Reaction of $\text{Ir}(\eta^3\text{-C}_3\text{H}_5)(\text{CO})(\text{PMe}_2\text{Ph})_2$ with *parahydrogen*

### 2.4.2.1 Reaction of $\text{Ir}(\eta^3\text{-C}_3\text{H}_5)(\text{CO})(\text{PMe}_2\text{Ph})_2$ (**15b**) with *parahydrogen* at 233 K

The reaction of  $\text{Ir}(\eta^3\text{-C}_3\text{H}_5)(\text{CO})(\text{PMe}_2\text{Ph})_2$  (**15b**) and *parahydrogen* is similar to that of the  $\text{PMe}_3$  analogue and yields **18bA** and **18bB** isomers with ratio of 1 : 1 at 233 K. Selected NMR data of **18bA** and **18bB**, obtained through monitoring this reaction, are listed in Table 25.

Table 25: Multinuclear NMR data for **18bA** and **18bB** (233K in toluene- $d_8$ )

				
Group / nucleus	Chemical shift ( $\delta$ ) and multiplicity	Coupling constants (Hz)	Chemical shift ( $\delta$ ) and multiplicity	Coupling constants (Hz)
<b><math>^1\text{H}</math></b>				
hydride	-11.20 (d, d)	$J_{\text{HH}} = -5$ $J_{\text{PH}} = 12$	-11.43 (d, d)	$J_{\text{HH}} = -7$ $J_{\text{PH}} = 18$
	-11.60 (d, d)	$J_{\text{HH}} = -5$ $J_{\text{PH}} = 17$	-11.74 (d, d)	$J_{\text{HH}} = -7$
<b><math>^{31}\text{P}</math></b>				
	-32.83	$J_{\text{PH}} = 12$ $J_{\text{PH}} = 17$	-39.5	$J_{\text{PH}} = 18$

### 2.4.2.1 Reaction of $\text{Ir}(\eta^3\text{-C}_3\text{H}_5)(\text{CO})(\text{PMe}_2\text{Ph})_2$ (**15b**) with *parahydrogen* at 298 K

When the reaction of  $\text{Ir}(\eta^3\text{-C}_3\text{H}_5)(\text{CO})(\text{PMe}_2\text{Ph})_2$  (**15b**) with  $\text{H}_2$  was examined at 298 K, similar intermediates and products to **15a** were detected. They are  $\text{Ir}(\eta^1\text{-C}_3\text{H}_5)(\text{CO})(\text{H})_2(\text{PMe}_2\text{Ph})_2$  (**19bB**),  $\text{HIr}(\text{CO})(\text{PMe}_2\text{Ph})_2$ , (**23bA**) and  $\text{H}_3\text{Ir}(\text{CO})(\text{PMe}_2\text{Ph})_2$  (**24bA** and **24bB**), as shown in Figure 56. **24bA** and **24bB** are formed in a ratio of 1 : 10 at 298 K. The NMR data for these species are presented in the following tables.

Chapter two

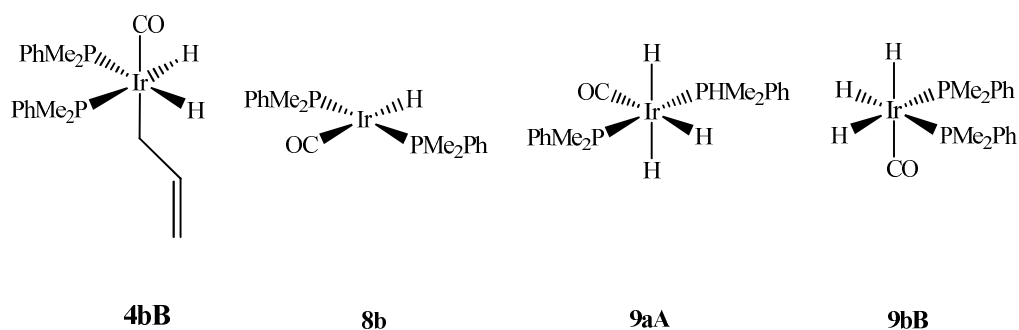


Figure 56: Intermediates and organometallic products that are detected in reaction of  $\text{Ir}(\eta^3\text{-C}_3\text{H}_5)(\text{CO})(\text{PMe}_2\text{Ph})_2$  (15b) with parahydrogen at 298 K

Table 26: Multinuclear NMR Data for 19aB (253 K in toluene- $d_8$ )

Group / nucleus	Chemical shift ( $\delta$ )	Multiplicity	Coupling constants (Hz)
<b><math>^1\text{H}</math></b>			
hydride	-10.06 (273 K) -10.12 (298 K)	2 <sup>nd</sup> order	$ \text{J}_{\text{PH}(\text{cis})} + \text{J}_{\text{PH}(\text{trans})}  = 124$
Reference: 12030901 and 11022803			

Table 27: NMR Data for 23bA (298 K in toluene- $d_8$ )

Group / nucleus	Chemical shift ( $\delta$ )	Multiplicity	Coupling constants (Hz)
<b><math>^1\text{H}</math></b>			
hydride	-9.23	t	$\text{J}_{\text{PH}} = 20.2$
<b><math>^{31}\text{P}</math></b>			
	-41.0	d	$\text{J}_{\text{PH}} = 20.2$
Reference: 11022803			

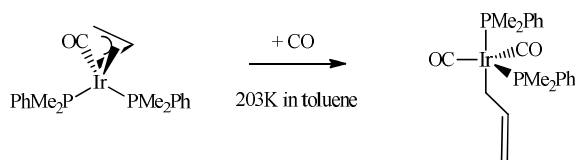
Table 28: Multinuclear NMR data of 24bA and 24bB

	Chemical shift ( $\delta$ ) and multiplicity	Coupling constants	Chemical shift ( $\delta$ ) and multiplicity	Coupling constants
<b><math>^1\text{H}</math></b>				
$\text{H}_a$	-10.19 (t, d)	$J_{\text{HP(cis)}} = 17$ $J_{\text{HH}} = -5$	-10.27 (t, t)	$J_{\text{PH(cis)}} = 21$ $J_{\text{HH}} = -2$
$\text{H}_b$	-10.74 (t, t)	$J_{\text{PH(cis)}} = 21.4$ $J_{\text{HH}} = -5$	-10.97 (2 <sup>nd</sup> order)	$J_{\text{HH}} = -2$ $ J_{\text{PH(cis)}} + J_{\text{PH(trans)}}  = 124$
<b><math>^{31}\text{P}</math></b>				
	-30.2		-41.3	
Reference: 11022503				

### 2.4.3 Reaction of $\text{Ir}(\eta^3\text{-C}_3\text{H}_5)(\text{CO})(\text{PMe}_2\text{Ph})_2$ (**15b**) with CO ( $^{12}\text{CO}$ and $^{13}\text{CO}$ )

#### 2.4.3.1 Reaction of $\text{Ir}(\eta^3\text{-C}_3\text{H}_5)(\text{CO})(\text{PMe}_2\text{Ph})_2$ (**15b**) with CO at 203 K ( $^{12}\text{CO}$ and $^{13}\text{CO}$ )

When a sample of  $\text{Ir}(\eta^3\text{-C}_3\text{H}_5)(\text{CO})(\text{PMe}_2\text{Ph})_2$  (**15b**) that was dissolved in toluene- $d_8$  was placed under CO at 233 K, the corresponding  $^{31}\text{P}$  NMR signals due to **15b** at  $\delta$  -33.96 and  $\delta$  -43.49 are replaced by two further doublets at  $\delta$  -33.9 and  $\delta$  -45.42, which share a common  $J_{\text{PP}}$  of 15 Hz. The  $^{31}\text{P}$  signal at  $\delta$  -33.9 has a  $^{13}\text{C}$  coupling of 31 Hz, whereas it is 11 Hz for the signal at  $\delta$  -43.3 when  $^{13}\text{CO}$  was used. When a  $^{13}\text{C}$  NMR spectrum was recorded, a doublet of doublets at  $\delta$  189.9 was observed for the new product, where  $J_{\text{PC}} = 31$  Hz and 11 Hz was indicated.



Equation 8: reaction of  $\text{Ir}(\eta^3\text{-C}_3\text{H}_5)(\text{CO})(\text{PMe}_2\text{Ph})_2$  (**15b**) with CO at 203 K

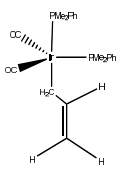
## Chapter two

In corresponding  $^1\text{H}$  NMR spectrum, four  $^1\text{H}$  NMR signals at  $\delta$  5.27 ( $J_{\text{HH}} = 16.55$  Hz),  $\delta$  4.87 ( $J_{\text{HH}} = 9.22$  Hz),  $\delta$  7.1 (overlapped) and  $\delta$  2.72 were detected due to an  $\eta^1\text{-C}_3\text{H}_5$  group. The 2D  $^1\text{H}$ - $^{31}\text{P}$  HMQC experiment linked the  $^1\text{H}$  NMR signals at  $\delta$  5.27 and  $\delta$  4.87 to the  $^{31}\text{P}$  signals at  $\delta$  -39.90 and  $\delta$  -45.42 respectively which were described in the preceding section.

This information suggests that the  $18e^-$  complex  $\text{Ir}(\eta^1\text{-C}_3\text{H}_5)(\text{CO})_2(\text{PMe}_2\text{Ph})_2$  (**28b**) has been detected, as shown in Equation 8. The NMR data of **28b** are listed in Table 29.

This reaction was not studied at higher temperature due to the formation of less informative carbonyl species.

**Table 29: Multinuclear NMR data for 28b (233 K in toluene- $d_8$ )**

			
Group / nucleus	Chemical shift ( $\delta$ )	Multiplicity	Coupling constants (Hz)
<b><math>^1\text{H}</math></b>			
<i>a</i> -PMe	1.07 (a)	s	
<i>e</i> -PMe	1.33 (b)	-	
$\eta^1$ -Allyl-CH <sub>2</sub> =	5.27	d	$J_{\text{HH}} = 16.6$
	4.87	d	$J_{\text{HH}} = 9.2$
$\eta^1$ -Allyl-CH	7.13	m	
$\eta^1$ -Allyl-IrCH <sub>2</sub>	2.78	d	
<b><math>^{31}\text{P}</math></b>			
<i>a</i> -PMe <sub>2</sub> Ph	-39.90	d, d	$J_{\text{PP}} = 15, J_{\text{PC}} = 31$
<i>e</i> -PMe <sub>2</sub> Ph	-45.42	d, d	$J_{\text{PP}} = 15, J_{\text{PC}} = 11$
<b><math>^{13}\text{C}</math></b>			
CO	189.9	d, d	$J_{\text{PC}} = 31, 11$
Reference:10061002			

### 2.4.4 Reaction of $\text{Ir}(\eta^3\text{-C}_3\text{H}_5)(\text{CO})(\text{PMe}_2\text{Ph})_2$ (**15b**) with CO and parahydrogen

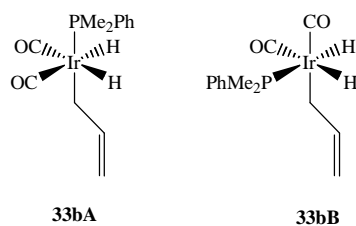


**Figure 57: The structure of 33bA and 33bB**

### Detection of 29bB

When a sample of  $\text{Ir}(\eta^3\text{-C}_3\text{H}_5)(\text{CO})(\text{PMe}_2\text{Ph})_2$  (**15b**) that was dissolved in toluene- $d_8$  was exposed to CO/*parahydrogen* (ratio 1 : 2 with total pressure of 3 atm.) mixture at 253 K, the known species **28b** was apparent according to the corresponding  $^1\text{H}$  NMR spectrum. However, when the sample was heated to 283 K, an enhanced hydride signal was observed at  $\delta$  -9.41 (d,  $J_{\text{HP}} = 22$  Hz). When a 2D  $^1\text{H}$ - $^{31}\text{P}$  HMQC experiment was recorded, a  $^{31}\text{P}$  centre at  $\delta$  -44.1 was correlated to this hydride signal. In addition, a  $^1\text{H}$ - $^{31}\text{P}$  HMQC spectrum demonstrated that the  $^{31}\text{P}$  signal at  $\delta$  -44.1 correlated to this and an a further polarized  $^1\text{H}$  NMR signal at  $\delta$  2.88. The  $^1\text{H}$  signal at  $\delta$  2.88 is again highly coupled, with  $J_{\text{PH}}$  of 8.6 Hz,  $J_{\text{HH}}$  of 8.8 Hz and 2.8 Hz which are due to the vinyl hydrogen and the hydride coupling respectively.

When  $^{13}\text{CO}$  is used, the hydride signal at  $\delta$  -9.41 is now strongly polarized. This arises because of the formation of an ABX spin-system. A further splitting of 52 Hz is now observed on the hydride signal due to coupling to  $^{13}\text{CO}$ . 2D  $^1\text{H}$ - $^{13}\text{C}$  HMQC experiments located the corresponding  $^{13}\text{C}$  centre at 173.0. These information confirm the formation of *cis-cis*- $\text{Ir}(\text{H})_2(\eta^1\text{-CH}_2\text{CH}=\text{CH}_2)(\text{CO})_2(\text{PPhMe}_2)$  (**33bA**). The NMR data of **33bA** is summarized in Table 30.

### Detection of 33bB

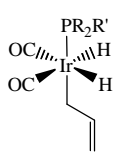
When the sample was heated to 293 K, two further coupled hydride signals were detected at  $\delta$  -9.36 and  $\delta$  -9.56, which shared a common coupling of -4 Hz. The signal at  $\delta$  -9.56 has a  $^{31}\text{P}$  splitting of 116 Hz due to a  $\text{PMe}_2\text{Ph}$  ligand that is *trans* to it, while the signal at  $\delta$  -9.56 only shows a *cis*  $^{31}\text{P}$  coupling of 20 Hz. Based on these information, the formation of

## Chapter two

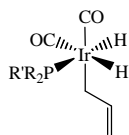
$\text{Ir}(\text{H})_2(\eta^1\text{-CH}_2\text{CH=CH}_2)(\text{CO})_2(\text{PPhMe}_2)$  (**33bB**) is indicated. The NMR data for **33bB** is listed in Table 31

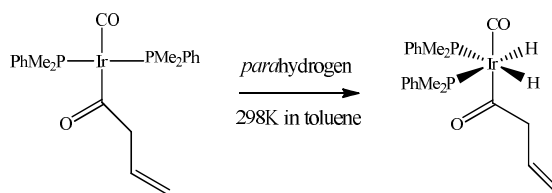
Both of **33bA** and **33bB** are hydrogen addition products of  $\text{Ir}(\eta^1\text{-CH}_2\text{CH=CH}_2)(\text{CO})_2(\text{PPhMe}_2)$  (**32b**), which is formed by phosphine loss from **28b**. However, a non-polarized signal due to the CO loss product  $\text{Ir}(\eta^1\text{-CH}_2\text{CH=CH}_2)(\text{CO})_2(\text{PPhMe}_2)$  (**19bB**) is also visible when the sample is warmed to 298 K. We note that **19bB** can also be detected without CO.

**Table 30: Multinuclear NMR data for 33bA (283 K in toluene- $d_8$ )**

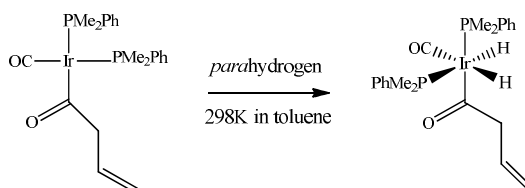
			
Group / nucleus	Chemical shift ( $\delta$ )	Multiplicity	Coupling constant (Hz)
<b><math>^1\text{H}</math></b>			
hydride	-9.41	d	$J_{\text{PH}} = 22, J_{\text{HH}} = 2.8,$ $ J_{\text{C}(\text{trans})\text{H}} + J_{\text{C}(\text{cis})\text{H}}  = 40$
Ir-CH <sub>2</sub>	2.88	t, d, d	$J_{\text{PH}} = 8, J_{\text{HH}} = 8.8, J_{\text{HH}} = -2.8$
<b><math>^{31}\text{P}</math></b>			
	-44.15	-	
<b><math>^{13}\text{C}</math></b>			
CO	172.9	-	
Reference: 11051101-24			

**Table 31: Multinuclear NMR data for 33bB (303K in toluene- $d_8$ )**

			
Group / nucleus	Chemical shift ( $\delta$ )	Multiplicity	Coupling constants (Hz)
<b><math>^1\text{H}</math></b>			
hydride	-9.36	d, d	$J_{\text{PH}} = 160, J_{\text{HH}} = -4$
	-9.56	d, d	$J_{\text{PH}} = 20, J_{\text{HH}} = -4$
Reference: 11051101-24			

Detection of acyl species **35bA***Equation 9: formation of 39bA*

In addition, a further 2<sup>nd</sup> order, non-polarized hydride signal was observable at  $\delta$  -9.70 at 298 K, suggesting the formation of another [AX]<sub>2</sub> spin system. The corresponding <sup>31</sup>P centre was detected at -38.2 according to the 2D <sup>1</sup>H-<sup>31</sup>P HMQC experiments. When an nOe pulse sequence was used, the hydride resonance at  $\delta$  -9.70 connected to a further proton signal at 3.78. This suggests the presence of acyl group in this complex. The corresponding 2D <sup>1</sup>H-<sup>1</sup>H COSY experiment linked three additional <sup>1</sup>H NMR signals at  $\delta$  6.49,  $\delta$  5.17 and  $\delta$  5.20 to the <sup>1</sup>H NMR signal at  $\delta$  3.78, thereby confirming this deduction. The new product is proposed to be **39bA**, the hydrogen addition product of **38bA**. NMR data for **39bA** is listed in Table 32.

*Equation 10: formation of 39bB*

When the sample was warmed further to 313 K, two strongly polarized signals are visible at  $\delta$  -8.56 and  $\delta$  -9.65. A series of NMR measurements confirm that **39bB**, the dihydrogen addition product of **38bB**, is formed. The NMR data for **39bB** is summarized in Table 33. **39bA** and **39bB** are the final products of this reaction if the sample temperature is kept below 333K.

Chapter two

Table 32: Selected multinuclear NMR data for 39bA (298 K in toluene- $d_8$ )

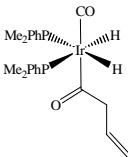
			
Group / nucleus	Chemical shift ( $\delta$ )	Multiplicity	Coupling constants (Hz)
<b><math>^1\text{H}</math></b>			
hydride	-9.70	d, d	$J_{\text{P}(\text{trans})\text{H}} = 120$ $J_{\text{P}(\text{cis})\text{H}} = 15$
CO- $\text{CH}_2$	3.87		$J_{\text{HH}} = 6.9$
= $\text{CH}$	6.49		
CH- $\text{CH}_2$	5.17, 5.20		
<i>PMe</i>	1.40, 1.55		
$\text{P}_{a-o, m}$ H	7.05, 7.23		
<b><math>^{31}\text{P}</math></b>			
	-38.2		$J_{\text{PP}} = 23$
<b><math>^{13}\text{C}</math></b>			
CO- $\text{CH}_2$	77.4		
CH- $\text{CH}_2$	114.03		



Table 33: Multinuclear NMR data for 39bB (298 K in toluene-*d*<sub>8</sub>)

Group / nucleus	Chemical shift (δ)	Multiplicity	Coupling constants (Hz)
<b><sup>1</sup>H</b>			
hydride H <sub>a</sub>	-9.65	d	$ J_{P(\text{trans})H} + J_{P(\text{cis})H}  = 122$
hydride H <sub>b</sub>	-8.56		$J_{CH} \approx 40$
CO-CH <sub>2</sub>	3.74		$J_{HH} = 7.2$
CH	6.42		
CH-CH <sub>2</sub>	5.14, 5.18		
P <sub>a</sub> Me	1.53, 1.57		
P <sub>b</sub> Me	1.29, 1.32		
P <sub>a</sub> -o,m H	7.12 6.94		
P <sub>b</sub> -ortho H	6.95, 7.04		
<b><sup>31</sup>P</b>			
P <sub>a</sub>	-38.2		$J_{PP} = 20$
P <sub>b</sub>	-47.5		$J_{PP} = 20$
<b><sup>13</sup>C</b>			
CO	-177.68		
CO-CH <sub>2</sub>	77.54		
CH=CH <sub>2</sub>	-		
CH=CH <sub>2</sub>	114.3		
Temperature	298 K		

### 2.4.5 Conclusion for 15b

The reaction of **15b** with hydrogen shows similarity with its PMe<sub>3</sub> analogue **15a**. At 233 K the phosphine loss products **18bA** and **18bB** are formed. Furthermore, hydrogenation at 298 K yields **24bA** and **24bB** as the final organometallic products.

## Chapter two

Reaction of **15b** with CO yields **28b** selectively at 203 K. The phosphine/CO loss products are detected as their dihydride addition products **33b** and **19b**. The CO insertion step happens at 313 K for **28b**. The detection of **39bA** and **39bC** suggests the presence of **38bA** and **38bB** in the reaction. **39bA** and **39bC** are stable products, lasting at room temperature for several days. This observation is different to that of **15a**, where **39bA** is formed selectively

## 2.5 NMR studies of fluxional behaviour of 15a-15e

### 2.5.1 Line shape simulation

The fluxionality of **15a-15e** was studied by line shape analysis. The NMR samples of **15** were prepared by dissolving ca. 50 mg of complex in 0.6 ml toluene- $d_8$ . The  $^{31}\text{P}$  NMR spectra of these samples were then recorded, stepwise, from 203 K to 293 K, in temperature intervals of 10 K. Calculated  $^{31}\text{P}$  NMR spectra were then obtained by simulation in gNMR and proved to be in good accordance with the experimental spectra. Figure 58 illustrates the calculated and experimental  $^{31}\text{P}$  NMR spectra for **15a** at 213 K and 293 K.

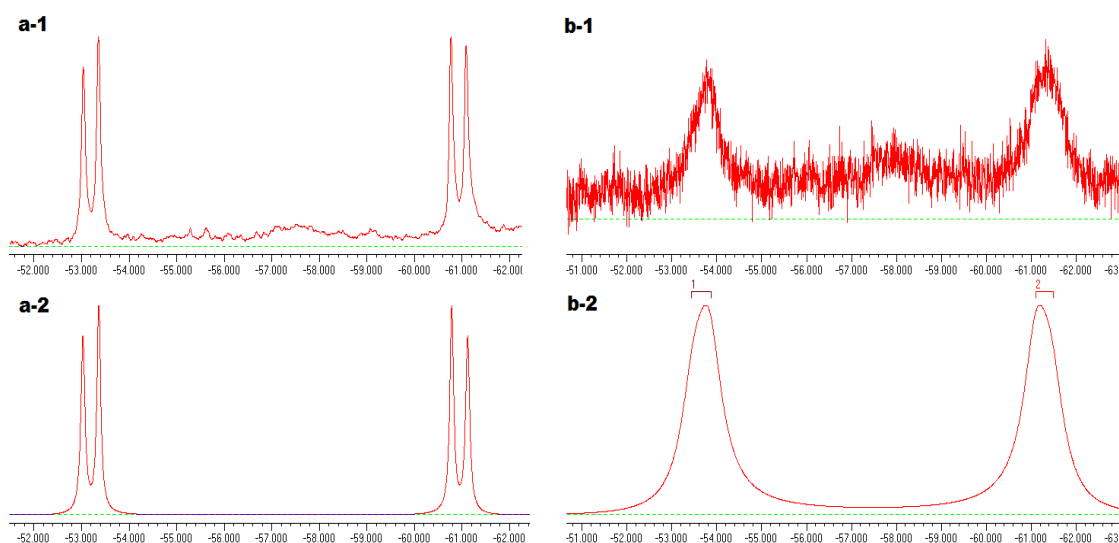


**Figure 58:** The line shape simulation of the  $^{31}\text{P}$  NMR spectra for **15a**. a) 203 K; b) 223K; 1): experimental spectrum; 2): calculated spectrum

### 2.5.2 Calculation of the activation parameters

The exchange rate constant for **15a** was determined to be  $40\text{ s}^{-1}$  at 203 K. Figure 59 shows an Eyring plot for **15a**. The Eyring approach was illustrated in **Section 1.6**. The activation parameters for this exchange reaction were then calculated. The  $\Delta G^\ddagger_{203}$ ,  $\Delta H^\ddagger$  and  $\Delta S^\ddagger$

values were estimated to be  $32.5 \pm 0.4 \text{ kJ mol}^{-1}$ ,  $36 \pm 2 \text{ kJ mol}^{-1}$  and  $17 \pm 10 \text{ J K}^{-1} \text{ mol}^{-1}$  respectively. The complete data associated with these calculations for **15a-15e** is attached in Appendix 1.

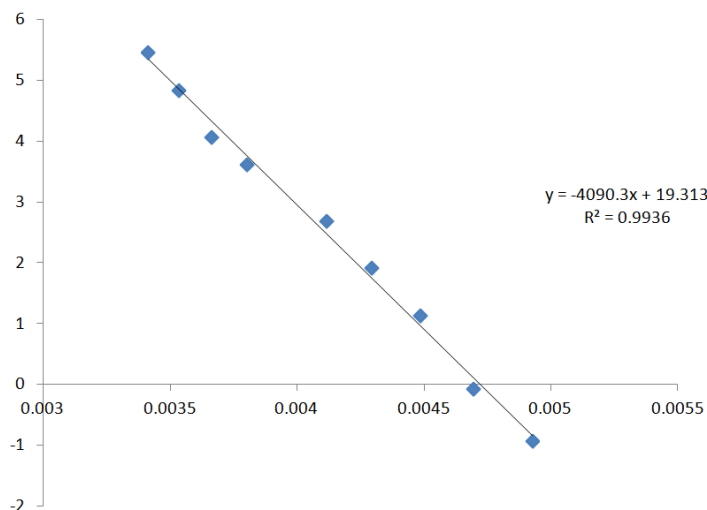


**Figure 59:** The Eyring plot for fluxional process of **15a**

**Table 34:** The activation parameters for **15a-15e**

T/K	$\Delta G_{203}^{\ddagger}/\text{kJ mol}^{-1}$	$\Delta H^{\ddagger}/\text{kJ mol}^{-1}$	$\Delta S^{\ddagger}/\text{J mol}^{-1} \text{ K}^{-1}$
<b>1a</b> , $\text{PMe}_3$	$32.5 \pm 0.4$	$36 \pm 2$	$17 \pm 10$
<b>1b</b> , $\text{PMe}_2\text{Ph}$	$33.5 \pm 0.3$	$31 \pm 2$	$-11 \pm 8$
<b>1c</b> , $\text{PMePh}_2$	$34.7 \pm 0.5$	$36 \pm 3$	$8 \pm 13$
<b>1d</b> , $\text{P}(p\text{-tol})_3$	$34.0 \pm 0.5$	$32 \pm 2$	$-9 \pm 14$
<b>1e</b> , $\text{PPh}_3^2$	$42.7 \pm 0.1$	$34 \pm 1$	$-43 \pm 3$

<sup>2</sup>: Previously calculated using the kinetic data collected by EXSY measurements

## 2.6 Conclusion

Compounds **15a-15e** were prepared according to the literature. The fluxionality of **15a-15e** was studied by line shape simulation. The free energy barriers to allyl rotation were found to increase in the order  $\text{PPh}_3 > \text{P}(p\text{-tol})_3 \sim \text{PMePh}_2 > \text{PMe}_2\text{Ph} > \text{PMe}_3$ . A precise trend is masked by the errors in these measurements although  $\Delta H^{\ddagger}$  is larger for  $\text{PMe}_3$  than  $\text{P}(p\text{-tol})_3$ . In addition  $\Delta S^{\ddagger}$  suggests that for  $\text{PPh}_3$  a more ordered transition state is involved. Here  $\text{PMe}_3$  is the better donor while  $\text{PPh}_3$  is the larger ligand. Both steric and electron effects therefore play a part in this process.

## Chapter two

Their reactions with H<sub>2</sub>, CO and a 1 : 2 mixture of CO and H<sub>2</sub> have been studied by *para*hydrogen assisted NMR methods. When **15** was treated with H<sub>2</sub> at 233 K, two isomers of Ir( $\eta^3$ -C<sub>3</sub>H<sub>5</sub>)(CO)(PR<sub>2</sub>R')(H)<sub>2</sub>, **18A** and **18B**, were formed and characterized. The elimination of organic product does not occur when the temperature is lower than 298 K, above which point the organic products propene and propane and the organometallic product **23** results. **23** is reactive and undergo hydrogen addition to give **24A** and **24B**, which are stable products.

The reaction of **15a-15b** with CO is very selective at 203 K, where two stable compounds **28a-28b** were formed. The ligand loss products are detected as their dihydride adducts **19** and **33**. CO insertion for **28b** happens at 313 K and yields a square planar complex **38b**, the hydrogen addition product of which, (**39bB** and **39bC**) were detected by NMR characterization. A similar reaction happens to **28a** at 308 K, where **39aB** is formed selectively. **39aB**, **39bA**, and **39bB** are stable over days at room temperature.

## Chapter 3 Studies of Rhodium catalysed hydroformylation

### 3.1 Introduction

### 3.2 Synthesis & characterization of $Rh(\eta^3-C_3H_5)(PPh_3)_2$ (**16**)

### 3.3 Control Reaction of $Rh(\eta^3-C_3H_5)(PPh_3)_2$ with parahydrogen

### 3.4 Control reaction of $Rh(\eta^3-C_3H_5)(PPh_3)_3$ with CO ( $^{12}CO$ or $^{13}CO$ )

### 3.5 Reaction of $Rh(\eta^3-C_3H_5)(PPh_3)_2$ with CO and $H_2$ in toluene- $d_8$

### 3.6 Conclusion

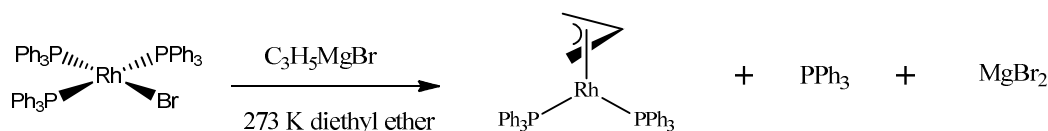
### 3.1 Introduction

In this chapter, the NMR study of rhodium catalyzed hydroformylation will be presented. The definitions, catalyst evolution, mechanism and selectivity of hydroformylation have been discussed in **Section 1.3**.

To understand the hydroformylation of dienes, a rhodium precursor,  $\text{Rh}(\eta^3\text{-C}_3\text{H}_5)(\text{PPh}_3)_2$  (**16**) was prepared and characterized, instead of  $\text{Rh}(\eta^3\text{-C}_3\text{H}_5)(\text{CO})(\text{PPh}_3)_2$  (**14**), as the latter type of compounds are highly unstable.<sup>75</sup> This work is presented in **Section 3.2**. Control reactions of **16** and  $\text{H}_2$  or  $\text{CO}$  are discussed in **Section 3.3** and **Section 3.4** respectively.

### 3.2 Synthesis & characterization of $\text{Rh}(\eta^3\text{-C}_3\text{H}_5)(\text{PPh}_3)_2$ (**16**)

#### 3.2.1 Synthesis



**Equation 11: Synthesis of  $\text{Rh}(\eta^3\text{-C}_3\text{H}_5)(\text{PPh}_3)_2$  (**16**)**

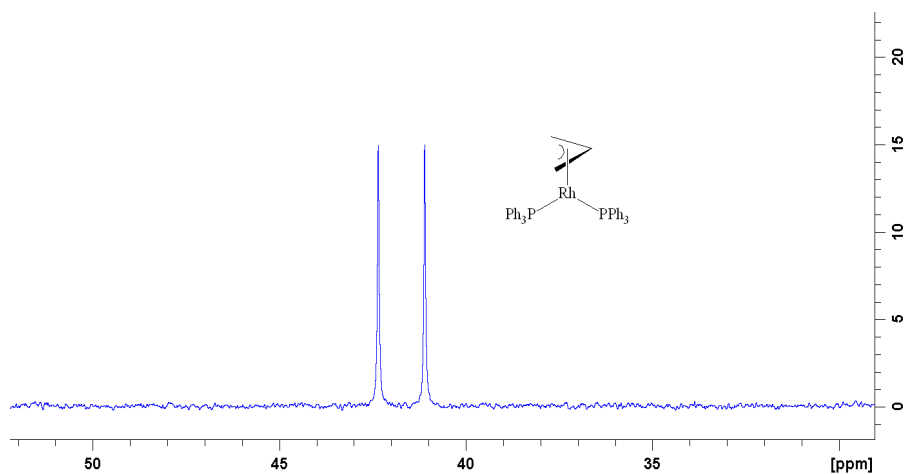


**Figure 60: The in-situ  $^{31}\text{P}$  NMR spectrum of **16** that was recorded in diethyl ether at 298 K. A drop of benzene- $d_6$  was added to this sample for shim and lock calibration**

**16** was prepared by treating  $\text{RhBr}(\text{PPh}_3)_3$  with 10 eq. of allyl magnesium bromide in diethyl ether according to Equation 11.<sup>149</sup> The detailed synthetic procedure for **16** is described in **Section 6.3**. The compound prepared in this manner proved to be of sufficient purity for an NMR study. As shown in Figure 60, the in-situ  $^{31}\text{P}$ <sup>148</sup> NMR spectrum indicates that **16** was the only organometallic species present in solution. Single crystals of **16** were grown at the

interface of diethyl ether/hexane mixture. The structure of **16** was therefore confirmed by both NMR and XRD characterization. The XRD characterization is presented in **Section 3.2.3**. Firstly, the NMR characterization will be discussed.

### 3.2.2 NMR characterization of $\text{Rh}(\eta^3\text{-C}_3\text{H}_5)(\text{PPh}_3)_2$ (**16**)

When a sample of **16** that was dissolved in toluene- $d_8$  was examined by  $^1\text{H}\{^{31}\text{P}\}$  NMR spectroscopy at 298 K, three  $^1\text{H}$  resonances were detected at  $\delta$  5.23 (m, 1H),  $\delta$  3.05 (d, 2H,  $J_{\text{HH}} = 7.0$  Hz), and  $\delta$  2.53 (d, 2H,  $J_{\text{HH}} = 13.0$  Hz). The resonance at  $\delta$  2.53 has a proton-phosphorus splitting of 4.2 Hz, whereas the  $^{31}\text{P}$  splittings on the other two resonances lie within the line width. A 2D  $^1\text{H}$ - $^1\text{H}$  COSY experiment revealed that the signal at  $\delta$  5.23 coupled with the other two  $^1\text{H}$  NMR signals described above. Figure 62 illustrates part of the 2D  $^1\text{H}$ - $^1\text{H}$  COSY NMR spectrum of **16**. The three resonances described above are therefore assigned to an  $\eta^3$ -allyl group, which is bound to the rhodium centre. These data are similar to those of known rhodium allyl species<sup>144,150-152</sup> The NMR properties of the  $\eta^3$  allyl ligands have been presented in **Section 1.7**.

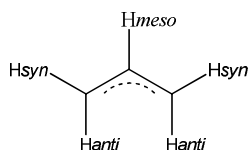


**Figure 61:** The structure of an  $\eta^3$ -allyl ligand

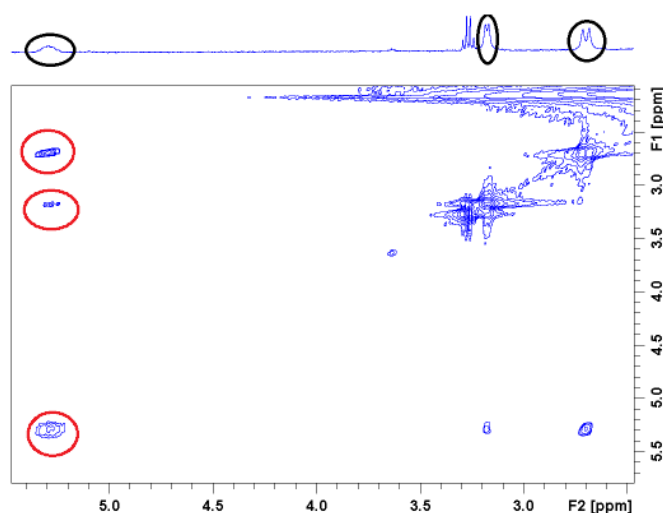


**Figure 62:** Part of a 2D  $^1\text{H}$ - $^1\text{H}$  COSY NMR spectrum that correlates the proton signals at  $\delta$  5.23,  $\delta$  3.05, and  $\delta$  2.53 due to the  $\eta^3$ -allyl group in **16**

### Chapter three

When an nOe pulse sequence was used, and the signal at  $\delta$  5.23 selectively irradiated, magnetization transfer to the signals at  $\delta$  3.05 and  $\delta$  7.55 was observed in addition to relayed transfer into a signal at  $\delta$  6.97. This confirms that the protons giving rise to the  $^1\text{H}$  NMR signals at  $\delta$  5.23 and  $\delta$  3.05 are arranged *cis* to one another and hence the signal at 3.05 is due to  $\text{H}_{\text{syn}}$  as shown in Figure 61. Additionally, when the signal at  $\delta$  3.05 was irradiated, it proved to correlate with two signals at  $\delta$  5.23 and  $\delta$  2.53 respectively. The NMR signal at  $\delta$  2.53 must arise from the  $\text{H}_{\text{anti}}$  of the allyl ligand. The *ortho*-H of the phosphine ligand was located by an nOe connection to a signal at  $\delta$  7.53. At this point, a second nOe measurement was completed in which the  $\delta$  7.53 signal was probed. In this spectrum, an nOe effect on the resonances at  $\delta$  5.23,  $\delta$  3.05, and  $\delta$  2.53 was seen. These results revealed the presence of  $\eta^3$  allyl ligand and two phosphine ligands in **16**. In addition, the equivalence of the two  $^{31}\text{P}$  ligands at this stage was also indicated.

In the corresponding  $^{31}\text{P}^{148}$  spectrum, only one signal was observed at  $\delta$  41.9 with a rhodium coupling of 202 Hz. This confirms the equivalent environment of the two phosphine ligands of **16** in solution. The corresponding  $^1\text{H}$ - $^{31}\text{P}$  HMQC experiment correlated this  $^{31}\text{P}$  NMR signal to three  $^1\text{H}$  NMR signals at  $\delta$  5.23,  $\delta$  3.05, and  $\delta$  2.53, which correspond to the  $\eta^3$ -allyl group. Figure 63 illustrates the correlation of the  $^{31}\text{P}$  NMR signal at  $\delta$  41.9 with the proton NMR signals at  $\delta$  3.05 and  $\delta$  2.53. The  $^{31}\text{P}$  NMR signal at  $\delta$  41.9 also coupled to two further  $^1\text{H}$  NMR signals at  $\delta$  7.53 and  $\delta$  6.97. These arise from the *o*- and *p*-hydrogen nuclei of the phenyl group of the phosphine. The *parahydrogen* of the phenyl group was detected at  $\delta$  6.97 by  $^1\text{H}$ - $^{13}\text{C}$  HMQC spectroscopy, which overlapped with the signal due to the *m*-hydrogen. However, they were differentiated in the second dimension when a 2D  $^1\text{H}$ - $^{13}\text{C}$  HMQC experiment was undertaken.



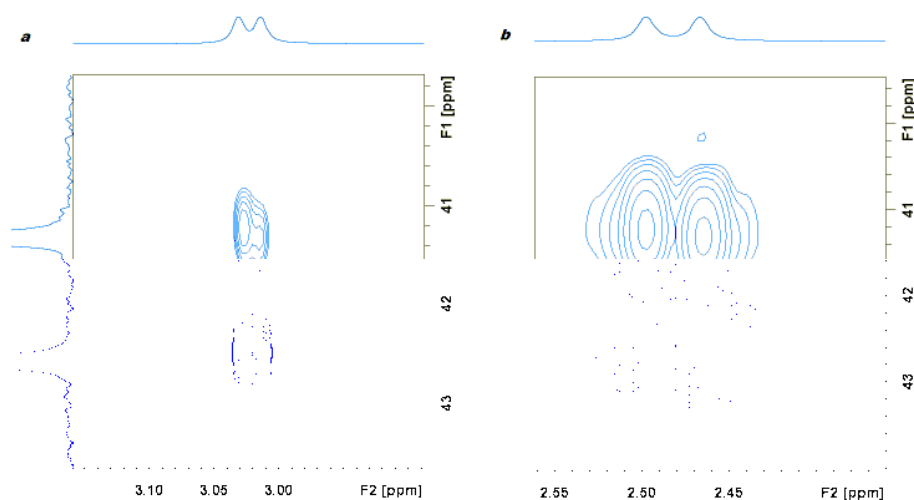


**Figure 63:** Expansion taken from a  $^1\text{H}$ - $^{31}\text{P}$  HMQC NMR spectrum that shows the correlations between the  $^{31}\text{P}$  signal at  $\delta$  41.9 and the proton signals at  $\delta$  3.05 (a), and  $\delta$  2.53 (b) due to **16**.

A  $^1\text{H}$ - $^{13}\text{C}$  HMQC experiment correlated the proton signal at  $\delta$  5.23 to a carbon nucleus that resonated at  $\delta$  46.95, whereas the proton signals at  $\delta$  3.05 and  $\delta$  2.53 coupled to a single carbon signal that appeared at  $\delta$  58.55. In addition, the  $^{13}\text{C}$  NMR signal at  $\delta$  58.55 possesses  $^{31}\text{P}$  and  $^{103}\text{Rh}$  couplings of 10 Hz respectively and is therefore quartet. Figure 64 illustrates part of the corresponding  $^1\text{H}$ - $^{13}\text{C}$  HMQC spectrum that linked the  $^1\text{H}$  NMR signals at  $\delta$  3.05 and  $\delta$  2.53 and the  $^{13}\text{C}$  NMR signal at  $\delta$  58.55. The other  $^{13}\text{C}$  signals for **16** were collected by  $^1\text{H}$ - $^{13}\text{C}$  HMQC methods. The NMR data for **16** is summarized in Table 35.

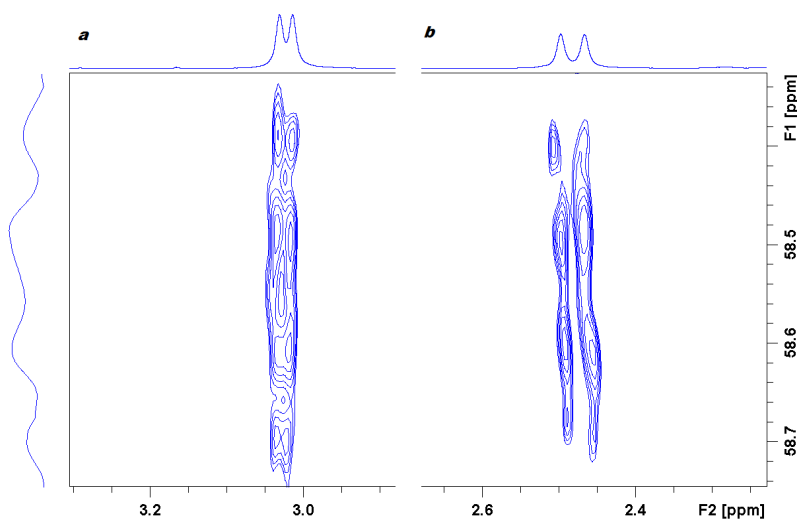


**Figure 64:** Plot of a  $^1\text{H}$ - $^{13}\text{C}$  HMQC NMR experiment which correlates the proton signals at  $\delta$  3.05 and  $\delta$  2.53 with a  $^{13}\text{C}$  NMR signal at  $\delta$  58.55, with  $J_{\text{PC}} = J_{\text{RhC}} = 10$  Hz.

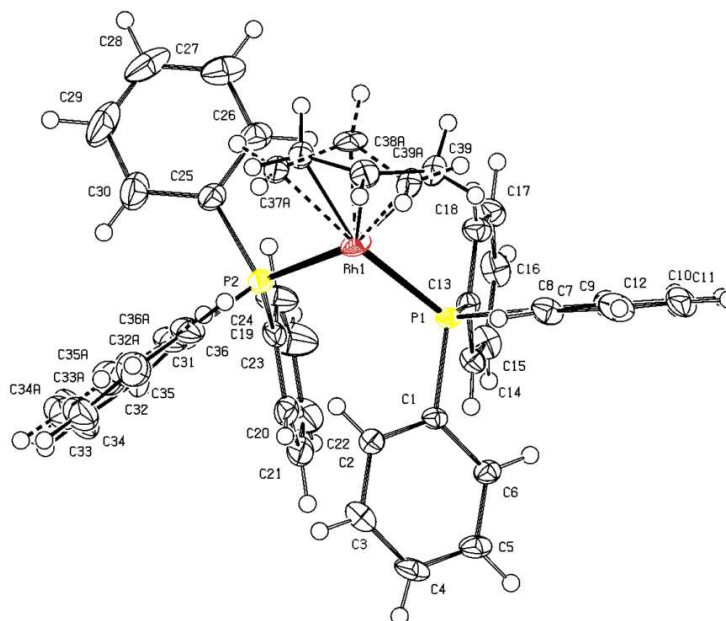
## Chapter three

Table 35: Multinuclear NMR data for **16** (298 K in toluene-*d*<sub>8</sub>)

Group / nucleus	Chemical shift (δ)	Multiplicity	Coupling constants (Hz)
<b><sup>1</sup>H</b>			
<i>meso</i> -CH	5.23 (1H)	m, d	$J_{HH} = 7.0, 13.0$ $J_{RhH} = 2.6, J_{PH} < 1$
<i>syn</i> -CH	3.05 (2H)	d, br	$J_{HH} = 7.0, J_{PH} < 1$
<i>anti</i> -CH	2.53 (2H)	d, d	$J_{HH} = 13.0, J_{PH} = 4.0$
<i>PPh</i> - <i>o</i> -H	7.53 (12H)	d, d	$J_{HH} = 7.0, J_{PH} \sim 7.0$
<i>PPh</i> - <i>m</i> -H	6.97 (12H)	m, overlapped	-
<i>PPh</i> - <i>p</i> -H	6.96 (6H)	m, overlapped	-
<b><sup>31</sup>P</b>			
	41.90	d	$J_{RhP} = 202$
<b><sup>13</sup>C</b>			
$\eta^3$ -Allyl-CH <sub>2</sub>	58.6	quart	$J_{PC} = 10.0, J_{RhC} = 10.0$
$\eta^3$ -Allyl-CH	46.9		-
<i>PPh</i> - <i>o</i> -C	134.0	d, d	$J_{PC} = 3.9, 7.9$
<i>PPh</i> - <i>m</i> -C	127.3		-
<i>PPh</i> - <i>p</i> -C	128.8		-

### 3.2.3 XRD studies

Single-crystal suitable for X-ray diffraction studies of **16** were obtained by addition of hexane to its diethyl ether solution. This enabled the solid to precipitate. Selected crystallographic data for **16** are presented in Table 36. Complete crystallographic data for **16** are provided in **Appendix 2**.



**Figure 65: Molecular structure of 16: ORTEP view showing 51.3% and 48.7% probability ellipsoids for 16A and 16B.**

**16** contains two conformations, **16A** and **16B** in the solid state that differ according to the arrangement of the allyl group with the two phosphine ligands. (**16A**: C<sub>37</sub>-C<sub>38</sub>-C<sub>39</sub>; **16B**: C<sub>371</sub>-C<sub>381</sub>-C<sub>391</sub> in Figure 65) The structures of **16A** and **16B** are illustrated in Figure 65. The occupancy of **16A** and **16B** was estimated to be 0.513 and 0.487 respectively. The metal centre in both forms display a slightly distorted square planar configuration. In addition, the two phosphine ligands are now non-equivalent in solid state, which is different to the situation in solution. Allyl rotation would lead to the necessary equivalence and <sup>31</sup>P NMR signal averaging in solution. This situation is common for η<sup>3</sup>-allyl transition metal complexes.<sup>130,153</sup>

Table 36: Selected bond lengths (Å) and angles (°) of 16A and 16B

Selected bond lengths of <b>11A</b> (Å)		Selected bond lengths of <b>11B</b> (Å)	
C <sub>39</sub> -Rh	2.225(8)	C <sub>391</sub> -Rh	2.109(9)
C <sub>37</sub> -Rh	2.131(7)	C <sub>371</sub> -Rh	2.248(13)
P <sub>1</sub> -Rh <sub>1</sub>	2.2403(8)	P <sub>1</sub> -Rh <sub>1</sub>	2.2403(8)
P <sub>2</sub> -Rh <sub>1</sub>	2.2582(9)	P <sub>2</sub> -Rh <sub>1</sub>	2.2582(9)
Selected bond angles of <b>16A</b>		Selected bond angles of <b>16B</b>	
P <sub>1</sub> -Rh <sub>1</sub> -C <sub>39</sub>	93.2(2)	P <sub>1</sub> -Rh <sub>1</sub> -C <sub>391</sub>	102.4(2)
P <sub>1</sub> -Rh <sub>1</sub> -C <sub>37</sub>	160.0(2)	P <sub>1</sub> -Rh <sub>1</sub> -C <sub>371</sub>	169.4(3)
P <sub>2</sub> -Rh <sub>1</sub> -C <sub>39</sub>	160.5(2)	P <sub>2</sub> -Rh <sub>1</sub> -C <sub>371</sub>	88.90(3)
P <sub>2</sub> -Rh <sub>1</sub> -C <sub>37</sub>	98.3(3)	P <sub>2</sub> -Rh <sub>1</sub> -C <sub>371</sub>	88.9(3)
P <sub>1</sub> -Rh <sub>1</sub> -P <sub>2</sub>	100.93(3)	P <sub>1</sub> -Rh <sub>1</sub> -P <sub>2</sub>	100.93(3)

No structure was found in the literature that is close to **16** (three coordinated rhodium  $\eta^3$ -allyl species). The benzyl analogue  $\text{Rh}(\eta^3\text{-CH}_2\text{-C}_6\text{H}_5)[\text{P}(i\text{-Pr})_3]_2$  was prepared and characterized by Werner.<sup>154</sup> The structural chemistry of  $\text{Rh}(\eta^3\text{-allyl})(\text{L})(\text{PR}_3)$  (where, L = CO, PF<sub>3</sub>) type complexes are known. Examples for six coordinated Rh(III) allyl species can also be found in the literature.<sup>150</sup> Table 37 presents a comparison of the parameters for these complexes using  $\text{Rh}(\eta^3\text{-allyl})(\text{PPh}_3)_2$ ,  $\text{RhCl}_2(\eta^3\text{-allyl})(\text{Xantphos})_2$ <sup>150</sup> and  $\text{Rh}[\eta^3\text{-C}_3\text{H}_4(\text{OMe})](\text{CO})(\text{PPh}_3)_2$ <sup>151</sup>. According to these data, the length of the metal-carbon bonds and metal-phosphorus bonds in **16** fall into the average value of the three species. It was also revealed that the bond angle in the allyl ligand was dependent on the nature of the complex. In **16**, this value is 121.1°, which in good accordance with theoretical value (120°). However, it is 124.9° in  $\text{RhCl}_2(\eta^3\text{-allyl})(\text{Xantphos})_2$  which could be caused by the bulky phosphine ligand, Xantphos. A substituent (OMe or Ph) on the allyl group decreases the bond angle of the allyl group.

**Table 37: A comparison of the structural parameters for **16** and other known rhodium allyl species**

Compound	Rh( $\eta^3$ -allyl)(PPh <sub>3</sub> ) <sub>2</sub>	RhCl <sub>2</sub> ( $\eta^3$ -allyl)(Xantphos) <sub>2</sub>	Rh[ $\eta^3$ -C <sub>3</sub> H <sub>4</sub> (OMe)](CO)(PPh <sub>3</sub> ) <sub>2</sub>
Rh-C <sub>1</sub>	2.225(8)	2.232(11)	2.179(4)
Rh-C <sub>2</sub>	2.131(11)	2.186(14)	2.145(4)
Rh-C <sub>3</sub>	2.131(7)	2.241(11)	2.233(4)
Rh-P <sub>1</sub>	2.2403(8)	2.394(2)	2.309(2)
Rh-P <sub>2</sub>	2.2582(9)	2.437(2)	2.399(1)
C <sub>1</sub> -C <sub>2</sub>	1.381(13)	1.414(18)	1.407(5)
C <sub>2</sub> -C <sub>3</sub>	1.376(10)	1.442(18)	1.393(5)
C <sub>1</sub> -C <sub>2</sub> -C <sub>3</sub>	121.1(10)	124.9(14)	114.3(4)

### 3.3 Control Reaction of Rh( $\eta^3$ -C<sub>3</sub>H<sub>5</sub>)(PPh<sub>3</sub>)<sub>2</sub> with *parahydrogen*

#### 3.3.1 Reaction of Rh( $\eta^3$ -C<sub>3</sub>H<sub>5</sub>)(PPh<sub>3</sub>)<sub>2</sub> with *parahydrogen* in toluene-d<sub>8</sub>

In order to follow the catalytic behaviour of **16** in hydroformylation, two control reactions were carried out. The first reaction aimed at understanding the reaction of **16** and *parahydrogen* and was undertaken over the temperature range 203 K to 273 K.

When a sample of **16** that was dissolved in toluene-d<sub>8</sub> under 3 atm. of *parahydrogen* was monitored by NMR spectroscopy at 203 K, no reaction was evident at this stage. However, when the sample was warmed to 243 K, a reaction was revealed by the detection of two broad hydride resonances at  $\delta$  -8.30 and  $\delta$  -15.18 with a ratio of 1 : 1. These hydride resonances were also visible when the reaction was monitored at 273 K. In addition, two polarised signals at  $\delta$  0.93 and  $\delta$  1.43 were seen due to the hydrogenation product propane at 273 K. We note that the polarization on organic products only lasts for several seconds at 273 K, suggesting very quick hydrogenation. The hydrogen peak was broad after the reaction, suggesting that it is exchanging with active species in solution. The H<sub>2</sub> signal sharpened when the sample was cooled to 243 K, which indicates the hydride-H<sub>2</sub> exchange is suppressed by cooling. We note that the hydride species formed in this reaction is stable at 273 K for several hours, which enables its full characterization.

### Chapter three

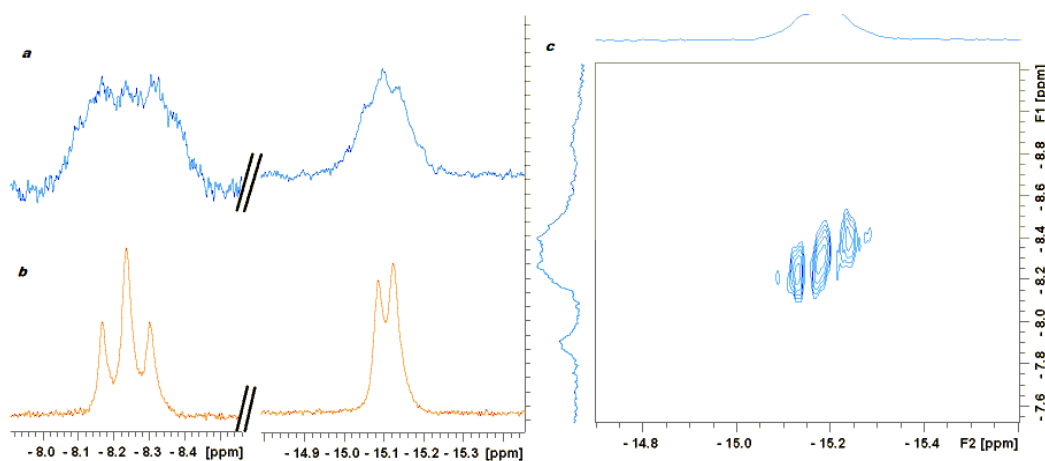


**Figure 66:** (a) and (b): Region of the 1D NMR spectra showing the hydride region that was recorded when 16 reacted with parahydrogen in toluene- $d_8$ ; (a):  $^1\text{H}$ ; (b):  $^1\text{H}\{^{31}\text{P}\}$ ; (c): Spots taken from the 2D  $^1\text{H}$ - $^1\text{H}$  COSY spectrum that links the two hydride resonances  $\delta$  -8.30 and  $\delta$  -15.18

In the 2D-COSY experiment, a weak correlation between these two signals was observed as shown in Figure 66, and hence these resonances can be attributed to ligands in the same species. The hydride resonance at  $\delta$  -8.30 simplifies into triplet in the corresponding  $^1\text{H}\{^{31}\text{P}\}$  NMR spectrum. It therefore couples to two rhodium nuclei through common couplings of 27.3 Hz, whereas the resonance at  $\delta$  -15.18 only couples to one rhodium nucleus through a coupling of 15.3 Hz. This indicates that the resonance at  $\delta$  -8.30 arises from a bridged hydride ligand, while the  $\delta$  -15.18 resonance arises from a terminal hydride. The corresponding  $^1\text{H}$  and  $^1\text{H}\{^{31}\text{P}\}$  NMR spectra for this species are illustrated in Figure 66.

In the corresponding  $^{31}\text{P}^{148}$  spectrum, two resonances were detected at  $\delta$  54.41 ( $J_{\text{RhP}} = 112.3$  Hz) and  $\delta$  49.22 ( $J_{\text{RhH}} = 162.4$  Hz, 51.1 Hz). The  $^{31}\text{P}$  NMR signal at  $\delta$  49.22 couples to both of hydride signals at  $\delta$  -8.30 and  $\delta$  -15.18, whereas the resonance at  $\delta$  54.41 only couples with the hydride resonance at  $\delta$  -15.18, according to corresponding 2D  $^1\text{H}$ - $^{31}\text{P}$  HMQC experiment. Figure 67 illustrates the expansion of the  $^1\text{H}$ - $^{31}\text{P}$  HMQC spectra that link the two hydride signals and the two  $^{31}\text{P}$  signals.

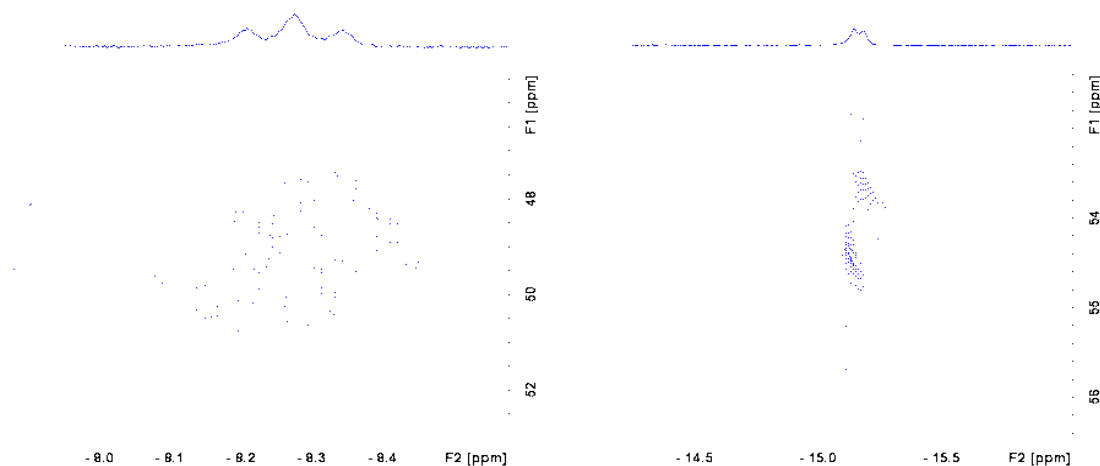


**Figure 67:** Expansions taken from a  $^1\text{H}$ - $^{31}\text{P}$  HMQC NMR spectrum showing the correlation of the hydride signals at  $\delta$  -8.30 and  $\delta$  -15.18 with two  $^{31}\text{P}$  centres at  $\delta$  54.41 and  $\delta$  49.22.

Based on the coupling pattern, we are dealing with Rh(III) and Rh(I) centres. The new product was therefore confirmed to be  $\text{Rh}(\text{H})_2(\text{PPh}_3)_2(\mu\text{-H})_2\text{Rh}(\text{PPh}_3)_2$  (**46**). The structure of **46** is shown in Figure 68, and the NMR data for **46** is summarized in Table 38. **46** is stable in toluene for a couple of days. Isolation of **46** was not achieved due to its high reactivity towards halogenated solvents and high solubility in most common solvents.

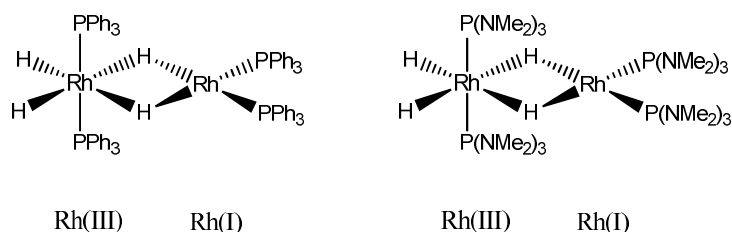
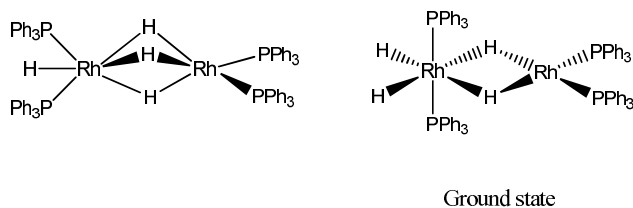


**Figure 68:** Structure of  $\text{Rh}(\text{H})_2(\text{PPh}_3)_2(\mu\text{-H})_2\text{Rh}(\text{PPh}_3)_2$  (**46**) and a similar complex,  $\text{Rh}(\text{H})_2[\text{P}(\text{NMe}_2)_3]_2(\mu\text{-H})_2\text{Rh}[\text{P}(\text{NMe}_2)_3]_2$

A closely related example to **46** is  $\text{Rh}(\text{H})_2[\text{P}(\text{NMe}_2)_3]_2(\mu\text{-H})_2\text{Rh}[\text{P}(\text{NMe}_2)_3]_2$ , which was studied by NMR and X-ray diffraction methods.<sup>155</sup> According to these studies,  $\text{Rh}(\text{H})_2[\text{P}(\text{NMe}_2)_3]_2(\mu\text{-H})_2\text{Rh}[\text{P}(\text{NMe}_2)_3]_2$  displays the configuration presented in Figure 68 in both solution and the solid state.

A range of dinuclear rhodium hydride complexes that bear phosphite ligands have also been reported.<sup>152,155</sup> NMR study showed that the resting state of one of them,  $\text{Rh}(\text{H})_4[\text{P}(\text{O}-i\text{-C}_3\text{H}_7)_3]_4$ , is  $\text{RhH}[\text{O}-i\text{-C}_3\text{H}_7)_3]_2(\mu\text{-H})_3\text{Rh}[\text{O}-i\text{-C}_3\text{H}_7)_3]_2$  rather than  $\text{Rh}(\text{H})_2[\text{P}(\text{O}-i\text{-C}_3\text{H}_7)_3]_2(\mu\text{-H})_2\text{Rh}[\text{P}(\text{O}-i\text{-C}_3\text{H}_7)_3]_2$ . The possible conformations of **46** are illustrated in Figure 69.

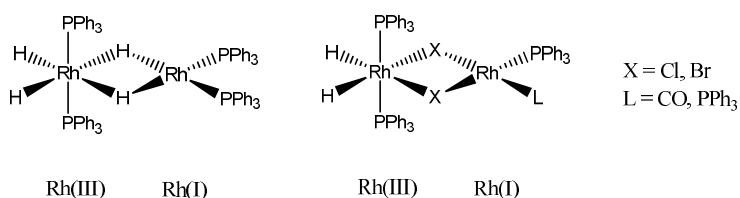
### Chapter three



**Figure 69:** The conformation of isomers of **46**

Catalytic hydrogenation by type **46** complexes was studied by Clement.<sup>156</sup> However, no mechanistic information was given in their report. As a repeat, two parallel samples that contains 1  $\mu\text{M}$  of  $\text{RhCl}(\text{PPh}_3)_3$  and **46** were prepared and 3  $\mu\text{l}$  of styrene was added to each of them. Two samples was degassed and placed under 3 atm. of hydrogen. The substrate in sample with catalyst **46** consumed in 45 s, while the other in 13 mins. That means the hydrogenation rate using **46** is approximately eighteen times quicker than well known Wilkinson's catalyst. These experiments are not standard kinetic measurements due to the diffusion problem in the NMR sample but to simply compare their reactivity. It was suggested by Mutterties that hydrogenation happens at the Rh(I) centre in **46** type complexes.<sup>152</sup>

We also note the similarity of these data to those previously reported for  $\text{Rh}(\text{H})_2(\text{PPh}_3)_2(\mu\text{-Cl})_2\text{Rh}(\text{PPh}_3)_2$ <sup>20</sup>,  $\text{Rh}(\text{H})_2(\text{PPh}_3)_2(\mu\text{-Cl})_2\text{Rh}(\text{PPh}_3)(\text{CO})$  and  $\text{Rh}(\text{H})_2(\text{PMe}_3)_2\text{Cl}(\mu\text{-H})(\mu\text{-Cl})\text{Rh}(\text{PMe}_3)(\text{CO})$ .<sup>157</sup> Figure 70 illustrates structures of these complexes.

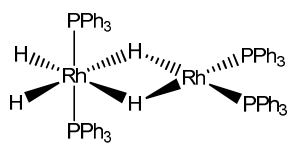


**Figure 70:** Structure of  $\text{Rh}(\text{H})_2(\text{PPh}_3)_2(\mu\text{-H})_2\text{Rh}(\text{PPh}_3)_2$  (**46**) and related complexes

In conclusion, the reaction of  $\text{Rh}(\eta^3\text{-C}_3\text{H}_5)(\text{PPh}_3)_2$  (**16**) with  $\text{H}_2$  in toluene is too fast for mechanistic study and a stable, dimeric hydride product **46** is formed. To trap the intermediates, extra ligands such as  $\text{CH}_3\text{CN}$  must be added.



Table 38: Multinuclear NMR data for **46** (273 K in toluene- $d_8$ )

			
Group / nucleus	Chemical shift ( $\delta$ )	Multiplicity	Coupling constants (Hz)
<b><math>^1\text{H}</math></b>			
bridged hdyride	-15.18 (2H)	d, t, br	$J_{\text{RhH}} = 15.3$ , $J_{\text{PH}} \sim 20$ $ J_{\text{HH}}  < 3$ .
terminal hydride	-8.30 (2H)	d, d t	$J_{\text{RhH}} = 27.3$ , $J_{\text{PH}} \sim 20$ $ J_{\text{HH}}  < 3$
$\text{P}_\text{B}\text{Ph-}o\text{-H}$	7.40	m	
$\text{P}_\text{B}\text{Ph-}m\text{-H}$	6.80	m	
$\text{P}_\text{B}\text{Ph-}p\text{-H}$	6.96	m	
$\text{P}_\text{A}\text{Ph-}o\text{-C}$	8.14	m	
$\text{P}_\text{A}\text{Ph-}m\text{-C}$	6.85	m	
$\text{P}_\text{A}\text{Ph-}p\text{-C}$	7.48	m	
<b><math>^{31}\text{P}</math></b>			
$\text{P}_\text{A}$	49.20	d	$J_{\text{RhP}} = 166.0$
$\text{P}_\text{B}$	54.40	d	$J_{\text{RhP}} = 111.9$
<b><math>^{13}\text{C}</math></b>			
$\text{P}_\text{A}\text{Ph-}o\text{-C}$	135.0		
$\text{P}_\text{A}\text{Ph-}m\text{-C}$	127.4		
$\text{P}_\text{A}\text{Ph-}p\text{-C}$	134.2		
$\text{P}_\text{B}\text{Ph-}o\text{-C}$	134.5		
$\text{P}_\text{B}\text{Ph-}m\text{-C}$	127.3		
$\text{P}_\text{B}\text{Ph-}p\text{-C}$	128.0	s	

### 3.3.2 Reaction of the detected product $\text{Rh}(\text{H})_2(\text{PPh}_3)_2(\mu\text{-H})_2\text{Rh}(\text{PPh}_3)_2$ (**46**) with CO

When a sample of  $\text{Rh}(\text{H})_2(\text{PPh}_3)_2(\mu\text{-H})_2\text{Rh}(\text{PPh}_3)_2$  (**46**) in toluene- $d_8$  was exposed to CO and monitored by NMR spectroscopy at room temperature, two broad hydrides signals were immediately detected at  $\delta$  -8.89 (br, peak width: 15 Hz) and  $\delta$  -9.64 (br) (with a ratio >

### Chapter three

10:1), The  $\delta$  -8.89 resonance coupled with a  $^{31}\text{P}$  nucleus that resonates at  $\delta$  36.9 (doublet,  $J_{\text{RhP}} = 139$  Hz) though a *cis* coupling according to a  $^1\text{H}$ - $^{31}\text{P}$  HMQC experiment. The  $^{103}\text{Rh}$ - $^{31}\text{P}$  coupling on the  $^{31}\text{P}$  NMR signals suggests that they arise from those of Rh(I) species. The NMR properties for this hydride resonance are almost identical with the known species  $\text{RhH}(\text{CO})(\text{PPh}_3)_3$  (**1**). (lit.  $^1\text{H}$ :  $\delta$  -8.90, peak width 10 - 15 Hz).<sup>33</sup> The hydride signal at  $\delta$  -9.64 was too weak for further characterization. Nevertheless, these two new products are ascribed to  $\text{RhH}(\text{CO})(\text{PPh}_3)_3$  (**1**) and  $\text{RhH}(\text{CO})_2(\text{PPh}_3)_2$  (**2ee**) for they are always in equilibrium under CO. The structures of **1** and **2ee** are illustrated in Figure 71.

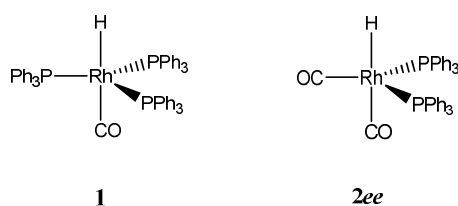
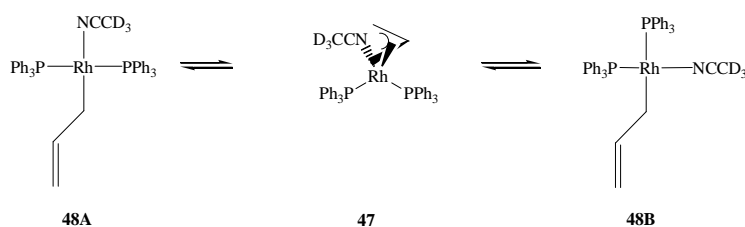


**Figure 71: Structure of  $\text{RhH}(\text{CO})(\text{PPh}_3)_3$  (**1**) and  $\text{RhH}(\text{CO})_2(\text{PPh}_3)_2$  (**2ee**)**

#### 3.3.3 Reaction of $\text{Rh}(\eta^3\text{-C}_3\text{H}_5)(\text{PPh}_3)_2$ with acetonitrile- $\text{d}_3$

The reaction of  $\text{Rh}(\eta^3\text{-C}_3\text{H}_5)(\text{PPh}_3)_2$  (**16**) with *parahydrogen* in acetonitrile- $\text{d}_3$  is much slower than it is in toluene- $\text{d}_8$ . However, the difficulty in this study lies in the poor solubility of **16** in acetonitrile at low temperature. When **16** was dissolved in an 1 : 1 mixture of toluene- $\text{d}_8$  and  $\text{CD}_3\text{CN}$ , no reaction was evident after 24 hours at 298 K. However, when a sample of **16** was dissolved in acetonitrile- $\text{d}_3$  and monitored by NMR spectroscopy at 298 K, a reaction product was detected due to the observation of three  $^1\text{H}$  NMR signals at  $\delta$  4.98,  $\delta$  2.60 and  $\delta$  2.04. The  $\delta$  4.98 signal was highly coupled. However, the detailed shape of this signal was not clear due to overlap. The  $^{31}\text{P}$  coupling on this signal was estimated to be less than 1.5 Hz. The  $^1\text{H}$  NMR signals at  $\delta$  2.04 was a doublet of triplets due to the coupling with a rhodium and two further phosphorus centres. The  $^1\text{H}$  NMR signal at  $\delta$  2.60 sharpened slightly on  $^{31}\text{P}$  decoupling. When a  $^1\text{H}$ - $^{31}\text{P}$  HMQC experiment was undertaken, connection of the  $^1\text{H}$  NMR signals at  $\delta$  4.98 and  $\delta$  2.04 to a  $^{31}\text{P}$  centre that resonates at  $\delta$  41.04 were observed, which possesses a rhodium coupling of 200.98 Hz. These are similar with the starting material **16**. Based on these data, the new product was assigned to be the solvated  $18\text{e}^-$  product  $\text{Rh}(\eta^3\text{-C}_3\text{H}_5)(\text{NCCD}_3)(\text{PPh}_3)_2$  (**47**). The NMR data for **47** is listed in Table 39.

In addition, two further  $\eta^1$ -allyl groups are evident in these NMR spectra as resonances at  $\delta$  4.01, 5.06, 5.24, 5.81 and at  $\delta$  3.10, 5.30, 5.23, 5.86 respectively when **16** reacts with acetonitrile at 298 K. However, these two species are low in intensity and very hard to characterise. The two doublet of doublets signals at around  $\delta$  5.0 are diagnostic of an  $\eta^1$ -allyl moiety. Now the Rh-CH<sub>2</sub> proton appears around  $\delta$  2.0 -  $\delta$  4.0. A *trans* electron withdrawing group such as CD<sub>3</sub>CN moves them to lower field. In addition, there are possibly four or five  $\eta^1$  allyl proton resonances depending on whether the CH<sub>2</sub> group protons signal are diastereotopic or not. According to their observed NMR information, and based on their consequent reaction products with *parahydrogen*, they are ascribed to **48A** and **48B** with structures illustrated in Scheme 31.



**Scheme 31:** When  $Rh(\eta^3-C_3H_5)(PPh_3)_2$  reacts with acetonitrile- $d_3$  at 298 K, three acetonitrile substitution and association products, **47**, **48A** and **48B** form immediately.

**Table 39:** NMR data for **47** (273 K in toluene- $d_8$ )

Group nucleus	Chemical shift ( $\delta$ )	Multiplicity	Coupling constants (Hz)
<b><math>^1H</math></b>			
	4.98,	m	$J_{HH} = 7.0, 12.4, J_{PH} < 1.5$
	2.60	d, br	$J_{HH} = 6.97$
	2.04	d, m	$J_{HH} = 12.4, J_{PH} \sim 3.5$
<b><math>^{31}P</math></b>			
	41.04	d	$J_{RHP} = 201.0$

### 3.3.4 Reaction of $Rh(\eta^3-C_3H_5)(PPh_3)_2$ with *parahydrogen* in acetonitrile- $d_3$ at 298K

### Chapter three

When the reaction of  $\text{Rh}(\eta^3\text{-C}_3\text{H}_5)(\text{PPh}_3)_2$  with *parahydrogen* in  $\text{CD}_3\text{CN}$  was monitored by NMR spectroscopy at 298 K, a number of polarized species were detected. These correspond to the organic materials, propene and propane, and a new inorganic product.

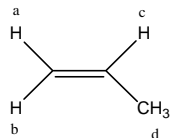


**Figure 72: Structure of propene**

The signals for propene appeared at  $\delta$  5.82, (1H, H<sub>c</sub>) 4.99, (1H, H<sub>a</sub>) 4.88 (1H, H<sub>b</sub>) and 1.67 (3H, H<sub>d</sub>) respectively. The resonances at  $\delta$  1.67, 4.99 and 4.88 showed strong PHIP, while the signal at  $\delta$  5.82 due to the H<sub>c</sub> had very little polarized component. The signals for propane that appear at  $\delta$  0.90 and  $\delta$  1.34 are strongly polarized. These results are illustrated in Figure 73.

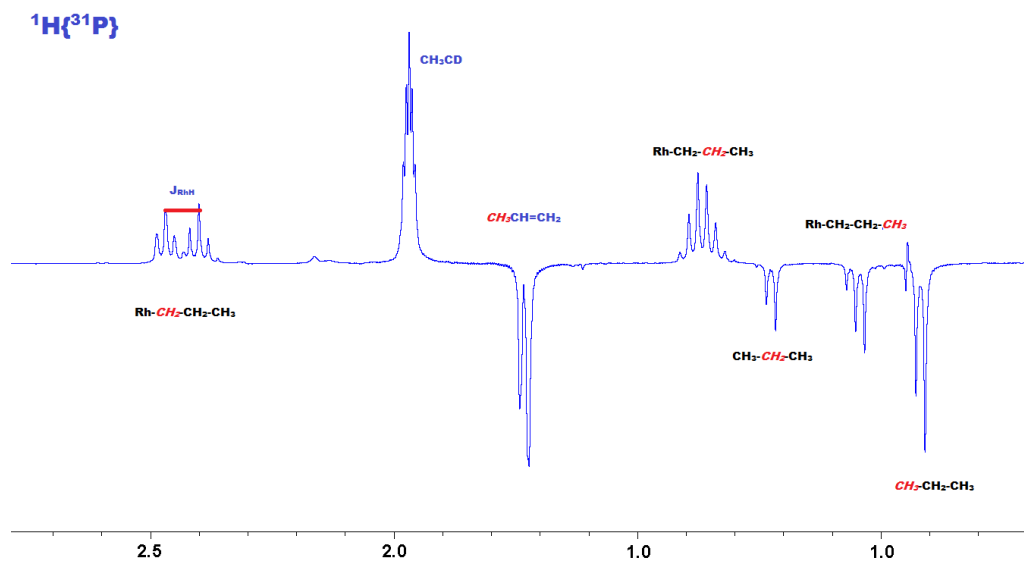


**Figure 73:  $^1\text{H}\{^{31}\text{P}\}$  NMR spectrum taken from the reaction of  $\text{Rh}(\eta^3\text{-C}_3\text{H}_5)(\text{PPh}_3)_2$  and *parahydrogen* at 298 K, where polarized signals due to propene, propane and a rhodium alkyl species are observed**

The most striking result in this study was the detection of the rhodium alkyl intermediate **49**. Figure 73 shows part of the  $^1\text{H}\{^{31}\text{P}\}$  NMR spectrum for this reaction at 298 K. The three signals at  $\delta$  2.43, 1.23 and 1.05 arise from a new species **49**; even though it could not be characterized fully. The signal at  $\delta$  2.43 appears as a doublet of triplets with  $J_{\text{RhH}} = 27$  Hz and  $J_{\text{HH}} = 7.57$  Hz and was therefore assigned to a  $\text{Rh-CH}_2$  motif. The signals at  $\delta$  2.43 and

$\delta$  1.05 share a  $^1\text{H}$ - $^1\text{H}$  coupling of 7.54 Hz. These are in good accordance with a Rh-CH<sub>2</sub>-CH<sub>2</sub>-CH<sub>3</sub> grouping. However, the rest of this species is not clear due to its short life time. A possible structure for **49** is illustrated in Figure 74.

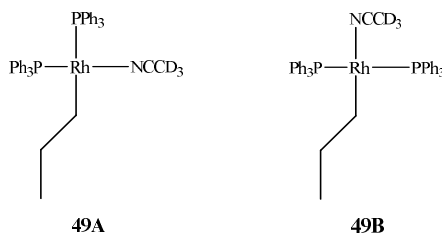


**Figure 74: Structures of 49A and 49B**

Two further hydride signals were detected at  $\delta$  -16.96 and  $\delta$  -17.14 due to the new products **50** and **51** after the reaction. Their chemical shift suggests that they are *trans* to acetonitrile. Both of these signals couple with two PPh<sub>3</sub> ligand that are arranged in a *cis* configuration as shown in the corresponding  $^1\text{H}$  and  $^1\text{H}\{^{31}\text{P}\}$  spectra. The corresponding  $^{31}\text{P}$  signals are detected at  $\delta$  42.4 and  $\delta$  44.1 respectively, as shown in Figure 75. The  $^{31}\text{P}$  NMR signal at  $\delta$  42.4 possesses a rhodium coupling of 108.0 Hz, while the signal at  $\delta$  44.1 of 111.2 Hz. This suggests that the new products are Rh(I) species.

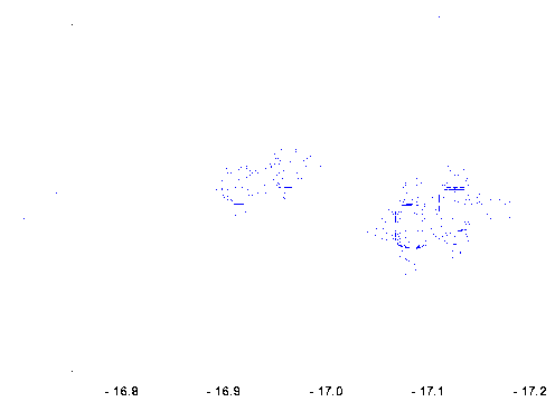


**Figure 75: The  $^1\text{H}$ - $^{31}\text{P}$  NMR spectrum that links the hydrides signals at  $\delta$  -16.96 and  $\delta$  -17.14 with their  $^{31}\text{P}$  neighbours.**

In order to understand the chemistry of the new hydride species, a series experiment was undertaken. We note that the NMR feature of these two hydride species are close to those of the known complex Rh(H)<sub>2</sub>(PPh<sub>3</sub>)<sub>2</sub>( $\mu$ -Br)<sub>2</sub>Rh(PPh<sub>3</sub>)<sub>2</sub> (**52**), which is a product by reacting RhBr(PPh<sub>3</sub>)<sub>3</sub> (**53**), the starting material to prepare **16**, with *parahydrogen*. However, when a

### Chapter three

mixture of  $\text{Rh}(\eta^3\text{-C}_3\text{H}_5)(\text{PPh}_3)_2$  and  $\text{RhBr}(\text{PPh}_3)_3$  in acetonitrile- $\text{d}_3$  was exposed to parahydrogen, a further signal at  $\delta$  17.54 due to  $\text{Rh}(\text{H})_2(\text{PPh}_3)_2(\mu\text{-Br})_2\text{Rh}(\text{PPh}_3)_3$  (**52**) was detected, besides the two hydride signals presented above. This excludes the possibility of being  $\text{Rh}(\text{H})_2(\text{PPh}_3)_2(\mu\text{-Br})_2\text{Rh}(\text{PPh}_3)_3$ .

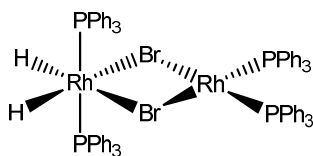


**Figure 76: Structure of  $\text{Rh}(\text{H})_2(\text{PPh}_3)_2(\mu\text{-Br})_2\text{Rh}(\text{PPh}_3)_3$  (**52**)**

The monohydride precursor  $\text{HRh}(\text{PPh}_3)_4$  (**54**) was also prepared by refluxing  $\text{RhCl}_3$  in ethanol. When a sample of  $\text{HRh}(\text{PPh}_3)_4$  was dissolved toluene- $\text{d}_8$ , a broad hydride resonance was observed at  $\delta$  -8.08 (width:  $\sim$  24 Hz). When a second sample of  $\text{HRh}(\text{PPh}_3)_4$  was dissolved acetonitrile- $\text{d}_3$  and monitored by NMR spectroscopy, no hydride signal was observed at 298 K. This suggests the fluxional element for  $\text{HRh}(\text{PPh}_3)_4$  and the new product. However, when the sample was cooled to 235 K, two hydride species are detected at  $\delta$  -17.06 and  $\delta$  -19.42 ( $J_{\text{RhH}} = 16.1$  Hz,  $J_{\text{PH}} = 8.47$  Hz). The new hydride signal at  $\delta$  -19.42 also couples with two *cis*  $^{31}\text{P}$  centres through a coupling of 12.6 Hz. Therefore, the hydride signals at  $\delta$  -16.96,  $\delta$  -17.14 are proposed to be  $\text{HRh}(\text{CD}_3\text{CN})_3(\text{PPh}_3)_2$ , (**50**) and  $\text{HRh}(\text{CD}_3\text{CN})_2(\text{PPh}_3)_2$  (**51**) respectively. The  $\text{PPh}_3$  ligands in all of these compounds are in *trans* to each other but *cis* to the hydride. The structures of these complexes are illustrated in Figure 77. Their NMR data is summarized in Table 40. The hydride signal at  $\delta$  -19.42 might arise from a unknown Rh(III) species, as the H-Rh coupling is significantly larger than that of the other two.

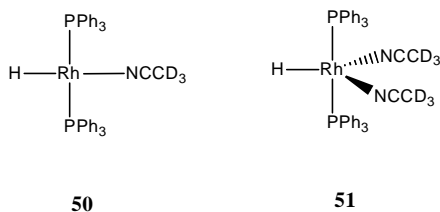


**Figure 77: Structure of **50**, **51****

We note the same difficulty to resolve the identity of these solvated hydride complexes in the literature.<sup>158</sup> **50** and **51** were not further characterized due to the high cost of  $\text{CD}_3\text{C}^{15}\text{N}$ .

Table 40: NMR data for the hydride species when **54** reacts with hydrogen

	HRh(CD <sub>3</sub> CN)(PPh <sub>3</sub> ) <sub>2</sub>	HRh(CD <sub>3</sub> CN) <sub>2</sub> (PPh <sub>3</sub> ) <sub>2</sub>	HRh(CD <sub>3</sub> CN)(CN)(CD <sub>3</sub> )(PPh <sub>3</sub> ) <sub>2</sub>
<b>Hydride</b>	δ -16.96 (d, d, d)	δ -17.14 (d, d, d)	δ 19.42 (d, d, d)
J <sub>PH</sub>	13.63 Hz	12.65 Hz	12.63 Hz
J <sub>RhH</sub>	19.14 Hz	16.87 Hz	8.47 Hz
<sup>31</sup> P	δ 42.4	δ 41.1	δ 39.55 (d, m)
J <sub>RhP</sub>	108.0	111.2	165.2

### 3.3.5 Reaction of Rh(η<sup>3</sup>-C<sub>3</sub>H<sub>5</sub>)(PPh<sub>3</sub>)<sub>2</sub> with parahydrogen in acetonitrile-d<sub>3</sub> at 273 K

A control reaction of **16** and parahydrogen in CD<sub>3</sub>CN was undertaken at 273 K. Experiments at lower temperature were not possible due to the precipitation of starting material. When a sample of **16** was dissolved in acetonitrile-d<sub>3</sub> and exposed to 3 atm. of parahydrogen and examined by NMR spectroscopy at 273 K, two thermal hydride resonances due to **50** and **51** were detected at δ -16.96 and δ -17.14 respectively.

In addition, four further polarized hydride resonances were also detected at δ -10.03, -10.47, -16.53 and -16.94. The corresponding COSY experiments grouped these signals at δ -10.47 and δ -16.94 to one complex **56A**, while the signal at δ -10.03 and δ -16.53 to another complex **56B**. Both **56A** and **56B** are hydrogen addition products. We note that the signal at δ -16.94 overlaps with the signal at δ -16.96 due to **50**. The <sup>1</sup>H-<sup>1</sup>H OPSY-COSY pulse program was used, in which the thermal resonance of **50** is suppressed, to reveal a correlation between the <sup>1</sup>H NMR signals at δ -16.94 and δ -10.47. Figure 78 shows the corresponding <sup>1</sup>H-<sup>1</sup>H COSY spectrum.

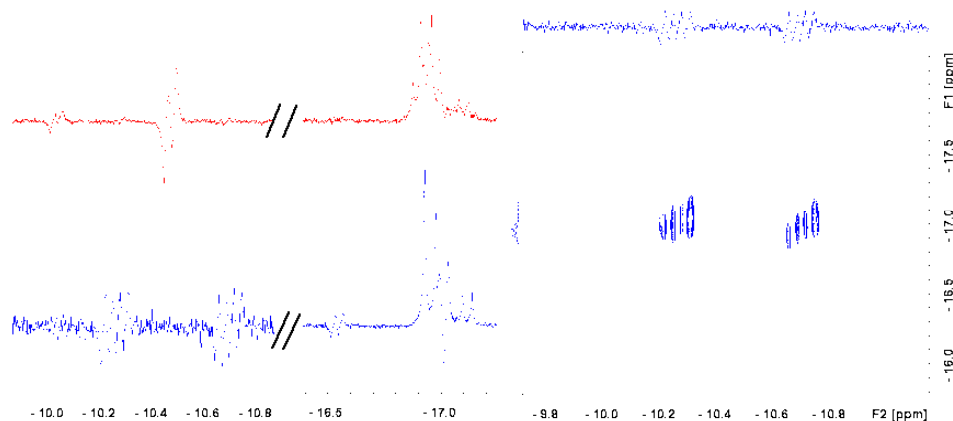
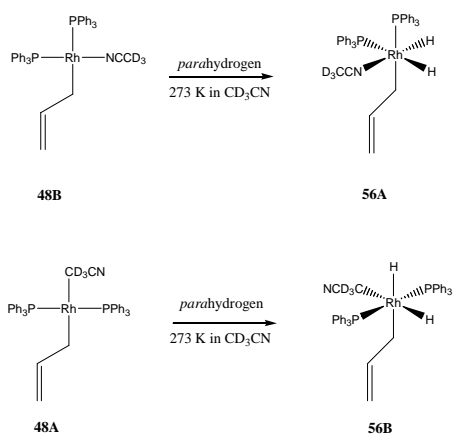


**Figure 78:** (a)  $^1\text{H}$  spectrum taken from the hydride region when **11** reacts with parahydrogen at 263K. (b) The  $^1\text{H}\{^{31}\text{P}\}$  spectrum. (c) Expansion of the COSY spectrum that correlates the  $^1\text{H}$  signals at  $\delta$  -10.47 and  $\delta$  -16.94.

The  $^1\text{H}$  NMR signal at  $\delta$  10.47 is doublet of quartet of doublets in appearance, with  $J_{\text{PH}} = 174$  Hz, 12 Hz,  $J_{\text{RhH}} = 22$  Hz and  $J_{\text{HH}} = 6.7$  Hz. It simplified into doublet of doublets on  $^{31}\text{P}$  decoupling. Its partner at  $\delta$  -16.94 shows only *cis*  $^{31}\text{P}$  coupling although the exact value is masked. However, its chemical shift suggests that it is *trans* to an acetonitrile ligand. Based on this information, the new compound contains two hydride ligands and one  $\text{PPh}_3$  ligand which is in *trans* to  $\text{H}_a$  and *cis* to  $\text{H}_b$ , another phosphine ligand which is *cis* with both  $\text{H}_a$  and  $\text{H}_b$ . The acetonitrile ligand is *trans* with  $\text{H}_b$ . The other coordination site must be occupied by an  $\eta^1$ -allyl ligand. However, the allyl ligand was detected due to short life time of **56A**. The structure of **56A** is illustrated in Scheme 32.

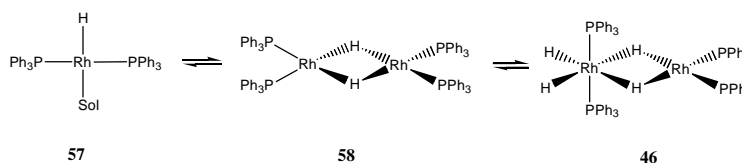


**Scheme 32:** The formation of **56A** and **56B**



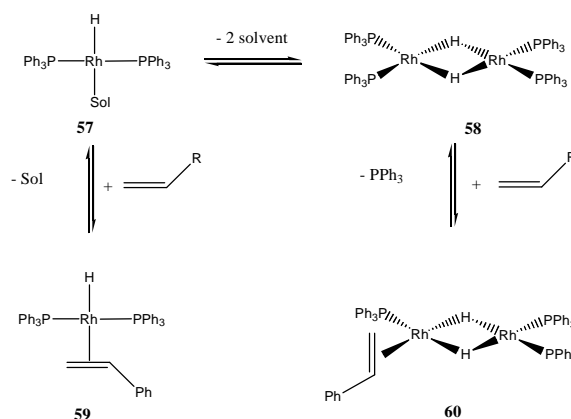
The  $^1\text{H}$  NMR signal at  $\delta$  -10.03 and  $\delta$  -16.53 only show two *cis*  $^{31}\text{P}$  couplings. There are therefore two  $\text{PPh}_3$  ligands in *cis* orientation. The other two sites in the new product must be occupied by an acetonitrile ligand and a  $\eta^1$ -allyl ligand. The structure of this compound was proposed to be **56B** and confirmed by NMR spectroscopy. The observation of **56A** and **56B** is possible for several minutes at 273 K. After reaction, the hydride signal due to **50** and **51** were again detected in the final products.

### 3.3.6 Discussion & Conclusion



**Scheme 33:** Possible mechanism for the formation of **46**

Hydrogenation of the allyl group of  $\text{Rh}(\eta^3\text{-C}_3\text{H}_5)(\text{PPh}_3)_2$  in toluene- $d_8$  is too fast for mechanistic study. After the reaction, a dimeric rhodium hydride species **46** is formed and fully characterized. **46** undergoes hydrogen exchange with free hydrogen above 243 K. Scheme 33 illustrates the possible mechanism for its formation hydride-hydrogen exchange pathway. The structure of **46** was confirmed by multinuclear NMR characterization. **46** are very active hydrogenation catalyst. The ‘real’ active species could be **46** or **57**.



**Scheme 34:** Possible pathways that explains the catalytic behaviour of **46** upon hydrogenation

The reaction of  $\text{Rh}(\eta^3\text{-C}_3\text{H}_5)(\text{PPh}_3)_2$  and *parahydrogen* in the presence of acetonitrile follows the same route, as shown in Scheme 34. A control reaction revealed that a large excess of acetonitrile stabilizes the intermediates and enables the observation of ligand

## Chapter three

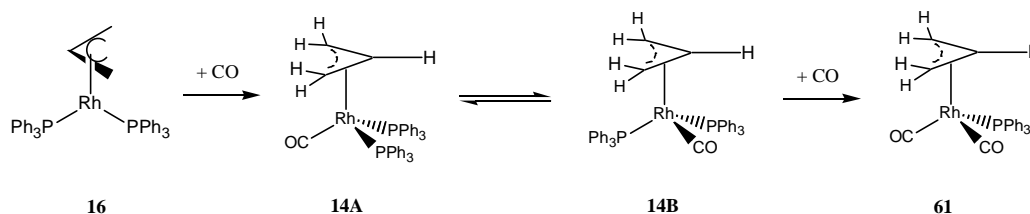
association and exchange products (**47**, **48**). Hydrogen addition to **48** yields **56A** and **56B** at 273 K, which were detected through PHIP (as shown in Figure 73). The first hydride transfer in **56** led to propene and  $\text{HRh}(\text{PPh}_3)_2(\text{CD}_3\text{CN})$  (**50**). Compound **50** associates with one or two  $\text{CD}_3\text{CN}$  ligands to form **51**.

It's most likely that the multistep hydrogenation of allyl group in **56** that yields propane happens without substrate liberation until it is complexly hydrogenated. In our study, a rhodium alkyl species **49** was detected by PHIP. The detection of **49** suggests that the two hydrides were transferred to the allyl group before binding the second hydrogen molecule. After the reaction, the hydrogenation product propane was detected by PHIP, while the signals due to **50** and **51** were not polarized at this stage.

### 3.4 Control reaction of $\text{Rh}(\eta^3\text{-C}_3\text{H}_5)(\text{PPh}_3)_3$ with CO ( $^{12}\text{CO}$ or $^{13}\text{CO}$ )

#### 3.4.1 Background

The reaction of  $\text{Rh}(\eta^3\text{-C}_3\text{H}_5)(\text{PPh}_3)_2$  and CO was expected to yield the CO association product  $\text{Rh}(\eta^3\text{-C}_3\text{H}_5)(\text{CO})(\text{PPh}_3)_2$  (**14**) and the further CO/ $\text{PPh}_3$  exchange product  $\text{Rh}(\eta^3\text{-C}_3\text{H}_5)(\text{CO})_2(\text{PPh}_3)$  (**61**), as illustrated in Scheme 35. Adding a large excess of CO converts these  $\eta^3$  allyl species to  $\eta^1$  allyl species. The reaction of **16** with CO was controlled by temperature in our study.



**Scheme 35:** Expected reaction of  $\text{Rh}(\eta^3\text{-C}_3\text{H}_5)(\text{PPh}_3)_2$  and CO leads to the formation of new  $\eta^3$ -allyl contained complexes **61**

Compound **14** was originally prepared and partly characterized by Brown and Wilkinson by reacting  $\text{HRh}(\text{CO})(\text{PPh}_3)_3$  with allene.<sup>75</sup> However, very little information was provided for this complex due to its low stability (even in the solid state under nitrogen) and its fluxionality. Two complexes that are close to **14** and contain bisphosphine ligands,  $\text{Rh}(\eta^3\text{-C}_3\text{H}_5)(\kappa^2\text{-R}_2\text{PCH}_2\text{P-}i\text{-Pr}_2)_2$ , where  $\text{R} = i\text{-Pr, Ph}$ , were prepared by Grignard reaction and its reactivity towards acid and CO was studied by Manger.<sup>131</sup>

The kinetic study of the CO/PPh<sub>3</sub> exchange reactions using the HRh(CO)(PPh<sub>3</sub>)<sub>3</sub> catalyst has been presented in **Section 1.3**. Close to my research, the reactivity of [Rh( $\eta^3$ -2-RC<sub>3</sub>H<sub>4</sub>)(P-*i*-Pr<sub>3</sub>)<sub>2</sub>] to CO was reported by Manger and a range of CO substitution/insertion products were detected.<sup>127,131</sup>

### 3.4.2 Reaction of Rh( $\eta^3$ -C<sub>3</sub>H<sub>5</sub>)(PPh<sub>3</sub>)<sub>2</sub> (**16**) with CO at 203 K

As a control, my research begins with the reaction of **16** with CO at 203 K for simplicity. When a sample of Rh( $\eta^3$ -C<sub>3</sub>H<sub>5</sub>)(PPh<sub>3</sub>)<sub>2</sub> was dissolved in toluene-d<sub>8</sub> under CO and monitored by NMR spectroscopy at 203 K, diagnostic signals are seen at  $\delta$  5.23,  $\delta$  3.05 and  $\delta$  2.53 due to **16**. They are immediately replaced by a further set of signals at  $\delta$  4.84,  $\delta$  2.91 and  $\delta$  1.72. These are due to a new  $\eta^3$ -allyl product. Figure 79 illustrates the <sup>1</sup>H-<sup>1</sup>H COSY spectrum that confirmed this. However, all three signals were broad at this point, suggesting high fluxionality. When an nOe pulse sequence was used, and the proton signal at  $\delta$  4.84 irradiated, it proved to connect to a proton signal at  $\delta$  2.91. When the signal at  $\delta$  2.91 was selectively excited, it correlated with the proton signals at  $\delta$  4.84 and  $\delta$  1.72. Hence the signals at  $\delta$  4.84,  $\delta$  2.91 and  $\delta$  1.72 were assigned to the *meso*-, *syn*- and *anti*-hydrogen respectively of an  $\eta^3$ -allyl ligand. Their NMR properties are in good accordance with those of  $\eta^3$ -allyl species as described in Section 1.7. In addition, the *ortho*- and *para*-hydrogen for the phenyl group were located at  $\delta$  7.50 and  $\delta$  6.99 when the proton signal at  $\delta$  4.84 was selectively irradiated. The assignment of these two signals was further proved by <sup>1</sup>H-<sup>31</sup>P HMQC correlations, as described below.

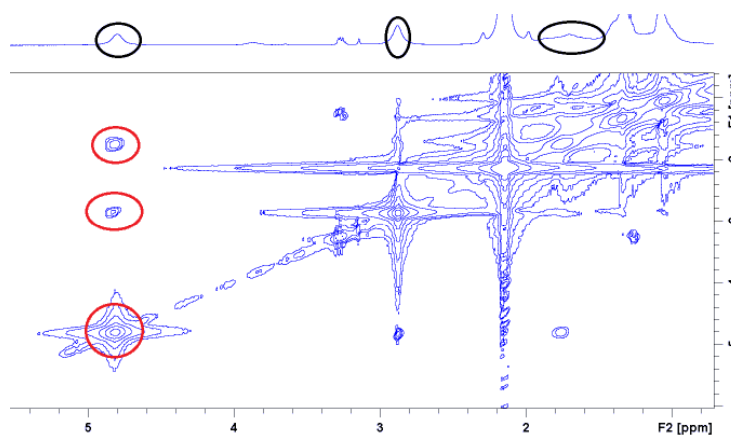


**Figure 79:** COSY experiments that correlates three proton signals at  $\delta$  4.84,  $\delta$  2.91, and  $\delta$  1.723 due to the  $\eta^3$ -allyl group in Rh( $\eta^3$ -C<sub>3</sub>H<sub>5</sub>)(CO)(PPh<sub>3</sub>)<sub>2</sub> (**14**)

### Chapter three

The  $^{31}\text{P}$  NMR spectrum of **14** is very complicated. Figure 80 illustrates the corresponding  $^{31}\text{P}$  NMR spectra at 188 K, 203 K and 233 K. When the sample was monitored by NMR at 183 K, two broad signals were detected at  $\delta$  30.19 and  $\delta$  47.72 in the corresponding  $^{31}\text{P}^{148}$  NMR spectrum, which carry rhodium couplings of 142.0 Hz and 153.3 Hz respectively. These two signals collapsed into a doublet at  $\delta$  38.41, with a rhodium coupling of 138.8 Hz upon warming to 233 K.

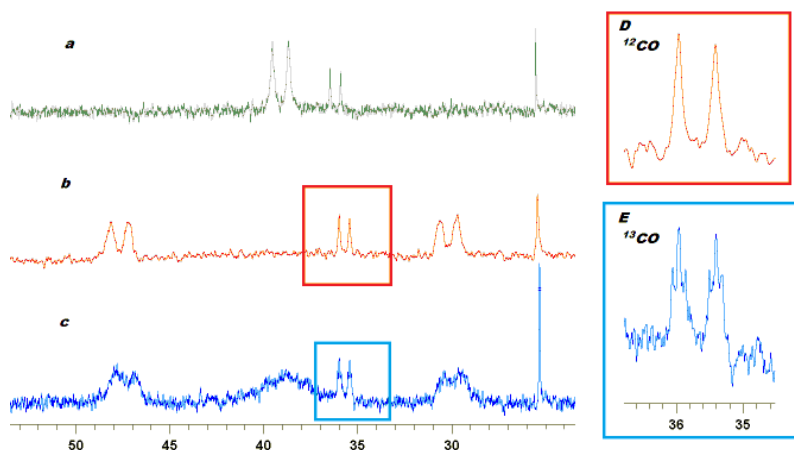


**Figure 80:** 1D  $^{31}\text{P}$  NMR spectra of  $\text{Rh}(\eta^3\text{-C}_3\text{H}_5)(\text{CO})(\text{PPh}_3)_2$  at 188 K, 203 K, and 233 K revealing its high fluxionality. (a): at 233 K using  $^{12}\text{CO}$ ; (b): at 188 K using  $^{12}\text{CO}$ ; (c): at 203 K using  $^{13}\text{CO}$ , D and E show expansion of the signal with/without  $^{13}\text{CO}$ .

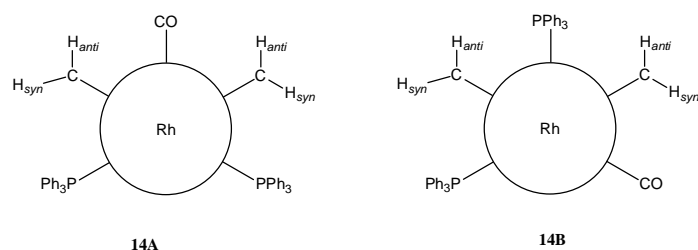
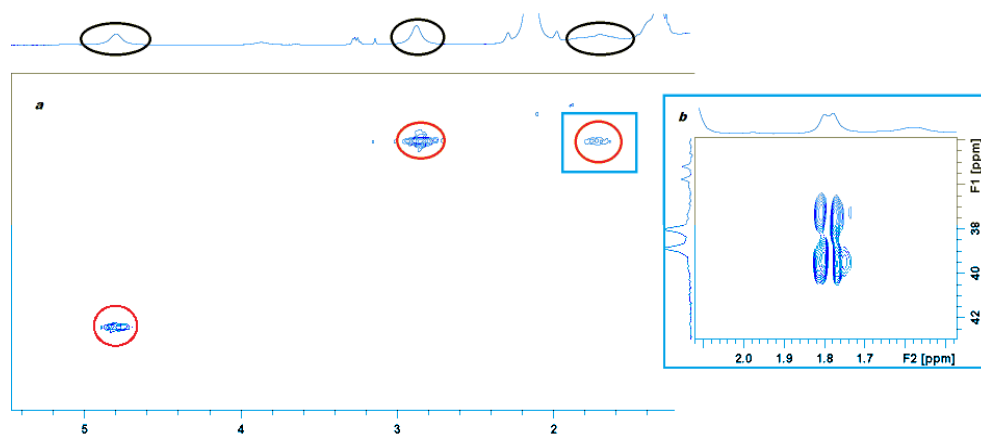


**Figure 81:** Two conformations of **14** in the toluene solution

When  $^{12}\text{CO}$  was replaced with  $^{13}\text{CO}$  and a  $^{13}\text{C}^{148}$  NMR spectrum recorded at 203 K, a doublet  $^{13}\text{C}$  resonance was detected at  $\delta$  198.06 and  $J_{\text{PC}}$  were within the line width at this stage. This  $^{13}\text{C}$  signal was assigned to the carbonyl group in **14**. In addition, an optimised  $^1\text{H}$ - $^{13}\text{C}$  HMQC experiment revealed that the *meso*-hydrogen at  $\delta$  4.84 in the allyl group was attached to a carbon nucleus which resonates at  $\delta$  82.0, while the *syn* and *anti*-hydrogen were connected to another carbon centre at  $\delta$  45.3. Figure 82 illustrates the correlations of these proton resonances and the corresponding carbon centres. These carbon data are in good accordance with the chemical shift for known  $\eta^3$ -allyl group containing products.

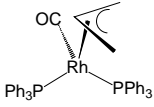
Carbon data for the phenyl group in **14** was collected by  $^1\text{H}$ - $^{13}\text{C}$  HMQC experiments and is listed in Table 41.

$^1\text{H}$ - $^{31}\text{P}$  correlations for **14** did not revealed anything substantial at 203 K. This can be ascribed to the fluctional behaviour of **14**. The  $^1\text{H}$ - $^{31}\text{P}$  HMQC experiments should work at 188 K. However, they were not completed with respect to protecting the probe. The structure of **14** can still be confirmed, as shown in Figure 82. It was the dominant species at this stage. (> 90 %)



**Figure 82:** The  $^1\text{H}$ - $^{13}\text{C}$  HMQC NMR spectrum that correlated three protons signals at  $\delta$  4.84,  $\delta$  2.82 and  $\delta$  1.77 with corresponding carbon resonances

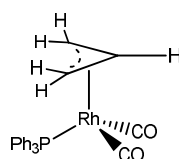
Table 41: Multinuclear NMR data for 14 (in toluene-*d*<sub>8</sub>)

			
Group / nucleus	Chemical shift (δ)	Multiplicity	Coupling constants (Hz)
<b><sup>1</sup>H</b>			
η <sup>3</sup> -Allyl-CH	4.82	br	
η <sup>3</sup> -Allyl-CH <sub>2</sub>	2.82	br	
η <sup>3</sup> -Allyl-CH <sub>2</sub>	1.77	br	
<i>o</i> -H	7.49	d, d	J <sub>HH</sub> = 3.81, J <sub>PH</sub> = 5.51
<i>m</i> -H	6.99	br	
<i>p</i> -H	7.37	br	J <sub>PH</sub> ~ 5
<b><sup>31</sup>P</b>			
	38.43 (233 K)		J <sub>RhP</sub> = 139
	29.76 and 47.32 (188K)		J <sub>RhP</sub> = 90
	30.19 and 47.72 (203 K)		J <sub>RhP</sub> = 142
<b><sup>13</sup>C</b>			
CO	198	d	J <sub>RhC</sub> = 70.6
η <sup>3</sup> -Allyl-CH	75.2 (188 K); 82.0 (203 K)	-	
η <sup>3</sup> -Allyl-CH <sub>2</sub>	43.0 (188 K), 45.2 (203 K)	-	
<i>o</i> -C	133.4	-	
<i>m</i> -C	128.46	-	
<i>p</i> -C	134.2	-	

#### Detection of Rh(η<sup>3</sup>-C<sub>3</sub>H<sub>5</sub>)(CO)<sub>2</sub>(PPh<sub>3</sub>) (61)

A further weak proton resonance was detected at δ 5.10 at 203 K due to the *meso*-hydrogen of another product. However, its partners were not detected at this stage due to its low intensity. When the sample was warmed to 233 K, the <sup>1</sup>H signal at δ 5.10 grew in but moved to δ 4.90. Meanwhile, *syn* and *anti*-hydrogen were detected at δ 2.82 (J<sub>HH</sub> = 3.8 Hz) and δ 1.77 (J<sub>HH</sub> = 8.9 Hz) respectively. The strength of these signals can also be promoted by adding more CO. Therefore they might arise from a further CO substitution product of **61**.

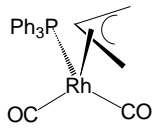
In the corresponding  $^{31}\text{P}^{148}$  NMR spectrum, a doublet signal was visible at  $\delta$  35.68 with  $J_{\text{RhP}} = 91$  Hz. When  $^{13}\text{CO}$  was used in a parallel experiment, this  $^{31}\text{P}$  resonance showed two further  $^{13}\text{C}$  splittings of 14 Hz. This suggests that there are two equivalent CO ligands in **61**, as shown in Figure 80. In the corresponding  $^{13}\text{C}^{148}$  NMR spectrum, a doublet of multiplet resonance was detected at 202.60, where  $J_{\text{RhC}} = 70$  Hz,  $J_{\text{CP}} = 14$  Hz. The compound is therefore confirmed to be  $\text{Rh}(\eta^3\text{-C}_3\text{H}_5)(\text{CO})_2(\text{PPh}_3)$  (**61**). The structure of **61** was illustrated in Figure 83. The NMR data of **61** are listed in Table 42



**Figure 83:** The structure of  $\text{Rh}(\eta^3\text{-C}_3\text{H}_5)(\text{CO})_2(\text{PPh}_3)$  (**61**)

If the sample was kept carefully at 203 K, no further product was detected, except  $\text{Rh}(\eta^3\text{-C}_3\text{H}_5)(\text{CO})(\text{PPh}_3)_2$  (**14**) and  $\text{Rh}(\eta^3\text{-C}_3\text{H}_5)(\text{CO})_2(\text{PPh}_3)$  (**61**). They are formed with a ratio of 9:1 by integrating the  $^{31}\text{P}$  and  $^{13}\text{C}$  signals. It is no surprise that this value decreases upon adding more CO.

Table 42: Selected multinuclear NMR data for 61 (in toluene- $d_8$ )

			
Group / nucleus	Chemical shift ( $\delta$ )	Multiplicity	Coupling constants (Hz)
<b><math>^1\text{H}</math></b>			
$\eta^3$ -Allyl-CH	4.94 (5.09) <sup>a</sup>	m	-
$\eta^3$ -Allyl-CH <sub>2</sub>	3.64	br	-
	3.39	br	-
<i>o</i> -H	8.06	overlap	-
<i>p</i> -H	7.01	overlap	-
<b><math>^{31}\text{P}</math></b>			
	35.68	d, t	$J_{\text{RhP}} = 91, J_{\text{CP}} = 14$
<b><math>^{13}\text{C}</math></b>			
CO	202.6	d, d	$J_{\text{RhP}} = 72, J_{\text{PC}} = 14$
<b>Temperature</b>	233 K (if un-noted), <sup>a</sup> at 203 K, in toluene- $d_8$		
Reference: 11050801 and 11031301			

### 3.4.3 Reaction of $\text{Rh}(\eta^3\text{-C}_3\text{H}_5)(\text{PPh}_3)_2$ with CO at 233 K

When the sample was warmed up to 233 K, two further  $\eta^1$ -allyl species were detected according to the corresponding  $^1\text{H}$ - $^1\text{H}$  COSY experiment. Figure 84 illustrates the corresponding  $^1\text{H}$ - $^1\text{H}$  COSY dataset at this stage.

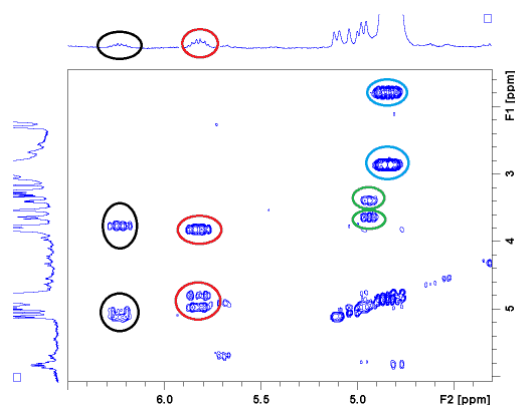


Figure 84: The  $^1\text{H}$ - $^1\text{H}$  COSY spectrum indicates the formation of two  $\eta^1$ -allyl contained products.



Two most notable sets of signals were detected at  $\delta$  3.76,  $\delta$  5.03,  $\delta$  5.12 and  $\delta$  6.23 and at  $\delta$  3.83,  $\delta$  4.83,  $\delta$  4.97 and  $\delta$  5.82 respectively. They are ascribed to be  $\eta^1$ -C<sub>3</sub>H<sub>5</sub> allyl species. <sup>1</sup>H-<sup>31</sup>P HMQC experiments revealed that the latter set of proton signals coupled with a <sup>31</sup>P signal at  $\delta$  29.5. However, none of these signals show substantial rhodium coupling. In addition, the <sup>1</sup>H NMR signal for Rh-CH<sub>2</sub>-CH=CH<sub>2</sub> was reported at 1 ~ 3.2 ppm higher than what is observed.<sup>127,150</sup> They are therefore ascribed to an acyl species. The former set of proton signals are ascribed to be *a*-Rh(CO-C<sub>3</sub>H<sub>5</sub>)(PPh<sub>3</sub>)(CO)<sub>3</sub> (**62A**) while the latter set to be *e*-Rh(CO-C<sub>3</sub>H<sub>5</sub>)(CO)<sub>3</sub>(PPh<sub>3</sub>) (**62B**). The structure of Rh(CO-C<sub>3</sub>H<sub>5</sub>)(PPh<sub>3</sub>)(CO)<sub>3</sub> (**62A**) and Rh(CO-C<sub>3</sub>H<sub>5</sub>)(CO)<sub>2</sub>(PPh<sub>3</sub>)<sub>2</sub> (**62B**) are illustrated in Figure 86. The arrangement of ligands is indicated by NMR information and general mechanism.

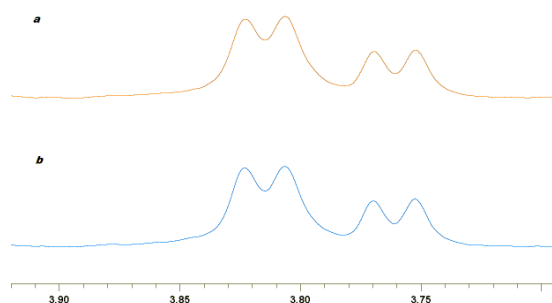


Figure 85: Part of the <sup>1</sup>H and <sup>1</sup>H{<sup>31</sup>P} NMR spectra of **62A** and **62B**

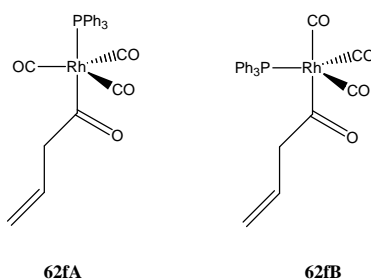


Figure 86: Structure of **62A** and **62B**

In addition, several weak signals due to further reaction products were also detected. On warming the sample to room temperature and re-cooling it to 203 K, a further set of signals were observed at  $\delta$  2.27,  $\delta$  4.70,  $\delta$  4.91 and  $\delta$  5.70. These signals were assigned to be an  $\eta^1$  allyl species *e*-Rh( $\eta^1$ -C<sub>3</sub>H<sub>5</sub>)(CO)<sub>3</sub>(PPh<sub>3</sub>) (**63B**) since no <sup>31</sup>P coupling was observed for this species. The branched acyl species (**60C**) was also detected at  $\delta$  3.43,  $\delta$  3.96,  $\delta$  2.63 and  $\delta$  2.87. <sup>1</sup>H-<sup>31</sup>P HMQC experiments correlate a <sup>31</sup>P signal at  $\delta$  16.7 to these signals. Resolving these species is impossible due to overlap.

### Chapter three

Intensive precipitation is observed at this stage, making NMR characterization difficult. In addition, a further set of resonance at  $\delta$  9.06,  $\delta$  5.93,  $\delta$  5.44 and  $\delta$  5.20 due to a new product **64** were observed. This new set of resonances might be formed by CO insertion into one of the C-H bond of the allyl group. However, its exact nature was not clear due to being unable to isolate the species responsible.

**Table 43: Complexes formed when the reaction of  $Rh(\eta^3-C_3H_5)(CO)(PPh_3)_2$  with  $^{13}CO$  was warmed to 233 K**

	<b>62A</b> $Rh(C_3H_5)(CO)_3(PPh_3)$	<b>62B</b> $Rh(C_3H_5)(CO)_2(PPh_3)_2$	<b>63</b> $Rh(\eta^1-C_3H_5)(CO)_3(PPh_3)$
$\eta^1$ -Allyl- $RhCH_2$	3.76	3.83	2.27
$\eta^1$ -Allyl= $CH_2$	5.03	4.83	4.70
$\eta^1$ -Allyl= $CH_2$	5.12	4.97	4.91
$\eta^1$ -Allyl- $CH$	6.23	5.82	5.70
		$^{31}P = 29.5$ $J_{RhP} = 134$ Hz, $J_{PP} = 42$ Hz)	
	<b>62C</b> $Rh(CO-i-C_3H_5)(CO)_3(PPh_3)$		<b>64</b> unknown
CO- $CH-CH_3$	3.43		9.06
CO- $CH-CH_3$	3.96		5.93
CH= $CH_2$	2.63	Olefinic $CH_2$	5.44
CH= $CH_2$	2.87		5.20
	$^{31}P = 16.75$		

### 3.5 Reaction of $Rh(\eta^3-C_3H_5)(PPh_3)_2$ with CO and $H_2$ in toluene- $d_8$

The reaction  $Rh(\eta^3-C_3H_5)(PPh_3)_2$  with CO and *parahydrogen* was then investigated and found not occur until the sample was heated to 343 K. However, the reaction shows no PHIP at this stage. The final product was identified as  $HRh(CO)_2(Ph_3)_2$  and the corresponding aldehyde was detected.

### 3.6 Conclusion

$Rh(\eta^3-C_3H_5)(PPh_3)_2$  was prepared and characterized by NMR and XRD methods. It proves to be a very active hydrogenation catalyst. The catalytic species is proposed to be

$\text{RhH}(\text{Sol})(\text{PPh}_3)_2$  (**57**), however, **57** is not stable and dimerizes to  $\text{Rh}(\text{PPh}_3)_2(\mu\text{-H})_2\text{Rh}(\text{PPh}_3)_2$  (**58**) in toluene. Hydrogen addition to **57** leads to a stable complex **46**. If  $\text{CH}_3\text{CN}$  was added prior the reaction with hydrogen,  $\text{RhH}(\text{Sol})(\text{PPh}_3)_2$  can be trapped as the  $\text{CH}_3\text{CN}$  adduct **50** and **51**.

The hydrogenation mechanism was further studied in  $\text{CH}_3\text{CN}$ . Reaction of **16** and  $\text{CH}_3\text{CN}$  affords **47** and **48** as ligand exchange products. Both of them can be characterized by conventional NMR methods. If *parahydrogen* is present at this stage, **48** can also be trapped as the dihydride form **56A** and **56B**. After hydrogenation, monohydride species **50** and **51** can also be detected after the reaction.

The interaction of  $\text{Rh}(\eta^3\text{-C}_3\text{H}_5)(\text{PPh}_3)_2$  with CO was also examined by NMR methods, where a range of  $\eta^3$ -allyl contained species **14** and **61** are formed. Both of **14** and **61** are fluxional molecules. The conversion of  $\eta^3$ -allyl to  $\eta^1$ -allyl in these species does not happen until the temperature reaches 233 K, where a range of CO insertion products, **62A-62C** form. These results are in good accordance with the literature.<sup>131</sup> Up to this point I have aimed to demonstrate the complexity of the rhodium system in relation to that of iridium. The allyl group in  $\text{Rh}(\eta^3\text{-C}_3\text{H}_5)(\text{PPh}_3)_2$  hydroformylates on exposing to CO/*parahydrogen*. A lowest reaction temperature at 343 K is required. However, the study at this temperature is not that fruitful compared with its cobalt analogue.

## **Chapter 4 NMR Study on Palladium Catalysed Carbonylation Mechanism**

*4.1: Results & Introduction*

*4.2 Control reactions for **12a***

*4.3 Diphenyl acetylene carbonylation catalysed by **12a***

*4.4 Diphenyl acetylene carbonylation catalysed by **12b***

*4.5 Studies using expanded substrates*

*4.6 Discussion & Conclusion*

## 4.1: Results & Introduction

### 4.1.1 Results

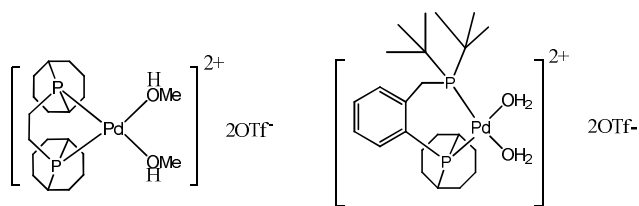
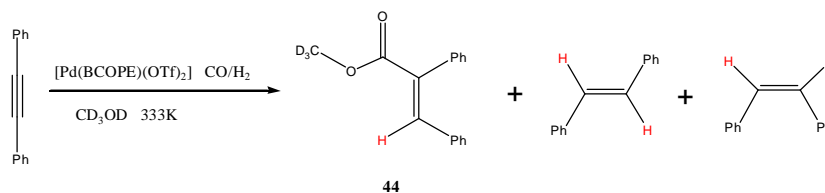


Figure 87: Structures of **12a** and **12b**

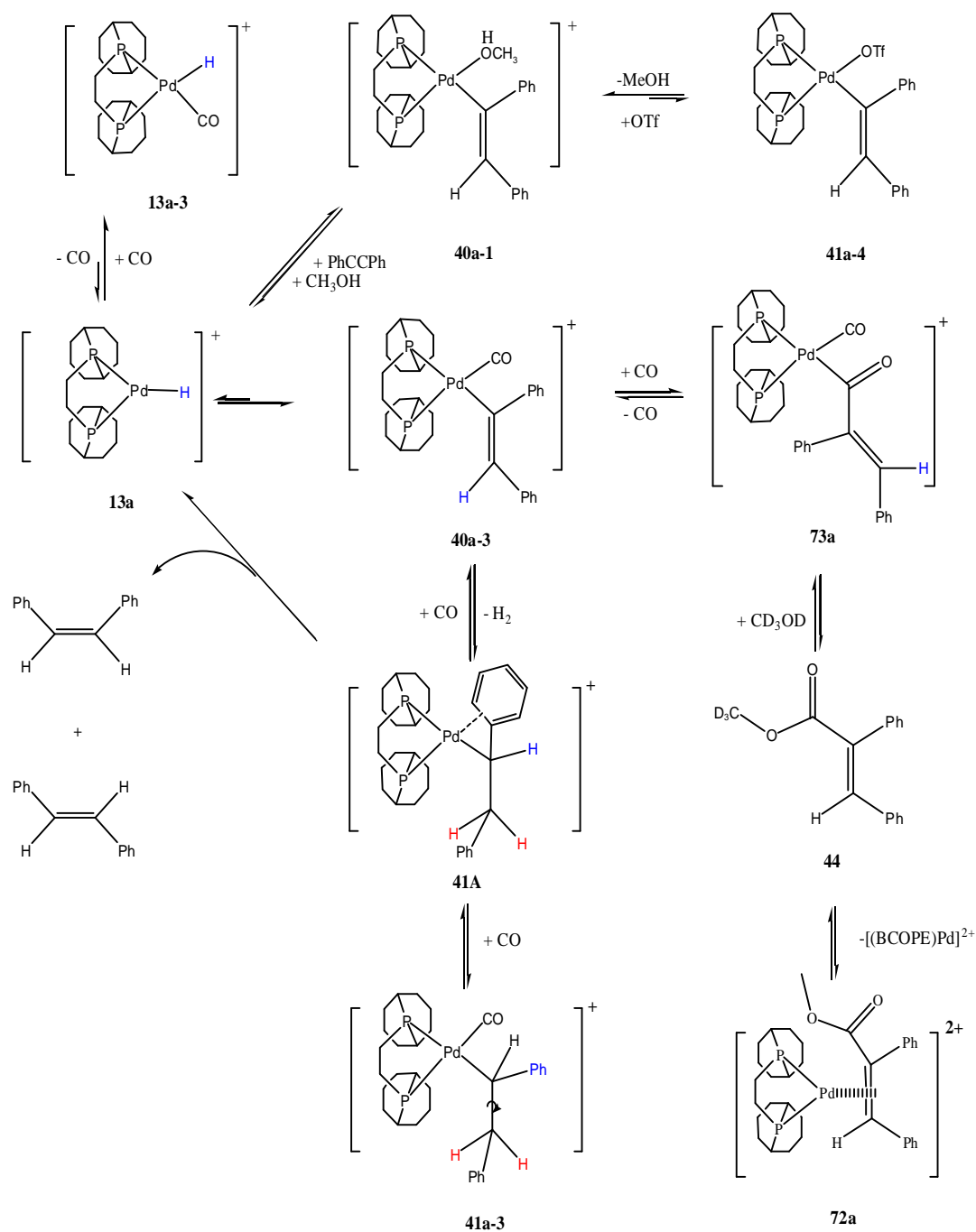
In this chapter, It is shown that  $[\text{Pd}(\text{BCOPE})(\text{CH}_3\text{OH})_2](\text{OTf})_2$  (**12a**) and  $[\text{Pd}(\text{tBuCOPE})(\text{H}_2\text{O})_2](\text{OTf})_2$  (**12b**), where  $\text{BCOPE} = [(\text{C}_8\text{H}_{14})\text{PCH}_2\text{-CH}_2\text{P}(\text{C}_8\text{H}_{14})]$  and  $\text{tBuCOPE} = [(\text{C}_8\text{H}_{14})\text{PC}_6\text{H}_4\text{CH}_2\text{P}(\text{tBu})_2]$ , react with CO,  $\text{H}_2$  and diphenyl acetylene to produce **5-1** under mild conditions, as illustrated in Figure 87. During the reaction for **12a**, Complexes **40a-1**, **40a-3**, **40a-4**, **41a**, **41a-3**, **42a**, **44**, **72a** and **73a** were detected as polarized NMR signals. These can be placed together in a mechanistic scheme as illustrated in Scheme 36. The reaction using **12b** shows similar results. I now describe the observations that justify these claims.



Equation 12: Diphenyl acetylene carbonylation in methanol gives **44** as the main product.

In this chapter, the synthesis of the catalysts, **12a** and **12b**, and the authentic compound **44** will be presented in Section 4.1.2. Section 4.1.2 also includes NMR and GC-MS characterization data for **44**. To understand the carbonylation mechanism, a series of control reactions are completed before bringing in the carbonylation reaction. These studies are discussed in Section 4.2. Sections 4.3 and 4.4 deal with the NMR studies of diphenyl acetylene carbonylation, catalyzed by **12a** and **12b** respectively. The carbonylation reactions using the expanded range of substrates, stilbene, styrene, and phenyl acetylene, are discussed in Section 4.5.

## Chapter four



**Scheme 36: Overall cationic mechanism for diphenyl acetylene carbonylation using the catalyst 12a**

### 4.1.2 Synthesis and characterization of the catalysts and expected product

#### 4.1.2.1 Synthesis of catalysts

Analytically pure  $[\text{Pd}(\text{BCOPE})(\text{CH}_3\text{OH})_2](\text{OTf})_2$  (**12a**) and  $[\text{Pd}(\text{tBuCOPE})(\text{OH}_2)_2](\text{OTf})_2$  (**12b**) were prepared by treating the corresponding dichloride complexes with silver triflate.

**12a** and **12b** were isolated by passing them through a short silica column, and then recrystallized from methanol. The detailed synthetic procedure is described in the experimental section. The purity of these products was confirmed by comparing their  $^{31}\text{P}$  NMR spectra with authentic data.<sup>46</sup> The corresponding  $^{31}\text{P}$  NMR spectrum of **12a** is shown in Figure 88, indicating that **12a** is the only organometallic species present.

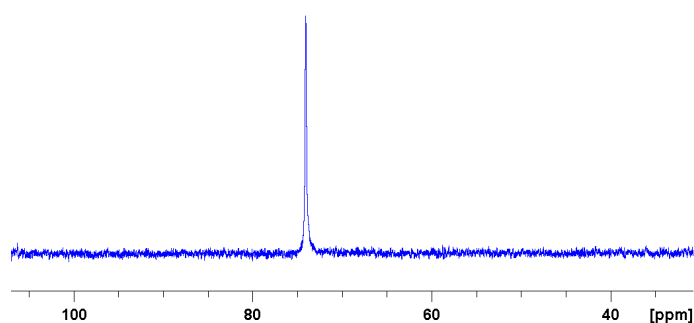


Figure 88: A  $^{31}\text{P}$  NMR spectrum of **12a**

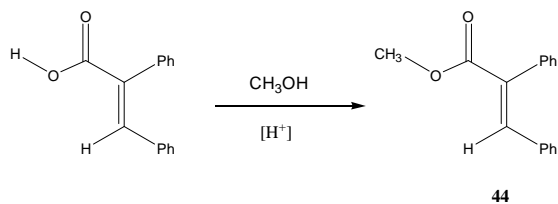
#### 4.1.2.2 Structures of catalysts

The molecular structure of **12a** was determined by Joaquín L. S. etc.<sup>46</sup> The palladium centre displays a square planar configuration with two phosphorus centre in a *cis* orientation. **12a** also processes two methanol solvates. The metal centre is further stabilized by two triflate counter anions via hydrogen bonding. **12b** proved to be a di-aqua complex and shows similar structural properties to **12a**. The structure and properties of the di-aqua complex of **12a** were studied by Miguel and co-workers.<sup>146</sup> These catalysts with different solvates show little difference in their catalytic performance. However, adding a large excess of water or methanol influences catalysis according to our study. This work will be further discussed in **Section 4.3.3**.

#### 4.1.2.3 Synthesis of the carbonylation product **44** and its NMR characterization

The ester product **44** was synthesised by treating a methanol solution of  $\alpha$ -phenyl-cinnamic acid with sulphuric acid, as shown in Equation 13, in yield: 80 %. Detailed synthetic procedure is described in the experimental chapter. The structure of **44** was confirmed by NMR and GC-MS methods.

## Chapter four



### Equation 13: Synthesis of $\alpha$ -phenyl-cinnamic acid methyl ester 44

When a  $^1\text{H}$  NMR spectrum of **44** was recorded in chloroform- $d_1$ , two signals are apparent at  $\delta$  3.82 and  $\delta$  7.88, with ratio 3:1. They are assigned to ' $\text{CH}_3$ ' and ' $=\text{CHPh}$ ' groups in **44**. When a 1D nOe experiment was used to excite the  $^1\text{H}$  NMR signal at  $\delta$  7.88, strong correlations were observed between the signals at  $\delta$  7.88 and  $\delta$  3.82, as well as the signals at  $\delta$  7.21 and  $\delta$  7.06. The signal at  $\delta$  7.06 must therefore arise from the *ortho*-hydrogen of a phenyl group. There are also weaker correlations between the signals at  $\delta$  3.82 and  $\delta$  7.21. The signal at  $\delta$  7.21 is assigned to the *ortho*-hydrogen of another phenyl group. This information confirms the *cis* orientation of the two phenyl groups on the double bond. Therefore the vinyl hydrogen and the carbonyl are also *cis*. The nOe correlations in **44** used to deduce this are illustrated in Figure 89.

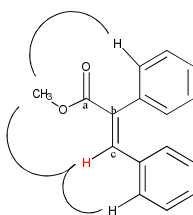


Figure 89: NOESY experiments reveal several spatially close protons in 45

Similarly, when a sample of  $\alpha$ -phenyl-cinnamic acid was examined by 2D NOESY experiments, a strong correlation was observed between the signal at  $\delta$  7.96 and  $\delta$  7.10. The signal at  $\delta$  7.10 arises from the *ortho*-hydrogen of the phenyl group. The rest of the NMR data of **44**, and  $\alpha$ -phenyl-cinnamic acid was collected by conventional 2D  $^1\text{H}$ - $^1\text{H}$  COSY and 2D  $^1\text{H}$ - $^{13}\text{C}$  HMQC experiments, as summarized in Table 44 and Table 45 respectively



Table 44: Multinuclear NMR data for  $\alpha$ -phenyl-cinnamic acid (298 K in methanol- $d_4$ )

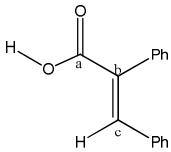
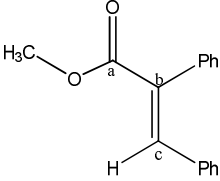
			
Group nucleus /	Chemical shift ( $\delta$ )	Multiplicity	Coupling constants (Hz)
<b><math>^1\text{H}</math></b>			
=CHPh	7.96 (1H)	s	
COOH	11.30 (1H)	s, br	
$\alpha$ -Phenyl	7.10 ( <i>o</i> -H) 7.20 ( <i>m</i> -H) 7.25 ( <i>p</i> -H)	d t t, overlap	$J_{\text{HH}} = 7.50$ $J_{\text{HH}} \sim 7.50$ $J_{\text{HH}} \sim 7.50$
$\beta$ -Phenyl	7.25 ( <i>o</i> -H) 7.39 ( <i>m</i> -H) 7.55 ( <i>p</i> -H)	d, overlap t t	$J_{\text{HH}} = 7.50$ $J_{\text{HH}} \sim 7.50$ $J_{\text{HH}} \sim 7.50$
<b><math>^{13}\text{C}</math></b>			
$\text{C}_{(a)}$	164	-	
$\text{C}_{(b)}$	130.3	-	
$\alpha$ -Phenyl	130.8	s	
	128.2	s	
	129.7	s	
$\beta$ -Phenyl	130.0	s	
	128.7	s	
	126.7	s	

Table 45: Multinuclear NMR data for 45 (298 K methanol-d<sub>4</sub>)

			
Group nucleus /	Chemical shift (δ)	Multiplicity	Coupling constants (Hz)
<b><sup>1</sup>H</b>			
=CHPh	7.84 (1H)	d, (using <sup>13</sup> CO) d, (using Ph <sup>13</sup> CCPh)	J <sub>C(a)H</sub> = 8.0 J <sub>CH</sub> = 3.5 and 156.0 (b and c)
CH <sub>3</sub>	3.82 (3H)	s	
α-Phenyl group	7.06 (1H, <i>o</i> -H)	d	J <sub>HH</sub> = 7.47
	7.18 (1H, <i>m</i> -H)	t	J <sub>HH</sub> ~ 7.47
	7.25 (1H, <i>p</i> -H)	t	J <sub>HH</sub> ~ 7.47
β-Phenyl group	7.21 (1H, <i>o</i> -H)	d	J <sub>HH</sub> = 7.47
	7.38 (1H, <i>m</i> -H)	t	J <sub>HH</sub> ~ 7.47
	7.52 (1H, <i>p</i> -H)	t	J <sub>HH</sub> ~ 7.47
<b><sup>13</sup>C</b>			
C <sub>(a)</sub>	164.0	-	J <sub>C(a)H</sub> = 8.0
C <sub>(b)</sub>	132.6	-	J <sub>C(a)H</sub> = 3.6
C <sub>(c)</sub>	140.5	-	J <sub>C(c)H</sub> = 156.0
CH <sub>3</sub>	52.5	s	-
α-Phenyl group	130.6 ( <i>o</i> -C)	-	
	129.8 ( <i>p</i> -C)	-	
α-Phenyl group	129.1 ( <i>o</i> -C)	-	
	127.9 ( <i>m</i> -C)	-	
	126.7 ( <i>p</i> -C)	-	

## 4.2 Control reactions for 12a

### 4.2.1 Reaction of 12a and *parahydrogen*

## 4.2.1.1 Background

The reaction of the Pd(BCOPE)(OH<sub>2</sub>)<sub>2</sub>(OTf)<sub>2</sub> (water adduct of **12a**) and H<sub>2</sub> was previously studied by Miguel and co-workers.<sup>146</sup> In their study, the palladium cluster **67a** was formed by treating with hydrogen in acidic solution (a solvent mixture of sulfolane 15 %, water 1%, ethanol 28%, and toluene-d<sub>8</sub> 56 % by weight), as shown in Figure 90. In **67a**, the two hydrides are symmetrically oriented, and resonate at δ -6.53. Both of them couple with six equivalent phosphine ligands and therefore appear as a septet, where J<sub>PH</sub> = 36 Hz.

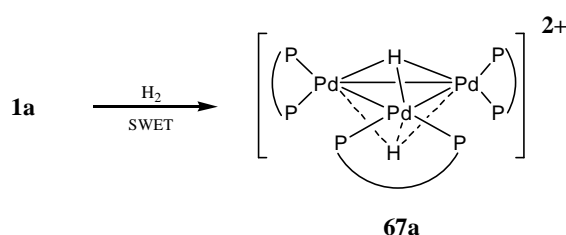


**Figure 90:** Reaction of [(BCOPE)Pd(H<sub>2</sub>O)<sub>2</sub>](OTf)<sub>2</sub> with hydrogen in acidic solution gives **67a**

The formation of this cluster is highly dependent on the nature of the phosphine ligand and the reducing reagent. Other hydride containing palladium clusters such as [Pd<sub>2</sub>(dipp)<sub>2</sub>(μ-H)<sub>2</sub>]<sup>2+</sup> (δ -2.50, J<sub>PH</sub>= 36 Hz)<sup>159</sup> and [Pd<sub>4</sub>(dppm)<sub>4</sub>(μ-H)<sub>2</sub>]<sup>+</sup> are known.<sup>160,161</sup> No other trimeric palladium clusters are found in the literature. However, a similar platinum [Pt<sub>3</sub>(dppm)<sub>3</sub>(H)<sub>2</sub>]<sup>2+</sup> (δ -3.68, J<sub>PH</sub>= 20 Hz) analogue was reported by Ramachandran.<sup>162</sup>

It was suggested that the formation of **67a** involved the palladium monohydride species [(BCOPE)PdH]<sup>+</sup> (**13a**) as the building block. However, no evidence for this detection was given.<sup>146</sup> This is not surprising as **13a** is neither electronically nor structurally saturated. However, **13a** can be trapped if suitable ligands are used to stabilize it. The reaction of **12b** with hydrogen in the presence of pyridine affords its pyridine adduct [Pd(BCOPE)(H)(pyridine)]<sup>+</sup> (**13b-2**).<sup>163</sup> *In-situ* NMR studies revealed a role of these pyridine adducts in the hydrogenation of diphenyl acetylene.<sup>46</sup> The corresponding solvate adduct of **13a** has never been observed. However, similar alcohol adducts can be generated *in-situ* and isolated when the phosphine 1, 2-(CH<sub>2</sub>PBu<sup>t</sup>)<sub>2</sub>C<sub>6</sub>H<sub>4</sub> is used.<sup>112</sup> The related complexes detected in the studies described in this thesis are summarized in Figure 91.

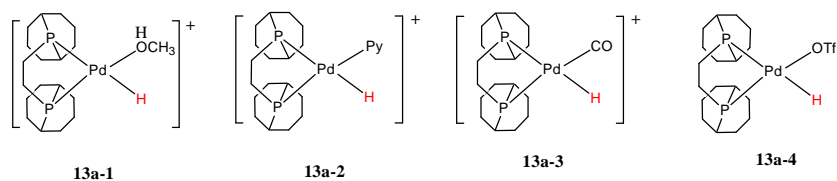


**Figure 91:** Structures of the monohydride species (13a) that are reported in this thesis

#### 4.2.1.2 Re-examination of the reaction of 12a and hydrogen

When a sample of **12a**, in dichloromethane- $d_2$ , was exposed to *parahydrogen* and examined by NMR spectroscopy at 315 K, (the boiling point of dichloromethane) no reaction was evident over several hours. No reaction was evident in methanol either. The key  $^{31}\text{P}$  NMR signal of **12a** remained visible at  $\delta$  74.4 throughout these studies. However, when a sample of **12a** that was dissolved in tetrachloroethane- $d_2$  was exposed to *parahydrogen* and monitored by NMR spectroscopy at 323 K, evidence for the formation of a new species was observed.

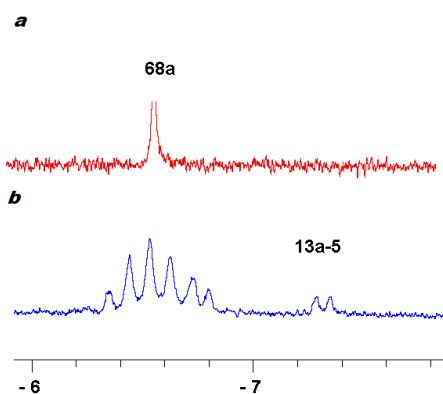
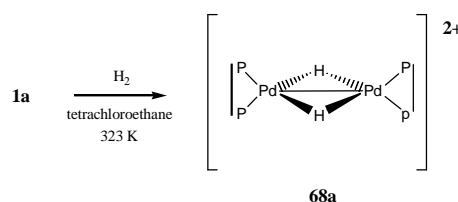


**Figure 92:** The hydride region of  $^1\text{H}$  (a, vertical scale: 32, 128 scans) and  $^1\text{H}\{^{31}\text{P}\}$  (b: vertical scale: 2; 4,000 scans) NMR spectra recorded to monitor the reaction of **12a** with *parahydrogen* in tetrachloroethane- $d_2$  at 323 K

This correspond to the detection of a weak,  $^{31}\text{P}$  coupled quintet (1 : 4 : 6 : 4 : 1) hydride resonance at  $\delta$  -6.53 in a 4000-scan  $^1\text{H}$  NMR experiment. This resonance simplifies into singlet on  $^{31}\text{P}$  decoupling, and has a  $^{31}\text{P}$  coupling of 36.0 Hz. Its shape does not change over the temperature range from 243 K to 323 K. The corresponding  $^1\text{H}$  and  $^1\text{H}\{^{31}\text{P}\}$  NMR spectra are shown in Figure 92. These results confirm that this molecule is rigid and contains four equivalent phosphine donors. Further characterisation was impossible due to its low intensity. On the basis that its chemical shift and the  $^{31}\text{P}$  coupling constant are very

similar to that of **68a**, they must be related. The hydride can be deduced to be a bridging and couple to four *cis*-phosphines.



**Equation 14: Reaction of 12a and hydrogen in the neutral non-alcoholic solvent, tetrachloroethane, gives rise to a palladium dimer at 323K**

After one day at 323 K, a second hydride signal was observed at  $\delta$  -7.02. This signal is 1<sup>st</sup> order with  $J_{\text{PH}} = 220.2$  Hz and 23.4 Hz respectively. It partly overlaps with the signal at  $\delta$  -6.53. This suggests the signal at  $\delta$  -7.02 arise from a palladium monohydride species with two phosphine ligands that are *trans* and *cis* to it. The compound therefore could be Pd(BCOPE)(H)(OTf) (**13a-4**) or the solvent adduct [Pd(BCOPE)(H)(sol)](OTf) (**13a-5**), where sol = tetrachloroethane. Further characterisation of this product was impossible due to its low intensity.

## 4.2.2 Reaction of 12a with CO

### 4.2.2.1 Background

Previous study has suggested that the reaction of [Pd(BCOPE)(OH<sub>2</sub>)<sub>2</sub>](OTf)<sub>2</sub> with CO yields the fluxional compound [Pd<sub>2</sub>(BCOPE)<sub>2</sub>(CO)<sub>2</sub>](OTf)<sub>2</sub> (**69a**).<sup>146</sup> The molecular structure of **69a** is shown in Figure 93. The definition and properties of fluxional molecules are described in the introduction section.<sup>135</sup>

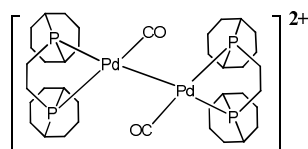


**Figure 93: Structure of [Pd<sub>2</sub>(BCOPE)<sub>2</sub>(CO)<sub>2</sub>](OTf)<sub>2</sub> (**69a**).**

**69a** gives a single, broad peak at  $\delta$  49.6 in the <sup>31</sup>P NMR spectrum according to previous studies. However, when the sample was cooled to 193 K, two signals, with a ratio of 1 : 1, were observed, indicating the inequivalence of the phosphine ligands. The inequivalence also applied to CO ligands. It is the exchanging of two isomers that leads to the signal

## Chapter four

averaging. We note the exchanging cannot totally be suppressed at 193 K, according to the line broadening effect.

### 4.2.2.2 Re-examination of the reaction of **12a** and CO

When a sample of **12a** in methanol- $d_4$  was exposed to 1 atm. of CO, a very slow reaction took place. The  $^{31}\text{P}$  resonance at  $\delta$  74.4 due to **12a** was gradually replaced by another resonance at  $\delta$  49.6 during this progress. This indicated the formation of new and symmetrical CO containing adduct since the new  $^{31}\text{P}$  resonance was a singlet. Based on this information, the new complex is  $[[\text{Pd}_2(\text{BCOPE})_2(\text{CO})_2](\text{OTf})_2]$  (**69a**). The reaction in dichloromethane shows similar results, suggesting that the reaction of **12a** and CO shows no solvent dependence. Although it is hard to calculate exact reaction rate of this reaction, the  $^{31}\text{P}$  NMR spectra suggest complete conversion to this product is achieved after one day at 298 K. When a sample containing the new product was examined at lower temperature, line broadening effects were observed in agreement with those of Miguel.<sup>146</sup>

### 4.2.3 Reaction of **12a**, CO and $\text{H}_2$ in methanol- $d_4$

#### 4.2.3.1 Background

Previous studies on the reaction of **12a**, CO and hydrogen suggest that a dinuclear palladium complex that contains a bridging hydride and carbonyl ligand, **42a**, is formed. The structure of **42a** is illustrated in Figure 94. **42a** is highly fluxional and yields a single hydride signal at  $\delta$  -5.54 in the  $^1\text{H}\{^{31}\text{P}\}$  NMR spectrum at room temperature. [2]

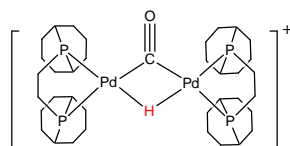
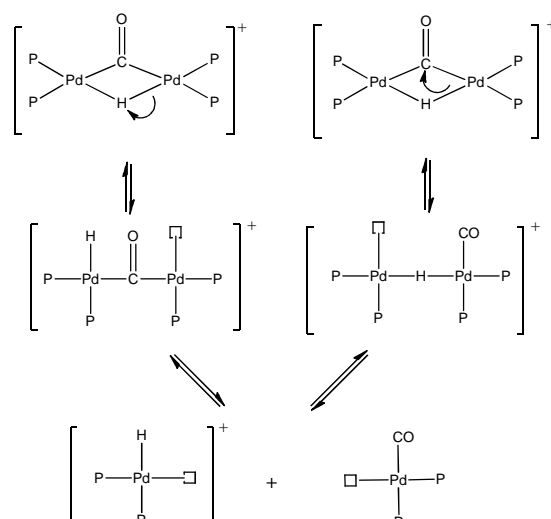


**Figure 94: Structure of 42a**

The chemistry of type **42a** complexes, with either bisphosphine or monophosphine ligands, is rich.  $[(\text{dipp})\text{Pd}(\mu\text{-H})(\mu\text{-CO})\text{Pd}(\text{dipp})][\text{Cl}]$  [dipp = 1,3-bis(diisopropylphosphino)propane] was prepared by methanolysis of  $[(\text{dipp})\text{Pd}(\text{Ph})\text{Cl}]$  or by treating  $[(\text{dipp})_2\text{Pd}]$  with HCl and CO.<sup>164</sup> Another example,  $[(\text{bdpp})\text{Pd}(\mu\text{-H})(\mu\text{-CO})\text{Pd}(\text{bdpp})][\text{Cl}]$ , where bdpp = 2,4-bis(diphenylphosphino)pentane, was reported by Toth.<sup>165,166</sup> Its formation and CO exchanging reaction were studied by NMR methods.<sup>165</sup> In late 1970s, the  $\text{PPh}_3$  analogue of

**42a** was prepared by treating  $[(\text{Ph}_3\text{P})_3\text{PdH}]\text{X}$ , where  $\text{X} = \text{CF}_3\text{COO}^-$ , with carbon monoxide.<sup>167</sup> Compounds with different counter anions such as  $\text{ClO}_4^-$  and  $\text{HC}(\text{SO}_2\text{CF}_3)_2^-$  were also prepared by other research groups.<sup>164,166</sup>

These binuclear palladium cations are non-rigid. This explains why the four phosphine ligands in **42a** type complexes are always NMR-equivalent at room temperature. In the  $\text{PPh}_3$  case, the phosphine exchange cannot be totally suppressed until the temperature is dropped to 163 K. The fluxional behaviour was further studied by line shape simulation where the activation parameters can be determined.<sup>167</sup> The positive activation entropy suggested a bridge breaking reaction, involving either Pd-H-Pd or Pd-C(O)-Pd, is undergone in the initial step. The corresponding Pd-C(O)-Pd or Pd-H-Pd type complexes could further cleave to  $\text{L}_2\text{PdH}$  or  $\text{L}_2\text{Pd}(\text{CO})$  fragments.



**Scheme 37: Intermediates involved in the formation and decomposition of 42a type compounds. For simplicity, the back bone of the phosphine ligand is neglected. The vacancy site should be occupied by solvent or other ligands.**

In both the monophosphine and bisphosphine cases, the formation of the bridged cation can be considered to be reversible, as illustrated in Scheme 37. Therefore, complexes of type **42a** are considered as a reservoir for the monohydride species  $[(\text{PR}_3)_2\text{PdH}]^+$ . Consequently **42a** shows similar catalytic behaviour to **12a**. Scheme 37 demonstrates how **42a** could be formed in solution; however, such progress is too quick to follow in protic solvents. The formation of **42a** is proposed to involve the very reactive intermediates  $[(\text{BCOPE})\text{PdH}]^+$  and  $(\text{BCOPE})\text{Pd}(\text{CO})$ . However, they are never detected.

## Chapter four

### 4.2.3.2 Re-examination of the reaction of **12a**, CO and H<sub>2</sub>

The reaction of **12a**, CO and H<sub>2</sub> was re-examined by NMR spectroscopy. When a sample of **1a** was dissolved in methanol and exposed to a mixture of CO and *parahydrogen*, no further reaction was observed over 30 minutes other than the slow conversion of **12a** to **69a**. This suggests that to form of **42a**, higher temperatures or other reagents, such as an acid, are required.

### 4.2.4 Reaction of **12a** with diphenyl acetylene

When a sample of **12a** and diphenyl acetylene in methanol-d<sub>4</sub> was examined between 298 K and 333 K, no reaction was observed and the <sup>31</sup>P signal of **12a** remained visible at δ 74.4 throughout the study.

### 4.2.5 Reaction of **12a** with diphenyl acetylene and CO in methanol-d<sub>4</sub>

When **12a** reacts with diphenylacetylene and CO in methanol-d<sub>4</sub> the formation of **69a** was indicated. No other reaction products were indicated, and GC-MS analysis of the resulting solution revealed only the presence of diphenyl acetylene.

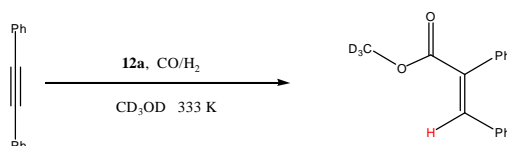
### 4.2.6 Short conclusion

The control reactions have revealed the need for H<sub>2</sub> and CO and the alkyne if catalysis is to occur. They suggest that the addition of CH<sub>3</sub>OH itself cannot catalyse the carbonylation of diphenyl acetylene.

## 4.3 Diphenyl acetylene carbonylation catalysed by **12a**

### 4.3.1 Introduction

#### 4.3.1.1 Reaction and study methods



#### Equation 15: *12a* catalysed diphenyl acetylene carbonylation

According to GC-MS, the reaction of diphenyl acetylene with CO/H<sub>2</sub> in the presence of **12a** gives the carbonylation product **44**. The yield proves dependent on the CO pressure. With 1



atm. of CO, the yield was 72 % after 30 mins at 333 K. In contrast, with 0.4 atm. of CO, the yield fell to 50 %. The by-products of this reaction are the hydrogenation products *cis*- and *trans*-stilbene. Reaction in dichloromethane gives only *cis*- and *trans*-stilbene. However, adding methanol to the dichloromethane sample does enable the formation of **44**, while adding water to the reaction in dichloromethane leads to formation of  $\alpha$ -phenyl-cinnamic acid.

This reaction was investigated by NMR methods in methanol (**Section 4.3.2**) and dichloromethane. (**Section 4.3.3**) I now examine the effect of Pd/CO ratio, temperature and substrate. By these studies, the diphenyl acetylene carbonylation mechanism was revealed as shown in **Section 4.1**.

#### 4.3.1.2 NMR parameters

NMR tubes that are equipped with Young' tap are used for this study. A typical NMR sample was prepared by dissolving 5 mg of catalyst and 10 mg of diphenyl acetylene in deuterated solvents. The sample was then degassed on high vacuum line ( $< 10^{-2}$  Pa) three times before exposing it to CO and *parahydrogen*. No difference was observed on using purified deuterated solvents according to standard methods or using these solvents as received.

#### 4.3.2 NMR study in methanol

##### 4.3.2.1 Overview

When a sample that contained **12a** and diphenyl acetylene (PhCCPh-d<sub>10</sub> or Ph<sup>13</sup>CCPh-d<sub>10</sub> in some cases) in methanol-d<sub>4</sub> was exposed to a mixture of CO/*parahydrogen* and monitored at 298 K, no enhanced NMR signals were evident at this point. However, when the sample was warmed to 308 K, several sets of strongly polarized resonances were observed after a short initiation time. These signals include the hydrogenation product *cis*- and *trans*-stilbene at  $\delta$  6.61 and  $\delta$  7.18 respectively. The corresponding <sup>1</sup>H{<sup>31</sup>P} NMR spectrum, which contains PhCCPh-d<sub>10</sub> as the substrate, is illustrated in Figure 95. The assignment of these signals will be detailed in the following section.

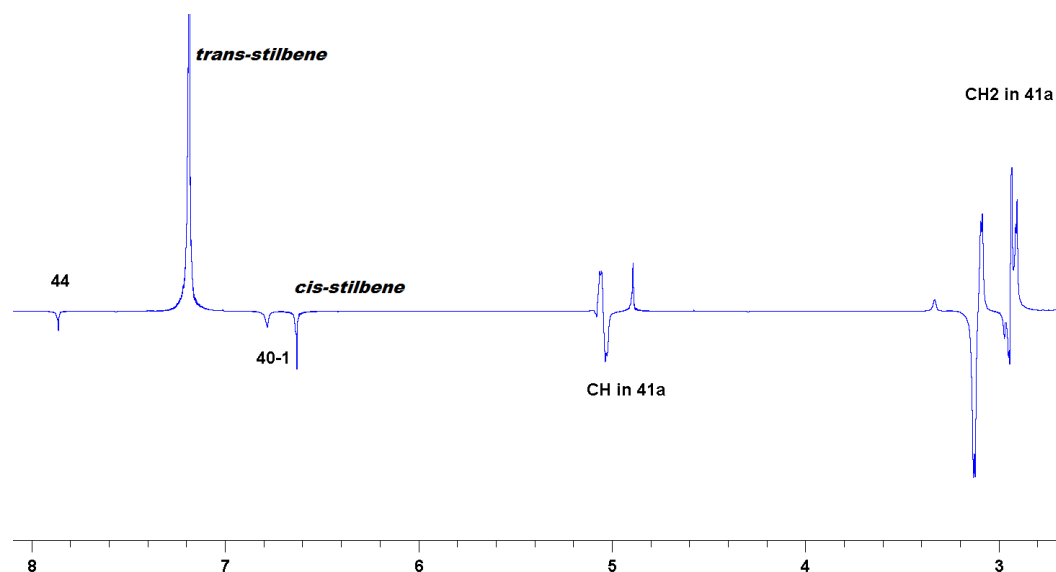


**Figure 95:** The  $^1\text{H}\{^{31}\text{P}\}$  NMR spectrum recorded during the reaction of **12a**, diphenyl acetylene- $d_{10}$ , CO and parahydrogen, suggesting the formation of a range of reaction intermediates and products at 323 K.

#### 4.3.2.2 Detection of species that does not contain CO

A dramatic increase in reactivity is observed upon adding CO when comparing the intensity of the enhanced signals with a parallel experiment without CO. The most notable PHIP enhanced signals appear at  $\delta$  5.02,  $\delta$  3.10 and  $\delta$  2.93 and are due to the known species **41a**. The intensity of **41a** signals increase by a factor of 16 when compared with experiments without CO. I conclude that adding CO not only leads to carbonylation but also promotes hydrogenation.

The NMR signals at  $\delta$  5.02,  $\delta$  3.10 and  $\delta$  2.93 due to **41a** are all mutually coupled. All of these signals simplify into doublet of doublets on  $^{31}\text{P}$  decoupling. The signal at  $\delta$  5.02 has 11.2 Hz and 15.0 Hz  $^1\text{H}$  couplings and therefore can be assigned to the '-CHPh' motif in the alkyl group, whereas the splittings are 15.0 Hz and -4.3 for the  $\delta$  3.10 resonance, and 15.0 Hz and -4.3 Hz for the  $\delta$  2.93 resonance. They can be assigned to the two protons of the 'CH<sub>2</sub>Ph' motif. Figure 96 illustrates the correlation of these three signals in the COSY plot.

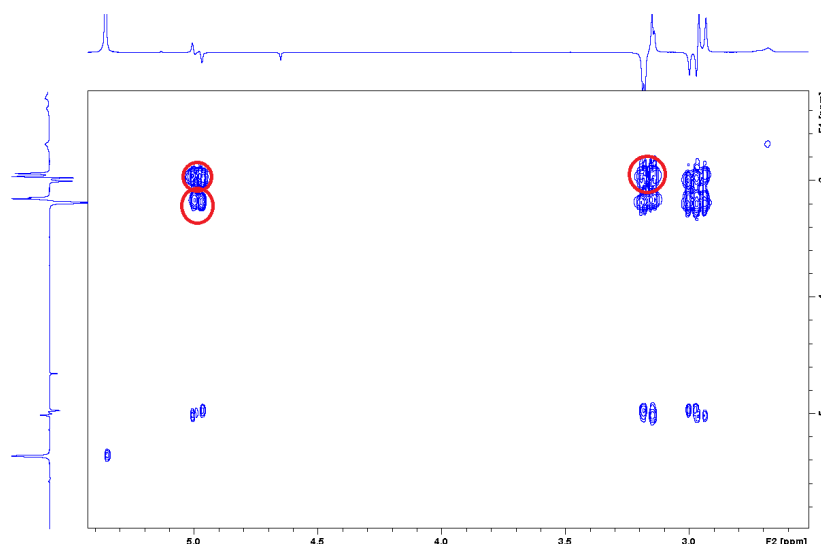


**Figure 96:** The correlation of the PHIP enhanced signals at  $\delta$  5.02,  $\delta$  3.10 and  $\delta$  2.93 due to **41a** is revealed by 2D  $^1\text{H}$ - $^1\text{H}$  COSY NMR.

Interestingly, the signals at  $\delta$  3.10 and  $\delta$  2.93 are strongly enhanced while the signal at  $\delta$  5.02 is only moderately enhanced. This difference is readily apparent when a  $^1\text{H}$ -OPSY NMR spectrum was recorded. As shown in Figure 97, the ratio of these peaks is approximately now 1:3:3 at 308 K. This ratio changes to 1:1.2:1.2 on warming to 323 K. Furthermore, when the reaction in  $\text{CD}_2\text{Cl}_2$  was undertaken at 308 K, the selectivity became even higher (cal. 1 : 19 : 19). These studies are presented in **Section 4.3.5**. This measurement monitors signals for sites, where the two protons from a single *parahydrogen* molecule are placed into both the ‘ $\text{CH}_2\text{Ph}$ ’ sites of **41a** with a higher probability than an  $\alpha\beta$  incorporation. This ratio difference reduces when the temperature increases, as the placement of two protons from a *parahydrogen* molecule into **41a** becomes less selective.

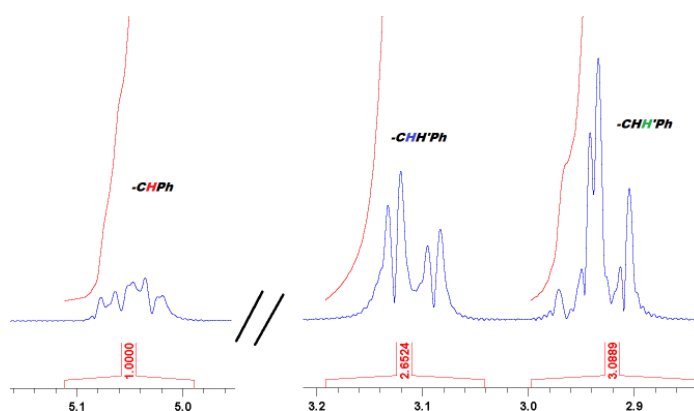


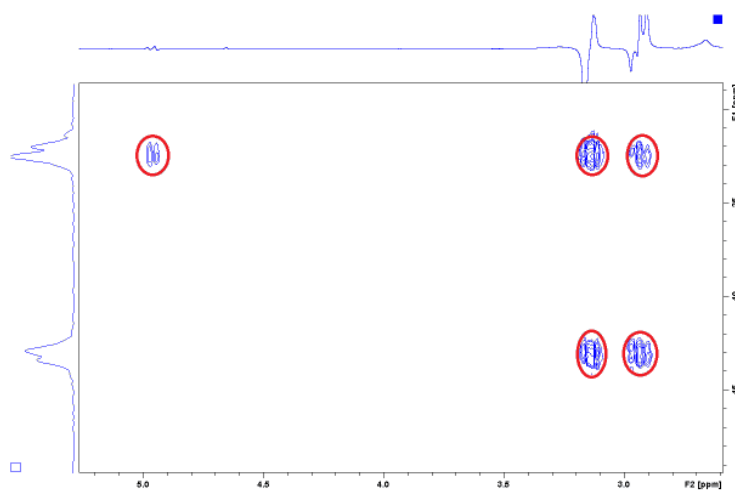
**Figure 97:** The integration of a  $^1\text{H}$  OPSY NMR spectrum shows the level of polarization that sits in the ‘ $\text{CHPh-CH}_2\text{Ph}$ ’ sites in **41a**

## Chapter four

According to a 2D  $^1\text{H}$ - $^{31}\text{P}$  HMQC experiment, all three protons couple to two inequivalent  $^{31}\text{P}$  signals at  $\delta$  32.2 and  $\delta$  42.1, which share a common coupling of 90.2 Hz. This suggests a *cis* orientation of two inequivalent phosphine donors.

Polarization on an *ortho*-hydrogen at  $\delta$  7.53 can be observed when diphenyl acetylene was used. However, when diphenyl acetylene- $\text{d}_{10}$  is used, the polarization at  $\delta$  7.53 disappears. In addition, no exchange between this *ortho*-hydrogen and dihydrogen is observed.

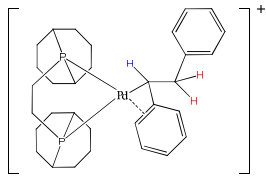
$^{13}\text{C}$  data were recorded when  $\text{Ph}^{13}\text{CCPh}$  was used. Figure 98 shows how these proton signals correlate with the newly formed  $^{13}\text{C}$  centres. The NMR data for **41a** is listed in Table 46.



**Figure 98:** Correlation of  $^1\text{H}$  and  $^{31}\text{P}$  signals at  $\delta$  32.2 and  $\delta$  42.1 using  $\pi/4$  2D  $^1\text{H}$ - $^{31}\text{P}$  HMQC experiments.

The chemistry of type **41a** complexes has been discussed in **Section 1.4.4**.

Table 46: Selected NMR data for **41a** (308 K in methanol-*d*<sub>4</sub>)

			
Group / nucleus	Chemical shift ( $\delta$ )	Multiplicity	Coupling constants (Hz)
<b><sup>1</sup>H</b>			
CHPh	5.02	d, d	$J_{HH} = -3.0, 10.0$
CH <sub>2</sub> Ph	2.93	d, d	$J_{HH} = 10.0, 15.2$
	3.10	d, d	$J_{HH} = -3.0, 15.2$
<i>ortho</i> -H	7.53	m	-
<b><sup>31</sup>P</b>			
P <sub>a</sub>	42.1	d	$J_{PP} = 90.2$
P <sub>b</sub>	32.2	d	$J_{PP} = 90.2$
<b><sup>13</sup>C</b>			
CHPh	62.3	d, d	$J_{CP} = 54.0, 16.2$
CH <sub>2</sub> Ph	35.2	d, d	$J_{CP} = 16.2, 5.4$

### Detection of **40a-1**

A further phosphorus coupled doublet of doublets was visible at  $\delta$  6.77 in these <sup>1</sup>H NMR spectra, with  $J_{PH}$  of 13.6 Hz and 6.8 Hz respectively. This signal was in emission, and disappeared when a dq-OPSY pulse sequence was used, whereas the signals for **41a** remained. This suggests that this signal arises from One-Proton-PHIP, whereas the signals for **41a** are due to PHIP. It simplifies into singlet on <sup>31</sup>P decoupling, and is therefore assigned to be the known species [(BCOPE)Pd(CPh=CHPh)(CD<sub>3</sub>OD)](OTf) (**40a-1**). The structure of **40a-1** is illustrated in Figure 99.

**40a-1** was also observable when no CO was used. However, its intensity increases by a factor of 4 if CO is used. A similar product, the pyridine adduct **40a-2** can also be trapped upon adding pyridine to this reaction. Type **40a** compounds that are related to this are summarized in Figure 99. Selective NMR data for **40a-1** is listed in Table 47.

## Chapter four

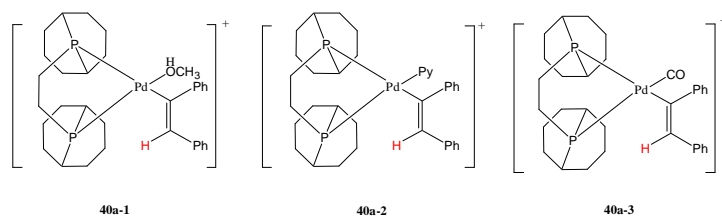
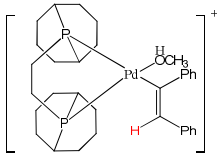
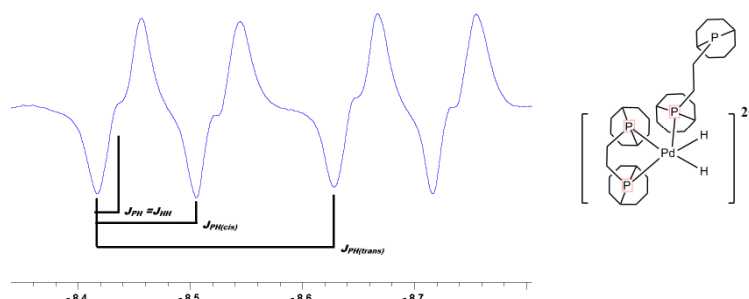


Figure 99: Structures of type 40a complexes

Table 47: Multinuclear NMR data for 40a-1 (308 K in methanol- $d_4$ )

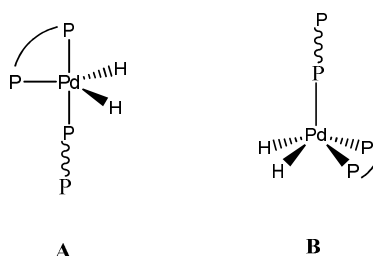
			
Group / nucleus	Chemical shift ( $\delta$ )	Multiplicity	Coupling constants (Hz)
$^1\text{H}$			
=CHPh	6.77	d, d	$J_{\text{PH}} = 13.6, 6.8$
$^{31}\text{P}$			
$\text{P}_{\text{trans}}$	21.8	m	$J_{\text{PH}} = 13.6$
$\text{P}_{\text{cis}}$	39.0	m	$J_{\text{PH}} = 6.8$
$^{13}\text{C}$			
Pd-C(Ph)=	161.2	-	-
PhCH=	130.6	-	-

So far, we have identified **41a** and **40a-3**. How are they formed? I now describe how the observation of these reaction intermediates to develop an answer to this question.

Detection of  $[(\kappa^2\text{-BCOPE})(\kappa^1\text{-BCOPE})\text{Pd}(\text{H})_2](\text{OTf})_2$  (70a)

**Figure 100:** (a): A  $\pi/4$  experiment taken from the reaction of **1a**, diphenyl acetylene and  $\text{CO}/p\text{-H}_2$  shows the signals at  $\delta$  -8.56 and  $\delta$  -8.59 have both in-phase and antiphase component.

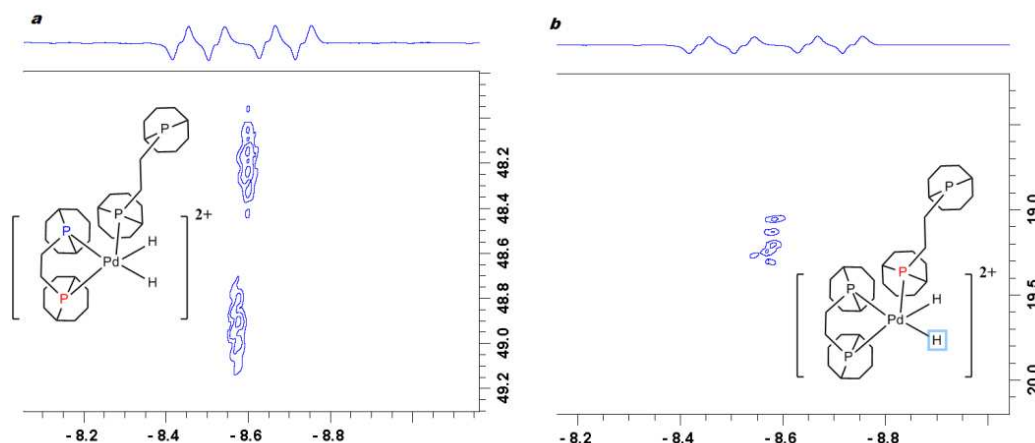
Firstly at 308 K, a polarized signal is detected at  $\delta$  -8.60. The corresponding  $^1\text{H}$  NMR spectrum is shown in Figure 100. This hydride resonance appears in a dq-OPSY experiment and hence arises from a  $\text{Pd}(\text{H})_2$  complex. Furthermore, the antiphase character is normally ascribed to inequivalent coupled dihydride resonances. The signal cluster at  $\delta$  -8.60 might arise from two very close hydride signals. The splitting of 105.4, 44.2 and 9 Hz suggested that there are three  $^{31}\text{P}$  couplings in this multiplet. Two possible products are shown in Figure 101. When these peaks are firstly examined, it is clear that 105.4, 44.2 and 9 Hz splittings are visible. In **Chapter 5**, a *trans* P-Pd-H couplings is revealed as being 174 Hz for  $[\text{HPd}(\text{PPh}_3)_3]^+$ . Furthermore, in  $[(\text{BCOPE})\text{PdH}(\text{py})]^+$ , the *trans* coupling is 223 Hz. This suggests that the hydride resonances observed does not have a *trans* phosphine and therefore excludes the possibility of being structure A.



**Figure 101:** Possible structures that fit the hydride signal at  $\delta$  -8.60

## Chapter four

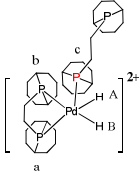
Based on the information that the 2D experiments provided, the cluster of the signal at  $\delta$  -8.60 is the AB pattern of two hydride signals at  $\delta$  -8.59 and  $\delta$  -8.61 with overlap. Both seem to have a large  $J_{\text{PH}}$  coupling of ca. 105.4 Hz and a smaller  $J_{\text{PH}}$  of ca. 44.2 Hz. This is an additional 10 Hz  $^{31}\text{P}$  splits to each signal. They also share a  $J_{\text{HH}}$  of ca. -10 Hz. The 2D  $^1\text{H}$ - $^{31}\text{P}$  HMQC experiments located three  $^{31}\text{P}$  centres at  $\delta$  19.16,  $\delta$  48.19, and  $\delta$  48.92 for this species. The  $^{31}\text{P}$  signal at  $\delta$  19.16 is  $^{31}\text{P}$  coupled triplet, with  $J_{\text{PP}} = 12.6$  Hz, this suggests its *cis* arrangement with other two  $^{31}\text{P}$  centres. Two further AB pattern  $^{31}\text{P}$  signals are detected at  $\delta$  48.19, and  $\delta$  48.92. They couple with each other as well as the  $^{31}\text{P}$  signal at  $\delta$  19.16, with  $J_{\text{PH}} = 29.4$  and 12.6 Hz respectively. These data confirm the arrangement of the hydride and phosphine ligands. In addition, according to the  $J_{\text{PH}(\text{cis})}$  coupling, we are detecting Pd(II) species rather than Pd(IV) species, which confirms the structure of this species to be of  $[(\kappa^2\text{-BCOPE})(\kappa^1\text{-BCOPE})\text{Pd}(\text{H})_2](\text{OTf})_2$  (**70a**). The structure of **70a** is illustrated in Figure 100.

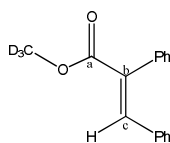


**Figure 102:** Correlation of hydride signals at  $\delta$  -8.56 and  $\delta$  -8.59 due to **12a** with  $^{31}\text{P}$  resonances



Table 48: Multinuclear NMR data for 70a (308 K in CD<sub>3</sub>OD)

			
Group / nucleus	Chemical shift ( $\delta$ )	Multiplicity	Coupling constants (Hz)
<b><sup>1</sup>H</b>			
Hydride A	-8.59	d, d, d, d	$J_{\text{PH}} = 105.4$ ( <i>trans</i> )
Hydride B	-8.61		$J_{\text{PH}} = 44.2$ ( <i>cis</i> ) $J_{\text{PH}} \sim 10$ ( <i>cis</i> ) $J_{\text{HH}} \sim -10$
<b><sup>31</sup>P</b>			
P <sub>c</sub>	19.16	t	$J_{\text{PP}} = 12.6$
P <sub>b</sub>	48.19	d, d	$J_{\text{PP}} = 29.4, 12.6$
P <sub>a</sub>	48.92	d, d	$J_{\text{PP}} = 29.4, 12.6$

4.3.2.3 Detection of the product: *cis*-PhCH=CPhCOOCD<sub>3</sub> (**44**)Figure 103: Structure of **44**.

So far, we have identified palladium species **41a** and **40a-1** in this reaction. However, a polarized signal for **44** is also seen. This signal appears at  $\delta$  7.84 as a singlet and in emission. It disappeared when a dq-OPSY pulse sequence was used, confirming its one-Proton-PHIP origin. When <sup>13</sup>CO was used, the <sup>1</sup>H resonance shows an extra 7.5 Hz splitting. This confirms that we are now dealing with a CO containing product. The coupling is typical for a vinyl proton and a carbonyl group that are *cis* orientated on a double bond. (*cis*: 4.5 Hz - 9 Hz, *trans*: > 10.5 Hz) The corresponding carbonyl group was located at  $\delta$  168.1 by a 2D <sup>1</sup>H-<sup>13</sup>C HMQC experiment. The corresponding <sup>13</sup>C NMR spectrum revealed that **44** is the only species that contains labelled <sup>13</sup>CO after the reaction, and indicated a high level of selectivity.

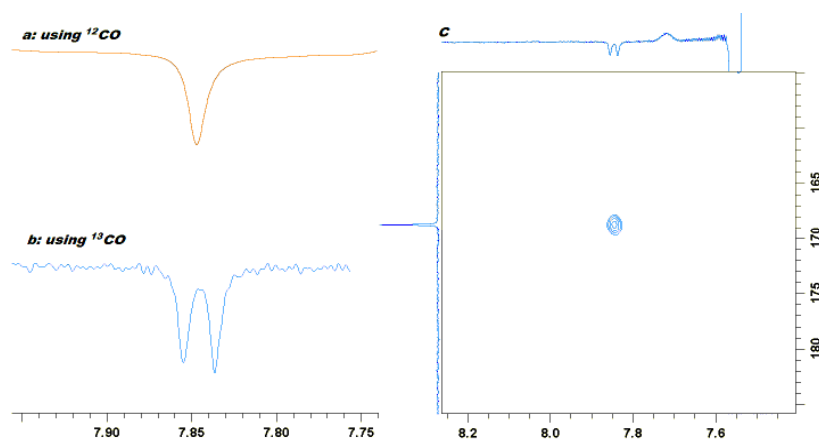
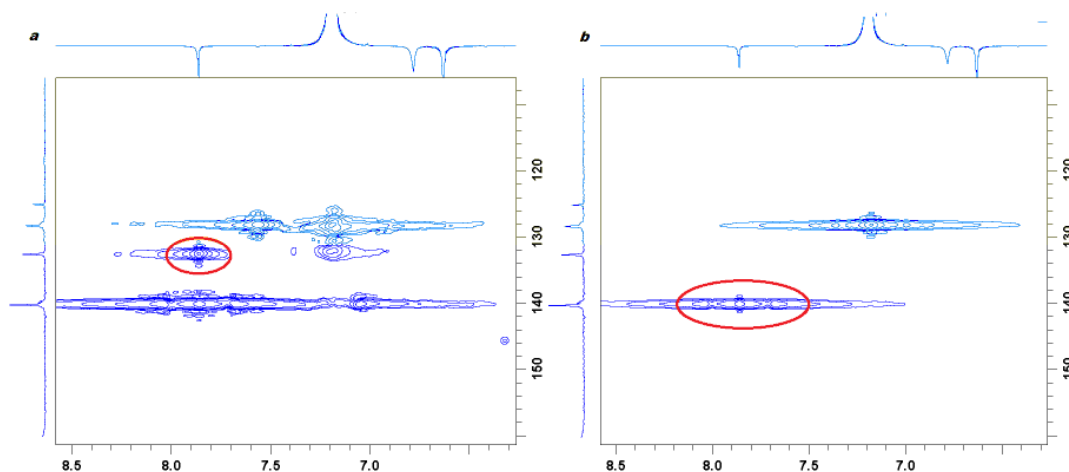


Figure 104: <sup>1</sup>H NMR spectra showing the region that contains the diagnostic signal for **44** when <sup>12</sup>CO (a) and <sup>13</sup>CO (b) were used. (c): the correlation of this proton signal to the carbon centre at  $\delta$  168.1 is recorded via a 2D measurement.

Additional information was provided when C<sub>5</sub>D<sub>5</sub><sup>13</sup>CCC<sub>6</sub>D<sub>5</sub> was used. This time the resonance at  $\delta$  7.84 showed extra <sup>13</sup>C splittings of 156 Hz and 3.5 Hz. A 2D <sup>1</sup>H-<sup>13</sup>C HMQC

experiment located the corresponding  $^{13}\text{C}$  NMR resonances at  $\delta$  132.6 and  $\delta$  140.5 for these two sites, which are both within the typical range of  $sp^2$  type carbon resonances. This information indicates that the proton resonates at  $\delta$  7.84 is attached to an  $sp^2$  type carbon centre.



**Figure 105:** Expansion of the  $^1\text{H}$ - $^{13}\text{C}$  HMQC dataset showing the correlation of the proton signal at  $\delta$  7.84 to the corresponding carbon centres at (a)  $\delta$  132.6 and (b)  $\delta$  140.5.

A GC-MS experiment supports the formation of the methoxycarbonylation product, *cis*- $\text{PhCH}=\text{CPhCOOCD}_3$  (**44**) by yielding a signal with  $m/z^+$  242, which corresponds to the molecular ion of **44**. Using diphenylacetylene- $d_{10}$  or  $\text{CH}_3\text{OH}$  leads to new signals at 252 and 239. **44** can therefore be formed in many isotopic states if different starting materials are used. These isomers are illustrated in Figure 106. Full NMR data of **44** is summarised in Table 45.

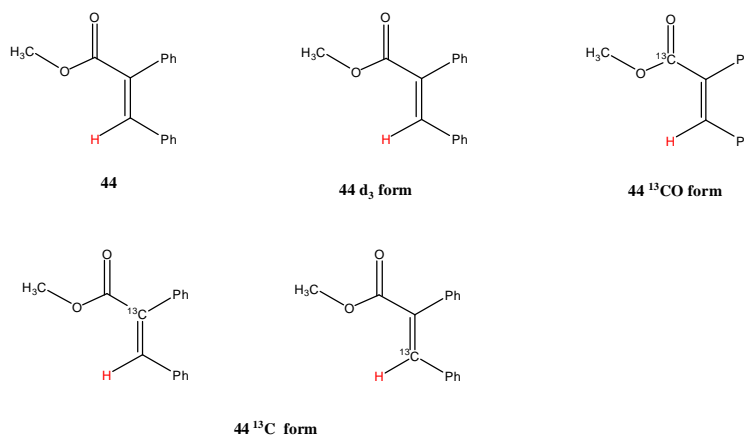


**Figure 106:**  $\alpha$ -phenyl-cinnamic ester derivatives detected in this study

## Chapter four

An overall 72 % yield for **44** was estimated by calibrating corresponding carbon spectra. This is in good accordance with GC-MS results. No doubt, the yield is highly dependent on CO pressure and could be improved. Reducing the Pd/substrate to CO/H<sub>2</sub> ratio proved to suppress the level of hydrogenation.

### 4.3.2.4 Detection of CO containing intermediates

#### Detection of [(BCOPE)Pd( $\mu$ -H)( $\mu$ -CO)Pd(BCOPE)][OTf] (**42a**)

In the very early stage of the reaction, a polarized hydride signal due to a known species, **42a**, is observed at  $\delta$  -5.34. <sup>146</sup> It appears as a <sup>31</sup>P coupled quintet, and collapses into a singlet on <sup>31</sup>P decoupling; with  $J_{PH} = 47.2$  Hz. A 2D <sup>1</sup>H-<sup>31</sup>P HMQC experiment correlated this hydride signal to a <sup>31</sup>P resonance at  $\delta$  20.9.

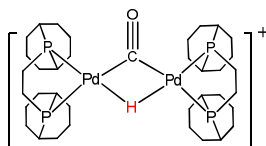


Figure 107: Structure of **42a**

As discussed in Section 4.2.3.1, previous studies confirm that type **42a** complexes show dynamic behaviour in solution due to the exchange of different configurations. This could be proved the temperature dependence of the corresponding <sup>1</sup>H and <sup>13</sup>C NMR spectra of type **42a** complexes. A similar complex, [(bdpp)Pd( $\mu$ -H)( $\mu$ -CO)Pd(bdpp)]Cl yields a <sup>31</sup>P coupled quintet at  $\delta$  -5.34, with  $J_{PH} = 44$  Hz at 298 K. However, when cooled to 223 K, this signal appeared as a triplet of triplets, with  $J_{PH} = 92$  and 5.4 Hz. These observations suggest the inequivalence of the phosphine ligands and further confirm the structure of **42a**.

The chemistry of **42a** was further explored by chemical methods in my study. This work will be presented in Section 4.3.4. This corresponds to the first intermediate detected that contains CO, as a result of CO being present in the reaction.

### 4.3.2.5 Detection of species of low-intensity

Further weak but enhanced signals are also visible at  $\delta$  6.90,  $\delta$  4.26 and  $\delta$  5.08 in the corresponding <sup>1</sup>H NMR spectrum. These species are not observed without CO.

**Detection of (BCOPE)Pd(CPh=CHPh)(OTf) (40a-4)**

The signal at  $\delta$  6.90 is broad and shows one-Proton PHIP. It disappears upon cooling the sample from 308 K to 298 K, reducing the catalyst/CO ratio or using the dq-OPSY program. However, it is visible when the reaction is undertaken in  $\text{CD}_2\text{Cl}_2\text{-d}_2$ . This excludes the possibility of it being a methanol adduct.

To understand how the reaction chemistry affects the detection of this complex, a series of experiments were conducted using different [Pd]/CO ratio. Table 49 lists the experimental conditions used in these studies. The typical  $^1\text{H}$  NMR spectra collected during these studies are illustrated in Figure 108.

**Table 49: Experimental conditions used when studying the CO dependence for 40a-4**

	Catalyst	solvent	substrate	CO	<i>p</i> -H <sub>2</sub>	Total	Other
A	6mg	0.6 ml	6 mg	1 atm.	2 atm.	3 atm.	
B	3mg	0.6 ml	6 mg	1 atm.	2 atm.	3 atm.	
C	1.5mg	0.6 ml	6 mg	1 atm.	2 atm.	3 atm.	
D	6mg	0.6 ml	6 mg	1 atm.	2 atm.	3 atm.	1ul H <sub>2</sub> O

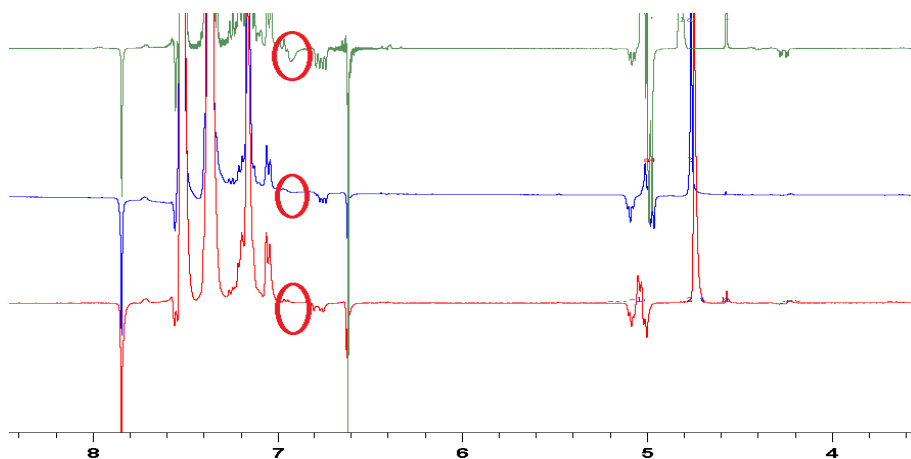


**Figure 108:  $^1\text{H}$  NMR spectra shows the dependence of [Pd]/CO ratio for the  $^1\text{H}$  NMR signal at  $\delta$  6.90**

## Chapter four

**Table 50: The impact of the [Pd]/CO ratio on the intensity of the related species**

[Pd]/CO ratio	$\delta$	Products and intermediates	Intensity		
↓	6.90	(BCOPE)Pd(CPh=CHPh) (OTf)	<b>40a-4</b>	↓	
	7.84	PhCH=CPhCOOCH <sub>3</sub>	<b>44</b>	↑	Carbonylation
	6.77	[(BCOPE)Pd(CPh=CHPh)(CH <sub>3</sub> OH)](OTf)	<b>40a-1</b>	↓	
	6.61	<i>cis</i> -PhCH=CHPh		↓	Hydrogenation
	5.08	[(BCOPE)Pd(CD <sub>3</sub> COCHPh=CHPh)(CO)](OTf)	<b>72a</b>	↑	Carbonylation intermediate
	5.02	[(BCOPE)Pd(PhCH-CH <sub>2</sub> Ph)](OTf)	<b>41a</b>	↓	Hydrogenation
	4.26	[(BCOPE)Pd(PhCH=CHPh)(CO)](OTf) <sub>2</sub>	<b>71a</b>	↓	Hydrogenation intermediate

According to these spectra, we conclude that the intensity of the <sup>1</sup>H NMR signal at  $\delta$  6.90 decrease when increasing the CO/Pd ratio. This signal also disappears on adding 1  $\mu$ l water to a sample in dichloromethane-d<sub>2</sub>. This species could be a palladium vinyl species that contains OTf<sup>-</sup> or a CO ligand. Its NMR properties are similar to those of known species [(BCOPE)Pd(CPh=CHPh)(CH<sub>3</sub>OH)](OTf) (**40a-1**) ( $\delta$  6.75) and [(BCOPE)Pd(CPh=CHPh)-(py)](OTf) (**40a-2**) ( $\delta$  6.70). A further experiment containing 5 mg of NaOTf gave rise of a very close peak at  $\delta$  6.96 (as described in **Section 4.3.3.6**). We finally conclude that the <sup>1</sup>H NMR signal at  $\delta$  6.90 arise from (BCOPE)Pd(CPh=CHPh)(OTf) (**40a-4**).

In addition, these NMR studies also show that the hydrogenation process was suppressed by increasing CO/[Pd] ratio, which indicates the potential improvement of the carbonylation yield.

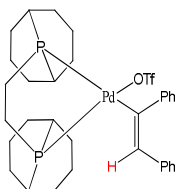


**Figure 109: Structure of 40a-4**

**Detection of [(BCOPE)Pd(PhCH=CHPh)(CO)](OTf) (71a)**

A further polarized signal appeared at  $\delta$  4.28. It is  $^{31}\text{P}$  coupled doublet of doublets, with  $J_{\text{PH}}$  of 13.0 Hz and 3.7 Hz. It simplifies into a singlet upon  $^{31}\text{P}$  decoupling. When a dq-OPSY experiment is used, this signal disappears. This suggests the formation of a new product **71a**. The comparison of  $^1\text{H}$  and  $^1\text{H}\{^{31}\text{P}\}$  spectra of **71a** was illustrated in Figure 110.

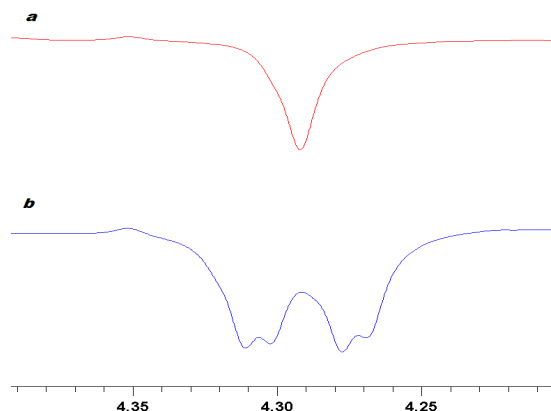


**Figure 110:** Region of the (a)  $^1\text{H}\{^{31}\text{P}\}$  (b)  $^1\text{H}$  and NMR spectra taken from the reaction of **12a**, diphenyl acetylene and  $\text{CO}/p\text{-H}_2$ .

When  $\text{Ph}^{13}\text{CCPh-d}_{10}$  was used as the substrate, further  $^{13}\text{C}$  splittings of 133.49 Hz and 3.30 Hz was observed for this signal. This suggests the possibility of a bound stilbene product, as the  $^1J_{\text{CH}}$  is much smaller than these found for free stilbene (157 Hz for *cis* and 152 Hz for *trans*). However, the detection of the corresponding  $^{31}\text{P}$  and  $^{13}\text{C}$  centres was not achieved due to its low intensity;

The new species must contain another ligand besides the stilbene, and two phosphines, as the phosphine donors are now inequivalent. These could be CO or OTf. I propose that this is the Pd(II) CO adduct [(BCOPE)Pd(PhCH=CHPh)(CO)](OTf)<sub>2</sub> (**71a**) because it is not observed without CO even though PhCH=CHPh is strongly polarised under these conditions.

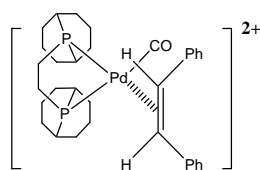


**Figure 111:** Possible structure for **71a**

## Chapter four

### Detection of [(BCOPE)Pd(CD<sub>3</sub>COCPh=CHPh)(CO)](OTf)<sub>2</sub> (**72a**)

A further weakly enhanced resonance was detected at  $\delta$  5.08, which is partly masked by the signal at  $\delta$  5.02 ('PhCH=' in **41a**). The signal at  $\delta$  5.02 is temperature dependent and moves to  $\delta$  4.97 when increasing the temperature to 313 K. In contrast, the signal at  $\delta$  5.08 is unaffected and therefore it is better recognized at 313 K. Figure 112 shows the corresponding <sup>1</sup>H and <sup>1</sup>H{<sup>31</sup>P} NMR spectra of this signal under variable conditions.

This signal is in emission, and does not couple to other proton signals. It is a <sup>31</sup>P coupled triplet when <sup>12</sup>CO is used where  $J_{\text{PH}} = 6.0$  Hz, as shown in Figure 112. This suggests that the two <sup>31</sup>P centres in this product are now equivalent. When <sup>13</sup>CO is used in this reaction, an extra <sup>13</sup>C splitting of 6.3 Hz is observed on this resonance. This value is very close to that found for **44**, indicating the proton that gives rise to this <sup>1</sup>H signal is *cis* to a <sup>13</sup>CO group on a double bond (> 9 Hz for *trans*). The proton signal at  $\delta$  5.08 is therefore ascribed to that of the three-coordinate ester adduct **72a**. The proposed structure of **72a** is shown in Figure 113.

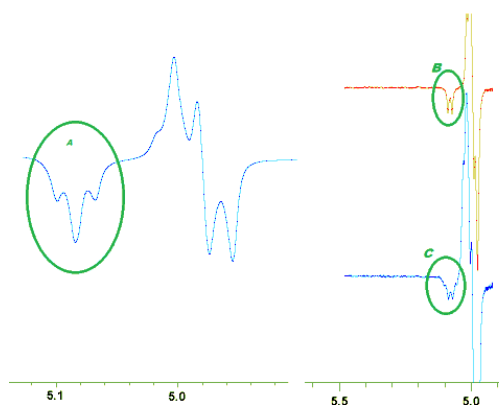


Figure 112: Expansion of the <sup>1</sup>H NMR signal at  $\delta$  5.08 under different conditions. (a): using normal CO at 313 K, (b): <sup>1</sup>H{<sup>31</sup>P} <sup>13</sup>CO at 308 K. C<sup>1</sup>H, <sup>13</sup>CO at 308 K

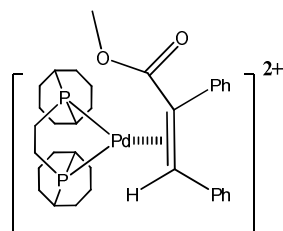


Figure 113: Structure of **72a**



### Detection of very weak species, 42a and 41a-3

Two additional polarized but very weak (almost equals to the  $^{13}\text{C}$  satellites for the signal due to **41a**) resonances at  $\delta$  4.55 and  $\delta$  5.23 were also detected. Both of these resonances show substantial  $^{31}\text{P}$  coupling and simplify to doublet of doublets on  $^{31}\text{P}$  decoupling. The corresponding  $^1\text{H}$  and  $^1\text{H} \{^{31}\text{P}\}$  spectra for these signals are shown in Figure 114. They must arise from the alkyl species as both of them show PHIP rather than one-Proton PHIP. They are proposed to be alkyl species that are stabilized by  $\text{OTf}^-$  and CO. However; any further characterization was not achieved due to their low intensity.

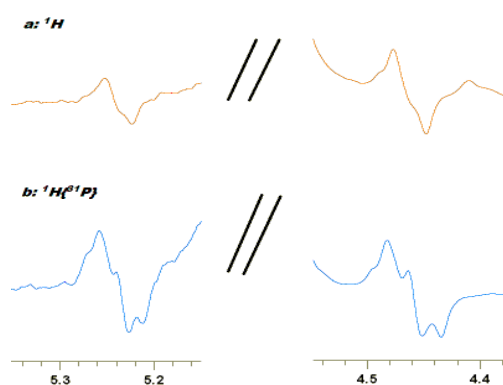


Figure 114:  $^1\text{H}$  and  $^1\text{H} \{^{31}\text{P}\}$  spectrum of additional alkyl complexes 42a-3 and 41a-3

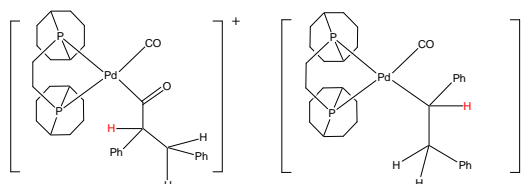


Figure 115: Structure of 42a and 41a-3

#### 4.3.2.6 Study with NaOTf: Detection of $\text{Pd}[(\text{BCOPE})(\text{CPh}=\text{CHPh})(\text{OTf})]$ (**40a-4**)

When a sample, which contains extra 5 mg NaOTf, was monitored by NMR spectroscopy, the broad signal due to **40a-4** was detected at  $\delta$  6.96 in the  $^1\text{H}$  NMR spectrum.

## Chapter four

### 4.3.2.7 Reaction of **12a**, diphenyl acetylene with CO and *parahydrogen* in ethanol- $d_6$

The reaction of **12a**, diphenyl acetylene, CO and hydrogen in ethanol was then followed. When a sample that contains **12a** and diphenyl acetylene in ethanol- $d_1$  was exposed to CO and  $H_2$ , another new anti-phase resonance was seen at  $\delta$  7.74, which simplified into singlet on  $^{13}C$  decoupling due to the removal of  $^3J_{CH} = 7.4$  Hz. The corresponding  $^{13}C$  carbonyl resonance for this species appears at  $\delta$  163.9, which is different from that detected for **44**. This change suggests that the ethyl ester **66** rather than the methyl ester was formed. In the meanwhile, the presence of **41a** is indicated by three mutually coupled resonances at  $\delta$  5.02,  $\delta$  3.14 and  $\delta$  2.94. The signals for **66** and *cis*-stilbene were found at  $\delta$  6.73 and  $\delta$  6.56 respectively. Selected NMR data for **66** is listed in Table 51.

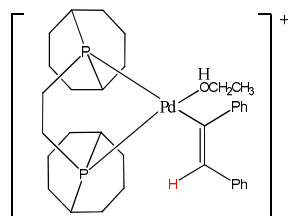


Figure 116: Structure of  $[Pd(BCOPE)(CPh=CHPh)(CH_3CH_2OD)](OTf)$  (**40-5**)

Table 51: NMR data for **66** (308 K in ethanol- $d_1$ )

Group / nucleus	Chemical shift ( $\delta$ )	Multiplicity	Coupling constants (Hz)
$^1H$			
=CH	7.74 (1H)	s	$J_{C(a)H} = 7.4$
CH <sub>3</sub>	1.34 (3H)	t	$J_{HH} = 7.13$
CH <sub>2</sub>	4.32 (2H)	quart	$J_{HH} = 7.13$
$^{13}C$			
C <sub>(a)</sub>	163.9		$J_{C(a)H} = 7.4$

#### 4.3.2.8 Short conclusion

In conclusion, **12a** proved to be an effective and selective hydrocarbonylation catalyst for diphenyl acetylene under very mild conditions (308 - 323 K, 3 atm. of synthetic gas). **12a** converts diphenyl acetylene to ester in the presence of alcohol. The total yield is 72 % under these conditions. No alkyne dimerization and CO co-polymerization product was detected. These results are supported by NMR and GC-MS studies, as described above.

In the NMR study in methanol, a wide range of carbonylation intermediates were detected by PHIP. They include the final ester product **44**, the ester adduct **72a**, and the vinyl species **40a-4**. They are believed to be closely related with the catalytic hydrocarbonylation cycle and strongly support the cationic mechanism of diphenyl acetylene hydrogenation and carbonylation.

The active hydride species **13a** was not directly detected during the catalysis in methanol; however, several hydride species including **42a** and **70a** are observed by PHIP. The formation of **42a** involves **13a** according to previous studies. The detection of **70a** and the *cis*-stilbene adduct **71a** gives evidence of the neutral mechanism for the diphenyl acetylene hydrogenation.

When diphenyl acetylene hydrogenation is hydrogenated to the alkyl complex **41a**, considerable level of selectivity was observed, where the two protons in a *para*hydrogen molecule are placed into the CH<sub>2</sub>Ph site in **41a**. The level of such selectivity was temperature dependent. The decreasing on selectivity can be explained by an increase tendency of neutral mechanism upon warming to 323 K.

The reaction in methanol was relatively fast. Therefore this reaction must be examined in non-protic solvents, such as CD<sub>2</sub>Cl<sub>2</sub>. The reaction of **12a**, diphenylacetylene, CO and H<sub>2</sub> in CD<sub>2</sub>Cl<sub>2</sub> was therefore followed.

#### 4.3.3 NMR studies of **12a** catalyzed carbonylation in dichloromethane-d<sub>2</sub>

##### 4.3.3.1 Control reaction

The reaction of **12a** with CO or H<sub>2</sub> was described in **Section 4.1**. When a sample of **12a** in dichloromethane-d<sub>2</sub> was exposed to CO/H<sub>2</sub> and monitored by NMR spectroscopy, no reaction was evident at 313 K. However, when diphenyl acetylene was added to this

## Chapter four

sample, two hydride species were immediately observed at  $\delta$  -5.54 and  $\delta$  -4.64. The quintet signal at  $\delta$  -5.54 was known as **42a**. The specification of new hydride complexes at  $\delta$  -4.64 will be discussed in following section.

### 4.3.3.2 Overview of reaction

When a sample of **12a**, diphenylacetylene in dichloromethane- $d_2$  was exposed to 1:2 mixture of CO/*parahydrogen* and monitored at 280 K, only a very weakly enhanced resonance at  $\delta$  3.12 due to **41a** was evident at this stage. However, the antiphase character of the hydrogen signal indicated that the exchanging of hydrogen and other active species was occurring.

Several strongly polarized resonances became visible after a short initiation period at 308 K. The  $^1\text{H}$  NMR signals at  $\delta$  2.94,  $\delta$  3.14 and  $\delta$  4.96 are due to **41a**. We note that the signal at  $\delta$  4.96 was only slightly polarized at this stage, compared with the other two signals at  $\delta$  2.94 and  $\delta$  3.14. The intensity of these three signals are estimated to be 1: 19: 19 at this stage. Such difference indicates higher level of selectivity (> 95%) than that was found in methanol (as described in **Section 4.3.3**). Reaction at 315 K still shows considerable selectivity (1: 3: 3).

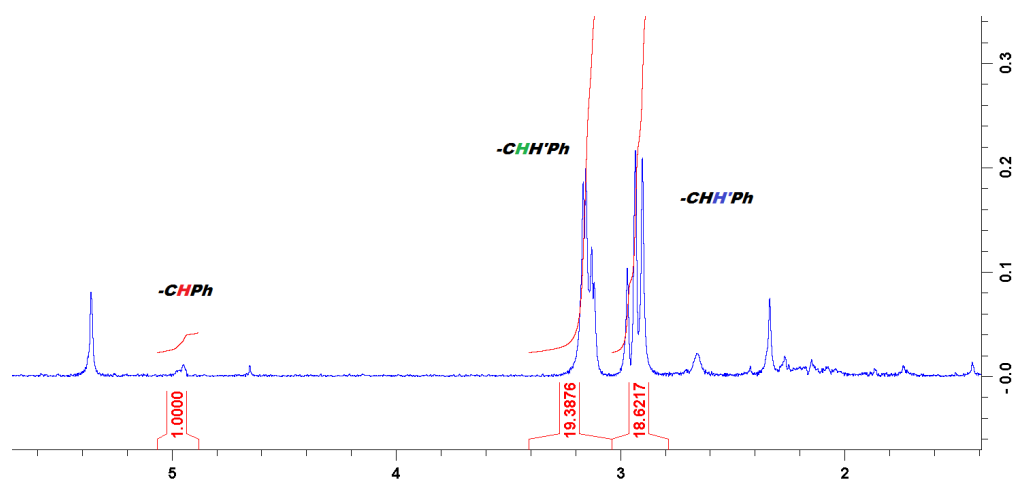


**Figure 117:**  $^1\text{H}$  NMR spectrum shows selective hydrogen addition to the ' $\text{CH}_2\text{Ph}$ ' site in **41a** when the reaction was undertaken in dichloromethane- $d_2$  at 308 K

Several other polarized resonances due to known species were also recognized: *cis*- and *trans*-stilbene at  $\delta$  6.61 and  $\delta$  7.18 respectively, **40a-4** at  $\delta$  6.90 and **42a** at  $\delta$  -5.54. The

signal due to **40a-1** at  $\delta$  6.78 was not visible until reaction temperature reaches 313 K, which is highest practicable temperature. Besides these specified signals, two new enhanced signals were observed at  $\delta$  7.89 and  $\delta$  -4.64, both of them show one-Proton-PHIP. Polarization on all of these signals can be regenerated on shaking and adding more parahydrogen.

#### 4.3.3.3 Detection of intermediates

##### Detection of [Pd(BCOPE)Pd(CO-CPh=CHPh)(CO)](OTf) (**73a**)

At 313 K, a polarized signal was detected at  $\delta$  7.89 in emission, which is phosphorus coupled doublet of doublets, with  $J_{\text{PH}}$  of 22 Hz and 3.5 Hz. Its chemical shift suggested that it arise from an acyl species ( $\delta$  7.6 to  $\delta$  8.2) rather than vinyl species ( $\delta$  6.6-  $\delta$  7.2). The 2D  $^1\text{H}$ - $^{31}\text{P}$  HMQC experiments correlated two phosphorus centres at  $\delta$  36.0 and  $\delta$  45.2 respectively. When  $\text{Ph}^{13}\text{CPh-d}_{10}$  was used, this signal shows extra  $^{13}\text{C}$  splitting of 156.2 Hz and 3.5 Hz, this correlates the signal at  $\delta$  7.89 to  $sp^2$  type carbon centres at  $\delta$  137.2 and 137.8.

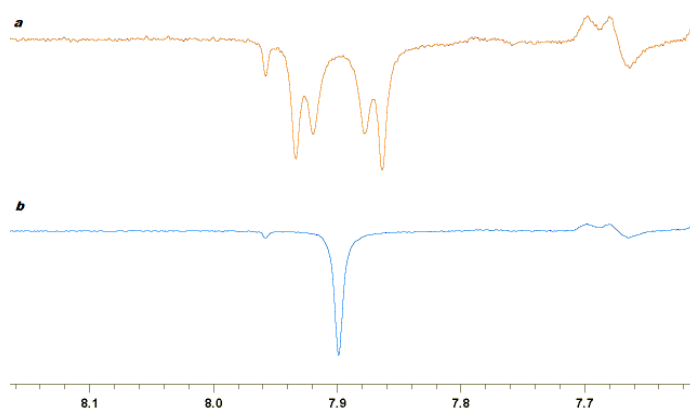


**Figure 118:** The  $^1\text{H}$  and  $^1\text{H} \{^{31}\text{P}\}$  spectra taken from the reaction of **1a**, diphenyl acetylene and  $\text{CO}/p\text{-H}_2$  in dichloromethane- $d_2$  at 313 K revealed the formation of an acyl species **73a**

According to the NMR information collected, **73a** must contain an acyl group and chelating BCOPE ligand. The other coordination site might be occupied by OTf or CO. In our further studies, lower the CO pressure to 0.3 atm. lead to a dramatic decrease in its intensity. In the meanwhile, this resonance also shows no solvent dependence when dichloromethane- $d_2$  is replaced by tetrachloroethane- $d_2$ . In conjunction with a related kinetic study using 1D EXSY experiments (See **Section 4.3.3.4**), the compound was assigned to be

## Chapter four

[(BCOPE)Pd(CO-CPh=CHPh)(CO)](OTf) (**73a**), The NMR data for **73a** is summarized in Table 52. In addition, when Ph<sup>13</sup>CCPh-d<sub>10</sub> was used as the substrate, a very weak resonance was detected at  $\delta$  7.69, which is normally masked by the background. According to the kinetic studies, this species is undergoing exchange with **73a**, and it could be PhCH=CHCOOTf. (**74**) The detail of this study will be provided in **Section 4.3.3.4**.

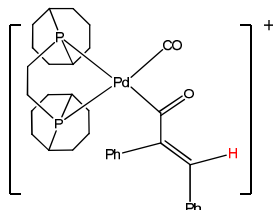


Figure 119: Structure of **73a**

Table 52: NMR data for **73a** (315 K in CD<sub>2</sub>Cl<sub>2</sub>)

Group / nucleus	Chemical shift ( $\delta$ )	Multiplicity	Coupling constants (Hz)
<b><sup>1</sup>H</b>			
	7.89	d, d d, d, t (using Ph <sup>13</sup> CCPh)	J <sub>PH</sub> = 22.3 and 3.5, J <sub>CH</sub> = 156.2 and 3.4
<b><sup>31</sup>P</b>			
P <sub>trans</sub>	36.0	d	J <sub>PH</sub> = 22.2
P <sub>cis</sub>	43.2	d	J <sub>PH</sub> = 3.5
<b><sup>13</sup>C</b>			
PhC=	137.2	d	J <sub>CH</sub> = 156.2
PhCH=	137.8	d	J <sub>CH</sub> = 3.4

### Detection of [PdH(BCOPE)(CO)](OTf) (**13a-3**)

In the high field of the <sup>1</sup>H NMR spectrum, a polarized doublet of doublets hydride signal was observed at  $\delta$  -4.64, with J<sub>PH</sub> of 189.9 Hz and 28.8 Hz. The corresponding <sup>1</sup>H and

$^1\text{H}\{^{31}\text{P}\}$  NMR spectra are illustrated in Figure 120. This signal simplifies into singlet on  $^{31}\text{P}$  decoupling, suggesting that it couple with two phosphine ligands that are *trans* and *cis* respectively. The phosphorus nucleus in *trans* was located at  $\delta$  46.0 by 2D  $^1\text{H}$ - $^{31}\text{P}$  HMQC experiments However, the other providing *cis* coupling was not detected and hence its binding is reversible. This is in agreement with the fact that add  $^{13}\text{CO}$  does not show an extra coupling.

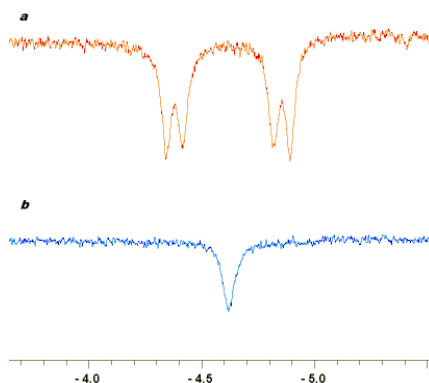


**Figure 120:** The  $^1\text{H}$  and  $^1\text{H}\{^{31}\text{P}\}$  NMR spectra showing the formation of a monohydride species **13a-3**

These data suggests this compound contains a chelating phosphine ligand and a hydride ligand. The other coordination site might be occupied by either CO or the solvent. This resonance shows no solvent dependence when tetrachloroethane- $\text{d}_2$  is used but strong CO pressure dependence. Therefore the compound was confirmed as  $[\text{PdH}(\text{BCOPE})(\text{CO})](\text{OTf})$  (**13a-3**).

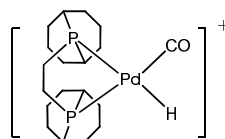


**Figure 121:** Structure of **13a-3**

#### 4.3.3.4 Reaction of (12a), diphenyl acetylene, with CO and $\text{H}_2$ in tetrachloroethane- $\text{d}_2$ at 343K

The reaction was further explored in tetrachloroethane- $\text{d}_2$  at 343 K, The reaction shows high similarities to the reaction in dichloromethane at 315 K, as described in last section.

## Chapter four

### 4.3.3.5 Kinetic study

A series of EXSY experiments were followed to probe the magnetization transfer between those species in  $\text{CD}_2\text{Cl}_2$ . When the signal at  $\delta$  7.89 due to **73a-3**, is selectively excited, reversible transfer into the signal at  $\delta$  7.69 (**74**) is indicated. This proceeds with an experimentally determined forward rate constant of  $0.69 \pm 0.03 \text{ s}^{-1}$  with a reverse rate constant of  $3.27 \pm 0.16 \text{ s}^{-1}$ . When the corresponding signal at  $\delta$  7.69 is probed, rapid transfer into the signal at  $\delta$  7.89 is indicated when the new rate constant is estimated to be  $3.8 \pm 0.16 \text{ s}^{-1}$ . These data suggest that these interconversions are facile with the equilibrium position lie to the left in favour of **73a**. The detailed calculation was attached in **Appendix 3**.

### 4.3.4 Impact of other reagents

A key question for this study lies in how hydrogen was activated. The presence of monohydride species has been revealed by the detection of **13a-2** and **13a-3**. It also has been suggested the formation of **42a** involves **13a** as the fragments. Therefore, a series of experiments were undertaken to explore the chemistry of **42a** by adding related reagents to the sample. The conditions of these experiments are summarized in Table 53. The results will be detailed in the following section.

**Table 53: Experiments used to study the impact of methanol**

	Catalyst	Solvent	CO	H <sub>2</sub>	Other reagents
1	3 mg	dichloromethane	1 bar	2 bar	CD <sub>3</sub> OD 1 $\mu\text{l}$
2	3 mg	dichloromethane	1 bar	2 bar	CD <sub>3</sub> OD 5 $\mu\text{l}$
3	3 mg	dichloromethane	1 bar	2 bar	CD <sub>3</sub> OD 10 $\mu\text{l}$
4	3 mg	dichloromethane	1 bar	2 bar	CH <sub>3</sub> OH 1 $\mu\text{l}$
5	3 mg	dichloromethane	1 bar	2 bar	CH <sub>3</sub> OH 5 $\mu\text{l}$
6	3 mg	dichloromethane	1 bar	2 bar	CH <sub>3</sub> OH 10 $\mu\text{l}$
7	3 mg	dichloromethane	1 bar	2 bar	D <sub>2</sub> O 1 $\mu\text{l}$
8	3 mg	dichloromethane	1 bar	2 bar	D <sub>2</sub> O 5 $\mu\text{l}$
9	3 mg	dichloromethane	1 bar	2 bar	D <sub>2</sub> O 10 $\mu\text{l}$
10	3 mg	dichloromethane	1 bar	2 bar	H <sub>2</sub> O 1 $\mu\text{l}$
11	3 mg	dichloromethane	1 bar	2 bar	H <sub>2</sub> O 5 $\mu\text{l}$
12	3 mg	dichloromethane	1 bar	2 bar	H <sub>2</sub> O 10 $\mu\text{l}$
13	3 mg	dichloromethane	1 bar	2 bar	NaCl saturated
14	3 mg	dichloromethane	1 bar	2 bar	NaOTf



#### 4.3.4.1 Methanol

Adding methanol to a  $\text{CD}_2\text{Cl}_2$  sample leads to the detection of a further characteristic signal for **44** at  $\delta$  7.84, which is not observed in  $\text{CD}_2\text{Cl}_2$  alone, as well as the signal at  $\delta$  7.89 due to **73a**. Slow conversion of **73a** to **44** can also be observed. In addition, adding methanol does not promote the formation of **42a**, although methanol has been reported to be the reducing reagent of Pd(II) to Pd(0) species.<sup>164</sup> Adding protio/deuterated methanol or different amount of it (1  $\mu\text{l}$ , 5  $\mu\text{l}$  and 10  $\mu\text{l}$ ) showed no difference. It can be concluded that the formation of **42a** does not involve methanol.

#### 4.3.4.2 Water

Adding water to the DCM sample leads to formation of  $\alpha$ -phenyl-cinnamic acid, by detecting a signal at  $\delta$  7.96 for the vinyl hydrogen. Adding water also ends the observation of the vinyl species **40a-3** at  $\delta$  6.90, the acyl species **73a** at  $\delta$  7.89, and the monohydride species **13a-3** at  $\delta$  -4.54. In contrast, adding water promotes the formation of **42a** dramatically. Figure 122 shows these observations.

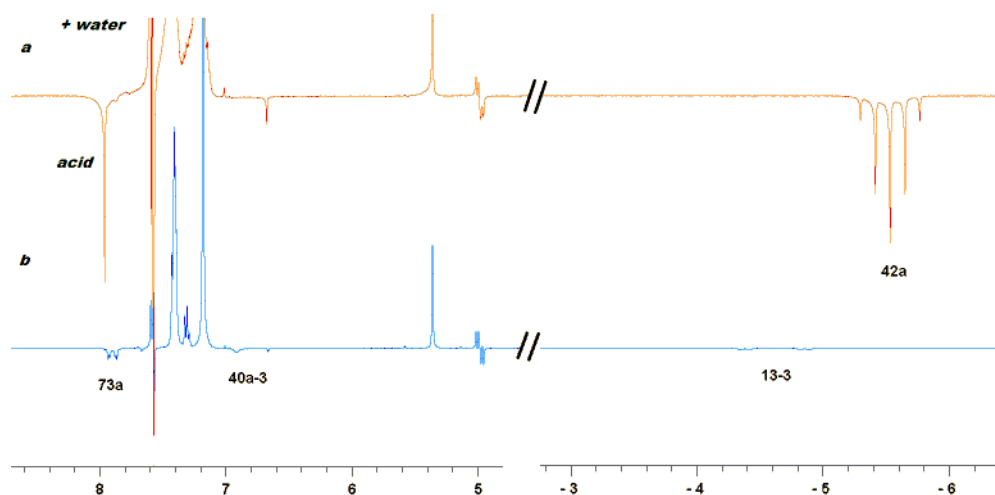


**Figure 122:** (a):  $^1\text{H}$  NMR spectrum upon adding 5  $\mu\text{l}$   $\text{H}_2\text{O}$  to the same sample. (b):  $^1\text{H}$  NMR spectrum taken from the reaction of **12a**, diphenyl acetylene with  $\text{CO}/\text{H}_2$ .

#### 4.3.4.3 NaCl

$\text{Cl}^-$  saturated dichloromethane- $\text{d}_2$  was prepared by shaking a suspension of NaCl in sonicating equipment for 2 hours. However, no difference was observed when this solvent was used for NMR study when compared with that employing normal dichloromethane- $\text{d}_2$ .

## Chapter four

It has been reported that adding sub stoichiometric amount of NaCl to an aqueous solution dramatically promotes these types of reactions.<sup>113</sup>

### 4.3.5 Short conclusion

Reaction of **12a** and diphenyl acetylene in dichloromethane- $d_2$  only gives only hydrogenation product in the absence of the nucleophile. Two key intermediates, the palladium acyl species **73a** and the palladium monohydride species **13a-3** are however detected here. Upon adding a stoichiometric amount of methanol to a dichloromethane sample, the slow formation of the ester **44** is observed. When methanol is replaced by water  $\alpha$ -phenyl-cinnamic acid is produced. We conclude that hydrogen rather than methanol contributes to the formation of these hydride species.<sup>164</sup>

## 4.4 Diphenylacetylene carbonylation catalysed by **12b**

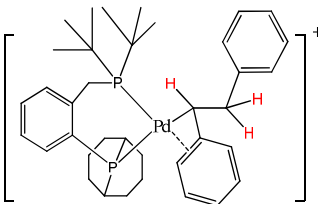
The reactions of  $[\text{Pd}(\text{}^t\text{BuCOPE})(\text{OH}_2)_2](\text{OTf})_2$  (**12b**) with diphenylacetylene and CO were then followed. This work will be presented briefly due to the similarity of these studies to those already described for **12a**.

### 4.4.1 Diphenylacetylene carbonylation catalysed by $[\text{Pd}(\text{}^t\text{BuCOPE})(\text{OH}_2)_2](\text{OTf})_2$ (**12b**) in methanol- $d_4$

When a sample of **12b** in methanol- $d_4$  was exposed to 1 atm. of CO, the solutions colour changed from colourless to yellow thereby indicating that the replacement of  $\text{OTf}^-$  by CO. When this sample was then exposed to 3 atm. of *parahydrogen* and monitored by NMR spectroscopy at 298 K, no enhanced NMR signals of the reaction were observed at this stage. However, when the sample was heated to 313 K, several enhanced proton signals were observed, these included those for the known hydrogenation products *cis*- and *trans*-stilbene at  $\delta$  6.61 and  $\delta$  7.18 respectively. The resonance for  $\text{H}_2$  also appears in antiphase suggesting that  $\text{H}_2$  is exchanging with active species in this solution.

A set of polarized signals were also seen at  $\delta$  5.02 and  $\delta$  2.99 and assigned to the known species **41b**. In contrast, to the previously described signals for **41a**, the signal at  $\delta$  5.02 which is due to the 'CHPh' motif was moderately enhanced while the resonances for the overlapping signals of the 'CH<sub>2</sub>Ph' motif were much weaker. A further emission signal can also be observed at  $\delta$  6.78 due to **40b-1**. **41b** and **40b-1** can in fact be seen without CO.<sup>46</sup> Selected NMR data for **41b** are presented in Table 54. A signal due to the carbonylation product **44** can also be observed, at  $\delta$  7.84, at this stage in the monitoring of this reaction.

Table 54: Selected multinuclear NMR data for **41b** (308 K CD<sub>2</sub>Cl<sub>2</sub>)

			
Group / Nucleus	chemical shift (δ)	multiplicity	coupling constant / Hz
<b><sup>1</sup>H</b>			
CH <sub>2</sub> Ph	2.96	m	
	3.03	m	
CHPh	4.94	m	
<b><sup>31</sup>P</b>			
(BCOPE)P	70.70	d	J <sub>PP</sub> = 60.3
<sup>t</sup> BuP	20.40	d	J <sub>PP</sub> = 60.3
<b><sup>13</sup>C</b>			
CH	64.0	d	J <sub>CP</sub> = 55.0
CH <sub>2</sub>	34.8	-	

When this sample was warmed further to 333 K, the <sup>1</sup>H NMR signals due to **41a** and **40a-1** disappeared. The signal at δ 7.84 due to **44** becomes much stronger at this point. Figure 123 illustrates the corresponding <sup>1</sup>H NMR spectrum at 333 K. The reaction was completed in 30 minutes, indicated by the disappearance of those intermediates. The enhancement of the δ 7.84 signal can be maintained for 30 minutes at 333 K, and regenerated by shaking or refilling the NMR tube with fresh *parahydrogen* and CO. This suggests that the carbonylation of diphenyl acetylene by **12b** is much faster than that by **12a**. Furthermore, given the long-term observation of hyperpolarisation in the signals of **44** the incorporation of a *parahydrogen* derived proton into it could be reversible. This effect was not observed with **12a**.

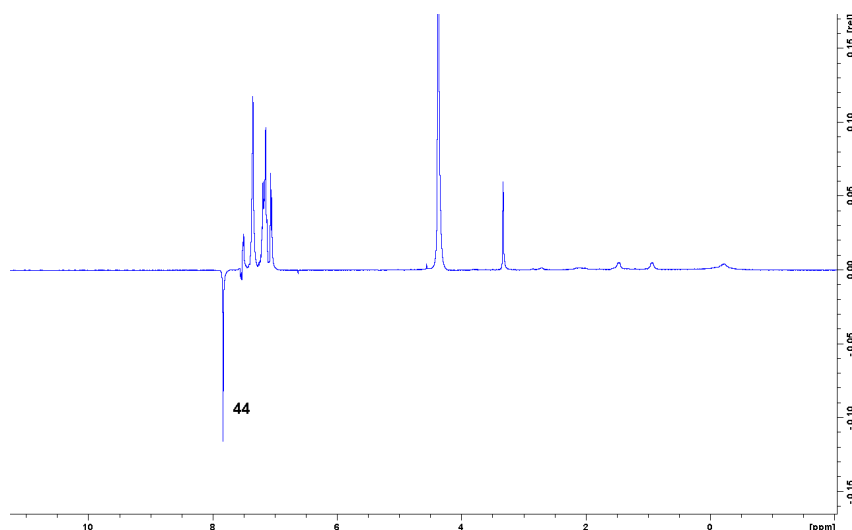


**Figure 123:** Region of the organic region of a  $^1\text{H}$  NMR spectrum that was recorded during the reaction of **12b**, diphenyl acetylene and  $\text{CO}/p\text{-H}_2$  at 333 K

These products, and the reaction intermediates **41b** and **40b-1** are known.<sup>46</sup> Their NMR data matches that previously reported. Five further antiphase signals are observed at  $\delta$  4.90,  $\delta$  5.21,  $\delta$  5.32,  $\delta$  -5.43 and  $\delta$  -5.41 during these measurements. They are similar in nature to those observed when the same reaction was undertaken with **12a** but have a transient existence due to the higher reactivity of this system, consequently only partial NMR data is available. Table 55 gives their NMR descriptions and the assignment of these signals.

The signal at  $\delta$  5.32 exhibits  $^1\text{H}$ -PHIP. I therefore conclude that it corresponds to the detection of the methyl ester of  $\alpha$ -phenyl-cinnamic acid as its chemical shift is very similar to that of **71a**. The signals at  $\delta$  4.90,  $\delta$  5.21 are attributed to two isomers of the *cis*-stilbene adduct shown which is related to **71bA** and **71bB**. These signals appear with an intensity ratio of 5 : 3 in accordance with the preferential formation of **71bA**.

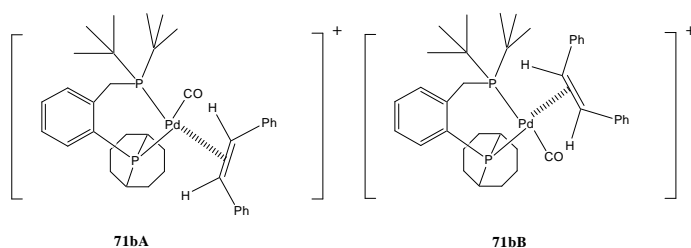


**Figure 124:** Structure of **71bA** and **71bB**

**Table 55: Intermediates detected in 12b catalysed diphenyl acetylene carbonylation and their NMR properties**

Assigned structure	Chemical shift ( $\delta$ )	Other NMR properties
	5.32	d, d, $J_{\text{PH}} = 6.2, 8.4$ Hz One-Proton PHIP
	5.21	t, $J_{\text{PH}} = 6.2$ Hz antiphase
	4.90	t, $J_{\text{PH}} = 6.2$ Hz antiphase

Further enhanced signals were evident at  $\delta$  -5.43 (quin,  $J_{\text{PH}} = 39$  Hz) and  $\delta$  -5.41 (quin,  $J_{\text{PH}} = 39$  Hz) due to two isomers of **43b** in these  $^1\text{H}$  NMR spectra. These assignments are based on the similarity in appearance of these enhanced signals to those of **43a**. The structures of these isomers are shown in Figure 125 and the averaging of the  $^{31}\text{P}$ -hydride couplings confirms that the H/CO arrangement within each isomer is undergoing interchange. The relative phosphine orientations do not change on this timescale and hence separate NMR signals are seen. In this case, **43b** is only detected when PHIP is employed.

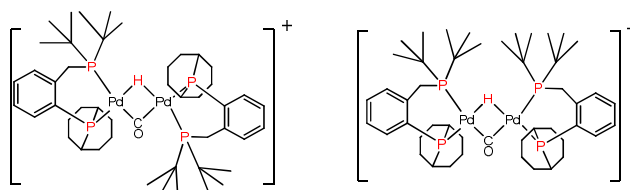


**Figure 125: Structures of 43bA and 43bB**

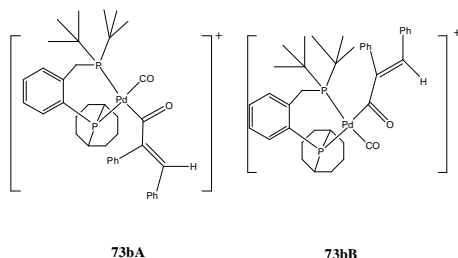
The product distribution of organic species was determined by GC-MS measurement in conjunction with calibrating the corresponding  $^{13}\text{C}$  NMR spectrum. When  $\text{Ph}^{13}\text{CCPh-d}_{10}$  was used, the yield of **44** was estimated as 55 % after 30 minutes of reaction. The levels of *cis* and *trans*-stilbene were estimated to be 44 % and 1 % respectively, Whilst **12b** shows

## Chapter four

higher catalytic activity than **12a** its selectivity for **44** is lower (55 % for **12b** vs 72 % for **12a**).

### 4.4.2 The reaction of **12b** diphenylacetylene, with CO and parahydrogen in dichloromethane-d<sub>2</sub>

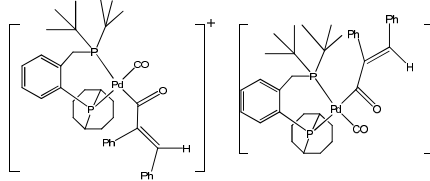
In order to detect the analogue of **73a**, a sample of **12b**, diphenylacetylene in dichloromethane-d<sub>2</sub> was exposed to CO/*p*-H<sub>2</sub> and examined by NMR spectroscopy at 315 K. Several polarized signals were observed immediately including the known species, **41b**, **40b-1**, and the two stilbene products that were described in methanol-d<sub>4</sub>. In addition, several new polarized signals were also observed. The most notable of these signals was centred at  $\delta$  7.90 and showed one-Proton-PHIP. It appears as a <sup>31</sup>P coupled doublet of doublets, with  $J_{\text{PH}} = 22.4$  Hz and 4.3 Hz respectively. This resonance simplified into a singlet on <sup>31</sup>P decoupling and when optimized 2D <sup>1</sup>H-<sup>31</sup>P HMQC experiments were recorded it correlated to two <sup>31</sup>P signals at  $\delta$  78.4 and  $\delta$  8.1. These are due to the <sup>t</sup>Bu-P and the BCOPE-P centres respectively. These resonances are all attributed to [Pd(<sup>t</sup>BuCOPE)(CO)(CPh=CHPh)](OTf) (**73bA**). The NMR data for **73bA** is summarized in Table 56.



**Figure 126: Structure of 73bA and 73bB**

A much weaker set of doublet of doublet signals which also appeared in emission was seen at  $\delta$  7.95. This signal is therefore very similar to that of **73bB**, but with much lower intensity (ca. 5 : 1 for **73bA**: **73bB**). It corresponds to the second isomer of **73b**. The *cis* coupling to phosphorus in **73b** for this signal proved to be 3.2 Hz, whereas the *trans* coupling was estimated at 20 Hz due to overlap. The *trans* <sup>31</sup>P centre for **73bB** was readily detected at  $\delta$  43.0 in the corresponding 2D <sup>1</sup>H-<sup>31</sup>P HMQC measurement, although its partner was not observed.

Table 56: Multinuclear NMR data for 73b isomers (315 K in toluene- $d_8$ )

				
Group / nucleus	Chemical shift ( $\delta$ ) and Multiplicity	Coupling constants (Hz)	Chemical shift ( $\delta$ ) and Multiplicity	Coupling constants (Hz)
$^1\text{H}$				
Vinyl-H	7.90	$J_{\text{PH}} = 22.4, 4.3$	7.95	$J_{\text{PH}} \sim 20, 3.2$
$^{31}\text{P}$				
cod-P	8.1	$J_{\text{PH}} = 22.4$	43.0	$J_{\text{PH}} = 3.2$
tBu-P	88.4	$J_{\text{PH}} = 4.3$		
Reference: 11022503				

### Detection of 13b-3 isomers

A further doublet of doublets was observed at  $\delta$  -5.45 in the hydride region. This signal coupled to two inequivalent phosphorus centres with couplings of 183.7 Hz (*trans*) and 19.3 Hz (*cis*) respectively. When a series of 2D  $^1\text{H}$ - $^{31}\text{P}$  HMQC experiments were recorded, a  $^{31}\text{P}$  centre which resonated at  $\delta$  7.9 proved to correlate to this signal via the *trans* coupling; the *cis* phosphine signal was located at  $\delta$  101.6. These two phosphine ligand signals share a common  $^{31}\text{P}$ - $^{31}\text{P}$  coupling of 36.7 Hz and are *cis* oriented. This hydride resonance is therefore assigned to  $[(^t\text{BuCOPE})\text{Pd}(\text{H})(\text{CO})](\text{OTf})$  (**13bA-3**) as it is only visible with CO. NMR data of **13bA-3** is listed in Table 57.

Another similar but much weaker hydride signal was also visible at  $\delta$  -6.36, which couples with two phosphorus centres with  $J_{\text{PH}} = 184.2$  Hz and 17.3 Hz respectively. It makes sense to ascribe this resonance to **13bB-3**, a second isomer. Figure 127 illustrates the  $^1\text{H}$  spectra for these two hydride signals and corresponding  $^1\text{H}$ - $^{31}\text{P}$  correlation for the hydride signal at  $\delta$  -5.45.

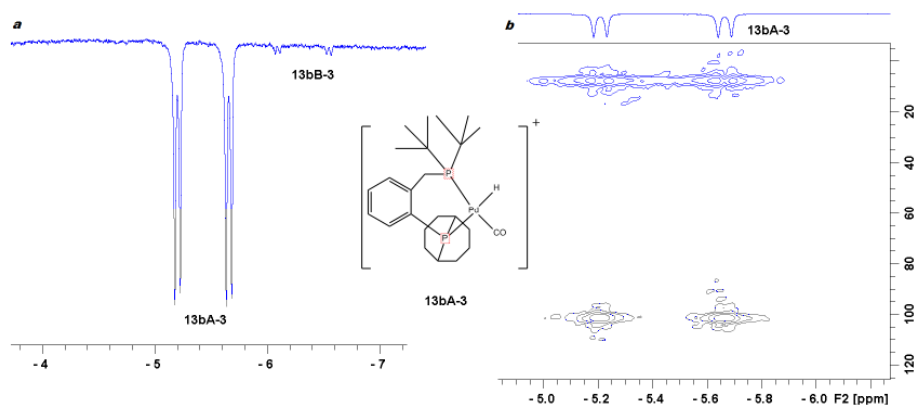


Figure 127: (a):  $^1\text{H}$  NMR spectra recorded at 323 K when 12b reacts with diphenylacetylene, CO and parahydrogen in dichloromethane- $d_2$  which reveal the formation of the monohydride complexes 13b-3; (b): expansion of a  $^1\text{H}$ - $^{31}\text{P}$  HMQC dataset showing correlations between these hydride signal of 13bA-3 and the resonances of its two  $^{31}\text{P}$  coupling partners.

Table 57: Multinuclear NMR data for 13b-3 isomers (315 K in  $\text{CD}_2\text{Cl}_2$ )

Group / nucleus	Chemical shift ( $\delta$ ) and multiplicity	Coupling constants (Hz)	Chemical shift ( $\delta$ ) and multiplicity	Coupling constants (Hz)
<b><math>^1\text{H}</math></b>				
hydride	-5.45 (d, d)	$J_{\text{PH}} = 183.7, 19.3$	-6.36 (d, d)	$J_{\text{PH}} = 184.2, 17.3$
<b><math>^{31}\text{P}</math></b>				
cod-P	19 (d)	$J_{\text{PH}} = 183.7$ $J_{\text{PP}} = 36.2$	-	
$^t\text{Bu-P}$	101.6 (d)	$J_{\text{PH}} = 19$ $J_{\text{PP}} = 36.2$	-	

#### 4.5 Studies using other substrates

This research was then expanded to all the study of *cis*-stilbene, styrene, and phenyl acetylene. These studies are presented in the following sections.



### 4.5.1 Carbonylation of *cis*-stilbene catalysed by **12a**

When a sample of **12a** and *cis*-stilbene in methanol was exposed to CO/*p*-H<sub>2</sub> and monitored by <sup>1</sup>H NMR spectroscopy, no enhanced signals were observed at 323 K. A thermal signal, at δ -5.54, due to **43a** was evident in this NMR spectrum. When the solution was analysed by GC-MS no carbonylation products were detected.

### 4.5.2 Carbonylation of styrene catalysed by **12a** and **12b**

#### 4.5.2.1 The reaction of **12a** and styrene in methanol-d<sub>4</sub>

When a sample of **12a** (3 mg) and styrene (3 μl) in methanol-d<sub>4</sub> was monitored at 298 K, no reaction was evident.

#### 4.5.2.2 The reaction of **12a**, styrene and CO in methanol-d<sub>4</sub>

When a sample of **12a** (3 mg) and styrene (3 μl) in methanol-d<sub>4</sub> was exposed to CO (1 bar), the slow conversion of **12a** into **69a** was indicated by the <sup>1</sup>H and <sup>31</sup>P NMR spectroscopy. The conversion of **12a** into **69a** was described previously in this thesis.

#### 4.5.2.3 The reaction of **12a**, styrene, with CO and *parahydrogen* in methanol-d<sub>4</sub>

When a sample of **12a** (3 mg) and styrene (3 μl) in methanol-d<sub>4</sub> was exposed to CO/*parahydrogen* and monitored by NMR spectroscopy at 298 K no reaction was evident besides the formation of **69a**. However, a very slow reaction took place over 2 hours at 308 K to form **75a**. The structure of **75a** is illustrated in Figure 128.

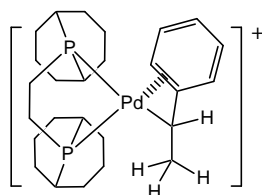


**Figure 128:** Structure of **75a**

Five non-polarized and newly formed resonances were detected at δ 1.44, δ 4.84, δ 6.92, δ 7.53 and δ 7.73 in the corresponding <sup>1</sup>H NMR spectrum. The signal at δ 1.44 is multiplet and simplifies into doublet on <sup>31</sup>P decoupling with J<sub>HH</sub> = 6.8 Hz, J<sub>PH</sub> = 10.2 Hz and 11.5 Hz. The δ 4.84 resonance is multiplet and simplifies to a quartet on <sup>31</sup>P decoupling, with J<sub>HH</sub> =

## Chapter four

6.8 Hz,  $J_{\text{PH}} = 6.8$  Hz. These two signals coupled according to 2D  $^1\text{H}$ - $^1\text{H}$  COSY measurements. Figure 129 shows the corresponding COSY dataset. Based on this information, a Pd-CHPh-CH<sub>3</sub> grouping that contains two phosphine ligands is indicted.

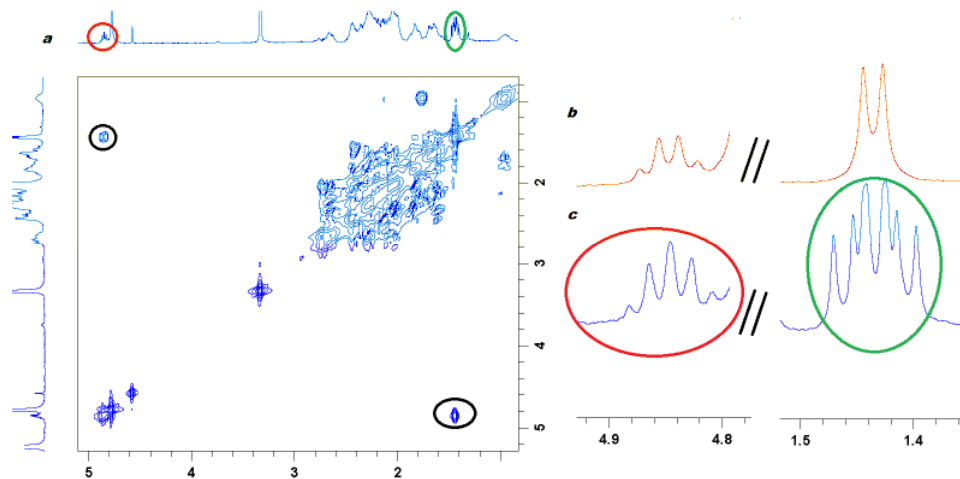


**Figure 129:** (a): A  $^1\text{H}$ - $^1\text{H}$  COSY dataset revealed the correlation of  $^1\text{H}$  NMR signals for 75a. (b): Expansions of the  $^1\text{H}$  and  $^1\text{H}\{^{31}\text{P}\}$  NMR spectra as shown to illustrate the  $\delta$  1.44 and  $\delta$  4.84 signals due to 75a

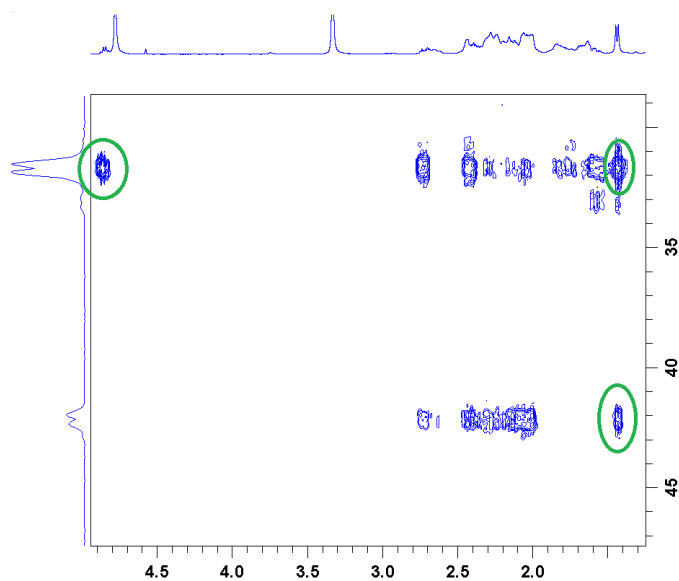


**Figure 130:** A  $^1\text{H}$ - $^{31}\text{P}$  HMQC dataset showing correlation between the signal at  $\delta$  1.43 and two  $^{31}\text{P}$  centres which resonate at  $\delta$  31.6 and  $\delta$  42.7 in 75a; the signal at  $\delta$  4.84 connects with just one  $^{31}\text{P}$  centre at  $\delta$  31.6.

When 2D  $^1\text{H}$ - $^{31}\text{P}$  HMQC experiments was undertaken, two inequivalent  $^{31}\text{P}$  NMR signals at  $\delta$  31.6 and  $\delta$  42.7 were located as described above. They share a common coupling of 55.3

Hz. The  $^1\text{H}$  resonance at  $\delta$  1.43 couples to both of the  $^{31}\text{P}$  signals, while the  $\delta$  4.84 resonance seems to couple to only the  $\delta$  31.6 signal. This information indicates the two  $^{31}\text{P}$  ligands in **75a** are inequivalent and *cis* orientated

In the low field region of the corresponding  $^1\text{H}$  NMR spectrum, three mutually coupled  $^1\text{H}$  NMR signals are detected at  $\delta$  6.92,  $\delta$  7.53 and  $\delta$  7.73. The signals at  $\delta$  6.92,  $\delta$  7.53 simplify into doublets and triplets respectively, whereas the signal at  $\delta$  7.73 remains unchanged, on  $^{31}\text{P}$  decoupling. The signal at  $\delta$  7.73 is therefore assigned to the *meta*-hydrogen of a phenyl group, while the rest are assigned to *ortho*- and *para*-hydrogens.

A  $^1\text{H}$ - $^{31}\text{P}$  HMQC experiment revealed that the  $\delta$  6.92 and  $\delta$  7.53 resonances both couple to the  $^{31}\text{P}$  resonance at  $\delta$  31.6. These data suggest that the signals at  $\delta$  1.44,  $\delta$  4.84,  $\delta$  6.92,  $\delta$  7.53 and  $\delta$  7.73 arise from the same species, **75a**. The structure of **75a** is shown in Figure 128 and is similar to **41a** and **41b**, although it can now be seen with the need for polarisation.<sup>46</sup> The characterisation of **75a** was expanded by recording a  $^1\text{H}$ - $^{13}\text{C}$  HMQC measurement which confirmed that the  $^1\text{H}$  NMR signal at  $\delta$  1.23 connected to a carbon centre at  $\delta$  14.5, whereas the  $\delta$  4.84 resonance coupled to a second  $^{13}\text{C}$  signal at  $\delta$  57.2. This NMR data is summarized in Table 58. We note **75a** is the only thermally stable product when **12a** reacts with styrene, CO and *para*hydrogen.

Chapter four

Table 58: Multinuclear NMR data for **75a** (298 K in CD<sub>3</sub>OD)

Group / nucleus	Chemical shift (δ)	Multiplicity	Coupling constants (Hz)
<b><sup>1</sup>H</b>			
CH <sub>3</sub>	1.23	m	J <sub>HH</sub> = 6.8, J <sub>PH</sub> = 10.2, 11.5
CH	4.84	quint	J <sub>HH</sub> = 6.8, J <sub>PH</sub> = 6.8
<i>o</i> -H	6.92	m	J <sub>HH</sub> = 7.7
<i>m</i> -H	7.53	m	J <sub>HH</sub> = 7.7 J <sub>HH</sub> = 7.4
<i>p</i> -H	7.73	m	J <sub>HH</sub> = 7.4
<b><sup>31</sup>P</b>			
	31.6	d	J <sub>PP</sub> = 55.3
	42.7	d	J <sub>PP</sub> = 55.3
<b><sup>13</sup>C</b>			
CH <sub>3</sub>	14.5	-	
CH	57.2	-	

4.5.2.4 Reaction of **12b**, styrene and CO in methanol-d<sub>4</sub>

The reaction of **12b**, styrene with CO/*p*-H<sub>2</sub> showed similar behaviour to that of **12a**, and sterically favoured **75bA** is formed selectively. The structure of **75bA** is illustrated in Figure 131. Selective NMR data of **75bA** are summarized in Table 59.

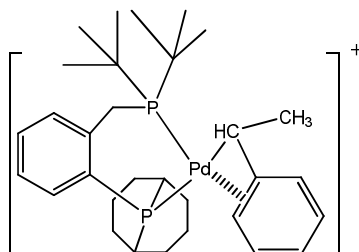


Figure 131: Structure of **75bA**

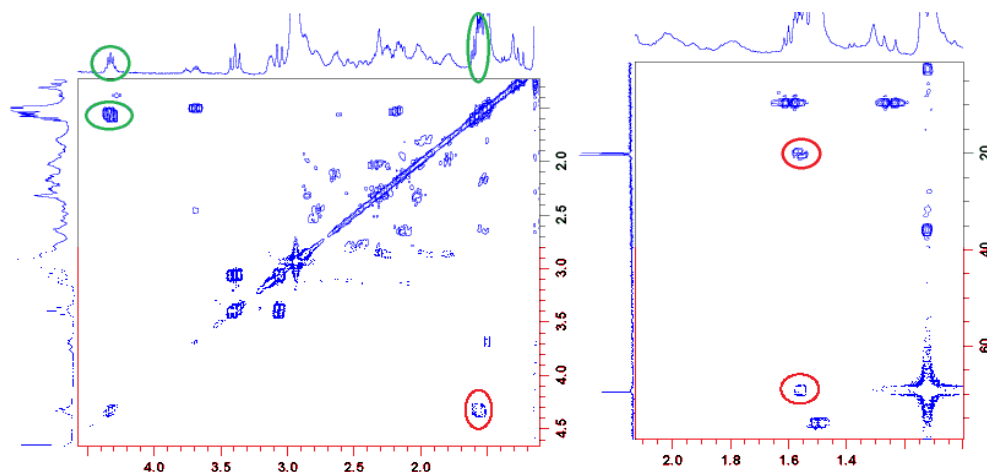


Figure 132: (a): The COSY dataset revealed the evidence of  $\text{CH}_3\text{-CH-Pd}$  group in 75bA. (b): Expansion of the  $^1\text{H}\text{-}^{31}\text{P}$  HMQC dataset that correlates the  $\text{CH}_3\text{-CH}$  group to two  $^{31}\text{P}$  centres

Table 59: Selective multinuclear NMR data for 75bA

Group nucleus	Chemical shift ( $\delta$ )	Multiplicity	Coupling constants (Hz)
<b><math>^1\text{H}</math></b>			
$\text{CH}_3$	1.57	m	$J_{\text{HH}} = 7$
$\text{CH}$	4.32	d	$J_{\text{HH}} = 7$
$o\text{-H}$	7.46	m, overlap	-
$m\text{-H}$	7.62	m, overlap	-
<b><math>^{31}\text{P}</math></b>			
	20.1		$J_{\text{PP}} = 58.2$
	69.3		$J_{\text{PP}} = 58.2$

### 4.5.3 Carbonylation of phenyl acetylene

## Chapter four

### 4.5.3.1 Reaction of Phenyl acetylene and **12a** in methanol-d<sub>4</sub>

Attempts to examine the reaction of **12a** and phenyl acetylene in methanol were unsuccessful due to the quick formation of a yellow solid. The new product contains very little NMR information and TLC and NMR failed. We assume that the hydride species plays a role in this progress. The reaction must be carried out in a non-protic solvent.

### 4.5.3.2 Reaction of **1a**, phenyl acetylene and CO/*p*-H<sub>2</sub> in dichloromethane-d<sub>2</sub>

The polymerization of phenyl acetylene was much slower in CD<sub>2</sub>Cl<sub>2</sub>. When a CD<sub>2</sub>Cl<sub>2</sub> sample of **12a**, phenyl acetylene under CO/*p*-H<sub>2</sub> was monitored by NMR spectroscopy, a reaction took place immediately. Two strongly polarized signals are seen at  $\delta$  1.23 and  $\delta$  4.84. Figure 133 illustrates this part of the corresponding <sup>1</sup>H and <sup>1</sup>H{<sup>31</sup>P} NMR spectra for this stage in the reactions time sequence. These polarised signals arise from the known species **75a**, as described in Section 4.5.2. We highlight the fact the signal of **75a** contains both inphase and antiphase components, suggesting their *parahydrogen* origin.

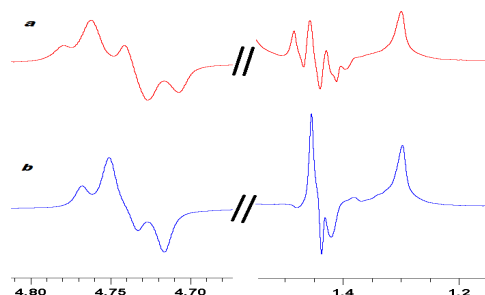


**Figure 133:** Region of the <sup>1</sup>H NMR spectrum when **12a** catalyses the reaction of phenyl acetylene and *parahydrogen*, indicating the formation of **75a**

## 4.6 Discussion & Conclusion

### 4.6.1 Discussion

Most of the reaction intermediates that have been described in this chapter are involved in both the hydrogenation and carbonylation reactions that have been described. The detection of these intermediates yields a good mechanistic map for these processes, where the substrate is diphenyl acetylene. The following discussion seeks to illustrate this by reference to **12a**; **12b** shows similar reactivity.

Two mechanisms have been proposed in the literature for the hydrogenation of a species such as diphenyl acetylene, as shown in Figure 134.<sup>46</sup> They are known as the cationic mechanism, which features the palladium hydride species **13a** as the catalytic precursor, and the neutral mechanism, which involves hydrogen addition to either Pd(II) or Pd(0) species.

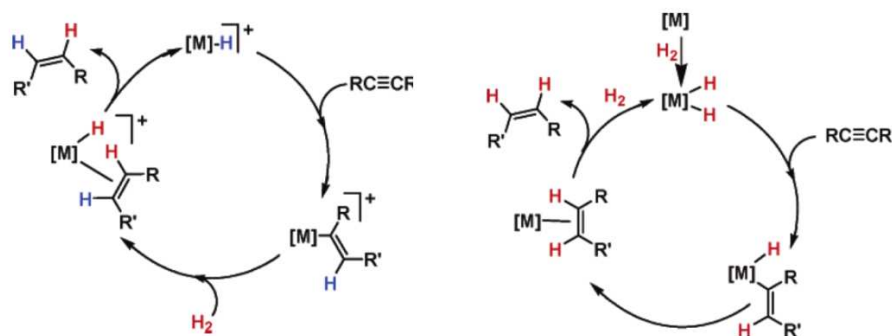
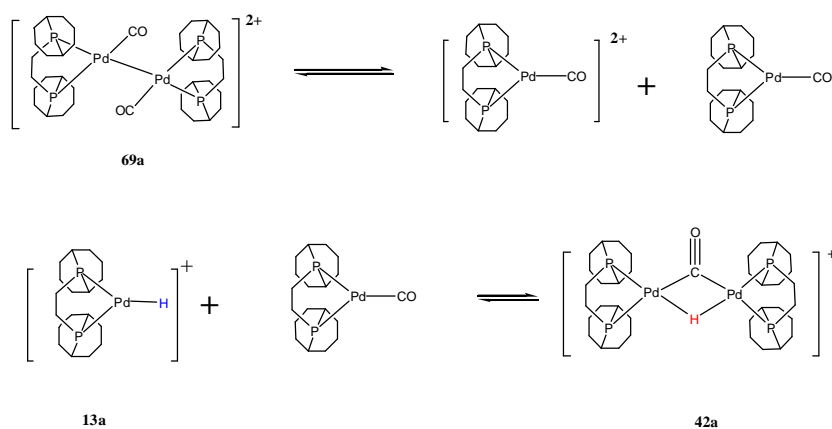


**Figure 134:** The proposed cationic and neutral mechanism for **12a** catalysed hydrogenation of diphenyl acetylene **46**

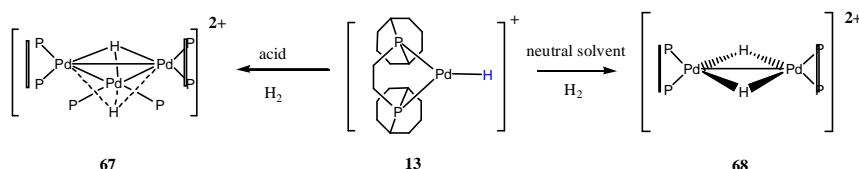
In this study, the formation of the highly unstable complex **13** was observed. This complex has been trapped as both pyridine (**13a-2**) and CO (**13a-3**) adducts. It dimerises in the absence of CO to form **68a**, and reacts with (BCOPE)Pd(CO) to form **43a**. Their interconversion is exemplified by the fact that **69a** (the CO adduct of **12a**) and **43a** show similar catalytic behaviour for hydrogenation or carbonylation. Furthermore their detection, as hyperpolarised hydride signals, implies kinetic activity since free *parahydrogen* derived protons must be incorporated into these molecules throughout these experiments.



**Scheme 38:** The interconversions of **13a**, **43a** and **69a**

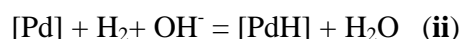
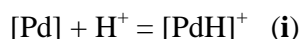
## Chapter four

There are in reality two possible pathways that could be envisaged to generate **13**. These are the protonation of (BCOPE)Pd(CO) or the addition of H<sub>2</sub> to **12a**. In the first route the hydride source would be the protic solvent and we might expect no hydride polarisation to result but more importantly without H<sub>2</sub> we see no reaction. Furthermore, in the control reaction where **12a** and hydrogen alone are employed, a palladium cluster is formed. The formations of such clusters are dependent on the metal concentration. Furthermore, when the reaction of **12a** with H<sub>2</sub> occurs in acidic solution, protonation proves to be much faster, as exemplified by the work by Miguel.<sup>146</sup> and the trimeric cluster **67** is formed. I have observed that when **12a** reacts with *parahydrogen* in a non-protic solution, where the reaction is slower, the cluster **68** is formed, as illustrated in Figure 135.

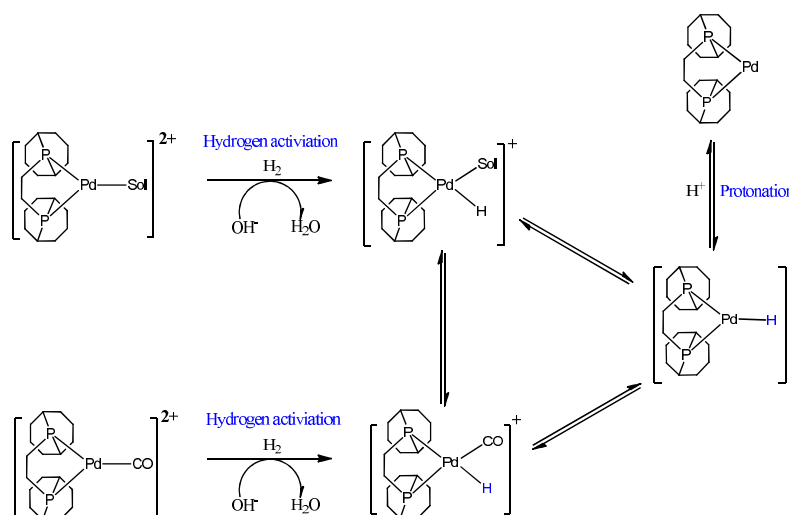


**Figure 135: The formation of palladium hydride clusters from complexes 13**

There are two possible pathways that describe how dihydrogen can be activated in this system. They are oxidative addition and heterolytic cleavage. Heterolytic cleavage can be promoted by adding a Brønsted base, such as Cl<sup>-</sup> to aid catalysis. Previous studies have suggested that the carbonylation reaction can be promoted by adding Cl<sup>-</sup>.<sup>113</sup> However, adding a large amount of Cl<sup>-</sup> actually prevents carbonylation. It has been suggested that Cl<sup>-</sup> serves as a base in these reactions. Water also promotes such a process according to my study. Upon comparing the results from H<sub>2</sub>O and D<sub>2</sub>O studies described here, confirmation that the hydride ligand come from hydrogen rather than water was obtained. Adding CH<sub>3</sub>OH to these solutions did not lead to an increase in the amount of **42a**.

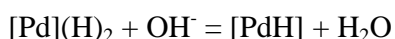
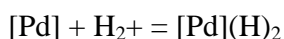






**Scheme 39: Possible pathways for the generation of active species 13 in 12a catalysed hydrogenation and hydrocarbonylation**

The detection of **70a**, a dihydrogen addition product, suggests that a neutral route is also possible. The formation of **70a** involves the hydrogen addition to a palladium (0) species  $(\kappa^2\text{-BCOPE})(\kappa^1\text{-BCOPE})\text{Pd}$ .  $\text{H}_2$  addition to  $(\eta^2\text{-BCOPE})\text{Pd}$  was not observed because while it would be expected to yield PHIP enhanced hydride signals none were detected. The addition product to  $(\kappa^2\text{-}^t\text{BuCOPE})\text{Pd}(\text{H})_2$  has been previously observed in these types of study.<sup>46</sup>



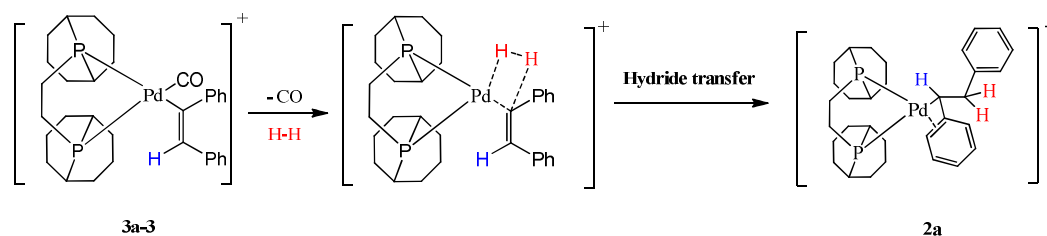
The detection of a palladium-stilbene complex **71a** and a palladium ester adduct, **72a** was also achieved. Palladium (0) bis-phosphine alkene complexes have been established to adopt a trigonal planar ligand arrangement.<sup>168,169</sup> In this case equivalent phosphines would result with *cis*-stilbene. In contrast palladium (II) bis-phosphine alkene complexes require a fourth ligand which in this case could be CO, methanol or OTf. Now the alkene binds so that the C-C bond lines out of the plane and consequently the two <sup>31</sup>P centres should be inequivalent. This situation is observed for **71a** and the formulation  $[(\text{BCOPE})\text{Pd}(\text{PhCH}=\text{CHPh})(\text{CO})](\text{OTf})_2$  is fully consistent with these data. In the case of **72a**,  $[(\text{BCOPE})\text{Pd}(\text{CD}_3\text{COCHPh}=\text{CHPh})(\text{CO})](\text{OTf})_2$  has been proposed. In this case, equivalent phosphines might be suggested because of the triplet character seen for the

## Chapter four

alkene proton resonance. The intensity of this signal precluded the location of a  $^{31}\text{P}$  signal. It should be noted however that if the P-P coupling is larger than the PH couplings a virtual coupling framework is created and hence even though they are inequivalent a triplet would be detected. It is also possible that the acyl group binds and  $[(\text{BCOPE})\text{Pd}(\text{CD}_3\text{COCPh}=\text{CHPh})](\text{OTf})_2$  results. Now the angle between the phosphorus centres would change, hence the PP coupling would alter and a virtual coupling might result. No virtual coupling was observed with **71a** suggestion  $J_{\text{PP}} < 13$  Hz. Such species however only account for at best ca. 5 % (according to the selectivity of hydrogen addition to **40a**, as described below) of the metal complexes in solution assuming equal PHIP enhancements.

The reaction of monohydride species **13a** with alkynes is well known, where a vinyl species is formed.<sup>143</sup> The vinyl species can be trapped as the methanol, pyridine adducts previously<sup>46</sup> and triflate salt. The chemistry of these vinyl species has been detailed in **Section 1.4.4.2**.

The formation of **41a** by hydrogen addition to **40a** shows considerable levels of reaction selectivity in methanol and an even higher level of selectivity in  $\text{CD}_2\text{Cl}_2$ . This deduction is based on the observation of an antiphase feature for the 'CH<sub>2</sub>' group of **41a** which is characteristic for PHIP dihydrogen addition products. For example, the 'CH<sub>2</sub>' group signal intensity proved to be 19 times higher than that of the 'CH' group. Therefore, the conversion of **40a** to **41a** must first follow a concerted pathway where the two hydrogen atoms come from a single molecule of H<sub>2</sub>. Secondly there are placed selectively into the 'PdC(Ph)= ' motif of **40a** as illustrated in Equation 16. This regio selectivity decreases on warming the sample because the PHIP enhancement levels for the three proton sites of **41a** become more equal.



### Equation 16: The selective hydrogen addition to 40a-3

This regio selectivity can be further proved by NOESY measurements. When the hydride signal at  $\delta -4.64$  due to  $[(\text{BCOPE})\text{PdH}(\text{CO})]^+$  (**13a-3**) was probed by NOESY at 308 K in

$\text{CD}_2\text{Cl}_2$ , magnetization transfer from this resonance into **41a** is observed, along with limited transfer into the CH site of **40a**. When the vinyl hydrogen of **41a** was probed in this way, only the magnetization transfer into the 'CH' group of **40a** rather than the 'CH<sub>2</sub>' group was observed. This confirms that H<sub>2</sub> addition to **41a** is followed by selective hydride transfer into the CH<sub>2</sub> site of **40a**.

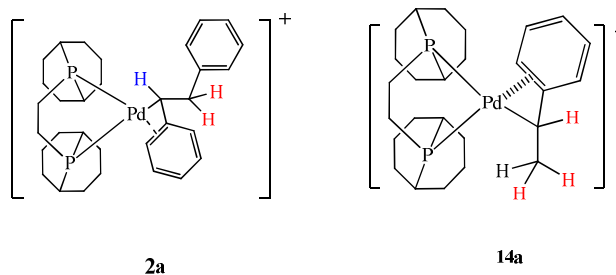


**Figure 136:** The structures of **40a** and **75a**, the colour labelling stands for the level of polarization. Blue: weak or moderate;

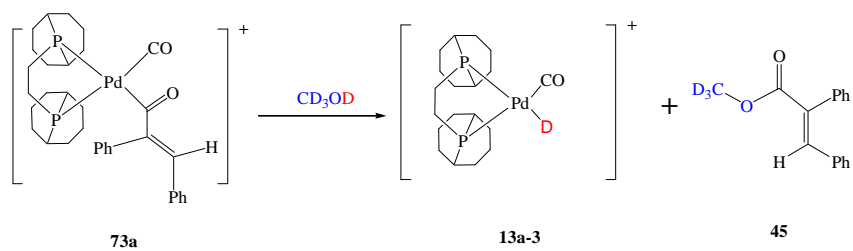
The selectivity could be caused by steric effects. Interestingly, when styrene was used as the substrate, the related complex **75a** was formed under normal conditions. In contrast, when **75a** was formed by adding H<sub>2</sub> to phenyl acetylene, no selectivity in the hydrogen transfer pathway was observed.

The  $\eta^3$  nature of the benzyl group in **41a** is well defined by the NMR characterization data. The styrene analogue **75a** shows similar structure. **41a** can convert to the thermally unfavoured  $\eta^1$  form **41a-3** when CO is present; full CO insertion into **41a** gives the acyl species **43a**. Both of these complexes have been detected through PHIP, albeit the signals are weak.

NOESY experiments also reveal that the conversion of **41a** to the hydrogenation products, *cis*- and *trans*-stilbene and the monohydride complex **13a-3** is possible. However, **75a** does not react with H<sub>2</sub> or CO at 323 K over 24 hours. These results are in accordance with the reported inert behaviour of alkenes.

The acyl complexes **73a** are formed by reversible CO insertion into **40a**. The alcoholysis of **73a** gives the carbonylation product **44** and the monodeuterium containing species **13a-3**. This explains why now the final product contains both <sup>1</sup>H and <sup>2</sup>D in the vinyl site.

## Chapter four



*Equation 17: Alcoholysis of 73a*

### 4.6.2 Overall mechanism of diphenyl acetylene carbonylation

The overall mechanism derived from these studies was presented earlier in **Section 4.1** in order aid the reader in appreciating these results.

**Chapter 5 NMR study on diphenyl acetylene hydrogenation using  
monophosphine supported palladium catalyst**

*5.1 Results*

*5.2 Synthesis and NMR characterization of Pd(PMePh<sub>2</sub>)<sub>2</sub>(OTf)<sub>2</sub> (**45**)*

*5.3 Control reactions*

*5.4 Study on Pd(PMePh<sub>2</sub>)<sub>2</sub>(OTf)<sub>2</sub> (**45**) catalyzed diphenyl acetylene hydrogenation*

*5.5 Discussion and Conclusion*

## Chapter five

### 5.1 Results

The NMR studies on the hydrogenation of diphenyl acetylene using  $\text{Pd}(\text{PMePh}_2)_2(\text{OTf})_2$  (**45**) will be presented in this chapter.

Now the control reactions reveal the formation of two monohydride species, **77** and **78**, when **45** reacts with hydrogen. These species are unstable and react further to form the dimeric complexes shown below via *ortho*-metalation. These products are characterized by NMR and MS methods.

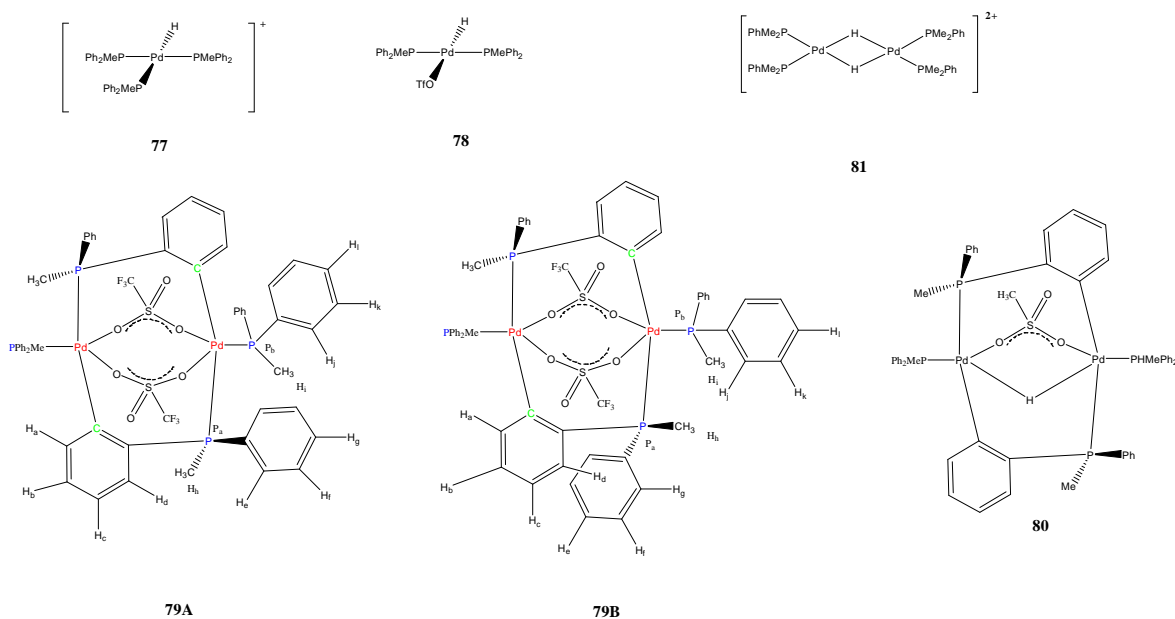


**Figure 137: Structures of the intermediates and products that are detected when **45** reacts hydrogen**

When **45** and diphenyl acetylene react with *para*hydrogen, the additional organometallic complexes, **82-84**, are detected by PHIP. The structures of these species are illustrated in Figure 138. They are different to these detected in the control reaction. Products related to **82-84** were also detected during the hydrogenation of diphenyl acetylene catalyzed by  $\text{Pd}(\text{PEt}_3)_2(\text{OTf})_2$ .<sup>45</sup>

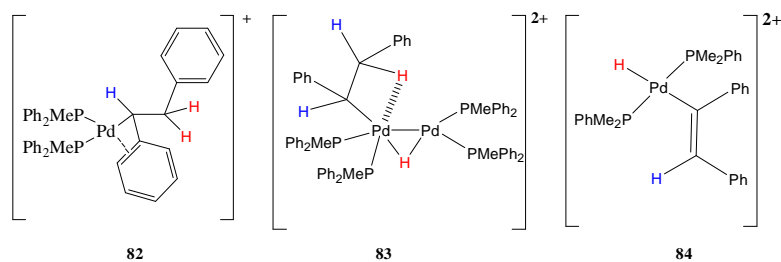


**Figure 138:** Additional organometallic products detected in **45** catalyzed diphenyl acetylene hydrogenation

## 5.2 Synthesis and NMR characterization of Pd(PMePh<sub>2</sub>)<sub>2</sub>(OTf)<sub>2</sub> (**45**)

Analytically pure Pd(MePPh<sub>2</sub>)<sub>2</sub>(OTf)<sub>2</sub> (**45**) was prepared by treating the corresponding chloride PdCl<sub>2</sub>(PMePh<sub>2</sub>)<sub>2</sub> (**76**) with silver triflate. **45** was recrystallized from methanol/hexane. The structure of **45** was confirmed by multinuclear NMR characterization and GC-MS. As shown in Figure 139, the corresponding <sup>31</sup>P NMR spectrum indicates that **45** is of sufficient purity for NMR study. Full NMR data for Pd(PMePh<sub>2</sub>)<sub>2</sub>(OTf)<sub>2</sub> (**45**) is summarized in Table 60.

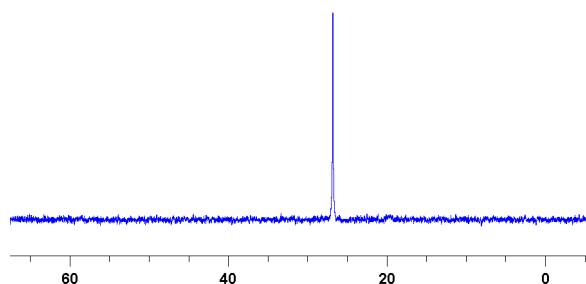


Figure 139: The  $^{31}\text{P}$  NMR spectrum of  $\text{Pd}(\text{PMePh}_2)_2(\text{OTf})_2$  (**45**) (298 K, in  $\text{CD}_2\text{Cl}_2$ )

Table 60: Multinuclear NMR data for **45** (298 K in  $\text{CD}_2\text{Cl}_2$ )

$  \begin{array}{c}  \text{PMePh}_2 \\    \\  \text{Ph}_2\text{MeP} - \text{Pd} - \text{OTf} \\    \\  \text{OTf}  \end{array}  $			
Group / nucleus	Chemical shift ( $\delta$ )	Multiplicity	Coupling constants (Hz)
<b><math>^1\text{H}</math></b>			
$\text{PCH}_3$	2.10 (6 H)	d, d	$J_{\text{PH}} = 12.4$ , $J_{\text{PH}} \sim 2.4$
<i>o</i> -H-Ph	7.53 (8 H)	quart	$J_{\text{HH}} = 7.7, 7.5$ , $J_{\text{PH}} = 7.6$
<i>m</i> -H-Ph	7.42 (8 H)	d, t	$J_{\text{HH}} = 7.7$ , $J_{\text{PH}} = 3.1$
<i>p</i> -H-Ph	7.59 (4 H)	t, d	$J_{\text{HH}} = 7.5$ , $J_{\text{PH}} = 1.3$
<b><math>^{31}\text{P}</math></b>			
$\text{PMePh}_2$	27.0	s	-
<b><math>^{13}\text{C}</math></b>			
$\text{PCH}_3$	13.1	d	$J_{\text{PC}} = 38.0$
<i>o</i> -C-Ph	132.6	overlap	-
<i>m</i> -C-Ph	129.4	d	$J_{\text{PC}} = 12.4$
<i>p</i> -C-Ph	132.8	overlap	-

## 5.3 Control reactions

### 5.3.1 Reaction of $\text{Pd}(\text{PMePh}_2)_2(\text{OTf})_2$ (**45**) with $\text{H}_2$

In order to follow the catalytic reaction of **45**, diphenyl acetylene and *p*-H<sub>2</sub>, two control reactions were undertaken. In the first of these, a dichloromethane-d<sub>2</sub> sample of **45** under 3



bar of *parahydrogen* was prepared and monitored by NMR spectroscopy at 298 K. The resulting  $^1\text{H}$  NMR spectrum revealed evidence for two hydride species, as illustrated in Figure 141. A 2D  $^1\text{H}$ - $^1\text{H}$  COSY experiment suggested that these signals did not couple with each other.

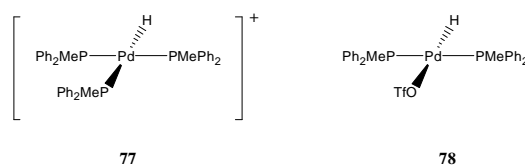


**Figure 140: Structures of  $[\text{PdH}(\text{PMe}_2\text{Ph})_3](\text{OTf})$  (77) and  $\text{PdH}(\text{PPh}_2\text{Me})_2(\text{OTf})$  (78)**

The first hydride resonance is centred at  $\delta$  -6.63. This signal couples with a  $^{31}\text{P}$  centre that is *trans* to it ( $J_{\text{PH}} = 188.0$  Hz) and two further  $^{31}\text{P}$  centres ( $J_{\text{PH}} = 9.3$  Hz) that are *cis*, to it as shown in Figure 141. The corresponding  $^{31}\text{P}$  centres were located at  $\delta$  1.0 and  $\delta$  10.4 respectively. This compound was specified to be  $[\text{PdH}(\text{PMe}_2\text{Ph})_3](\text{OTf})$  (77) by comparing its NMR properties with those of the known species  $[\text{PdH}(\text{PPh}_3)_3](\text{O}_2\text{CCF}_3)$  (hydride:  $\delta$  -7.0, d, t;  $J_{\text{PH}} = 174$  Hz, 13.5 Hz).<sup>167</sup> The structure of 77 is illustrated in Figure 140.

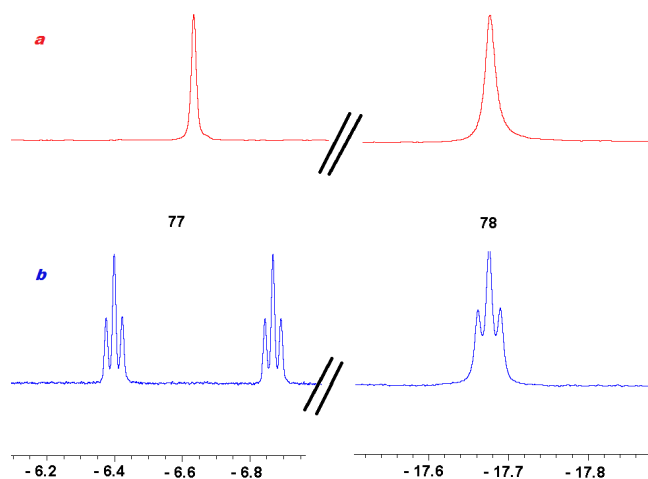


**Figure 141: Selective regions of (a):  $^1\text{H}\{^{31}\text{P}\}$  and (b):  $^1\text{H}$  NMR spectra that illustrate the formation of 77 and 78 when 45 reacts with hydrogen.**

A second, broad hydride signal was observed at  $\delta$  -17.80 at 298 K. This signal sharpened when a  $^1\text{H}\{^{31}\text{P}\}$  pulse sequence was used. When a  $^1\text{H}$  NMR spectrum was recorded at 248 K, this signal moved to  $\delta$  -17.67 and became triplet, with two  $^{31}\text{P}$  couplings of 5.7 Hz. This signal collapsed into singlet when  $^{31}\text{P}$  was selectively decoupled. Base on this information

## Chapter five

and its similarity with the known species  $\text{PdH}(\text{OTf})(\text{P}^t\text{Bu}_3)_2$  ( $\delta -17.2$ ,  $J_{\text{PH}} = 5.2$  Hz),<sup>170</sup> the new product is  $\text{PdH}(\text{OTf})(\text{PPh}_2\text{Me})_2$  (**78**). The structure of **78** is illustrated in Figure 140. **77** and **78** are in equilibrium in solution. The NMR data for **77** and **78** are summarized in Table 61 and Table 62 respectively. However, they are not stable and transform into other species in solution.

**Table 61: Selective NMR data for 77 (298 K in  $\text{CD}_2\text{Cl}_2$ )**

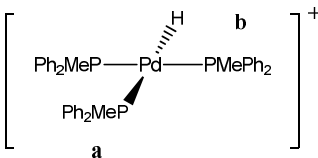
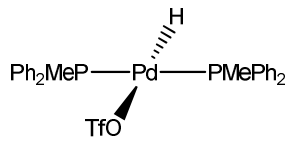
			
Group nucleus	Chemical shift ( $\delta$ )	Multiplicity	Coupling constants (Hz)
<b><math>^1\text{H}</math></b>			
Hydride	-6.67	d, t	$J_{\text{PH}} = 188.0, 8.5$
$\text{CH}_3\text{-P}_b$	1.71	T	$J_{\text{PH}} = 3.0$
$\text{CH}_3\text{-P}_a$	1.31	D	$J_{\text{PH}} = 7.7$
<i>o</i> - $\text{P}_a\text{Ph}$	7.41	-	
<i>p</i> - $\text{P}_a\text{Ph}$	7.42	-	
<i>o</i> - $\text{P}_b\text{Ph}$	7.15		$J_{\text{PH}} = 11.4, J_{\text{HH}} = 8.0$
<i>p</i> - $\text{P}_b\text{Ph}$	7.31		
<b><math>^{31}\text{P}</math></b>			
$\text{P}_a\text{MePh}_2$	0.83	d, d	$J_{\text{PH}} = 188.0, J_{\text{PP}} = 31.0$
$\text{P}_b\text{MePh}_2$	9.96	T	$J_{\text{PH}} = 9.3, J_{\text{PP}} = 9.3$

Table 62: Selective NMR data for 78 (248 K in CD<sub>2</sub>Cl<sub>2</sub>)

Group / nucleus	Chemical shift (δ)	Multiplicity	Coupling constants (Hz)
			
<b><sup>1</sup>H</b>			
hydride	-17.80 (298 K) -17.67	s, br t	-J <sub>PH</sub> = 5.7, virtual coupling
Me	2.11	t	J <sub>PH</sub> = 3.0, virtual coupling
<i>o</i> -PPh	7.66	-	
<i>p</i> -PPh	7.49	-	
<i>m</i> -PPh	7.56	-	
<b><sup>31</sup>P</b>			
PMePh <sub>2</sub>	11.09	d	J <sub>PH</sub> = 5.7

### Detection of catalyst decomposition products

When the reaction time is prolonged, a range of further products are detected. Most of these are formed by *ortho*-metalation (C-H activation) of a phenyl group of the phosphine ligand. The structures of the two main products are illustrated in Scheme 40. These are stereo isomers that differ according to orientation of the phosphines Me and Ph substituent.

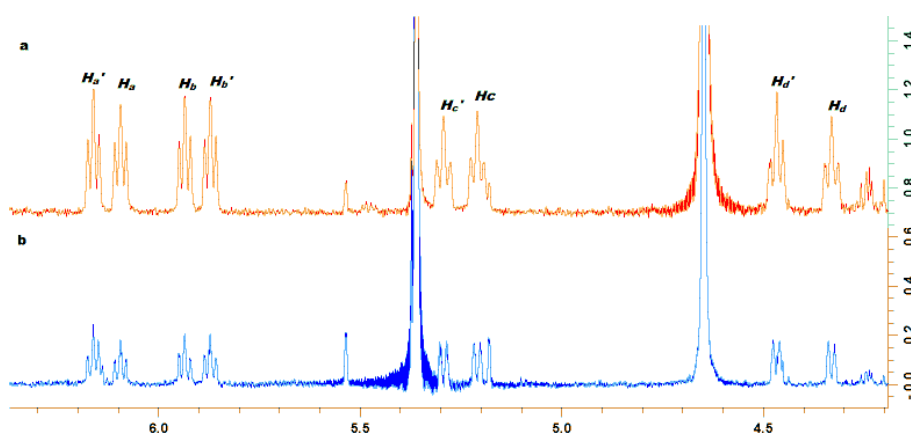
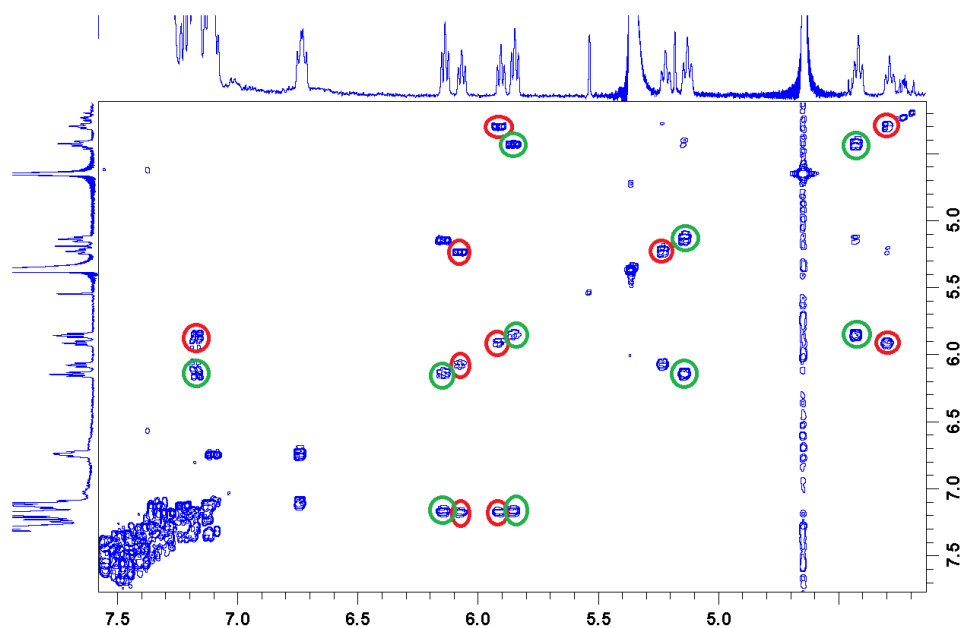


Figure 142: Selected regions of the NMR spectra used to indicate the formation of 79. (a): <sup>1</sup>H and (b) <sup>1</sup>H{<sup>31</sup>P}

## Chapter five

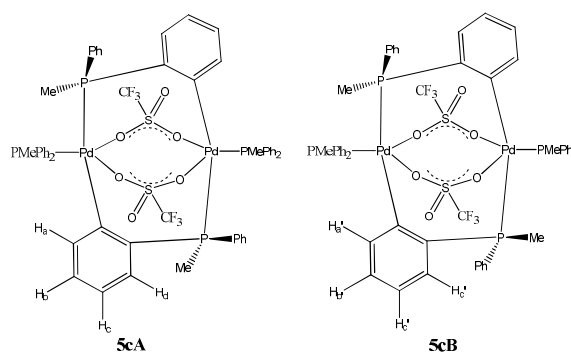
In the organic region of the corresponding  $^1\text{H}$  NMR spectrum, one set of signals is seen at  $\delta$  4.33 (t,  $J_{\text{HH}} = 7.60$  Hz), 5.21 (t,  $J_{\text{HH}} = 7.60$  Hz), 5.93 (t,  $J_{\text{HH}} = 6.9$  Hz), and 6.09 (t,  $J_{\text{HH}} = 6.9$  Hz) due to **5cA** which are correlated according to 2D  $^1\text{H}$ - $^1\text{H}$  COSY experiments. The signals at  $\delta$  4.33 and  $\delta$  5.21 show substantial  $^{31}\text{P}$  couplings of 8.01 Hz and 7.81 Hz respectively, whereas the  $^{31}\text{P}$  couplings for the signals at  $\delta$  5.93 and  $\delta$  6.09 lie within the line width. The  $^1\text{H}$  NMR signals at  $\delta$  4.33 and  $\delta$  5.21 arise from *o*, and *p*-hydrogen of the activated phenyl group. The  $^1\text{H}$  NMR signals at  $\delta$  5.93 and  $\delta$  6.09 couple with a further  $^1\text{H}$  signal at  $\delta$  7.17, which is assigned as the *m*-hydrogen of the other  $\text{PMePh}_2$  ligand (no coupling to  $^{31}\text{P}$ ).

The corresponding  $^{31}\text{P}$  NMR signal for the activated phosphine ligand was detected at 27.32 according to the 2D  $^1\text{H}$ - $^{31}\text{P}$  HMQC experiments. This  $^{31}\text{P}$  NMR signal exhibits virtual coupling. The resonance due to the methyl group, and the *o*, and *p*-hydrogens of the remaining phosphine were located at  $\delta$  1.86, (d,  $J_{\text{PH}} = 9.16$  Hz),  $\delta$  7.54, (d,  $J_{\text{PH}} = 12.70$  Hz) and  $\delta$  7.45, (t,  $J_{\text{PH}} = 10.50$  Hz) in the 2D  $^1\text{H}$ - $^{31}\text{P}$  HMQC experiments.



**Figure 143:** 2D  $^1\text{H}$ - $^1\text{H}$  COSY dataset that connects the  $^1\text{H}$  NMR signals for **79A** and **79B**

NOe experiments also connected the  $^1\text{H}$  NMR signals at  $\delta$  4.33 and  $\delta$  1.86 (Me) of the activated phosphine ligand to three other  $^1\text{H}$  NMR signals at  $\delta$  7.16,  $\delta$  7.31 and  $\delta$  7.42 due to a second phosphine ligand. The corresponding 2D  $^1\text{H}$ - $^{31}\text{P}$  HMQC experiments located the  $^{31}\text{P}$  NMR signal at  $\delta$  -7.60 and a  $^1\text{H}$  signal at  $\delta$  2.13 due to the methyl group. The  $^{31}\text{P}$  NMR signal again exhibits virtual coupling.



**Scheme 40:** Structures of **79A** and **79B**, the dominant C-H activation products

The second isomer of **79B** was characterized likewise by NMR methods. Mass spectroscopy experiments confirm that **5c** contains two palladium atoms and two triflate ligands.

The structures of **79A** and **79B** are further supported by the fact that when the reaction is repeated with Pd(PPh<sub>3</sub>)<sub>2</sub>(OTf)<sub>2</sub> only one analogous product is detected. The structures of **79A** and **79B** are illustrated in Scheme 50, and their NMR data is summarized in Table 63.

**Table 63:** Multinuclear NMR data of **79A** and **79B**

	Chemical shift ( $\delta$ ) and multiplicity	Coupling constants	Chemical shift ( $\delta$ ) and multiplicity	Coupling constants
<b><sup>1</sup>H</b>				
H <sub>a</sub>	6.09	J <sub>HH</sub> = 7.00	6.16 (d)	J <sub>HH</sub> = 7.00
H <sub>b</sub>	5.21 (t)	J <sub>HH</sub> = 7.80 J <sub>PH</sub> = 7.81	5.13 (t)	J <sub>HH</sub> = 8.01 J <sub>PH</sub> = 8.05

*Chapter five*

H <sub>c</sub>	5.93 (t)	J <sub>HH</sub> = 7.04	5.87 (t)	J <sub>HH</sub> = 6.92
H <sub>d</sub>	4.33 (t)	J <sub>HH</sub> = 7.40 J <sub>PH</sub> = 8.01	4.46 (t)	J <sub>HH</sub> = 8.10 J <sub>PH</sub> = 8.41
H <sub>e</sub>	7.45 (t)	J <sub>HH</sub> = 10.50	7.41 (m, overlapped)	-
H <sub>f</sub>	7.17	J <sub>HH</sub> = 12.70	7.18	J <sub>HH</sub> = 12.70
H <sub>g</sub>	7.54 (d)	J <sub>HH</sub> = 12.70, 10.50	7.42 (m, overlapped)	-
H <sub>h</sub>	1.86 (d)	J <sub>PH</sub> = 8.94	1.83 (d)	J <sub>PH</sub> = 8.94
H <sub>i</sub>	2.13 (d, overlapped)	-	2.16 (d, overlapped)	-
H <sub>j</sub>	7.16 (overlapped)	-	7.34 (overlapped)	-
H <sub>k</sub>	7.31	-	7.43	-
H <sub>l</sub>	7.42	-	7.68	-
<b><sup>31</sup>P</b>				
P <sub>a</sub>	27.01 (d, t) 2 <sup>nd</sup> order		26.20 (d, t) 2 <sup>nd</sup> order	
P <sub>b</sub>	-7.64		-7.60	
<b><sup>13</sup>C</b>				
C <sub>a</sub>	116.53 (m)	-	113.37 (t, m)	J <sub>PC</sub> = 9.83
C <sub>b</sub>	116.98 (quart)	J <sub>PC</sub> = 15.66, 11.48	101.54 (t, m)	J <sub>PC</sub> = 11.41
C <sub>c</sub>	114.2 (quart)	J <sub>PC</sub> = 14.85, 10.79	117.45 (t, m)	J <sub>PC</sub> = 7.42
C <sub>d</sub>	103.60 (quart)	J <sub>PC</sub> = 18.96, 11.51	108.99 (quart)	J <sub>PC</sub> = 12.79, 12.71
C <sub>e</sub>	128.97-129.88		128.97-129.88	
C <sub>f</sub>				
C <sub>g</sub>	132.66	J <sub>PC</sub> = 10.50		
C <sub>h</sub>	9.47 (d)	J <sub>PC</sub> = 35.81	8.86 (d)	J <sub>PC</sub> = 34.82
C <sub>i</sub>	14.74 (d)	J <sub>PC</sub> = 27.52	14.86 (d)	J <sub>PC</sub> = 28.50
C <sub>j</sub>				
C <sub>k</sub>	129.25	-	129.33	-
C <sub>l</sub>	128.97-129.88		130.44 (quart)	J <sub>PC</sub> = 22.96, 7.83

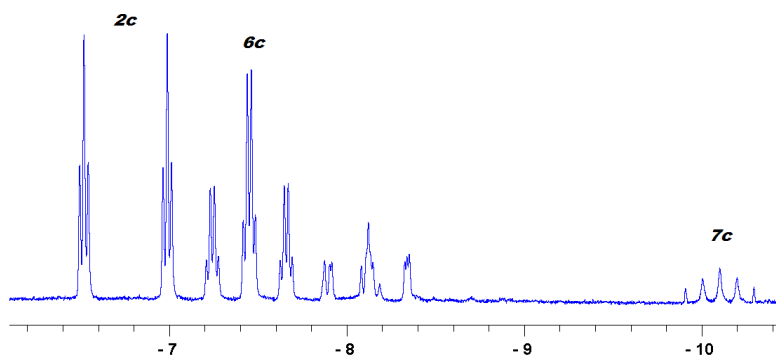


**Figure 144:** Region of the  $^1\text{H}$  NMR spectrum showing the formation of several hydride contained species when **45** reacts with parahydrogen

**79** contains no hydride ligand but when a  $^1\text{H}$  NMR spectrum is recorded at this stage, several species that contains bridged hydride ligands are also detected. None of these signals couple with each other and therefore they must arise from different monohydride species.

One of them, **80**, contains a bridged hydride that resonates at  $\delta$  -7.38 (t, quart,  $J_{\text{PH}} = 82.8$  Hz, 9.0 Hz). This suggests that the hydride couples with two  $^{31}\text{P}$  centres though a *transoid* coupling and three  $^{31}\text{P}$  centres through *cisoid* coupling. There are two equivalent  $^{31}\text{P}$  centres that provide the *trans* coupling which resonate at  $\delta$  5.47. Two distinct  $^{31}\text{P}$  centres are  $\delta$  -3.68 and  $\delta$  -6.37 for the *cis* coupling. Consequently there are two equivalent  $^{31}\text{P}$  centres, and one unique  $^{31}\text{P}$  centre which provide these couplings. All of these  $^{31}\text{P}$  NMR signals are highly phosphorus-phosphorus coupled multiplets. Furthermore, **80** does not contain an ortho metallated phosphine according to the 2D  $^1\text{H}$ - $^{31}\text{P}$  HMQC dataset. A possible structure for this complex illustrated in Figure 145. This information and the rest of the NMR data for **80** are summarized in Table 64.

Another hydride at  $\delta$  -8.06 due to new products shows similar *trans* couplings but a different number of *cis* couplings. They could be  $\text{PPh}_3/\text{OTf}^-$  exchange products. However, these products are not specified due to the low intensity and obscure coupling pattern.

## Chapter five

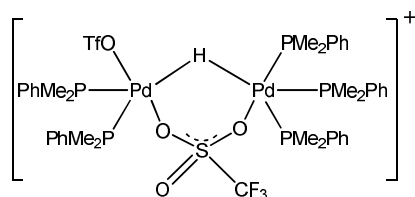


Figure 145: Possible structure for **80**

The hydride signal at  $\delta$  -10.02 is short lived. It appears as a quintet with  $J_{\text{PH}}$  of 39.3 Hz at 298 K. However, when the sample was cooled to 248 K, this signal is a complex triplets, which appears to possess 2<sup>nd</sup> order character. It must arise from a dynamic complex (**81**). The possible structure for **8c** is illustrated in Figure 147.

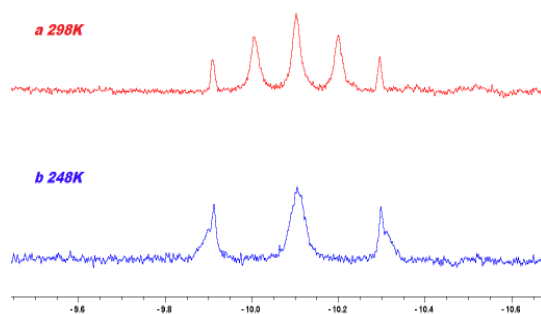


Figure 146: The <sup>1</sup>H NMR spectra at 248 K and 298 K suggested the dynamic behaviour for **81**

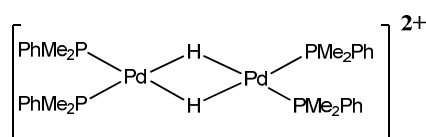


Figure 147: The structure of **81**



Table 64: NMR data for 78 (298 K in CD<sub>2</sub>Cl<sub>2</sub>)

Group / nucleus	Chemical shift ( $\delta$ )	Multiplicity	Coupling constants (Hz)
<b><sup>1</sup>H</b>			
hydride	-7.38 (1H)	t, quart	J <sub>PH</sub> = 82.8, 9.0
Me-C	1.67	d	J <sub>PH</sub> = 7.83
Me-B	1.03		
Me-A	1.01		
<i>o</i> -H	6.69 (3H)	d, d	J <sub>HH</sub> = 7.7, J <sub>PH</sub> = 11.5, 7.7, 1.0
<i>m</i> -H	7.09 (overlap)	t	J <sub>HH</sub> = 7.7, 8.0
<i>p</i> -H	7.34 (overlap)		
<b><sup>31</sup>P</b>			
<i>Trans</i> -C	5.49	m	J <sub>PH</sub> = 82.8,
<i>Cis</i> -A	-3.68	doublet	J <sub>PP</sub> = 50, 27.8, J <sub>PH</sub> = 9.0
<i>Cis</i> -B	-6.37	doublet	J <sub>PP</sub> = 50, 28.1, J <sub>PH</sub> = 9.0

Table 65: NMR data for 79 (in CD<sub>2</sub>Cl<sub>2</sub>)

Group / nucleus	Chemical shift ( $\delta$ )	Multiplicity	Coupling constants (Hz)
<b><sup>1</sup>H</b>			
hydride	-10.10 (298 K) -10.02 (248 K)	quint (298 K) d, d, d (248K)	J <sub>PH</sub> = 39.3 Hz 2 <sup>nd</sup> order, 2 <sup>nd</sup> order

### 5.3.2 Reaction of 45 and diphenyl acetylene

## Chapter five

When a sample of **45** and diphenyl acetylene in methanol- $d_4$  was examined between 298 K and 333 K, no reaction was observed and the  $^{31}\text{P}$  signal of **45** remained visible at  $\delta$  27.0 throughout the study.

### 5.4 Study on $\text{Pd}(\text{PMePh}_2)_2(\text{OTf})_2$ (**45**) catalyzed diphenyl acetylene hydrogenation

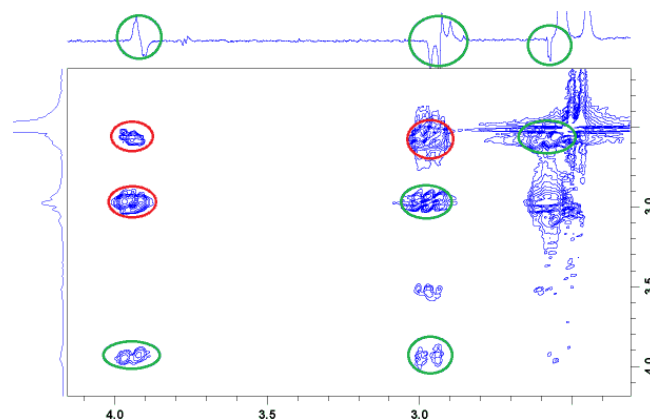
#### 5.4.1 NMR studies

##### 5.4.1.1 Detection of $[\text{Pd}(\text{PMePh}_2)_2(\text{CHPh-CH}_2\text{Ph})](\text{OTf})$ (**82**)

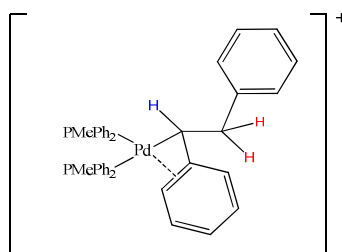
When a sample of  $\text{Pd}(\text{PMePh}_2)_2(\text{OTf})_2$  (**45**) and diphenyl acetylene that was dissolved in dichloromethane- $d_2$  under 3 atm. of *parahydrogen* was monitored by NMR spectroscopy at 298 K, no polarized signal was observed. However, when the sample was warmed to 308 K, a new set of polarized signals were detected at  $\delta$  2.95 and  $\delta$  2.57. Meanwhile, polarized signals for *cis* and *trans*-stilbene were also visible at  $\delta$  6.61 and  $\delta$  7.18 respectively.

The  $^1\text{H}$  NMR signals at  $\delta$  2.95 and  $\delta$  2.57 coupled with each other and both simplified into doublet of doublets. They share a common coupling of 3.70 Hz. The properties of these two signals are very similar with the known alkyl species that contain BCOPE or  $\text{PEt}_3$  ligands.<sup>45</sup> However, the third signal for this alkyl group was not visible until the sample was warmed to 313 K. When a 2D  $^1\text{H}$ - $^1\text{H}$  COSY experiment was undertaken at 313 K, a  $^1\text{H}$  NMR signal at  $\delta$  3.90 was correlated to  $^1\text{H}$  NMR signals at  $\delta$  2.95 and  $\delta$  2.57. This suggests high selectivity for hydrogen addition to place two protons in the 'CH<sub>2</sub>Ph' motif in **82** at 308 K. We also note that the signal at  $\delta$  2.57 overlaps with the signals of the phosphine. The correlations between these three signals were however clearly illustrated if an OPSY-COSY NMR spectrum was recorded. Figure 148 presents the 2D  $^1\text{H}$ - $^1\text{H}$  OPSY-COSY NMR spectrum, where all the thermal  $^1\text{H}$  NMR signals in this region are completely suppressed.

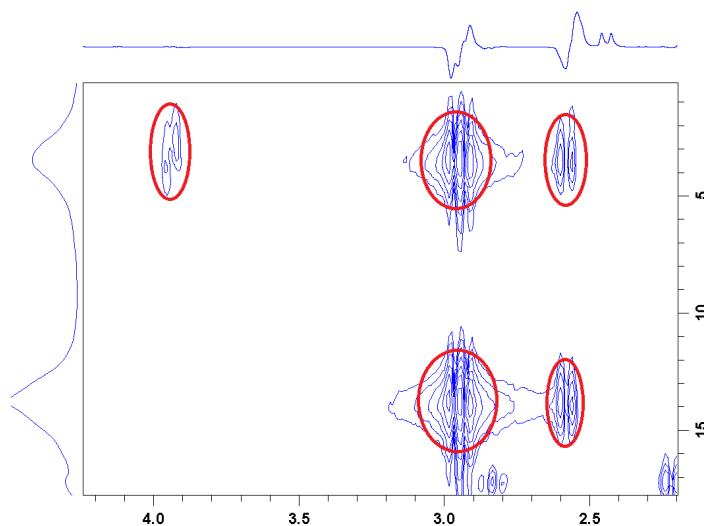
When a 2D  $^1\text{H}$ - $^{31}\text{P}$  HMQC experiment was recorded, the correlation of these  $^1\text{H}$  NMR signals and two  $^{31}\text{P}$  centres that resonated at  $\delta$  2.4 and  $\delta$  14.3 was observed. Figure 150 illustrates part of the  $^1\text{H}$ - $^{31}\text{P}$  HMQC dataset. When mono-labelled  $\text{Ph}^{13}\text{CCPh}$  was used as the substrate, the corresponding  $^1\text{H}$ - $^{13}\text{C}$  HMQC experiment correlates the  $^1\text{H}$  NMR signals at  $\delta$  2.57 and  $\delta$  2.95 to a  $^{13}\text{C}$  centre at  $\delta$  35.05, whereas the  $^1\text{H}$  NMR signal at  $\delta$  3.90 to another  $^{13}\text{C}$  centre at  $\delta$  73.41, which further confirms the structure of **82**. The structure of  $[\text{Pd}(\text{PMePh}_2)_2(\text{CHPh-CH}_2\text{Ph})](\text{OTf})$  (**82**), is shown in Figure 149. NMR data for **82** is summarized in Table 66.



**Figure 148:** Expansion of the 2D  $^1\text{H}$ - $^1\text{H}$  OPSY-COSY NMR spectrum that links the polarized signals at  $\delta$  2.95,  $\delta$  2.57 and  $\delta$  3.90, with internal  $^1\text{D}$  OPSY spectra and external  $^1\text{D}$   $\pi/4$   $^1\text{H}$  NMR spectrum as horizontal and vertical projections respectively.

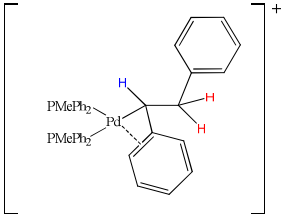


**Figure 149:** Structure of  $[\text{Pd}(\text{PMePh}_2)_2(\text{CHPh-CH}_2\text{Ph})](\text{OTf})$  (82)



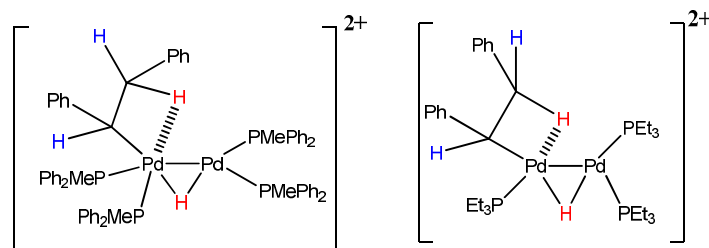
**Figure 150:** The 2D  $^1\text{H}$ - $^{31}\text{P}$  HMQC dataset that correlates the  $^1\text{H}$  NMR signals at  $\delta$  2.95,  $\delta$  2.57 and  $\delta$  3.90 to two  $^{31}\text{P}$  centres at  $\delta$  2.4 and  $\delta$  14.3

Table 66: Multinuclear NMR data for **82** (308 K in CD<sub>3</sub>OD)

			
Group / nucleus	Chemical shift (δ)	Multiplicity	Coupling constants (Hz)
<b><sup>1</sup>H</b>			
CH <sub>2</sub> Ph	2.95 (1H)	m, using (Ph- <sup>13</sup> CCPh)	J <sub>HH</sub> = 14.7, J <sub>HH</sub> = 11.7, J <sub>PH</sub> ~ 2.7 J <sub>CH</sub> = 124.4
CH <sub>2</sub> Ph	2.57 (1H)	m using (Ph- <sup>13</sup> CCPh)	J <sub>HH</sub> = 14.7, J <sub>HH</sub> = 3.7, J <sub>PH</sub> ~ 3.0 J <sub>CH</sub> = 128.1
CHPh	3.90 (1H)	d, d, d	J <sub>HH</sub> = 11.7, 3.7, J <sub>PH</sub> = 8.3
<b><sup>31</sup>P</b>			
PMePh <sub>2</sub> ( <i>cis</i> to alkyl)	2.4	-	
PMePh <sub>2</sub> ( <i>trans</i> to alkyl)	14.3	-	
<b><sup>13</sup>C</b>			
CH <sub>2</sub>	34.9	d, d	J <sub>PC</sub> = 20.5, 7.5
CH	73.4	d, d	J <sub>PC</sub> = 34.3, 25.4

#### 5.4.1.2 Detection of compound **83**

The polarization on **83** lasts for 15 min at 308 K, which aiding in its full characterization. However, when a concentrated sample that contains 20 mg catalyst and 20 mg diphenyl acetylene was monitored at 315 K, two short lived intermediates were detected by observing two polarized hydride signals at δ -7.34 and δ -10.04. These are different to those seen in the reaction of **45** and hydrogen.



**Figure 151:** Structure of new product **83** that is detected in the  $\text{Pd}(\text{PMePh}_2)_2(\text{OTf})_2$  catalysed hydrogenation of diphenyl acetylene and its known  $\text{PEt}_3$  analogue.

The hydride signal at  $\delta$  -7.34 coupled with two equivalent  $^{31}\text{P}$  centres through a 81.2 Hz and two further  $^{31}\text{P}$  centres through 13.4 Hz respectively, As shown in Figure 152. The latter  $^{31}\text{P}$  centre was located  $\delta$  17.2 according to the corresponding 2D  $^1\text{H}$ - $^{31}\text{P}$  HMQC experiments. In addition, the hydride signal also coupled with another proton signal though a coupling of 4.4 Hz. The antiphase character suggests that these two protons must from the same *parahydrogen* molecule.

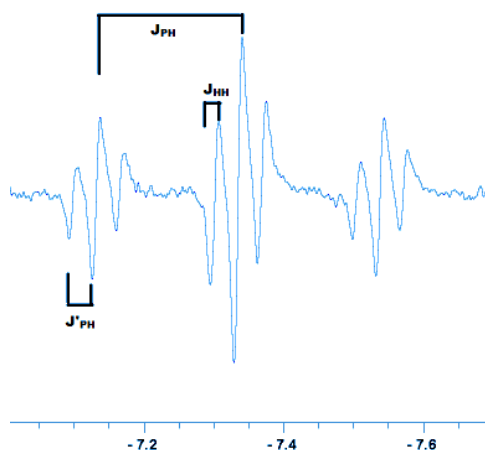


**Figure 152:** Region of the  $^1\text{H}$  NMR spectrum and the coupling assignment for hydride resonance at  $\delta$  -7.34 due to **83**

When 2D  $^1\text{H}$ - $^1\text{H}$  COSY pulse sequence was used, the hydride signal at  $\delta$  -7.34 was correlated to a  $^1\text{H}$  NMR signal at  $\delta$  2.84. This signal at  $\delta$  2.84 has both *in*-phase and *anti*-phase components, which is in constant with the hydride signal at  $\delta$  -7.34. This confirms their *parahydrogen* origin. In addition, the signal at  $\delta$  2.84 couples with two polarized signals at  $\delta$  2.23 and  $\delta$  3.62 according to the 2D  $^1\text{H}$ - $^1\text{H}$  COSY experiment, as shown in Figure 153. They therefore arise from another alkyl species. According to the 2D  $^1\text{H}$ - $^{31}\text{P}$

## Chapter five

HMQC experiment, both of the signals at  $\delta$  2.84 and  $\delta$  -7.34 coupled with a  $^{31}\text{P}$  centre that resonates at  $\delta$  17.2.

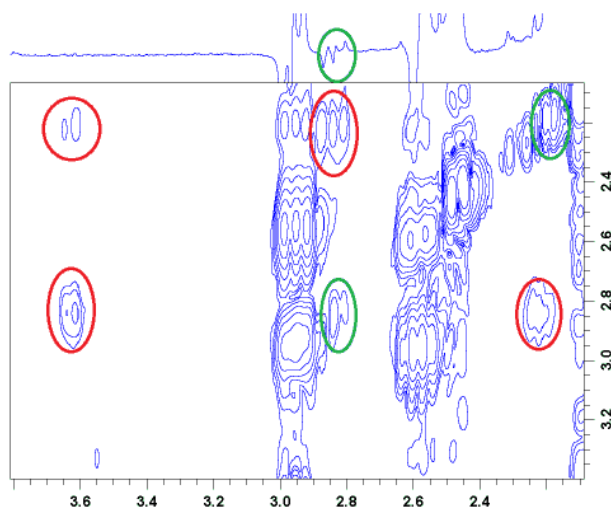
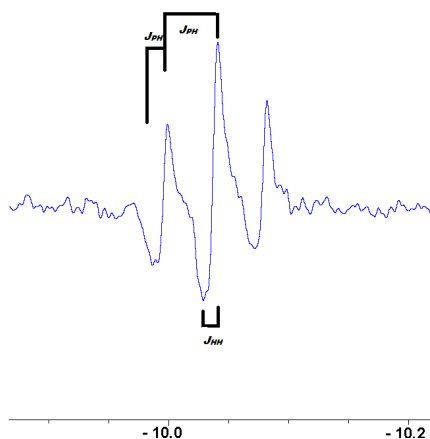


**Figure 153:** Expansion of the 2D  $^1\text{H}$ - $^1\text{H}$  COSY dataset showing the correlation between the  $^1\text{H}$  NMR signals at  $\delta$  2.23,  $\delta$  2.84 and  $\delta$  3.62

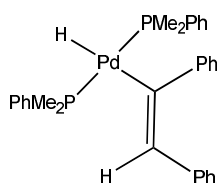
This compound is proposed to be **83**, as illustrated in Figure 151. The low intensity and the short life time prohibit further NMR characterization.

### 5.4.1.3 Detection of compound 84

A further triplet of doublet hydride signal was detected at  $\delta$  -10.1. It coupled with two equivalent  $^{31}\text{P}$  centres though a coupling of 16.8 Hz and a further proton centre though a coupling 3.8 Hz. Figure 154 illustrates the  $^1\text{H}$  NMR spectrum for this signal. When 2D  $^1\text{H}$ - $^1\text{H}$  COSY experiment was undertaken, the hydride resonance at  $\delta$  -10.1 was correlated to a  $^1\text{H}$  NMR signal at  $\delta$  5.57, which slightly sharpen on  $^{31}\text{P}$  decoupling. Both of these two signals at  $\delta$  -10.10 and  $\delta$  5.57 coupled with a  $^{31}\text{P}$  NMR signal at  $\delta$  8.50, according to corresponding  $^1\text{H}$ - $^{31}\text{P}$  HMQC dataset. Therefore the  $^1\text{H}$  NMR signal at  $\delta$  -10.1 and  $\delta$  5.57 are indirectly linked.



**Figure 154:** Region of the  $^1\text{H}$  NMR spectrum and coupling assignment for hydride resonance at  $\delta$  -10.10 due to **84**

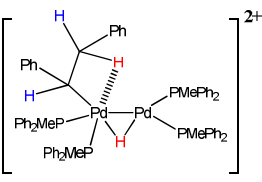


**Figure 155:** Structure of **84**

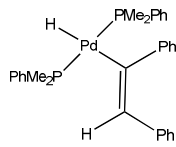
The NMR properties of the signal at  $\delta$  -10.1 are very similar with known palladium vinyl hydride species according to previous study on  $\text{Pd}(\text{PEt}_3)_2(\text{OTf})_2$  catalysed diphenyl acetylene hydrogenation.<sup>45</sup> Therefore the new product is proposed to be  $\text{Pd}(\text{H})(\text{CPh}=\text{CHPh})(\text{PMePh}_2)_2$  (**84**). The structure of **84** is illustrated in Figure 155.

## Chapter five

**Table 67: Multinuclear NMR data for 83 (315 K in CD<sub>2</sub>Cl<sub>2</sub>)**

			
Group / nucleus	Chemical shift (δ)	Multiplicity	Coupling constants (Hz)
<b><sup>1</sup>H</b>			
Hydride	-7.34	t, t, d	J <sub>PH</sub> = 81.2, 13.4, J <sub>HH</sub> = 13.5
	2.20	overlap	J <sub>HH</sub> = 11.7, 17.9
	2.84	d, d, d	J <sub>HH</sub> = 17.9, 4.0, J <sub>PH</sub> ~ 10
	3.62	d, d, t	J <sub>HH</sub> = 11.7, 4.0, J <sub>PH</sub> ~ 2.0
<b><sup>31</sup>P</b>			
PMePh <sub>2</sub> on Pd(II)	17.2	m	J <sub>PH</sub> = 13.4
<b><sup>13</sup>C</b>			
CH <sub>2</sub>	36.54	m	-

**Table 68: Selected multinuclear NMR data for 84 (313 K in CD<sub>2</sub>Cl<sub>2</sub>)**

			
Group / nucleus	Chemical shift (δ)	Multiplicity	Coupling constants (Hz)
<b><sup>1</sup>H</b>			
Hydride	-10.1	t, d	J <sub>PH</sub> = 16.8, J <sub>HH</sub> = 3.8
	5.51	d	J <sub>HH</sub> = 3.8
<b><sup>31</sup>P</b>			
PMePh <sub>2</sub> on Pd(II)	8.50	d	J <sub>PH</sub> = 16.8

### 5.4.2 ESI-MS investigation

A range of ESI-MS measurements were carried out upon this reaction, using identical reaction conditions to that are used in the NMR investigation with necessary dilution (required for ESI-MS measurements). It revealed the presence of [Pd(Ph-C=CH-



$\text{Ph}(\text{PMePh}_2)_2]^+$  and  $[\text{PdH}(\text{PMePh}_2)_3]^+$  by the observation of signals at  $M/Z^+$  686.9 and 709.0.

## 5.5 Discussion and Conclusion

$\text{Pd}(\text{PMePh}_2)_2(\text{OTf})_2$  (**45**) catalyses diphenyl acetylene hydrogenation into *cis*, *trans*-stilbene and diphenyl ethane. During this reaction, three intermediates, **82-84**, are detected. The structures of **82-84** are illustrated in Figure 156.

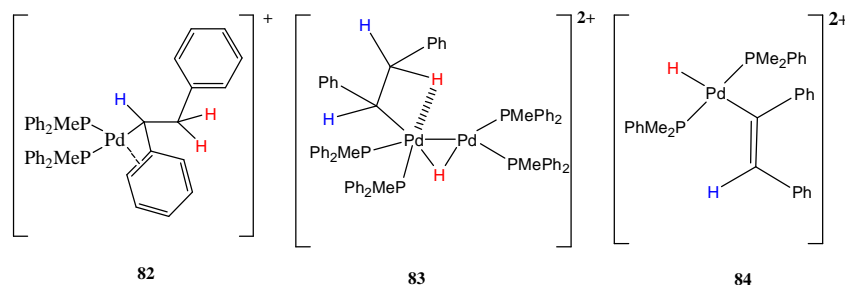


**Figure 156: Summary of structures of 82-84**

The detection of **82** suggests monohydride (i. e. cationic) mechanism. The formation of **82** shows high level of selectivity on hydrogen addition into the 'CH<sub>2</sub>Ph' motif. It can be concluded that at lower temperature (308 K), the monohydride/cationic mechanism dominates. This is in accordance with catalysts that contain bisphosphines. The dimeric alkyl complex, **83**, is detected when a concentrated sample and higher reaction temperature are applied. At this time, another neutral complex **84** is detected. The detection of **84** supports the neutral mechanism, which only happens at higher temperature.

## **Chapter 6 Experimental**

*6.1 General Conditions*

*6.2 Synthesis for **Chapter 2***

*6.3 Synthesis for **Chapter 3***

*6.4 Synthesis for **Chapter 4 and 5***

## 6.1 General Conditions

### 6.1.1 General Conditions

All manipulations undertaken for my thesis were carried out under inert atmosphere conditions, using standard Schlenk techniques (with vacuum of up to  $10^{-2}$  mbar, with  $N_2$  or Ar as an inert atmosphere) or high vacuum techniques ( $10^{-4}$  mbar). Dry  $N_2$  and Ar were purchased from BOC Gases. Storage and manipulation of samples was carried out using standard glovebox techniques under an atmosphere of  $N_2$ , using an Alvic Scientific Gas Shield glovebox equipped with a freezer ( $-32$  °C), vacuum pump, and  $N_2$  purge facilities.

**Solvents:** Solvents were obtained as analytical grade from Fisher. They were purified according to the standard procedures. Diethyl ether, THF, hexane, dioxane and toluene were dried by refluxing over sodium wire under nitrogen, while dichloromethane and methanol were dried over calcium hydride. Acetone was dried over  $CaSO_4$  and distilled. All of the solvents were stored under vacuum in ampoule.

**Deuterated solvents:** The deuterated solvents, methanol- $d_4$ ,  $CD_2Cl_2$ - $d_2$ , toluene- $d_8$ , tetrachloroethane- $d_2$  and acetonitrile- $d_3$  were purchased from Aldrich and purified according to standard procedures. All of the solvents are stored under vacuum in ampoule.

**NMR instrument:** NMR spectra were obtained on Bruker Avance 400 and Avance 700 spectrometers. The Bruker Avance 400 spectrometer was connected to a liquid nitrogen dewar through a tube and evaporator.

## 6.2 Synthesis for chapter 2

Iridium trichloride trihydrate was bought from Precious Metal Online and used as received. Other reagents used in this section were purchased from Aldrich and used as received.

$[Ir(COD)Cl]_2$ ,  $[IrBr_2(CO)_2][TBA]$ ,  $[IrCl_2(CO)_2][TBA]$ ,  $IrBr(CO)(PPhMe_2)_2$ ,  $IrBr(CO)(PMe_3)_2$ ,  $IrCl(CO)(PPh_3)_2$ ,  $IrCl(CO)[P(p-tol)_3]_2$ , and  $IrCl(CO)(PPh_2Me)_2$  were prepared using reported methods.<sup>171,172 173 174 175</sup> The NMR spectra for these products matched with those taken from the literature. The target material, **12a-12e**, were synthesized by Grignard reaction from Vaska's type complexes.<sup>75</sup>

### 6.2.1 Synthesis of $IrCl(CO)(PMe_3)_2$ (**12a**)

In view of the complexity in preparing this material full details are provided.

## Chapter six

**a):** 500 mg of  $[\text{IrCl}(\text{COD})]_2$  (0.75 mmol) was suspended in 500  $\text{cm}^3$  of hexane in a one-litre round bottom flask that was equipped with nitrogen inlet and the condenser. A hexane solution of  $\text{PMe}_3$  (0.228 g/3 mmol in 20 ml hexane) was added drop wise to the suspension within 2 hours. The solution was stirred for 15 mins under nitrogen. The reaction mixture was filtered. The filtrate contains  $\text{IrCl}(\text{CO})(\text{PMe}_3)_2$ .

**b):** CO was introduced to the pale yellow solution after removing the  $\text{N}_2$ . The white precipitation formed during this progress was collected by filtration, which is known as  $\text{IrCl}(\text{CO})_2(\text{PMe}_3)_2$ .

**c):**  $\text{IrCl}(\text{CO})_2(\text{PMe}_3)_2$  was placed in a ampule, which is connected to the high vacuum line. The sample was pumped for 2-6 hours, when *in-situ* NMR shows complete conversion to  $\text{IrCl}(\text{CO})(\text{PMe}_3)_2$ . (Yield: 0.62 g, 75%)

**d):** Crude  $\text{IrCl}(\text{CO})(\text{PMe}_3)_2$  was dissolved in a maximum amount of hexane, and repeat **b** and **c** step.

Selected spectroscopic data for  $\text{IrCl}(\text{CO})(\text{PMe}_3)_2$  : in  $\text{d}_6$ -benzene, 295 K

$^1\text{H}$ ,  $\delta$  1.26 (t,  $J_{\text{PH}} = 3.5$  Hz  $\text{PMe}_3$ );  $^{31}\text{P}$ ,  $\delta$  -15.12 (s), Lit.  $\delta$  -13.5 (s) <sup>173</sup>

Selected spectroscopic data for  $\text{IrCl}(\text{CO})_2(\text{PMe}_3)_2$

$^{31}\text{P}$ ,  $\delta$  -23.88 (s), Lit.  $\delta$  -19.2 <sup>173</sup>

## 6.3 Synthesis for Chapter 3

$\text{Rh}(\eta^3\text{-C}_3\text{H}_5)(\text{PPh}_3)_2$  was prepared by reacting  $\text{RhBr}(\text{PPh}_3)_3$  with allyl magnesium bromide according to the literature. <sup>149</sup> The product was of sufficient purity for further study. The crystal for XRD study was grown at the interface of a hexane/toluene solution.

## 6.4 Synthesis for Chapter 4 and 5

### 6.4.1 Synthesis of complexes

#### 6.4.1.1 Reagents

$\text{PdCl}_2$  was purchased from Johnson Matthey and  $\text{PhCN}$  from Lancaster. The BCOPE and  $^t\text{BuCOPE}$  ligands were prepared at Shell and the University of Bristol. Other reagents were obtained from Aldrich and used as received.

#### 6.4.1.2 Synthesis for Chapter 4 and 5

$\text{Pd}(\text{PhCN})_2\text{Cl}_2$ ,  $\text{Pd}(\text{BCOPE})\text{Cl}_2$ ,  $\text{Pd}(\text{}^t\text{BuCOPE})\text{Cl}_2$  and  $\text{Pd}(\text{PPh}_2\text{Me})_2\text{Cl}_2$  were prepared according to the literature.<sup>45,46</sup>

#### 6.4.2 NMR sample preparation

For the hydrogenation studies, solutions of the palladium catalyst (ca. 5 mM; ca. 2.5 mg of catalyst in 500 $\mu\text{L}$  of deuterated solvent) were placed in a Young's tap capped NMR tube. A ca. 40-fold excess of diphenylacetylene- $\text{d}_{10}$  (ca. 20 mg; ca. 0.22 M) was then added and the reaction with  $p\text{-H}_2$  (3-3.5 atm) monitored.

## Appendices

## Appendix 1: Calculation of the activation parameters of 15a-15e

$$K = k$$

For  $\text{Ir}(\eta^3\text{-C}_3\text{H}_5)(\text{CO})(\text{PMe}_3)_2$  (15a)

Table 69: Ligand exchange rate constants for 15a from 203 K to 293 K

T/K	k/s <sup>-1</sup>
203	40
213	100
223	350
233	800
243	1800
263	4900
273	8000
283	18000
293	350000

Table 70: Eyring plot data for 15a

Temperature	1/T	lnk/T	ln2k/T
203	0.004926	-1.62433	-0.93118
213	0.004695	-0.75612	-0.06297
223	0.004484	0.450761	1.143909
233	0.004292	1.233573	1.92672
243	0.004115	2.002481	2.695628
263	0.003802	2.924836	3.617984
273	0.003663	3.377725	4.070872
283	0.003534	4.15268	4.845827
293	0.003413	4.782931	5.476078

A linear regression analysis of the Eyring was undertaken to determine the values for DG, DH and DS in Section 2.5 of the thesis. The rate constants are multiplied by 2 in order to account for there being an equal probability of crossing the transition state to product or returning to the ground state conformation.<sup>148</sup> The listed errors come directly from the

upper and lower 95% confidence limits of these data. The same analysis method was employed for compounds **15a-15d**. The following sections list their raw exchange rate data.

**For Ir( $\eta^3$ -C<sub>3</sub>H<sub>5</sub>)(CO)(PMe<sub>2</sub>Ph)<sub>2</sub> (15b)**

*Table 71: The reaction rate and rate constants for 15b from 203 K to 293 K*

T/K	k/ s <sup>-1</sup>
203	30
213	55
223	120
233	250
243	600
263	1600
273	3600
283	5000
293	6400

**For Ir( $\eta^3$ -C<sub>3</sub>H<sub>5</sub>)(CO)(PMePh<sub>2</sub>)<sub>2</sub> (15c)**

*Table 72: The reaction rate and rate constants for 15c from 203 K to 293 K*

T/K	k/s <sup>-1</sup>
205	12
215	35
225	100
235	300
245	600
265	2000
275	3200
298	9000

**For Ir( $\eta^3$ -C<sub>3</sub>H<sub>5</sub>)(CO)[P-(p-tol)<sub>3</sub>]<sub>2</sub> (15d)**

## Appendices

**Table 73: The reaction rate and rate constants for 15d from 203 K to 293 K**

<b>T/K</b>	<b>k/s<sup>-1</sup></b>
205	20
215	60
225	100
235	160
245	280
255	800
265	1400
275	2800
285	4600



## Appendix 2: The crystallographic data for 16

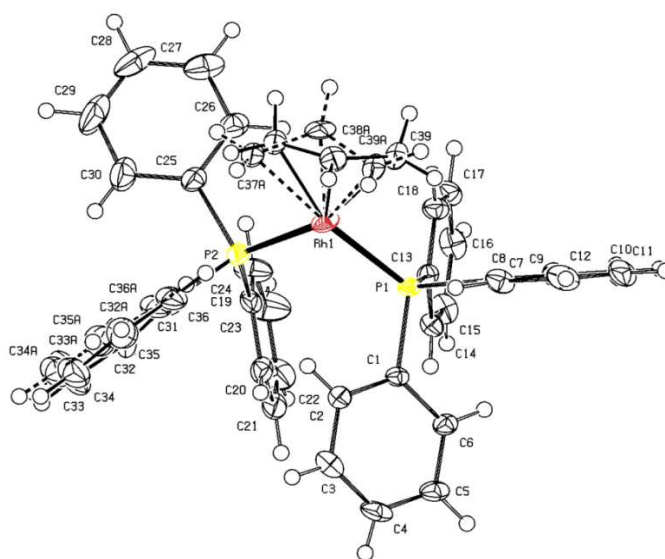


Table 1 Crystal data and structure refinement for sbd1202

Identification code	sbd1202
Empirical formula	$C_{39}H_{35}P_2Rh$
Formula weight	668.52
Temperature/K	110.00(10)
Crystal system	triclinic
Space group	P-1
$a/\text{\AA}$	10.1721(12)
$b/\text{\AA}$	10.4426(11)
$c/\text{\AA}$	17.5032(18)
$\alpha/^\circ$	89.514(8)
$\beta/^\circ$	75.659(10)
$\gamma/^\circ$	63.140(11)
Volume/ $\text{\AA}^3$	1595.4(3)
Z	2
$\rho_{\text{calc}}/\text{mg}/\text{mm}^3$	1.392
$m/\text{mm}^{-1}$	0.662
F(000)	688.0
Crystal size/ $\text{mm}^3$	$0.2617 \times 0.121 \times 0.0623$
$2\theta$ range for data collection	5.74 to 64.24 $^\circ$
Index ranges	$-14 \leq h \leq 13$ , $-15 \leq k \leq 15$ , $-24 \leq l \leq 24$
Reflections collected	15864
Independent reflections	9911[R(int) = 0.0465]
Data/restraints/parameters	9911/0/432

## Appendices

Goodness-of-fit on  $F^2$  1.122  
Final R indexes [ $I \geq 2\sigma(I)$ ]  $R_1 = 0.0602$ ,  $wR_2 = 0.1182$   
Final R indexes [all data]  $R_1 = 0.0801$ ,  $wR_2 = 0.1310$   
Largest diff. peak/hole /  $e \text{ \AA}^{-3}$  1.36/-2.12

Table 2 Fractional Atomic Coordinates ( $\times 10^4$ ) and Equivalent Isotropic Displacement Parameters ( $\text{\AA}^2 \times 10^3$ ) for sbd1202.  $U_{\text{eq}}$  is defined as 1/3 of the trace of the orthogonalised  $U_{ij}$  tensor.

Atom	x	y	z	U(eq)
C1	6213(3)	5512(3)	6565.3(17)	18.0(6)
C2	6715(4)	5226(4)	7250.2(19)	23.4(6)
C3	7419(4)	3817(4)	7433(2)	29.6(8)
C4	7619(4)	2683(4)	6937(2)	30.1(8)
C5	7146(4)	2953(4)	6248(2)	26.8(7)
C6	6459(4)	4349(3)	6056.1(19)	21.6(6)
C7	6671(3)	7076(3)	5327.5(18)	20.2(6)
C8	8168(4)	6834(4)	5270(2)	26.7(7)
C9	9218(4)	6552(4)	4531(2)	31.7(8)
C10	8788(4)	6501(4)	3842(2)	35.5(9)
C11	7324(4)	6729(4)	3888(2)	33.9(8)
C12	6263(4)	7019(4)	4630.3(19)	26.0(7)
C13	3578(3)	7798(3)	6116.0(17)	18.8(6)
C14	2951(4)	6854(4)	6122.7(18)	21.3(6)
C15	1536(4)	7324(4)	5968(2)	29.6(7)
C16	736(4)	8721(4)	5804(2)	30.7(8)
C17	1344(4)	9667(4)	5802(2)	28.8(7)
C18	2743(4)	9219(4)	5959.7(19)	24.6(7)
C19	2227(4)	8046(4)	8198.8(18)	24.0(7)
C20	2823(4)	6545(4)	8140.2(18)	26.5(7)
C21	1943(4)	5891(4)	8033.8(19)	31.7(8)
C22	494(5)	6708(5)	7973(3)	43(1)
C23	-117(6)	8200(5)	8031(3)	55.6(13)
C24	749(5)	8856(4)	8144(2)	38.6(9)
C25	1983(4)	10734(4)	8734.6(19)	26.0(7)
C26	1509(4)	11747(4)	8216(2)	31.6(8)
C27	436(5)	13173(4)	8506(3)	44(1)
C28	-154(5)	13583(5)	9307(3)	53.1(13)
C29	319(5)	12594(6)	9826(3)	57.1(14)
C30	1373(5)	11157(5)	9549(2)	41.6(10)
C31	4167(5)	8046(4)	9136(2)	36.3(9)

C32	3572(14)	7454(17)	9681(9)	36(2)
C32A	3015(18)	7790(20)	9801(12)	36(2)
C33	4247(12)	6856(14)	10304(7)	46(2)
C33A	3499(15)	7159(18)	10424(9)	46(2)
C34	5651(14)	6768(13)	10308(7)	45(2)
C34A	4886(17)	6947(16)	10513(9)	45(2)
C35	6361(13)	7311(14)	9705(6)	39.5(18)
C35A	5849(17)	7299(17)	9977(8)	39.5(18)
C36	5700(20)	7930(20)	9101(10)	32(2)
C36A	5370(20)	7860(30)	9291(12)	32(2)
C37	5339(14)	10776(13)	7743(5)	26.8(16)
C37A	5380(16)	10589(14)	8017(6)	26.8(16)
C38	6568(10)	10080(9)	7082(4)	27.7(17)
C38A	5557(10)	10842(8)	7206(5)	27.0(17)
C39	6351(10)	9950(10)	6347(5)	25.8(13)
C39A	6710(11)	9748(10)	6618(5)	25.8(13)
P1	5387.6(9)	7384.8(8)	6336.4(5)	17.38(16)
P2	3448.3(10)	8880.2(9)	8294.8(5)	21.78(17)
Rh1	5171.0(3)	9018.8(3)	7244.55(16)	23.85(8)

Table 3 Anisotropic Displacement Parameters ( $\text{\AA}^2 \times 10^3$ ) for sbd1202. The Anisotropic displacement factor exponent takes the form:  $-2\pi^2[h^2a^{*2}U_{11} + \dots + 2hka \times b \times U_{12}]$

Atom	$U_{11}$	$U_{22}$	$U_{33}$	$U_{23}$	$U_{13}$	$U_{12}$
C1	15.8(13)	16.1(14)	21.9(14)	3.5(11)	-2.3(11)	-8.6(11)
C2	25.9(16)	21.4(16)	21.6(15)	2.4(12)	-4.2(12)	-11.1(14)
C3	28.9(18)	34(2)	29.7(18)	14.5(15)	-10.9(14)	-16.6(16)
C4	27.7(18)	21.9(17)	40(2)	14.1(15)	-4.2(15)	-13.5(15)
C5	25.0(16)	18.3(15)	36.6(18)	4.5(13)	-2.2(13)	-12.8(13)
C6	21.7(15)	19.4(15)	24.8(15)	1.5(12)	-2.3(12)	-12.5(13)
C7	19.0(14)	14.5(14)	23.3(15)	5.6(11)	-1.9(11)	-6.5(12)
C8	19.8(15)	27.0(17)	33.0(18)	9.7(14)	-4.6(13)	-12.0(14)
C9	18.1(15)	28.4(18)	42(2)	12.0(15)	-2.0(14)	-8.8(14)
C10	34(2)	30.5(19)	29.2(18)	9.1(15)	6.3(15)	-12.2(16)
C11	37(2)	38(2)	22.0(16)	6.3(15)	-2.7(14)	-16.2(17)
C12	24.4(16)	26.3(17)	26.4(16)	5.7(13)	-5.8(13)	-11.6(14)
C13	17.0(14)	18.7(14)	18.7(14)	0.9(11)	-1.4(11)	-8.2(12)
C14	21.8(15)	24.1(16)	21.3(15)	6.6(12)	-7.0(12)	-12.9(13)
C15	25.0(17)	39(2)	29.5(17)	7.2(15)	-8.4(13)	-18.4(16)
C16	19.1(16)	43(2)	28.0(17)	8.6(15)	-10.3(13)	-11.0(16)
C17	23.5(16)	25.8(17)	28.5(17)	7.6(14)	-4.5(13)	-5.7(14)

## Appendices

C18	21.5(15)	20.5(16)	28.1(16)	4.3(13)	-3.1(12)	-8.4(13)
C19	33.8(18)	26.9(17)	18.2(14)	5.9(12)	-5.6(12)	-20.8(15)
C20	32.4(18)	30.4(18)	19.8(15)	-0.7(13)	1.2(13)	-21.2(15)
C21	46(2)	33.4(19)	23.3(16)	2.0(14)	-1.4(15)	-29.0(18)
C22	55(3)	51(3)	51(2)	16(2)	-23(2)	-44(2)
C23	50(3)	47(3)	95(4)	27(3)	-40(3)	-34(2)
C24	40(2)	28.8(19)	59(3)	15.0(18)	-22.5(19)	-21.5(18)
C25	27.1(17)	24.2(17)	26.8(16)	-1.3(13)	0.2(13)	-15.8(14)
C26	31.7(19)	25.0(18)	36.1(19)	-0.2(15)	-1.7(15)	-15.3(15)
C27	35(2)	27(2)	68(3)	2.5(19)	-8(2)	-16.1(17)
C28	38(2)	30(2)	74(3)	-22(2)	7(2)	-12.4(19)
C29	54(3)	57(3)	42(2)	-25(2)	15(2)	-24(3)
C30	45(2)	46(3)	28.8(19)	-5.0(17)	1.8(16)	-24(2)
C31	60(3)	28.2(19)	30.2(19)	3.2(15)	-23.3(17)	-22.7(19)
C32	51(8)	35(7)	17(5)	0(4)	-2(5)	-20(6)
C32A	51(8)	35(7)	17(5)	0(4)	-2(5)	-20(6)
C33	59(7)	62(6)	36(4)	22(4)	-28(6)	-38(7)
C33A	59(7)	62(6)	36(4)	22(4)	-28(6)	-38(7)
C34	69(8)	45(4)	40(6)	17(4)	-30(5)	-36(7)
C34A	69(8)	45(4)	40(6)	17(4)	-30(5)	-36(7)
C35	48(6)	41(3)	39(6)	7(4)	-19(4)	-25(4)
C35A	48(6)	41(3)	39(6)	7(4)	-19(4)	-25(4)
C36	41(7)	26(3)	39(7)	10(4)	-14(5)	-23(4)
C36A	41(7)	26(3)	39(7)	10(4)	-14(5)	-23(4)
C37	40(2)	27(4)	21(5)	0(4)	-1(4)	-25(3)
C37A	40(2)	27(4)	21(5)	0(4)	-1(4)	-25(3)
C38	37(5)	30(4)	29(4)	5(3)	-11(3)	-25(4)
C38A	31(4)	17(4)	39(5)	4(3)	-5(3)	-19(3)
C39	34(4)	33(3)	22(4)	-3(3)	-2(2)	-28(3)
C39A	34(4)	33(3)	22(4)	-3(3)	-2(2)	-28(3)
P1	16.9(4)	14.8(4)	20.4(4)	3.3(3)	-2.5(3)	-8.7(3)
P2	28.4(4)	19.8(4)	20.1(4)	0.8(3)	-5.1(3)	-14.3(3)
Rh1	22.50(13)	18.34(13)	32.03(15)	-2.1(1)	-1.18(10)	-13.66(10)

Table 4 Bond Lengths for sbd1202.

Atom	Atom	Length/Å	Atom	Atom	Length/Å
C1	C2	1.395(4)	C25	P2	1.847(3)
C1	C6	1.402(4)	C26	C27	1.391(5)
C1	P1	1.833(3)	C27	C28	1.369(6)
C2	C3	1.391(5)	C28	C29	1.369(7)

C3	C4	1.381(5)	C29	C30	1.392(6)
C4	C5	1.388(5)	C31	C32	1.305(17)
C5	C6	1.384(5)	C31	C32A	1.552(19)
C7	C8	1.402(4)	C31	C36	1.495(17)
C7	C12	1.393(5)	C31	C36A	1.25(2)
C7	P1	1.848(3)	C31	P2	1.844(4)
C8	C9	1.393(5)	C32	C33	1.42(2)
C9	C10	1.389(6)	C32A	C33A	1.35(3)
C10	C11	1.379(5)	C33	C34	1.392(13)
C11	C12	1.401(4)	C33A	C34A	1.376(17)
C13	C14	1.394(4)	C34	C35	1.393(12)
C13	C18	1.403(4)	C34A	C35A	1.356(15)
C13	P1	1.831(3)	C35	C36	1.39(2)
C14	C15	1.392(5)	C35A	C36A	1.43(3)
C15	C16	1.381(5)	C37	C38	1.381(13)
C16	C17	1.381(5)	C37	Rh1	2.131(12)
C17	C18	1.383(5)	C37A	C38A	1.423(11)
C19	C20	1.396(5)	C37A	Rh1	2.248(13)
C19	C24	1.381(5)	C38	C39	1.376(10)
C19	P2	1.848(3)	C38	Rh1	2.131(7)
C20	C21	1.393(5)	C38A	C39A	1.397(12)
C21	C22	1.360(6)	C38A	Rh1	2.107(7)
C22	C23	1.386(6)	C39	Rh1	2.225(8)
C23	C24	1.386(6)	C39A	Rh1	2.109(9)
C25	C26	1.383(5)	P1	Rh1	2.2403(8)
C25	C30	1.392(5)	P2	Rh1	2.2582(9)

Table 5 Bond Angles for sbd1202.

Atom	Atom	Atom	Angle/°	Atom	Atom	Atom	Angle/°
C2	C1	C6	118.8(3)	C35A	C34A	C33A	122.5(14)
C2	C1	P1	118.2(2)	C36	C35	C34	121.5(10)
C6	C1	P1	122.9(2)	C34A	C35A	C36A	116.2(13)
C3	C2	C1	120.7(3)	C35	C36	C31	117.8(8)
C4	C3	C2	120.0(3)	C31	C36A	C35A	126.6(10)
C3	C4	C5	119.8(3)	C38	C37	Rh1	71.1(6)
C6	C5	C4	120.6(3)	C38A	C37A	Rh1	65.6(5)
C5	C6	C1	120.1(3)	C37	C38	Rh1	71.1(6)
C8	C7	P1	117.1(2)	C39	C38	C37	121.1(9)
C12	C7	C8	118.6(3)	C39	C38	Rh1	75.3(5)
C12	C7	P1	124.2(2)	C37A	C38A	Rh1	76.4(6)

## Appendices

C9	C8	C7	120.6(3)	C39A	C38A	C37A	119.2(10)
C10	C9	C8	120.0(3)	C39A	C38A	Rh1	70.7(5)
C11	C10	C9	120.2(3)	C38	C39	Rh1	67.9(4)
C10	C11	C12	120.0(3)	C38A	C39A	Rh1	70.6(5)
C7	C12	C11	120.7(3)	C1	P1	C7	97.91(13)
C14	C13	C18	118.4(3)	C1	P1	Rh1	115.30(10)
C14	C13	P1	126.0(2)	C7	P1	Rh1	119.29(11)
C18	C13	P1	115.6(2)	C13	P1	C1	107.48(14)
C15	C14	C13	120.1(3)	C13	P1	C7	101.31(14)
C16	C15	C14	120.9(4)	C13	P1	Rh1	113.51(10)
C17	C16	C15	119.5(3)	C19	P2	Rh1	122.77(10)
C16	C17	C18	120.3(3)	C25	P2	C19	100.95(16)
C17	C18	C13	120.9(3)	C25	P2	Rh1	108.56(11)
C20	C19	P2	119.8(3)	C31	P2	C19	101.67(17)
C24	C19	C20	118.1(3)	C31	P2	C25	103.62(17)
C24	C19	P2	122.1(3)	C31	P2	Rh1	116.72(15)
C21	C20	C19	120.6(4)	C37	Rh1	C37A	13.3(3)
C22	C21	C20	120.4(4)	C37	Rh1	C38	37.8(3)
C21	C22	C23	119.8(4)	C37	Rh1	C39	66.8(3)
C22	C23	C24	120.1(4)	C37	Rh1	P1	160.0(2)
C19	C24	C23	121.0(4)	C37	Rh1	P2	98.3(3)
C26	C25	C30	119.2(3)	C37A	Rh1	P2	88.9(3)
C26	C25	P2	117.2(2)	C38	Rh1	C37A	45.4(3)
C30	C25	P2	123.5(3)	C38	Rh1	C39	36.7(2)
C25	C26	C27	120.4(4)	C38	Rh1	P1	124.4(2)
C28	C27	C26	120.1(4)	C38	Rh1	P2	134.2(2)
C27	C28	C29	120.1(4)	C38A	Rh1	C37	25.1(3)
C28	C29	C30	120.7(4)	C38A	Rh1	C37A	38.0(3)
C25	C30	C29	119.5(4)	C38A	Rh1	C38	25.7(3)
C32	C31	C32A	17.6(11)	C38A	Rh1	C39	42.9(3)
C32	C31	C36	119.2(10)	C38A	Rh1	C39A	38.7(3)
C32	C31	P2	127.7(8)	C38A	Rh1	P1	135.2(2)
C32A	C31	P2	115.6(8)	C38A	Rh1	P2	120.0(2)
C36	C31	C32A	131.2(11)	C39	Rh1	C37A	78.3(3)
C36	C31	P2	112.7(7)	C39	Rh1	P1	93.2(2)
C36A	C31	C32	104.4(11)	C39	Rh1	P2	160.5(2)
C36A	C31	C32A	115.8(11)	C39A	Rh1	C37	58.6(3)
C36A	C31	C36	15.4(12)	C39A	Rh1	C37A	67.8(4)
C36A	C31	P2	127.7(8)	C39A	Rh1	C38	22.8(3)
C31	C32	C33	121.8(13)	C39A	Rh1	C39	16.8(3)
C33A	C32A	C31	117.6(14)	C39A	Rh1	P1	102.4(2)
C34	C33	C32	120.4(11)	C39A	Rh1	P2	156.7(2)

C32A	C33A	C34A	120.5(15)	P1	Rh1	C37A	169.4(3)
C33	C34	C35	118.9(11)	P1	Rh1	P2	100.93(3)

Table 6 Torsion Angles for sbd1202.

<b>A</b>	<b>B</b>	<b>C</b>	<b>D</b>	<b>Angle/°</b>
C1	C2	C3	C4	-0.4(5)
C1	P1	Rh1	C37	130.9(10)
C1	P1	Rh1	C37A	92.9(16)
C1	P1	Rh1	C38	107.8(3)
C1	P1	Rh1	C38A	138.4(4)
C1	P1	Rh1	C39	128.6(3)
C1	P1	Rh1	C39A	114.3(3)
C1	P1	Rh1	P2	-64.97(11)
C2	C1	C6	C5	1.9(5)
C2	C1	P1	C7	124.4(3)
C2	C1	P1	C13	-131.0(2)
C2	C1	P1	Rh1	-3.3(3)
C2	C3	C4	C5	1.4(5)
C3	C4	C5	C6	-0.7(5)
C4	C5	C6	C1	-1.0(5)
C6	C1	C2	C3	-1.2(5)
C6	C1	P1	C7	-51.0(3)
C6	C1	P1	C13	53.6(3)
C6	C1	P1	Rh1	-178.7(2)
C7	C8	C9	C10	-0.3(5)
C7	P1	Rh1	C37	14.9(10)
C7	P1	Rh1	C37A	-23.1(16)
C7	P1	Rh1	C38	-8.3(3)
C7	P1	Rh1	C38A	22.3(4)
C7	P1	Rh1	C39	12.5(3)
C7	P1	Rh1	C39A	-1.7(3)
C7	P1	Rh1	P2	178.94(12)
C8	C7	C12	C11	-0.1(5)
C8	C7	P1	C1	-75.1(3)
C8	C7	P1	C13	175.2(3)
C8	C7	P1	Rh1	49.9(3)
C8	C9	C10	C11	0.0(6)
C9	C10	C11	C12	0.3(6)
C10	C11	C12	C7	-0.2(6)
C12	C7	C8	C9	0.4(5)

## Appendices

C12	C7	P1	C1	102.5(3)
C12	C7	P1	C13	-7.2(3)
C12	C7	P1	Rh1	-132.5(3)
C13	C14	C15	C16	0.3(5)
C13	P1	Rh1	C37	-104.4(10)
C13	P1	Rh1	C37A	-142.4(16)
C13	P1	Rh1	C38	-127.6(3)
C13	P1	Rh1	C38A	-97.0(4)
C13	P1	Rh1	C39	-106.8(3)
C13	P1	Rh1	C39A	-121.0(3)
C13	P1	Rh1	P2	59.64(11)
C14	C13	C18	C17	-1.2(5)
C14	C13	P1	C1	0.0(3)
C14	C13	P1	C7	102.2(3)
C14	C13	P1	Rh1	-128.7(2)
C14	C15	C16	C17	-0.7(5)
C15	C16	C17	C18	0.2(5)
C16	C17	C18	C13	0.8(5)
C18	C13	C14	C15	0.7(4)
C18	C13	P1	C1	177.3(2)
C18	C13	P1	C7	-80.6(2)
C18	C13	P1	Rh1	48.6(2)
C19	C20	C21	C22	1.0(5)
C19	P2	Rh1	C37	157.6(4)
C19	P2	Rh1	C37A	167.1(4)
C19	P2	Rh1	C38	171.5(3)
C19	P2	Rh1	C38A	144.2(3)
C19	P2	Rh1	C39	118.5(6)
C19	P2	Rh1	C39A	164.8(7)
C19	P2	Rh1	P1	-16.90(14)
C20	C19	C24	C23	-0.3(6)
C20	C19	P2	C25	-158.7(3)
C20	C19	P2	C31	-52.1(3)
C20	C19	P2	Rh1	80.7(3)
C20	C21	C22	C23	-1.0(6)
C21	C22	C23	C24	0.4(7)
C22	C23	C24	C19	0.3(7)
C24	C19	C20	C21	-0.3(5)
C24	C19	P2	C25	24.5(3)
C24	C19	P2	C31	131.0(3)
C24	C19	P2	Rh1	-96.2(3)
C25	C26	C27	C28	0.2(6)



C25	P2	Rh1	C37	40.6(3)
C25	P2	Rh1	C37A	50.0(4)
C25	P2	Rh1	C38	54.4(3)
C25	P2	Rh1	C38A	27.2(3)
C25	P2	Rh1	C39	1.5(6)
C25	P2	Rh1	C39A	47.7(7)
C25	P2	Rh1	P1	-133.94(12)
C26	C25	C30	C29	-1.1(6)
C26	C25	P2	C19	-91.2(3)
C26	C25	P2	C31	163.8(3)
C26	C25	P2	Rh1	39.1(3)
C26	C27	C28	C29	0.5(7)
C27	C28	C29	C30	-1.6(8)
C28	C29	C30	C25	1.9(7)
C30	C25	C26	C27	0.1(6)
C30	C25	P2	C19	90.3(3)
C30	C25	P2	C31	-14.7(4)
C30	C25	P2	Rh1	-139.4(3)
C31	C32	C33	C34	-5.9(19)
C31	C32A	C33A	C34A	9(2)
C31	P2	Rh1	C37	-75.9(3)
C31	P2	Rh1	C37A	-66.5(4)
C31	P2	Rh1	C38	-62.1(3)
C31	P2	Rh1	C38A	-89.4(3)
C31	P2	Rh1	C39	-115.0(6)
C31	P2	Rh1	C39A	-68.8(7)
C31	P2	Rh1	P1	109.50(13)
C32	C31	C32A	C33A	42(4)
C32	C31	C36	C35	-6(2)
C32	C31	C36A	C35A	-8(3)
C32	C31	P2	C19	-21.2(8)
C32	C31	P2	C25	83.3(8)
C32	C31	P2	Rh1	-157.5(8)
C32	C33	C34	C35	1.7(18)
C32A	C31	C32	C33	-129(6)
C32A	C31	C36	C35	9(2)
C32A	C31	C36A	C35A	7(3)
C32A	C31	P2	C19	-36.1(9)
C32A	C31	P2	C25	68.3(9)
C32A	C31	P2	Rh1	-172.4(8)
C32A	C33A	C34A	C35A	-2(3)
C33	C34	C35	C36	0(2)

## Appendices

C33A C34A C35A C36A -2(2)  
C34 C35 C36 C31 3(2)  
C34A C35A C36A C31 -1(3)  
C36 C31 C32 C33 8.1(18)  
C36 C31 C32A C33A -10(2)  
C36 C31 C36A C35A -172(9)  
C36 C31 P2 C19 151.6(9)  
C36 C31 P2 C25 -104.0(9)  
C36 C31 P2 Rh1 15.3(9)  
C36A C31 C32 C33 3.4(18)  
C36A C31 C32A C33A -11(2)  
C36A C31 C36 C35 11(6)  
C36A C31 P2 C19 155.1(15)  
C36A C31 P2 C25 -100.4(15)  
C36A C31 P2 Rh1 18.8(15)  
C37 C38 C39 Rh1 -56.7(8)  
C37 C38 Rh1 C37A -16.5(8)  
C37 C38 Rh1 C38A 43.2(7)  
C37 C38 Rh1 C39 130.9(9)  
C37 C38 Rh1 C39A 150.5(13)  
C37 C38 Rh1 P1 167.3(5)  
C37 C38 Rh1 P2 -22.7(7)  
C37A C38A C39A Rh1 61.2(9)  
C37A C38A Rh1 C37 6.3(13)  
C37A C38A Rh1 C38 -91.8(10)  
C37A C38A Rh1 C39 -153.2(9)  
C37A C38A Rh1 C39A -128.1(10)  
C37A C38A Rh1 P1 -167.7(6)  
C37A C38A Rh1 P2 39.1(8)  
C38 C37 Rh1 C37A 119(3)  
C38 C37 Rh1 C38A -44.5(7)  
C38 C37 Rh1 C39 -29.5(6)  
C38 C37 Rh1 C39A -12.9(6)  
C38 C37 Rh1 P1 -32.0(13)  
C38 C37 Rh1 P2 163.8(5)  
C38 C39 Rh1 C37 30.3(6)  
C38 C39 Rh1 C37A 23.1(6)  
C38 C39 Rh1 C38A 39.6(5)  
C38 C39 Rh1 C39A -26.7(13)  
C38 C39 Rh1 P1 -150.6(5)  
C38 C39 Rh1 P2 73.0(9)  
C38A C37A Rh1 C37 -12(2)

C38A C37A Rh1	C38	37.5(5)
C38A C37A Rh1	C39	18.3(6)
C38A C37A Rh1	C39A	32.1(6)
C38A C37A Rh1	P1	55(2)
C38A C37A Rh1	P2	-146.9(6)
C38A C39A Rh1	C37	-20.8(6)
C38A C39A Rh1	C37A	-31.5(6)
C38A C39A Rh1	C38	-41.5(8)
C38A C39A Rh1	C39	94.6(16)
C38A C39A Rh1	P1	152.6(5)
C38A C39A Rh1	P2	-29.1(11)
C39 C38 Rh1	C37	-130.9(9)
C39 C38 Rh1	C37A	-147.3(8)
C39 C38 Rh1	C38A	-87.7(9)
C39 C38 Rh1	C39A	19.6(10)
C39 C38 Rh1	P1	36.4(6)
C39 C38 Rh1	P2	-153.5(4)
C39A C38A Rh1	C37	134.4(12)
C39A C38A Rh1	C37A	128.1(10)
C39A C38A Rh1	C38	36.3(6)
C39A C38A Rh1	C39	-25.1(5)
C39A C38A Rh1	P1	-39.6(7)
C39A C38A Rh1	P2	167.2(5)
P1 C1 C2	C3	-176.8(3)
P1 C1 C6	C5	177.3(2)
P1 C7 C8	C9	178.2(3)
P1 C7 C12	C11	-177.7(3)
P1 C13 C14	C15	177.9(2)
P1 C13 C18	C17	-178.7(2)
P2 C19 C20	C21	-177.3(2)
P2 C19 C24	C23	176.6(4)
P2 C25 C26	C27	-178.5(3)
P2 C25 C30	C29	177.3(3)
P2 C31 C32	C33	-179.6(8)
P2 C31 C32A C33A		179.2(13)
P2 C31 C36	C35	-179.9(12)
P2 C31 C36A C35A		175.4(14)
Rh1 C37 C38	C39	58.7(8)
Rh1 C37A C38A C39A		-58.3(7)

## Appendices

Table 7 Hydrogen Atom Coordinates ( $\text{\AA}\times 10^4$ ) and Isotropic Displacement Parameters ( $\text{\AA}^2\times 10^3$ ) for sbd1202.

Atom	x	y	z	U(eq)
H2	6540(40)	5990(40)	7590(20)	28
H3	7770(40)	3640(40)	7880(20)	35
H4	8080(40)	1820(40)	7110(20)	36
H5	7294	2171	5904	32
H6	6070(40)	4570(40)	5590(20)	26
H8	8450(40)	6820(40)	5790(20)	32
H9	10227	6395	4497	38
H10	9505	6309	3338	43
H11	7036	6689	3415	41
H12	5255	7178	4659	31
H14	3500(40)	5960(40)	6180(20)	26
H15	1114	6675	5976	35
H16	-110(50)	9060(40)	5670(20)	37
H17	798	10629	5691	35
H18	3143	9883	5963	30
H20	3840	5963	8173	32
H21	2356	4870	8003	38
H22	-97	6257	7892	52
H23	-1131	8773	7993	67
H24	319	9880	8185	46
H26	1919	11467	7660	38
H27	112	13862	8147	53
H28	-893	14556	9504	64
H29	-77	12892	10382	69
H30	1672	10471	9912	50
H32	2662	7421	9662	43
H32A	2005	8056	9770	43
H33	3736	6513	10719	55
H33A	2876	6863	10803	55
H34	6118	6345	10716	54
H34A	5182	6537	10968	54
H35	7317	7259	9707	47
H35A	6789	7180	10053	47
H36	6211	8260	8679	38
H36A	6031	8119	8915	38
H37A	4565	11760	7698	32
H37B	5571	10680	8263	32
H37C	4433	11294	8408	32
H37D	6308	10216	8210	32

*Appendices*

H38	7624	9555	7151	33
H38A	4817	11764	7057	32
H39A	7253	9260	5926	31
H39B	5693	10852	6157	31
H39C	7749	9289	6697	31
H39D	6704	9917	6061	31

## List of abbreviations

### List of abbreviations

Me =	Methyl	dppb =	1,4-Bis(diphenylphosphino)butane
PPh <sub>3</sub> =	Triphenylphosphine	<i>o, m, p</i> =	ortho, meta, para
PMe <sub>3</sub> =	Trimethylphosphine	acac =	Acetylacetonate
PMe <sub>2</sub> Ph =	Dimethylphenylphosphine	OAc <sup>-</sup> =	Acetate ion
THF =	Tetrahydrofuran	dppe =	1,2-Bis(diphenylphosphino)ethane
<sup>i</sup> Pr =	iso-Propyl	OTf =	Trifluoromethanesulfonate
<sup>t</sup> Bu =	tert-Butyl	TBA =	Tetrabutylammonium
Ph =	Phenyl	<i>fac</i> =	Facial isomer
Cy =	Cyclohexyl	<i>mer</i> =	Meridional isomer
Ac =	Acetyl	Py =	Pyridine
L =	Neutral ligand	<i>e</i> =	Equatorial
X =	Ionic ligand	<i>a</i> =	Apical
COD =	Cyclooctadiene	PE =	Polyethylene
BCOPE =	(C <sub>8</sub> H <sub>14</sub> )PCH <sub>2</sub> -CH <sub>2</sub> P(C <sub>8</sub> H <sub>14</sub> )	PP =	Polypropene
<sup>t</sup> BuCOPE =	(C <sub>8</sub> H <sub>14</sub> )PC <sub>6</sub> H <sub>4</sub> CH <sub>2</sub> P( <sup>t</sup> Bu) <sub>2</sub>	Sol. =	Solvent
TPPTS =	3,3',3''-Phosphanetriyltris(benzene-sulfonic acid) trisodium salt	BINAS =	Sulfonated 2,2'-bis(diphenylphosphino)-1,1'-binaphthyl sodium salt

### Spectroscopy

NMR =	Nuclear magnetic resonance	XRD =	X-Ray diffraction
1D =	One dimensional	PHIP =	Parahydrogen induced polarization
2D =	Two dimensional	s =	Singlet
COSY =	Homonuclear correlation spectroscopy	d =	Doublet
HMQC =	Heteronuclear correlation spectroscopy	t =	Triplet

## *List of abbreviations*

HSQC =	Heteronuclear Single Quantum Coherence	quart =	Quartet
HMBC =	Heteronuclear Multiple Bond Correlation	quin =	Quintet
nOe =	Nuclear Overhauser effect	d, d =	Doublet of doublets
OPSY =	Only parahydrogen spectroscopy	d, d, d =	Doublet of doublet of doublets
NOESY =	Nuclear Overhauser Enhancement Spectroscopy	d, t =	Doublet of triplets
EXSY =	Exchange spectroscopy	IR =	Infrared

### *Units*

ml =	Millilitre	mol =	Mole
Å =	Ångström	s =	Seconds
µl =	microlitre	min =	Minutes
mg =	milligram	δ =	Chemical shift (ppm)
mmol =	millimole	ppm =	Parts per million
MHz =	megahertz	g =	Gramme
°C =	Degrees Celsius	K =	Kelvin
atm. =	Atmosphere	Hz =	Hertz

## References

### References

- (1) *R&D Magazine* **2005**, 20.
- (2) Perutz, R. N. *Chem. Rev.* **1985**, 85, 97.
- (3) Walter, M. G.; Warren, E. L.; McKone, J. R.; Boettcher, S. W.; Mi, Q.; Santori, E. A.; Lewis, N. S. *Chem. Rev.* **2010**, 110, 6446.
- (4) Rüttinger, W.; Dismukes, G. C. *Chem. Rev.* **1997**, 97, 1.
- (5) Li, S. F.; Guo, Z. X. *J. Phys. Chem. C* **2010**, 114, 11456.
- (6) Laitar, D. S.; Müller, P.; Sadighi, J. P. *J. Am. Chem. Soc.* **2005**, 127, 17196.
- (7) Kobayashi, T.; Takahashi, H. *Energy Fuels* **2003**, 18, 285.
- (8) Kang, P.; Cheng, C.; Chen, Z.; Schauer, C. K.; Meyer, T. J.; Brookhart, M. J. *Am. Chem. Soc.* **2012**, 134, 5500.
- (9) Kumar, A.; Kołaski, M.; Lee, H. M.; Kim, K. S. *J. Phys. Chem. A* **2008**, 112, 5502.
- (10) Oyama, S. T.; Somorjai, G. A. *J. Chem. Educ.* **1988**, 65, 765.
- (11) Kiss, G. *Chem. Rev.* **2001**, 101, 3435.
- (12) Kollár, L. *Modern Carbonylation Methods* Wiley-VCH, 2008.
- (13) Herrmann, W. A.; Kohlpaintner, C. W. *Angew. Chem. Int. Ed. Engl.* **1993**, 32, 1524.
- (14) Leeuwen, P. W. N. M. v. *Homogeneous Catalysis: Understanding The Art*; Kluwer Academic Publishers: Dordrecht / Boston / London.
- (15) Zuidema, E.; Daura-Oller, E.; Carbó, J. J.; Bo, C.; van Leeuwen, P. W. N. M. *Organomet.* **2007**, 26, 2234.
- (16) Kuil, M.; Soltner, T.; van Leeuwen, P. W. N. M.; Reek, J. N. H. *J. Am. Chem. Soc.* **2006**, 128, 11344.
- (17) Bronger, R. P. J.; Kamer, P. C. J.; van Leeuwen, P. W. N. M. *Organomet.* **2003**, 22, 5358.
- (18) Leeuwen, P. W. N. M. v.; Claver, C. *Rhodium catalyzed hydroformylation*, 2001; Vol. 22.
- (19) Douglas, B. E.; McDaniel, D. H.; Alexander, J. J. *Concepts and Models of Inorganic Chemistry, 3<sup>rd</sup> Edition*; John Wiley & Sons, Inc, 1994.
- (20) Duckett, S. B.; Newell, C. L.; Eisenberg, R. *J. Am. Chem. Soc.* **1994**, 116, 10548.



- (21) Young, J. F.; Osborn, J. A.; Jardine, F. H.; Wilkinson, G. *Chem. Commun.* **1965**, 131.
- (22) Osborn, J. A.; Wilkinson, G.; Young, J. F. *Chem. Commun.* **1965**, 17.
- (23) Crabtree, R. H. *The Organometallic Chemistry of the Transition Metals*, 5<sup>th</sup> Edition Wiley-Interscience, 2009.
- (24) Yadav, M. S. *Quick Review in Inorganic Chemistry* Anmol Publications Pvt. Ltd, 2005.
- (25) Vaska, L. *Acc. Chem. Res.* **1968**, 1.
- (26) Chock, P. B.; Halpern, J. *J. Am. Chem. Soc.* **1966**, 88.
- (27) Vaska, L.; DiLuzio, J. W. *J. Am. Chem. Soc.* **1962**, 84.
- (28) Hallman, P. S.; Evans, D.; Osborn, J. A.; Wilkinson, G. *Chem. Commun.* **1967**, 305.
- (29) Chinn, M. S.; Heinekey, D. M. *J. Am. Chem. Soc.* **1990**, 112, 5166.
- (30) Godard, C.; Duckett, S. B.; Polas, S.; Tooze, R.; Whitwood, A. C. *Dalton. Trans.* **2009**, 2496.
- (31) Godard, C.; Duckett, S. B.; Polas, S.; Tooze, R.; Whitwood, A. C. *J. Am. Chem. Soc.* **2005**, 127, 4994.
- (32) Godard, C.; Duckett, S. B.; Henry, C.; Polas, S.; Toose, R.; Whitwood, A. C. *Chem. Commun.* **2004**, 1826.
- (33) Brown, J. M.; Kent, A. G. *J. Chem. Soc., Perkin Trans.* **1987**, 1597.
- (34) Bianchini, C.; Oberhauser, W.; Orlandini, A.; Giannelli, C.; Frediani, P. *Organomet.* **2005**, 24, 3692.
- (35) Diebolt, O.; van Leeuwen, P. W. N. M.; Kamer, P. C. J. *ACS Catalysis* **2012**, 2, 2357.
- (36) Tromp, M.; Sietsma, J. R. A.; van Bokhoven, J. A.; van Strijdonck, G. P. F.; van Haaren, R. J.; van der Eerden, A. M. J.; van Leeuwen, P. W. N. M.; Koningsberger, D. C. *Chem. Commun.* **2003**, 128.
- (37) Koningsberger, D. C.; Mojet, B. L.; van Dorssen, G. E.; Ramaker, D. E. *Top. Catal.* **2000**, 10, 143.
- (38) Tromp, M.; van Bokhoven, J. A.; van Haaren, R. J.; van Strijdonck, G. P. F.; van der Eerden, A. M. J.; van Leeuwen, P. W. N. M.; Koningsberger, D. C. *J. Am. Chem. Soc.* **2002**, 124, 14814.
- (39) Yagupsky, G.; Wilkinson, G. *J. Chem. Soc. A.* **1969**, 725.

## References

- (40) Brown, C. K.; Wilkinson, G. J. *Chem. Soc. D.* **1971**, 70.
- (41) Duckett, S. B.; Mewis, R. E. *Acc. Chem. Res.* **2012**.
- (42) Bianca K. Muñoz, E. S. G., Cyril Godard, Ennio Zangrando, Carles Bo, Aurora Ruiz, and Carmen Claver *Eur. J. Inorg. Chem.* **2008**.
- (43) Pruett, R. L.; Smith, J. A. *J. Org. Chem.* **1969**, 34, 327.
- (44) Evans, D.; Osborn, J. A.; Wilkinson, G. J. *Chem. Soc. A.* **1968**, 3133.
- (45) Joaquín López-Serrano, S. B. D., and Agustí Lledós *J. Am. Chem. Soc.* **2006**, 128, 9596.
- (46) Joaquín López-Serrano, S. B. D., Stuart Aiken, Karina Q. Almeida Leñero, Eite Drent, John P. Dunne, Denis Konya and Adrian C. Whitwood *J. Am. Chem. Soc.* **2007**, 129, 6513.
- (47) Joaquín López-Serrano, S. B. D., John P. Dunne, Cyril Godard and Adrian C. Whitwood *Dalton. Trans.* **2008**.
- (48) Antolovic, D.; Davidson, E. R. *J. Am. Chem. Soc.* **1987**, 109, 5828.
- (49) Gleich, D.; Schmid, R.; Herrmann, W. A. *Organomet.* **1998**, 17, 4828.
- (50) Tang, D.; Qin, S.; Su, Z.; Hu, C. *Organomet.* **2006**, 26, 33.
- (51) Huo, C.-F.; Li, Y.-W.; Beller, M.; Jiao, H. *Organomet.* **2005**, 24, 3634.
- (52) Powell, J.; Shaw, B. L. *J. Chem. Soc. A.* **1968**, 583.
- (53) Siegel, H.; Himmele, W. *Angew. Chem. Int. Ed. Engl.* **1980**, 19, 178.
- (54) Breit, B. *Acc. Chem. Res.* **2003**, 36, 264.
- (55) Franke, R.; Selent, D.; Börner, A. *Chem. Rev.* **2012**, 112, 5675.
- (56) Hebrard, F. d. r.; Kalck, P. *Chem. Rev.* **2009**, 109, 4272.
- (57) Schulz, H. F.; Bellstedt, F. *Product R&D* **1973**, 12, 176.
- (58) Barborak, J. C.; Cann, K. *Organomet.* **1982**, 1, 1726.
- (59) Youichi Ishii, K. M., Kenji Kamita, and Masanobu Hidai *J. Am. Chem. Soc.* **1997**, 119, 6448.
- (60) R. Kummer, H. J. N., H. Hohenschutz and M. Strohmeyer In *Advances in Chemistry* American Chemical Society: 1974; Vol. 132, p 19.
- (61) Adkins, H.; Krsek, G. *J. Am. Chem. Soc.* **1949**, 71, 3051.
- (62) Gholap, R. V.; Kut, O. M.; Bourne, J. R. *Ind. Eng. Chem. Res.* **1992**, 31, 2446.
- (63) Huo, C.-F.; Li, Y.-W.; Beller, M.; Jiao, H. *Organomet.* **2003**, 22, 4665.

## References

- (64) Versluis, L.; Ziegler, T.; Baerends, E. J.; Ravenek, W. *J. Am. Chem. Soc.* **1989**, *111*, 2018.
- (65) Heck, R. F.; Breslow, D. *J. Am. Chem. Soc.* **1962**, *84*, 2499.
- (66) Heck, R. F.; Breslow, D. S. *J. Am. Chem. Soc.* **1961**, *83*, 4023.
- (67) Clark, A. C.; Terapane, J. F.; Orchin, M. *J. Org. Chem.* **1974**, *39*, 2405.
- (68) Vidal, J. L.; Walker, W. E. *Inorg. Chem.* **1981**, *20*, 249.
- (69) Li, C.; Widjaja, E.; Garland, M. *J. Am. Chem. Soc.* **2003**, *125*, 5540.
- (70) Slauch, L. H.; Mullineaus, R. D.; Patent, U. S., Ed.; U.S. Pat. 3239569; U.S. Pat. 3239570: Unites States of America, 1966.
- (71) Slauch, L. H.; Mullineaux, R. D. *J. Organomet. Chem.* **1968**, *13*, 469.
- (72) Yagupsky, G.; Brown, C. K.; Wilkinson, G. *J. Chem. Soc. A.* **1970**, 1392.
- (73) Brown, C. K.; Wilkinson, G. *J. Chem. Soc. A.* **1970**, 2753.
- (74) O'Connor, C.; Yagupsky, G.; Evans, D.; Wilkinson, G. *Chem. Commun.* **1968**, 420.
- (75) Brown, C. K.; Mowat, W.; Yagupsky, G.; Wilkinson, G. *J. Chem. Soc. A.* **1971**, 850.
- (76) Bath, S. S.; Vaska, L. *J. Am. Chem. Soc.* **1963**, *85*, 3500.
- (77) Laplaca, S. J.; Ibers, J. A. *J. Am. Chem. Soc.* **1965**, 85.
- (78) Yagupsky, G.; Brown, C. K.; Wikinson, G. *J. Chem. Soc. D.* **1969**, 1244.
- (79) Pruett, R. L. S., J. A. S. 1968.
- (80) Omastu, T. 1989.
- (81) Billig, E. A., A. G. and Bryant, D. R. ; Patent, U. S., Ed. United States of America, 1987.
- (82) Sanger, A. R. *J. Mol. Catal.* **1978**, *3*, 221.
- (83) Sanger, A. R.; Schallig, L. R. *J. Mol. Catal.* **1977**, *3*, 101.
- (84) Pittman, C. U.; Hirao, A. *J. Org. Chem.* **1978**, *43*, 640.
- (85) Matsumoto 1986.
- (86) Aubry, D. A.; Bridges, N. N.; Ezell, K.; Stanley, G. G. *J. Am. Chem. Soc.* **2003**, *125*, 11180.

## References

- (87) Kamer, P. C. J.; van Leeuwen, P. W. N. M.; Reek, J. N. H. *Acc. Chem. Res.* **2001**, *34*, 895.
- (88) Williams, G. L.; Parks, C. M.; Smith, C. R.; Adams, H.; Haynes, A.; Meijer, A. J. H. M.; Sunley, G. J.; Gaemers, S. *Organomet.* **2011**, *30*, 6166.
- (89) van der Veen, L. A.; Boele, M. D. K.; Bregman, F. R.; Kamer, P. C. J.; van Leeuwen, P. W. N. M.; Goubitz, K.; Fraanje, J.; Schenk, H.; Bo, C. *J. Am. Chem. Soc.* **1998**, *120*, 11616.
- (90) van der Veen, L. A.; Keeven, P. H.; Schoemaker, G. C.; Reek, J. N. H.; Kamer, P. C. J.; van Leeuwen, P. W. N. M.; Lutz, M.; Spek, A. L. *Organomet.* **2000**, *19*, 872.
- (91) Casey, C. P.; Whiteker, G. T.; Melville, M. G.; Petrovich, L. M.; Gavney, J. A.; Powell, D. R. *J. Am. Chem. Soc.* **1992**, *114*, 5535.
- (92) Wasserscheid, P.; Waffenschmidt, H. In *Ionic Liquids*; American Chemical Society: 2002; Vol. 818, p 373.
- (93) Webb, P. B.; Sellin, M. F.; Kunene, T. E.; Williamson, S.; Slawin, A. M. Z.; Cole-Hamilton, D. J. *J. Am. Chem. Soc.* **2003**, *125*, 15577.
- (94) Institute, N. I. P., Ed. France, 1977; Vol. Fr. Pat. 2,314,910.
- (95) van Rooy, A.; Orij, E. N.; Kamer, P. C. J.; van Leeuwen, P. W. N. M. *Organomet.* **1995**, *14*, 34.
- (96) Bruke, P. M.; Organization, W. I. P., Ed. United States of America, 1997.
- (97) Heck, R. F. *Acc. Chem. Res.* **1969**, *2*, 10.
- (98) Freemanla, M. A.; Young, D. A. *Inorg. Chem.* **1986**, *25*, 1556.
- (99) Tolman, C. A. *J. Am. Chem. Soc.* **1970**, *92*, 2953.
- (100) Tolman, C. A. *Chem. Rev.* **1977**, *77*, 313.
- (101) Bartik, T.; Himmler, T.; Schulte, H. G.; Seevogel, K. *J. Organomet. Chem.* **1984**, *272*, 29.
- (102) Dierkes, P.; W. N. M. van Leeuwen, P. *J. Chem. Soc., Dalton Trans.* **1999**, *0*, 1519.
- (103) Ojima, I. *Chem. Rev.* **1988**, *88*, 1011.
- (104) Lazzaroni, R.; Raffaelli, A.; Settambolo, R.; Bertozzi, S.; Vitulli, G. *J. Mol. Catal.* **1989**, *50*, 1.
- (105) Lazzaroni, R.; Uccello-Barretta, G.; Scamuzzi, S.; Settambolo, R.; Caiazza, A. *Organomet.* **1996**, *15*, 4657.
- (106) Fyhr, C.; Garland, M. *Organomet.* **1993**, *12*, 1753.

- (107) Garland, M.; Pino, P. *Organomet.* **1991**, *10*, 1693.
- (108) Lazzaroni, R.; Settambolo, R.; Uccello-Barretta, G.; Caiazzo, A.; Scamuzzi, S. *J. Mol. Catal. A: Chem.* **1999**, *143*, 123.
- (109) Wu, X.-F.; Neumann, H.; Beller, M. *Chem. Rev.* **2012**, *113*, 1.
- (110) Zung, T. T.; Bruk, L. G.; Temkin, O. N. *Mendeleev Commun.* **1994**, *4*, 2.
- (111) Clegg, W.; Eastham, G. R.; Elsegood, M. R. J.; Heaton, B. T.; Iggo, J. A.; Tooze, R. P.; Whyman, R.; Zacchini, S. *Organomet.* **2002**, *21*, 1832.
- (112) Clegg, W.; Eastham, G. R.; Elsegood, M. R. J.; Heaton, B. T.; Iggo, J. A.; Tooze, R. P.; Whyman, R.; Zacchini, S. *J. Chem. Soc., Dalton Trans.* **2002**, 3300.
- (113) Konya, D.; Almeida Leñero, K. Q.; Drent, E. *Organomet.* **2006**, *25*, 3166.
- (114) Takaya, J.; Iwasawa, N. *J. Am. Chem. Soc.* **2008**, *130*, 15254.
- (115) She, L.; Li, X.; Sun, H.; Ding, J.; Frey, M.; Klein, H.-F. *Organomet.* **2006**, *26*, 566.
- (116) Gatti, G.; López, J. A.; Mealli, C.; Musco, A. *J. Organomet. Chem.* **1994**, *483*, 77.
- (117) Fitton, P.; McKeon, J. E.; Ream, B. C. *J. Chem. Soc. D.* **1969**, 370.
- (118) Klein, H.-F.; Bickelhaupt, A.; Lemke, M.; Sun, H.; Brand, A.; Jung, T.; Röhr, C.; Flörke, U.; Haupt, H.-J. *Organomet.* **1997**, *16*, 668.
- (119) Atkinson, K. D.; Cowley, M. J.; Elliott, P. I. P.; Duckett, S. B.; Green, G. G. R.; López-Serrano, J. n.; Whitwood, A. C. *J. Am. Chem. Soc.* **2009**, *131*, 13362.
- (120) Pravica, M. G.; Weitekamp, D. P. *Chem. Phys. Lett.* **1988**, *145*, 255.
- (121) Permin, A. B.; Eisenberg, R. *J. Am. Chem. Soc.* **2002**, *124*, 12406.
- (122) Aguilar, J. A.; Elliott, P. I. P.; Lopez-Serrano, J.; Adams, R. W.; Duckett, S. B. *Chem. Commun.* **2007**, 1183.
- (123) Reich, H. J. <http://www.chem.wisc.edu/areas/reich/nmr/05-hmr-16-virt-coupl.htm>, 2012.
- (124) Atwood, H. J. L. a. J. D. *J. Am. Chem. Soc.* **1989**, *111*.
- (125) Lloyd, L. S.; Adams, R. W.; Bernstein, M.; Coombes, S.; Duckett, S. B.; Green, G. G. R.; Lewis, R. J.; Mewis, R. E.; Sleigh, C. J. *J. Am. Chem. Soc.* **2012**.
- (126) John, K. D.; Salazar, K. V.; Scott, B. L.; Baker, T.; Sattelberger, A. P. *Chem. Commun.* **2000**.
- (127) Martin Schäfer, J. W. a. H. W. *J. Chem. Soc., Chem. Commun.* **1991**.
- (128) Martinengo, P. C. A. S. *Inorg. Chem.* **1966**, *6*.

## References

- (129) Green, M. L. H.; Nagy, P. L. I. *Adv. Organomet. Chem.* **1965**, Volume 2, 325.
- (130) Wheeler, R. M. a. A. G. *Nature* **1968**, 217.
- (131) Manger, M.; Wolf, J.; Teichert, M.; Stalke, D.; Werner, H. *Organomet.* **1998**, 17, 3210.
- (132) Tsuji, J.; Takahashi, K.; Minami, I.; Shimizu, I. *Tetrahedron Lett.* **1984**, 25, 4783.
- (133) Trost, B. M.; Van Vranken, D. L. *J. Am. Chem. Soc.* **1993**, 115, 444.
- (134) Trost, B. M.; Mignani, S. M.; Nanninga, T. N. *J. Am. Chem. Soc.* **1988**, 110, 1602.
- (135) McKee, M. L. *WIREs Comput Mol Sci* **2011**, 1, 943.
- (136) Abatjoglou, A. G.; Billig, E.; Bryant, D. R. *Organomet.* **1984**, 3, 923.
- (137) Matsubara, T.; Koga, N.; Ding, Y.; Musaev, D. G.; Morokuma, K. *Organomet.* **1997**, 16, 1065.
- (138) Gleich, D.; Herrmann, W. A. *Organomet.* **1999**, 18, 4354.
- (139) del Rio, I.; de Lange, W. G. J.; van Leeuwen, P. W. N. M.; Claver, C. *J. Chem. Soc., Dalton Trans.* **2001**, 1293.
- (140) Lightburn, T. E.; De Paolis, O. A.; Cheng, K. H.; Tan, K. L. *Org. Lett.* **2011**, 13, 2686.
- (141) Wang, X.; Buchwald, S. L. *J. Am. Chem. Soc.* **2011**, 133, 19080.
- (142) Chikkali, S. H.; Bellini, R.; de Bruin, B.; van der Vlugt, J. I.; Reek, J. N. H. *J. Am. Chem. Soc.* **2012**.
- (143) Fang, X.; Zhang, M.; Jackstell, R.; Beller, M. *Angew. Chem. Int. Ed.* **2013**, 52, 4645.
- (144) John, K. D.; Salazar, K. V.; Scott, B. L.; Baker, R. T.; Sattelberger, A. P. *Organomet.* **2000**, 20, 296.
- (145) Kevin D. John, R. M., Griselda Hernandez, Jennifer C. Green, Richard L. Martin, R. Thomas Baker, and Alfred P. Sattelberger *Organomet.* **2002**, 21.
- (146) Baya, M.; Houghton, J.; Konya, D.; Champouret, Y.; Daran, J.-C.; Almeida Leñero, K. Q.; Schoon, L.; Mul, W. P.; Oort, A. B. v.; Meijboom, N.; Drent, E.; Orpen, A. G.; Poli, R. *J. Am. Chem. Soc.* **2008**, 130, 10612.
- (147) de la Fuente, V.; Waugh, M.; Eastham, G. R.; Iggo, J. A.; Castellón, S.; Claver, C. *Chem. Eur. J.* **2010**, 16, 6919.
- (148) Campbell, C. H.; Green, M. L. H. *J. Chem. Soc. A.* **1971**, 3282.
- (149) Reilly, C. A.; Thyret, H. *J. Am. Chem. Soc.* **1967**, 89, 5144.

## References

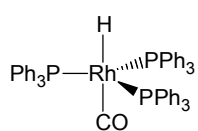
- (150) Richard J. van Haaren, E. Z., Jan Fraanje, Kees Goubitz, Paul C.J. Kamer, Piet W.N.M. van Leeuwen, Gino P.F. van Strijdonck *C. R. Chimie* **2002**, 431.
- (151) Kohtaro Osakada, J.-C. C., Take-aki Koizumi, Isao Yamaguchi, and Takakazu Yamamoto *Organomet.* **1996**, 14.
- (152) Sivak, A. J.; Muetterties, E. L. *J. Am. Chem. Soc.* **1979**, 101, 4878.
- (153) Incorvia, J. W. F. a. M. *J. Inorg. Chem.* **1968**, 7.
- (154) Werner, H.; Schäfer, M.; Nürnberg, O.; Wolf, J. *Chem. Ber.* **1994**, 127, 27.
- (155) Meier, E. B.; Burch, R. R.; Muetterties, E. L.; Day, V. W. *J. Am. Chem. Soc.* **1982**, 104, 2661.
- (156) Clement, D. A.; Nixon, J. F.; Poland, J. S. *J. Organomet. Chem.* **1974**, 76, 117.
- (157) Duckett, S. B.; Eisenberg, R. *J. Am. Chem. Soc.* **1993**, 115, 5292.
- (158) Ingleson, M. J.; Brayshaw, S. K.; Mahon, M. F.; Ruggiero, G. D.; Weller, A. S. *Inorg. Chem.* **2005**, 44, 3162.
- (159) Fryzuk, M. D.; Lloyd, B. R.; Clentsmith, G. K. B.; Rettig, S. J. *J. Am. Chem. Soc.* **1994**, 116, 3804.
- (160) Gauthron, I.; Gagnon, J.; Zhang, T.; Rivard, D.; Lucas, D.; Mugnier, Y.; Harvey, P. D. *Inorg. Chem.* **1998**, 37, 1112.
- (161) Meilleur, D.; Rivard, D.; Harvey, P. D.; Gauthron, I.; Lucas, D.; Mugnier, Y. *Inorg. Chem.* **2000**, 39, 2909.
- (162) Ramachandran, R.; Puddephatt, R. *J. Inorg. Chem.* **1993**, 32, 2256.
- (163) Johnason A, H., University of York, 2008.
- (164) Portnoy, M.; Frolow, F.; Milstein, D. *Organomet.* **1991**, 10, 3960.
- (165) Toth, I.; Elsevier, C. J. *Organomet.* **1994**, 13, 2118.
- (166) Portnoy, M.; Milstein, D. *Organomet.* **1994**, 13, 600.
- (167) Zudin, V. N.; Chinakov, V. D.; Nekipelov, V. M.; Likholobov, V. A.; Yermakov, Y. I. *J. Organomet. Chem.* **1985**, 289, 425.
- (168) Krause, J.; Bonrath, W.; Poerschke, K. R. *Organomet.* **1992**, 11, 1158.
- (169) Hahn, C.; Vitagliano, A.; Giordano, F.; Taube, R. *Organomet.* **1998**, 17, 2060.
- (170) Yoshida, T.; Otsuka, S. *J. Am. Chem. Soc.* **1977**, 99, 2134.
- (171) Forster, D. *Inorg. Nucl. Chem. Lett.* **1969**, 5, 433.

## **References**

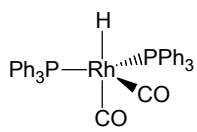
- (172) Seth, P. N. A.; Underhill, A. E.; Watkins, D. M. *Inorg. Nucl. Chem. Lett.* **1980**, *16*, 1.
- (173) Field, L. D.; Lawrenz, E. T.; Ward, A. J. *Polyhedron* **1999**, *18*, 3031.
- (174) Burk, M. J.; Crabtree, R. H. *Inorg. Chem.* **1986**, *25*, 931.
- (175) Kang, J. P. C. a. J. W. *J. Am. Chem. Soc.* **1967**, *89*.



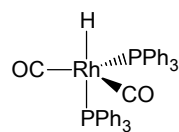
## Structure of complexes



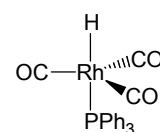
1



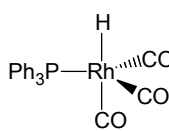
2ee



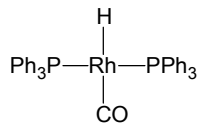
2ae



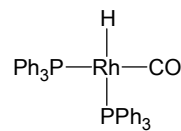
3a



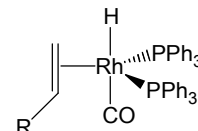
3e



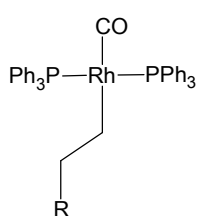
4t



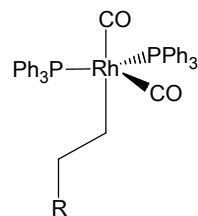
4c



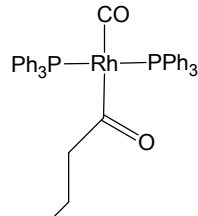
5



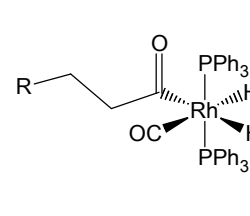
6



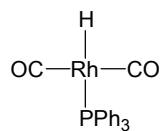
7



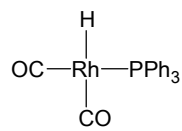
8



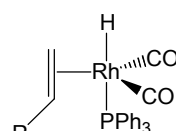
9



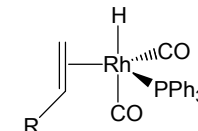
10t



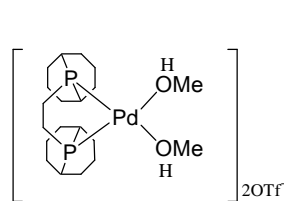
10c



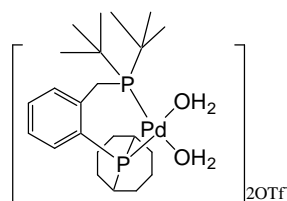
11e



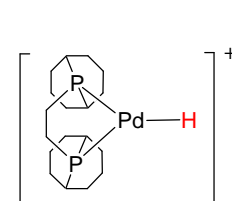
11a



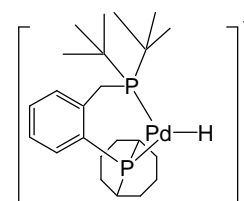
12a



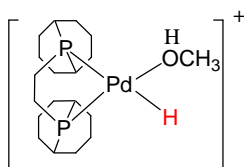
12b



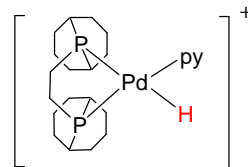
13a



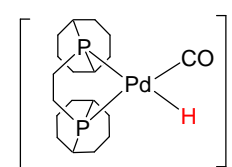
13b



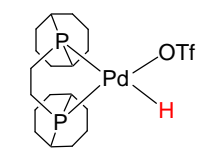
13a-1



13a-2

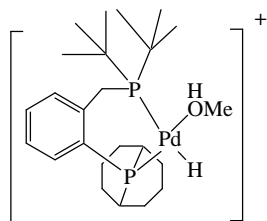


13a-3

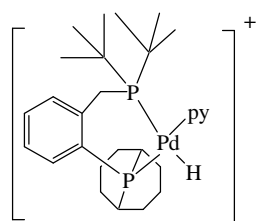


13a-4

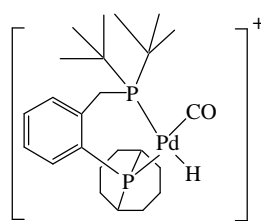
## Structure of complexes



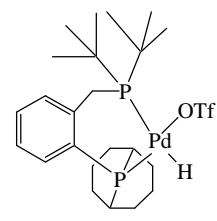
13bA-1



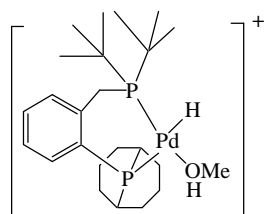
13bA-2



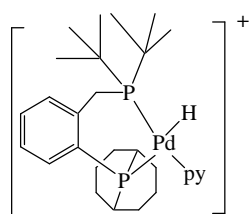
13bA-3



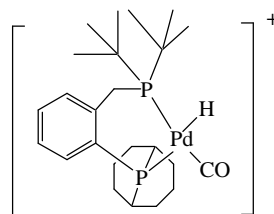
13bA-4



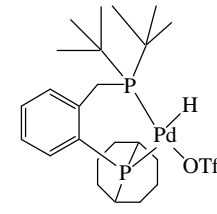
13bB-1



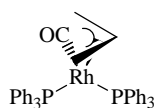
13bB-2



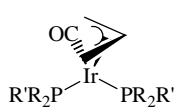
13bB-3



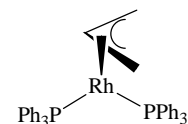
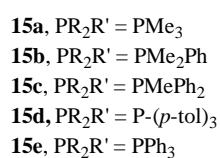
13bB-4



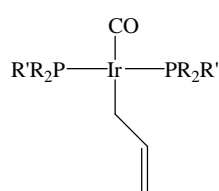
14



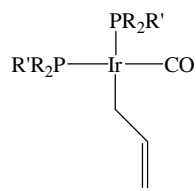
15



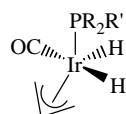
16



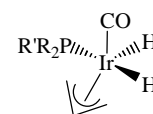
17aA-17eA



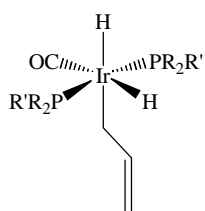
17aB-17eB



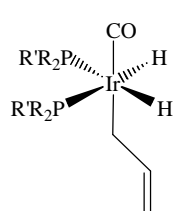
18aA- 18eA



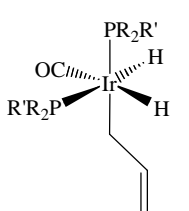
18aB - 18eB



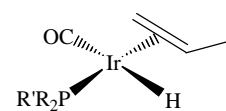
19aA-19eA



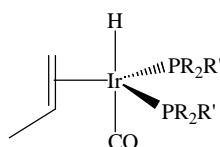
19aB-19eB



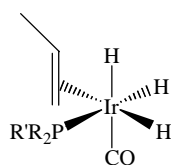
19aC-19eC



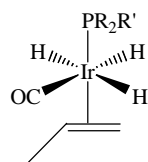
20a-20e



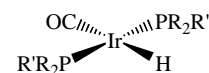
21a-21e



22aA-22eA

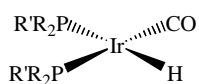


22aB-22eB

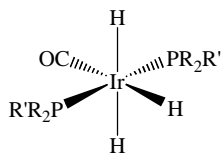


23aA-23eA

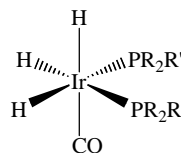
*Structure of complexes*



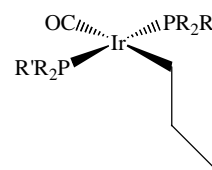
**23aB-23eB**



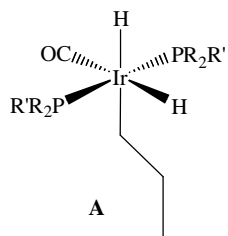
**24aA-24eA**



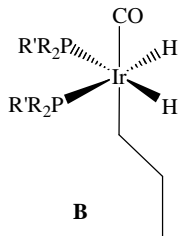
**24aB-24eB**



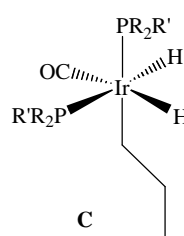
**25a-25e**



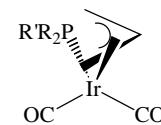
**26aA-26eA**



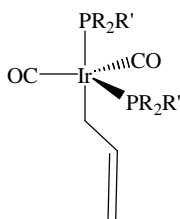
**26aB-26eB**



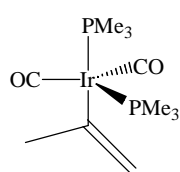
**26aC-26eC**



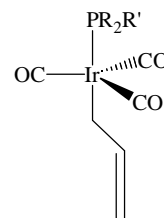
**27a-27e**



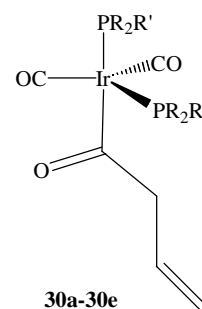
**28a-28e**



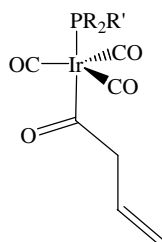
**28a-2**



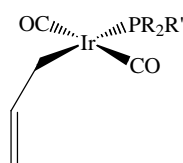
**29a-29e**



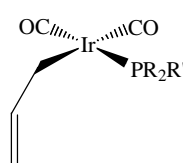
**30a-30e**



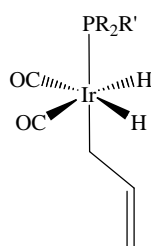
**31a-31e**



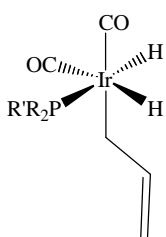
**32aA-32eA**



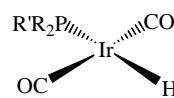
**32aB-32eB**



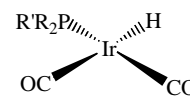
**33aA-33eA**



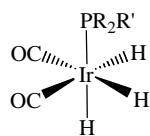
**33aB-33eB**



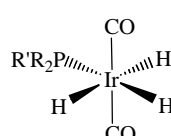
**34aA-34eA**



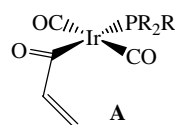
**34aB-34eB**



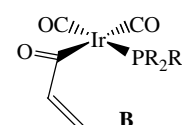
**35aA-35eA**



**35aB-35eB**

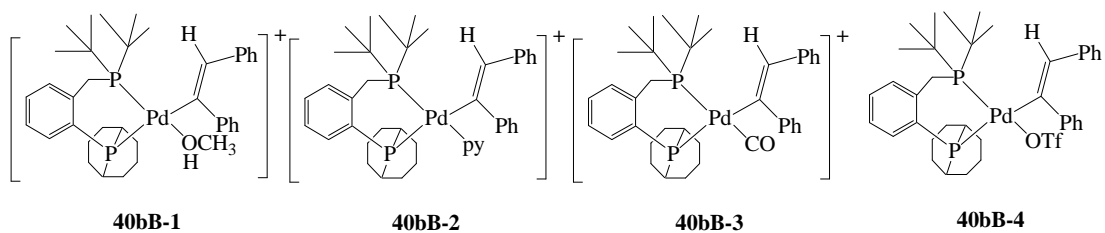
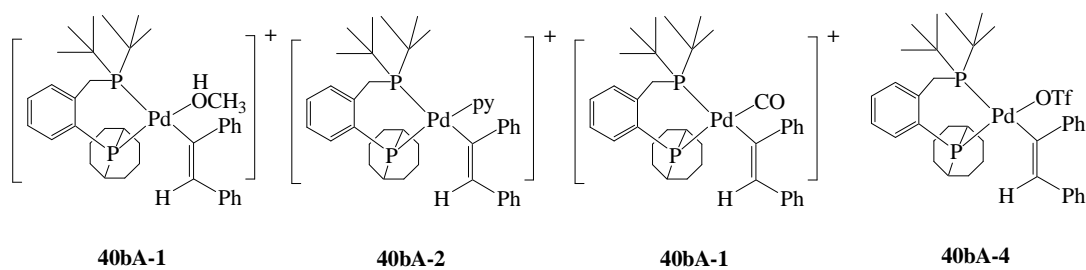
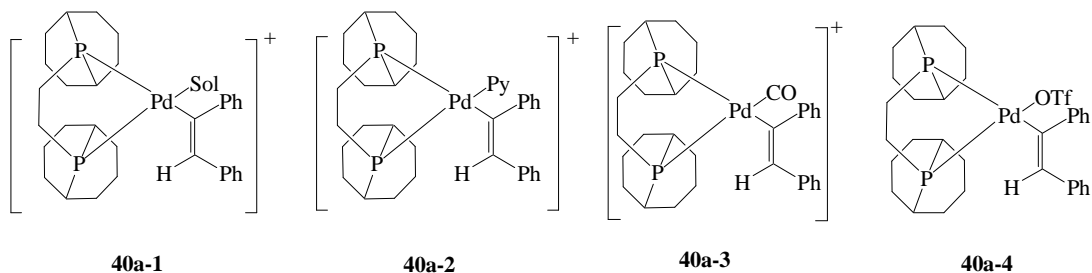
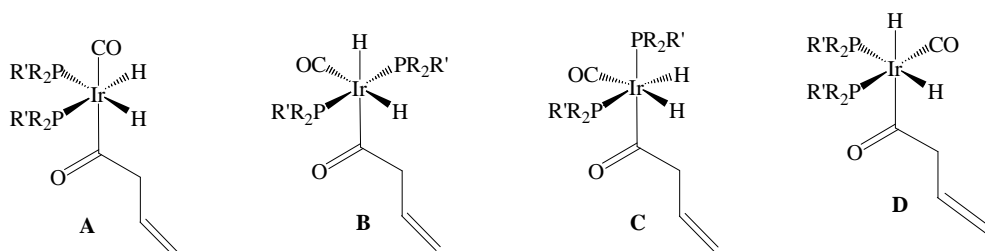
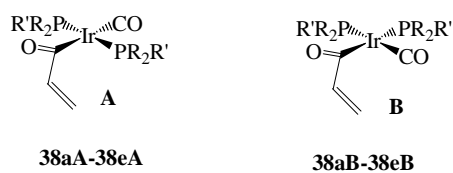
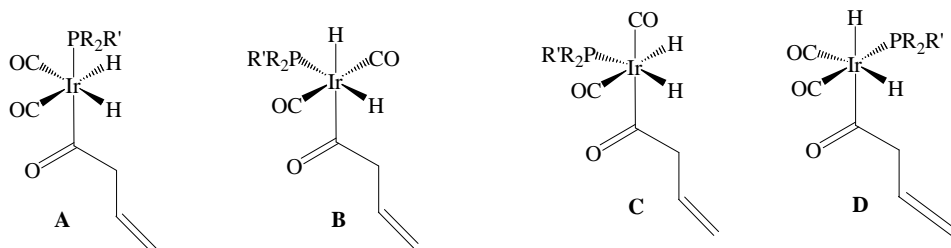


**36aA-36eA**

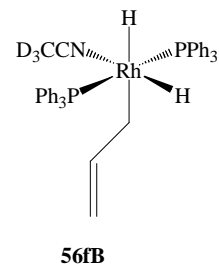
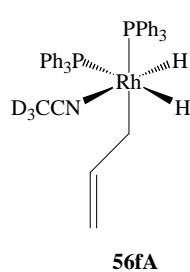
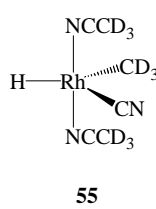
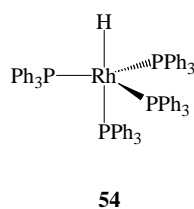
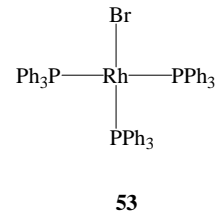
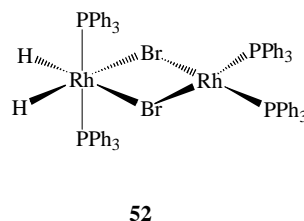
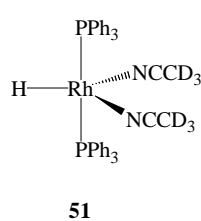
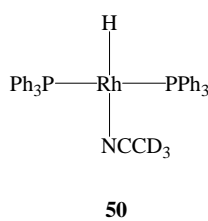
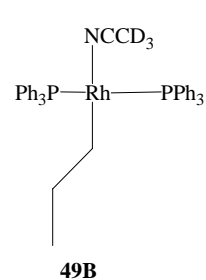
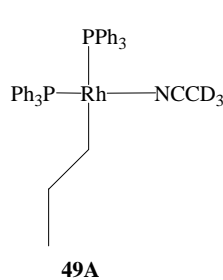
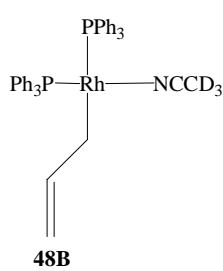
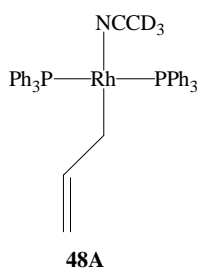
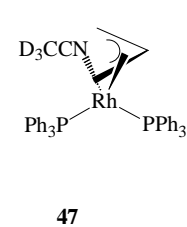
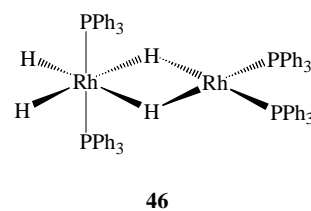
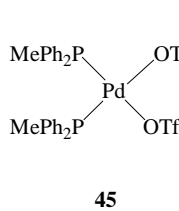
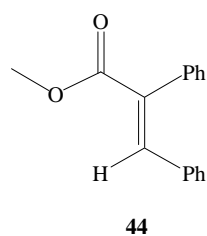
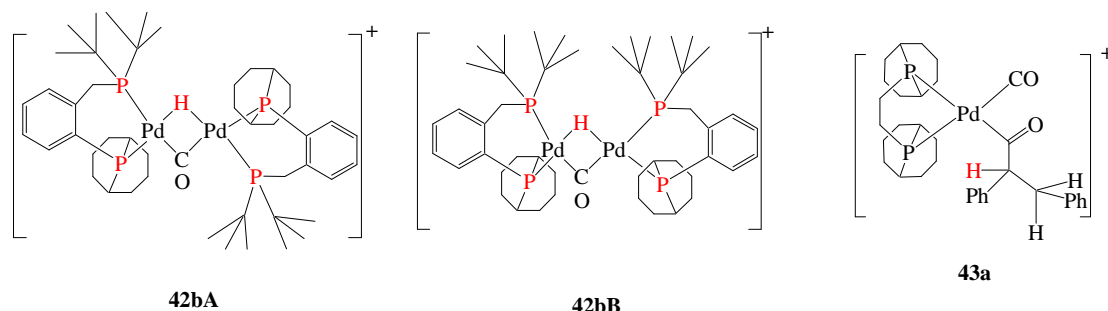
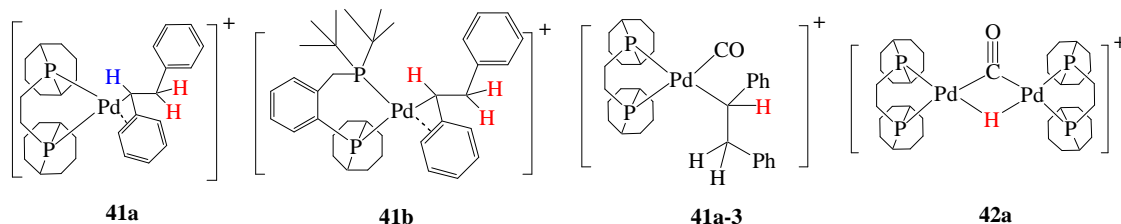


**36aB-36eB**

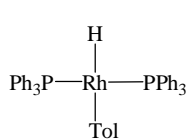
*Structure of complexes*



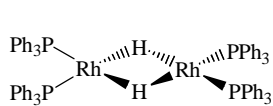
Structure of complexes



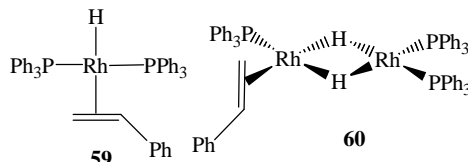
## Structure of complexes



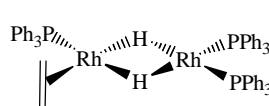
57



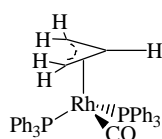
58



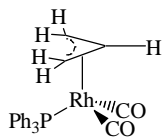
59



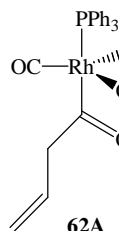
60



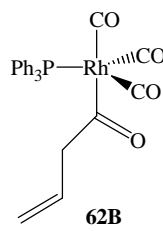
61A



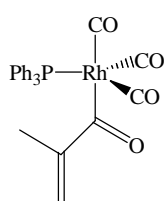
61B



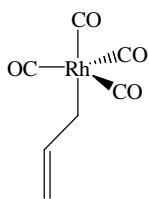
62A



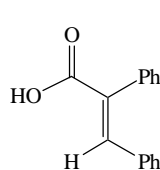
62B



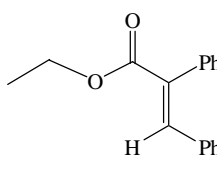
62C



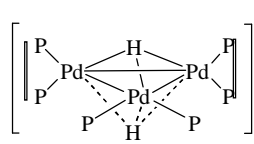
63



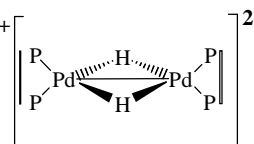
65



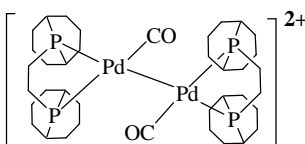
66



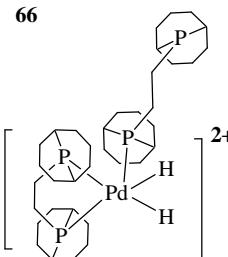
67a



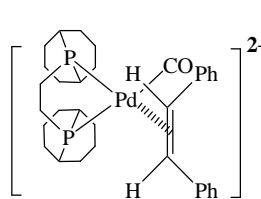
68a



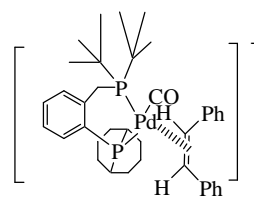
69a



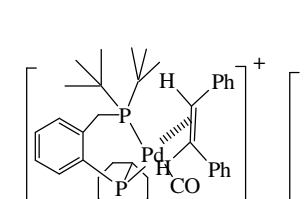
70a



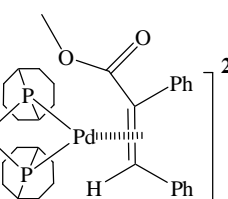
71a



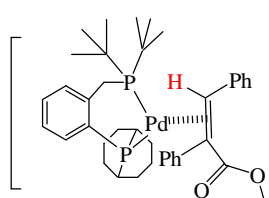
71bA



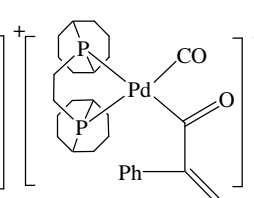
71bB



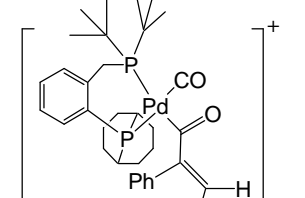
72a



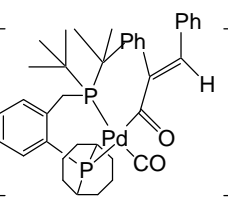
72b



73a



73bA



73bB

Structure of complexes

